

**Stone deterioration and replacement of natural building stones  
at the Cologne cathedral  
A contribution to the preservation of cultural heritage**

Dissertation  
zur Erlangung des mathematisch-naturwissenschaftlichen Doktorgrades  
„Doctor rerum naturalium“  
der Georg-August-Universität Göttingen

im Promotionsprogramm Geowissenschaften  
der Georg-August University School of Science (GAUSS)

vorgelegt von  
**Birte Johanna Graue**  
aus Lauterbach, Hessen

Göttingen, 2013

### Betreuungsausschuss

Prof. Dr. Siegfried Siegesmund

Abteilung Strukturgeologie und Geodynamik

Geowissenschaftliches Zentrum der Georg-August-Universität Göttingen

Prof. Dr. Bernhard Middendorf

Abteilung Werkstoffe des Bauwesens und Bauchemie

Institut für konstruktiven Ingenieurbau der Universität Kassel

### Mitglieder der Prüfungskommission

Referent: Prof. Dr. Siegfried Siegesmund

Geowissenschaftliches Zentrum der Georg-August-Universität Göttingen

Korreferent: Prof. Dr. Rolf Snethlage

Apl. Professor für Angew. Mineralogie der LMU München i.R.

Wetzelstr. 24, 96047 Bamberg

### Weitere Mitglieder der Prüfungskommission

Prof. Dr. Bernhard Middendorf

Abteilung Werkstoffe des Bauwesens und Bauchemie

Institut für konstruktiven Ingenieurbau der Universität Kassel

Prof. Dr. Karl-Heinz Pörtge

Geographisches Institut

Georg-August-Universität Göttingen

Prof. Dr. Hans Ruppert

Abteilung Sedimentologie und Umweltgeologie

Geowissenschaftliches Zentrum der Georg-August-Universität Göttingen

Prof. Dr. Sharon Webb

Abteilung Experimentelle und Angewandte Mineralogie

Geowissenschaftliches Zentrum der Georg-August-Universität Göttingen

Tag der mündlichen Prüfung: 27.03.2013

## Preface

The present work has been undertaken within the framework of a research project founded by the Deutsche Bundestiftung Umwelt (DBU-AZ-28253-45) named “*Untersuchung und Simulation der Verwitterung ausgewählter Naturwerksteine und ihrer Interdependenzen mit historischen und neuzeitlichen Baumaterialien am Dom zu Köln*“.

The thesis incorporates the following publications and manuscripts:

Graue B, Siegesmund S, Middendorf B (2011) Quality assessment of replacement stones for the Cologne Cathedral: mineralogical and petrophysical requirements. *Environ. Earth Sci.*, 63:1799–1822 (chapter four and five)

Graue B, Siegesmund S, Middendorf B, Oyhantcabal P (2012) Requirements for replacement stones at the Cologne cathedral – a systematic approach to general criteria of compatibility. 12th Int. Congr. Deterioration and Conservation of Stone. Columbia University, New York City (chapter nine)

Graue B, Siegesmund S, Simon K, Licha T, Oyhantcabal P, Middendorf B (2012) Environmental impact on stone decay: crust formation at the Cologne cathedral. 12th Int. Congr. Deterioration and Conservation of Stone. Columbia University, New York City (chapter eight)

Graue B, Siegesmund S, Oyhantcabal P, Naumann R, Licha T, Simon K (2013) The effect of air pollution on stone decay: the decay of the Drachenfels trachyte in industrial, urban and rural environments– a case study of the Cologne, Altenberg and Xanten cathedrals. *Environ Earth Sci.* DOI. 10.1007/s12665-012-2161-6 (chapter three, four, five and eight)

Graue B, Siegesmund S, Schumacher T (2013) Steinverwitterung und Natursteinaustausch am Kölner Dom. In: *Naturstein als Element der Kulturlandschaft*. Siegesmund S, Snethlage R (eds.) (submitted) (chapter two and nine)





**Abstract**

The present work deals with the deterioration of natural building stones as a function of mineralogical and petrophysical properties in different environmental and building-physical contexts. Taking Cologne cathedral as an example, the diversity of construction materials found in this monument and the resulting problems of the interference of these materials with each other in terms of their deterioration will be elucidated. Physical and chemical deterioration processes are empirically ascertained through laboratory testing and experiments, and are correlated to the specific petrophysical properties determined in the various stones. Decay phenomena observed *in situ* and the processes connected with these are investigated. To evaluate the different pollution impacts, the decay in three different environmental situations is examined: at industrial Cologne, at urban Xanten and at rural Altenberg. A major influence of air pollution on stone deterioration is ascertained for not only carbonate stone but also silicate stones. Taking the Drachenfels trachyte as an example, mineral composition, textural features, and petrophysical properties are correlated with the observed decay phenomena and the ascertained physical and chemical deterioration mechanisms in an overall context. These results lead to a model of deterioration of the Drachenfels trachyte. In regard to the replacement of natural building stones as a preservation measure for historic monuments, the gained insights from the analyses and laboratory experiments are discussed and existing general criteria for replacement stones are considered more differentiated. The various feedback mechanisms of the different building stones in respect of petrophysical characteristics and deterioration behavior are evaluated. Based on this assessment a selection system can be developed that, supports the evaluation of the compatibility of historical and modern replacement stones for historical buildings and contributes to the preservation of cultural monuments.

During its 600-year history, over 50 different building stones have contributed to the construction of Cologne cathedral. The present work considers eight main building stones. The investigated “cathedral stones” are the Drachenfels trachyte, the Stenzelberg latite, the Obernkirchen and Schlaitdorf sandstones, the Krensheim Muschelkalk, the Londorf basalt lava as well as the Montemerlo trachyte and the Bozanov sandstone. A use of similar natural building stones is ascertained for the Xanten and Altenberg cathedrals. These three monuments built at the same time in the 13<sup>th</sup> century show the use of similar stones not only during the first phase of building, but also in their later construction and restoration. Chapter 2 of the present work introduces these three monuments and the use of building stones in them. The question of appropriate replacement material has been around for long time, since the medieval used Drachenfels trachyte was no longer available for construction work in the 19<sup>th</sup> century.

The environmental situations of the three cathedrals differ greatly: while Cologne cathedral is located in an industrial area, the urban environment at Xanten shows only minor industrial impacts, whereas Altenberg is located in a rural forested environment. Chapter 3 describes in more detail these differing environmental conditions. Furthermore, microclimatic measurements of moisture balance and temperature distribution within different building stones at Cologne cathedral are presented. Detectors are placed at different depths inside each building stone *in situ* oriented in different building expositions. These measurements will aid understanding of correlations and interactions of moisture and temperature distribution with observed decay phenomena and investigated deterioration processes.

The building stones at the three monuments in different environmental conditions show similar decay patterns. The Cologne cathedral suffers severe stone deterioration, which endangers the structure of the building. The Drachenfels trachyte shows pronounced deterioration phenomena such as contour scaling, flaking and structural disintegration to crumbling and total fabric collapse. Other main building stones e.g. sandstones, carbonates, and volcanic rocks, show significant degradation as well. The different deterioration phenomena of the three buildings are illustrated in Chapter 4. At Xanten and Altenberg cathedrals similar deterioration phenomena are detected, but intensity of decay is significantly less pronounced. Deterioration processes in the different building stones are comparable. They are controlled by the mineralogical composition and texture of the stones, which in turn influence the petrophysical properties. This indicates that the intensity of decay at the three monuments varies with the different environmental situations.

The petrophysical properties and specific characteristics of the eight investigated building stones of the Cologne cathedral are ascertained. In Chapter 5 petrographic and petrophysical characteristics are investigated as well as moisture, thermal and strength properties. These properties are correlated to each other in terms of their influence and dependence on each other. They are also discussed in respect of their influence on the typical deterioration phenomena of each stone.

In Chapter 6 experiments and tests on physical weathering are described. The specific drying behavior of the eight “cathedral stones” is discussed, as well as their reactions in cyclic freeze-thaw and salt weathering tests. The test results are correlated to the specific properties of the eight stones and compared to the decay observed *in situ*.

The results of chemical experiments are discussed in Chapter 7 are presented to aid understanding of stones’ reactions in chemical weathering. A general assessment is given of the stones’ resistivity against acidic attack, and their dissolution behavior in different leachants is also investigated. Possible chemical weathering reactions are discussed to elucidate how natural building stones behave under various environmental conditions.

After the ascertainment of extrinsic factors (building climatic and environmental conditions etc.) and intrinsic factors (such as petrophysical properties, mineral composition, textural features, etc.) in the various stones, as well as the empiric assessment of their physical and chemical deterioration behavior, the next consequential step was to investigate *in situ* the different, highly complex interacting weathering reactions and deterioration processes of a physical and chemical character. Chapter 8 presents these investigations in three different locations at Cologne, Xanten and Altenberg. The formation of black weathering crusts as the main indicator for pollution-related stone decay varies significantly between industrial, urban and rural environments. It can also be shown that gypsum crusts not only form on carbonate but as well on silicate stone. The crust formation on the Drachenfels trachyte is mainly controlled by extrinsic factors, and adjacent stone may contribute. A model of deterioration is developed for the Drachenfels trachyte illustrating the interactions and feedback mechanisms of stone characteristics as well as physical and chemical deterioration process in the context of pollution impact.

The final chapter returns to the question of adequate replacement stones. On the background of the several investigations and the gained knowledge, possible interferences of different adjacent building stones are illustrated. The general requirements for replacement stones are summarized in terms of mineralogical, optical and petrophysical properties. The strong divergence of the ascertained parameters of the investigated stones (i.e. mineral composition, porosity, water absorption and saturation, drying characteristics, moisture and thermal dilatation, strength properties, etc.) shows, that the constraints for a replacement material make it almost impossible to find an ideal stone, if parameters are not differentiated stronger. Properties and characteristics are correlated and assessed in terms of their significance for material behavior and in view of the observed deterioration phenomena and processes. They are ranked as “material index” and “decay index”. The correlation of these rankings determines their relevance for replacement criteria: the imperative “key parameters” are indicated. These are the parameters the replacement stone should match; they should be met within the stated requirements for replacement stones. This evaluation leads to a systematic approach developing general criteria of compatibility in selecting replacement materials for historic monuments comprising more than one natural building stone material. It also supports the evaluation of the compatibility of historical and modern replacement stones within a building.

The gained knowledge will aid to establish restoration and conservation concepts, especially in terms of evaluating material compatibilities and the respective selection of replacement materials; thus contributing to the development and implementation of preservation measures for historic stone monuments.



## Zusammenfassung

Die vorliegende Arbeit beschäftigt sich mit der Verwitterung von Naturwerkstein als Funktion von mineralogischen und petrophysikalischen Eigenschaften unter unterschiedlichen umwelt- und bauphysikalischen Bedingungen. Am Beispiel des Kölner Doms wird zum einen die große Anzahl an unterschiedlichen Baumaterialien, die in diesem Bauwerk angetroffen werden, vorgestellt. Darüber hinaus werden auch die daraus resultierenden Probleme von Interferenzen der verschiedenen Materialien untereinander in Hinblick auf ihre Verwitterung beleuchtet. Physikalische und chemische Verwitterungsprozesse werden anhand von Laborversuchen und Tests empirisch erfasst. Diese werden mit den festgestellten spezifischen petrophysikalischen Eigenschaften der unterschiedlichen Gesteine korreliert und im Zusammenhang mit den *in situ* festgestellten Verwitterungsphänomenen und –prozessen diskutiert. Um die unterschiedlichen Einflüsse der Verwitterungs- und Umweltbelastungen zu evaluieren, wird die Natursteinverwitterung an drei Standorten – dem industriell geprägten Köln, Xanten mit einem städtischen Klima und im ländlichen Altenberg im Bergischen Land – vergleichend studiert. Hierbei zeigt sich der starke Einfluss der Luftverschmutzung auf die Natursteinverwitterung nicht nur für karbonatische sondern auch für silikatische Gesteine. Beispielhaft werden am Drachenfels Trachyt die Mineralkomposition, die Gefügeeigenschaften und die petrophysikalischen Eigenschaften des Gesteins im Gesamtzusammenhang miteinander korreliert und mit den festgestellten Schadensphänomenen und den ermittelten physikalischen und chemischen Verwitterungsprozessen abgeglichen. Aus diesen Erkenntnissen heraus wird ein Modell zur Verwitterung dieses Naturwerksteins entwickelt. In Hinblick auf Natursteinersatz als Erhaltungsmaßnahme für historische Kulturgüter aus Stein werden die Untersuchungsergebnisse, die Erkenntnisse aus den Laborversuchen und den Diskussionen zusammengeführt und bestehende grundsätzliche Anforderungen an ein Ersatzgestein weiter differenziert. Die verschiedenen Wechselwirkungsmechanismen der unterschiedlichen Naturwerksteine, die in einem Bauwerk verbaut sind, werden vor dem Hintergrund ihrer petrophysikalischen Charakteristika sowie ihres Verwitterungsverhaltens bewertet. Basierend auf dieser Beurteilung wird eine Auswahl-Systematik entwickelt, die die Evaluierung der Verträglichkeit von historischen und modernen Austauschgesteinen für historische Bauwerke unterstützt.

Aufgrund seiner langen über 600 Jahre währenden Baugeschichte ist der Kölner Dom aus über 50 verschiedenen Bausteinen errichtet. Die vorliegende Arbeit bezieht sich dabei auf acht Haupt-Bausteine. Die untersuchten „Dom-Bausteine“ sind der Drachenfels Trachyt, der Stenzelberg Latit, der Obernkirchener und der Schlaitdorfer Sandstein, der Krensheimer Muschelkalk, die Londorfer Basaltlava sowie der Montemerlo Trachyt und der Bozanov

Sandstein. Eine Verwendung ähnlicher Naturwerksteine ist auch beim Xantener und beim Altenberger Dom festzustellen, die ebenfalls aus dem 13. Jahrhundert stammen. Für diese drei mittelalterlichen Bauwerke wurden nicht nur zu ihrer Entstehungszeit sondern auch in späteren Restaurierungs- und Wiederinstandsetzungsmaßnahmen ähnliche Bausteine verwendet. Kapitel 2 der vorliegenden Arbeit stellt die drei Kathedralen in ihrem bauhistorischen Kontext vor und zeigt die Verwendung der unterschiedlichen Naturwerksteine auf. Es erwies sich schon zu ihrer Erbauungszeit und auch zu Zeiten des Weiterbaus, dass die Frage nach einem adäquaten Ersatzgestein entscheidend war, seit der ursprünglich verwendete Drachenfels Trachyt ab dem 19. Jahrhundert für Weiterbau- und Instandsetzungsmaßnahmen nicht mehr zur Verfügung stand.

Die Umweltbedingungen an den drei Standorten unterscheiden sich sehr stark: Der Kölner Dom ist in einem industriell geprägten Raum zu finden, das städtische Klima von Xanten zeigt geringe industrielle Prägung, während Altenberg in einer ländlichen waldreichen Gegend liegt. Diese drei unterschiedlichen Umweltbedingungen der Kathedralen werden in Kapitel 3 beleuchtet. Darüber hinaus, werden mikroklimatische Feuchtigkeits- und Temperatur-Messungen und die entsprechenden Verteilungen in verschiedenen Bausteinen des Kölner Doms vorgestellt. Sensoren wurden *in situ* platziert in unterschiedlichen Tiefen innerhalb der jeweiligen Bauwerksteine und in unterschiedlich exponierten Bereichen des Bauwerks. Diese Messungen sollen dazu beitragen, die Wechselwirkungen von Feuchtigkeits- und Temperatur-Verteilung in den Bauwerksgesteinen mit den festgestellten Schäden und untersuchten Verwitterungsprozessen zu korrelieren.

Die Naturwerksteine an den drei Bauwerken in den unterschiedlichen Umweltbedingungen zeigen ähnliche Verwitterungsmuster. Am Kölner Dom ist eine sehr starke Naturstein-Verwitterung festzustellen, die die statische Sicherheit von Gebäudeteilen mitunter gefährdet. Der Drachenfels Trachyt zeigt ausgeprägte Verwitterungsmerkmale, wie Schalen- und Schuppenbildung, strukturelle Entfestigung und Bröckelzerfall bis hin zum Totalverlust. Auch die anderen Bauwerksgesteine wie Sand- und Kalksteine sowie vulkanische Gesteine zeigen signifikante Verwitterung. Die unterschiedlichen Verwitterungsphänomene sind in Kapitel 4 dargestellt. Am Xantener und Altenberger Dom wurden ähnliche Verwitterungsmerkmale festgestellt, allerdings in viel geringerem Umfang und geringerer Intensität. Die Prozesse, die die Verwitterung begründen, sind vergleichbar. Diese werden von der mineralogischen Zusammensetzung und den Gefügeeigenschaften der jeweiligen Steine bestimmt, die wiederum die petrophysikalischen Eigenschaften beeinflussen. Dadurch wird deutlich, dass die unterschiedliche Intensitätsausprägung an den drei Bauwerken in den unterschiedlichen umweltspezifischen Bedingungen begründet liegt.

Die Eigenschaften und gesteinspezifischen Charakteristika der acht untersuchten „Dom-Bausteine“ sind festgestellt worden. In Kapitel 5 werden ihre petrographischen und

petrophysikalischen Eigenschaften sowie ihr Feuchte- und Temperaturverhalten als auch ihre Festigkeitsparameter bestimmt. Diese Eigenschaften werden miteinander korreliert in Hinblick auf ihren wechselwirkenden Einfluss und ihre Abhängigkeiten untereinander und sie werden in Hinblick auf ihren Einfluss auf die typischen Verwitterungsphänomene der einzelnen Steine diskutiert.

Kapitel 6 beschreibt Experimente und Tests zur physikalischen Verwitterung von Naturwerksteinen. Das Trocknungsverhalten der acht „Dom-Bausteine“ sowie ihr Verhalten bei zyklischer Frost-Tau-Belastung und Salzbelastung werden diskutiert. Die Test-Ergebnisse werden mit den gesteinspezifischen Eigenschaften korreliert und mit dem *in situ* beobachteten Verfall verglichen.

Die Ergebnisse von verschiedenen chemischen Experimenten werden in Kapitel 7 diskutiert und sollen zum Verständnis von chemischen Verwitterungsreaktionen der unterschiedlichen Steine beitragen. Neben einer generellen Beurteilung ihrer Säureresistenz soll ihr Lösungsverhalten in unterschiedlichen Lösungen untersucht werden. Mögliche chemische Verwitterungsreaktionen werden diskutiert, um das Verhalten der Naturwerksteine in unterschiedlichen Umweltbedingungen zu beleuchten

Nachdem die einzelnen extrinsischen Faktoren (u.a. Klima- und Umweltbedingungen) sowie die intrinsischen Faktoren der einzelnen Steine (petrophysikalische Eigenschaften und Mineralkomposition sowie Gefügeeigenschaften, etc.) erfasst und ihr physikalisches und chemisches Verwitterungsverhalten in Tests empirisch festgestellt wurde, werden in einem nächsten Schritt diese verschiedenen, sehr komplexen wechselwirkenden Verwitterungsreaktionen und –prozesse physikalischer und chemischer Art *in situ* untersucht. Kapitel 8 stellt die Untersuchungen an den verschiedenen Bauwerksteinen der drei unterschiedlichen Standorte des Kölner, Xantener und Altenberger Doms vor. Die Bildung schwarzer Verwitterungskrusten als Hauptindikator für die Natursteinverwitterung im Zusammenhang mit Luftverschmutzung variiert sehr stark in diesen drei unterschiedlichen – industriell geprägten, städtischen und ländlichen – Klimata. Darüber hinaus wird gezeigt, dass sich nicht nur auf Karbonatgesteinen schwarze Verwitterungskrusten bilden, sondern auch auf silikatischen Naturwerksteinen. Die Krustenbildung auf dem Drachenfels Trachyt ist hauptsächlich durch extrinsische Faktoren bestimmt, dabei können benachbarte Gesteine zu dieser Krustenbildung mit beitragen. Für den Drachenfels Trachyt wird ein Verwitterungsmodell entwickelt, das die Wechselwirkung der verschiedenen Rückkopplungsmechanismen physikalischer und chemischer Verwitterungsprozesse als Funktion intrinsischer und extrinsischer Faktoren darstellt.

Im abschließenden Kapitel wird die anfangs gestellte Frage nach einem adäquaten Ersatzgestein aufgegriffen. Vor dem Hintergrund der unterschiedlichen durchgeführten Untersuchungen und daraus gewonnenen Erkenntnisse werden mögliche Wechselwirkungen

der unterschiedlichen miteinander verbauten Werksteine beleuchtet. Grundsätzliche Anforderungen an Ersatzgesteine umfassen mineralogische, optische und petrophysikalische Eigenschaften. Die starke Divergenz der festgestellten Steinparameter der verschiedenen untersuchten Gesteine (Mineralkomposition, Porosität, Wasseraufnahme und –sättigung, Trocknungsverhalten, Feuchte- und Temperaturdehnung, Festigkeitsparameter, etc.) zeigt, dass es anhand dieses Anforderungskataloges fast unmöglich ist, ein ideales Ersatzgestein zu finden, falls die Parameter nicht differenzierter betrachtet werden. Dazu wird die Summe der Eigenschaften und Charakteristika in Hinblick auf ihre Signifikanz für die Materialeigenschaften und das Materialverhalten auf der einen Seite sowie für die Ausprägung von Schadensphänomenen und ihr Verwitterungsverhalten auf der anderen Seite miteinander korreliert und bewertet. Anhand einer entsprechenden Punktevergabe werden ein „Material-interner Index“ und ein „Verwitterungs-Index“ erstellt. Aus diesen beiden Bewertungs-Skalen ergeben sich die „Schlüssel-Parameter“ des Originalgesteins, die bei einem Kompatibilitätsabgleich mit einem potenziellen Austauschgestein im Rahmen des genannten Anforderungskataloges übereinstimmen sollten. Diese systematische Herangehensweise der Evaluierung führt zu einer Entwicklung von allgemeinen Qualitätskriterien für die Kompatibilität zur Auswahl geeigneter Ersatzgesteine für historische Bauwerke, in denen mehr als ein Naturwerkstein verbaut ist. Sie trägt zur Beurteilung der Verträglichkeit von historischen und modernen Austauschmaterialien in einem Bauwerk bei.

Die neu gewonnenen Erkenntnisse sollen also einen Beitrag leisten bei der Aufstellung von Sanierungs- und Konservierungskonzepten, im Besonderen bei der Evaluierung von Materialkompatibilitäten und der entsprechenden Auswahl von Ersatzgestein, und damit die Entwicklung und Umsetzung von qualitativ hochwertigen Erhaltungsstrategien für Baudenkmäler aus Naturwerkstein unterstützen.



**Table of contents**

Preface .....	i
Abstract .....	iii
Zusammenfassung .....	vii
Table of contents .....	xi
1 General Introduction .....	1
1.1 Aims of the thesis .....	1
1.2 Deterioration of natural building stone .....	3
1.2.1 Physical deterioration .....	4
1.2.2 Chemical deterioration .....	9
1.2.3 Biological deterioration .....	12
1.3 The impact of air pollution on stone decay .....	13
1.4 Stone deterioration at the Cologne cathedral .....	14
1.5 Interferences of adjacent stones .....	16
1.6 Cultural heritage preservation needs for adequate replacement stones .....	16
1.7 History of the selection of replacement stones for the Drachenfels trachyte .....	17
1.8 Requirements for replacement stones .....	17
2 The cathedrals – construction history of the Cologne, Xanten and Altenberg cathedrals .....	19
3 The cathedrals' environments .....	25
3.1 Industrial, urban and rural environment .....	25
3.2 Material temperature and moisture balance in the building stones .....	27
3.2.1 Material and methods .....	27
3.2.2 In situ-measurements .....	29
3.2.3 Acquired data .....	33
3.3 Conclusions .....	37
4 Stone decay at the cathedrals .....	41
4.1 Decay features of the “cathedral stones” .....	41
4.2 Comparison of the decay at the three different locations .....	47
5 The building stones of the Cologne cathedral .....	51
5.1 Geology at the Cologne cathedral .....	51
5.2 Petrography of the “cathedral stones” .....	53
5.2.1 Density, porosity, pore size distribution .....	57
5.3 Moisture properties .....	60
5.3.1 Capillary water absorption .....	60
5.3.2 Water saturation coefficient .....	61
5.3.3 Sorption/ Desorption .....	62

5.3.4	Water vapor diffusion resistance .....	63
5.3.5	Hydric and hygric dilatation.....	63
5.4	Thermal Dilatation.....	65
5.5	Mechanical properties.....	66
5.5.1	Uniaxial compressive strength.....	66
5.5.2	Flexural strength .....	66
5.5.3	Tensile strength .....	67
5.6	Deterioration phenomena and physical decay processes .....	67
6	Aspects of physical weathering.....	75
6.1	Drying properties.....	75
6.2	Freeze–thaw weathering tests .....	80
6.3	Salt-weathering tests .....	89
7	Aspects of chemical weathering.....	95
7.1	Acid buffering capacity .....	95
7.1.1	Material and methods .....	95
7.1.2	Results.....	95
7.1.3	Discussion .....	96
7.2	Leaching with methane-sulfonic-acid at pH 4 .....	97
7.2.1	Material and methods .....	97
7.2.2	Results.....	98
7.2.3	Discussion .....	99
7.3	Leaching experiments.....	102
7.3.1	Material and methods .....	102
7.3.2	Detection of pH changes .....	104
7.3.3	Leached fractions .....	104
7.3.4	Discussion .....	116
7.4	Leaching processes in natural building stone .....	116
7.4.1	Correlation of leachability, grain size and leachant .....	117
7.4.2	Dependency upon the leachant.....	118
7.4.3	Interaction of weathering reactions.....	120
7.4.4	Comparison of experimental and natural weathering rates .....	121
7.4.5	Conclusion .....	122
8	The effect of air pollution on stone decay .....	125
8.1	Material and methods .....	127
8.2	Black weathering crusts on the natural building stones .....	129
8.2.1	Crust classification.....	129
8.2.2	Mineralogy and fabric of black weathering crusts.....	131

8.2.3	Geochemical characterization .....	134
8.2.4	Microscale chemical investigation .....	136
8.2.5	The polycyclic aromatic hydrocarbon fingerprint .....	139
8.3	Discussion.....	141
8.3.1	Crust formation on Drachenfels trachyte in comparison to limestone.....	141
8.3.2	Sulfur and calcium sources.....	142
8.3.3	Interferences of adjacent stones.....	145
8.3.4	Exposition and crust formation .....	147
8.4	Correlation of crust formation and stone decay .....	149
8.5	The clay mineral content in the Drachenfels trachyte .....	155
8.6	Conclusions .....	157
9	Multifactorial selection system for replacement stones.....	161
9.1	Introduction .....	161
9.2	General requirements for replacement stones.....	163
9.3	Recognition and measurement of parameters.....	169
9.3.1	Assessment and ranking .....	170
9.3.2	Correlation and matching.....	173
9.4	Multivariate statistics.....	176
9.5	Development of a classification scheme for the selection of replacement stones.....	178
10	General conclusions .....	179
11	Outlook .....	185
	References .....	187
	Acknowledgement.....	197
	Curriculum Vitae.....	199
	Appendix .....	201



## 1 General Introduction

### 1.1 Aims of the thesis

The cathedral of Cologne is one of the most outstanding monuments in Northern Europe and, with 6.5 million visitors per year, the most popular tourist attraction in Germany. Since 1996 the largest gothic church has been honored as UNESCO world heritage site. Its unique construction history began in 1248 and extends over a period of over 600 years. Due to this very long building time, Cologne cathedral is built with over 50 different building stones. The Drachenfels trachyte from the quarries of the Siebengebirge has been mainly used as the natural building stone for construction in Cologne since the Roman period. The Rhine River provided an excellent means of transporting good stone material from quarries along the Rhine and its connecting rivers (Wolff 2004). In Figure 2.4, the lithological survey map illustrates that the issue of stone procurement was very important throughout the construction period of the cathedral. At the beginning of the 16<sup>th</sup> century, construction was halted and only recommenced at the beginning of the 19<sup>th</sup> century. At that time, the Drachenfels trachyte was no longer available. Initial renovations were carried out with latite from the “Stenzelberg” and a few other materials from the quarries of the Siebengebirge. In the middle of the 19<sup>th</sup> century, the second construction phase used sandstone from “Schlaitdorf”, in southern Germany. Later on, the “Obernkirchen” sandstone from Lower Saxony and from 1918 until the 1940s the “Krensheim Muschelkalk” were implemented. In the 1950s, the decay-resistant basalt lava from “Londorf” was used. The materials currently applied are trachyte from “Montemerlo” (Italy) for the replacement of the deteriorated Drachenfels trachyte, as well as Czech sandstone from “Bozanov”, which has been used to replace the weathered Schlaitdorf sandstone (Scheuren 2004; Schumacher 2004).

The increasing deterioration of the building materials from the historic and more recent construction history has endangered the structure of the cathedral. The continuously present scaffolding at the cathedral indicates the constant need for stone preservation works. The issue of stone deterioration is as old as the monuments themselves. Through the examination of deterioration and research on the preservation of the Drachenfels trachyte, deterioration far beyond the usually expected extent was ascertained (Dombauhütte Köln 2006). Apparently the type of adjacent natural building stones plays a key role. Already, in earlier times, a stronger deterioration of the trachyte was observed in context with carbonate stone (Kraus 1985a; Schumacher 2004; von Plehwe-Leisen et al. 2007). Wolff (1992) detected severe deterioration of the Schlaitdorf sandstone placed next to Londorf basalt lava. Negative interferences of the used stones and mortars are assumed.

Starting with the question of whether several natural building stones which are placed together in one building context will interfere with each other, the thesis pursues several objectives:

(a) *Petrographic and petrophysical characterization of the investigated “cathedral stones”.*

The petrophysical properties and characteristics of the eight building stones from the Cologne cathedral will be ascertained: mineral composition, density, porosity, pore size distribution, capillary water uptake, water uptake by adsorption, saturation degree, water vapor diffusion resistance, moisture and thermal dilatation, as well as strength properties. The ascertained properties will be correlated with each other and their influence on the decay of the stones will be deduced.

(b) *Outline of the physical and chemical deterioration processes in terms of the ascertained parameter in these stones.*

Laboratory tests and experiments on physical weathering will be conducted concerning the drying characteristics, freeze-thaw-weathering behavior and salt deterioration resistance of the “cathedral stones”. The chemical weathering behavior will be investigated through laboratory experiments with regard to the stones' acid resistivity and leachabilities. The correlation of the ascertained properties with one another and the observed decay phenomena, as well as the results of the laboratory tests, will help to understand deterioration processes within the stones investigated.

(c) *Detection of the impact of environmental pollution on the natural building stone deterioration.*

Black weathering crusts are usually seen as the main indicator of pollution-related stone decay (Henley 1967; Del Monte et al. 1981; Wolff 1986; Ausset et al. 1992; Derbez and Lefèvre 1996; Esbert et al. 1996; Charola and Ware 2002; Brimblecombe 2003; Sabbioni 2003, etc.). Crust formation on the stones at Cologne, Xanten and Altenberg cathedrals will be investigated in terms of the different industrial, urban and rural environments. Differences of crust formation on carbonate and silicate rocks and the different impact of air pollution at the three sites will be detected.

(d) *Understanding of deterioration processes in the Drachenfels trachyte.*

The Drachenfels trachyte is the natural building stone of the Rhineland region used since the Roman period (Berres 1996). This unique stone shows severe deterioration phenomena which endanger its cultural heritage. The present work will investigate the main factors, i.e., the parameters of the stone, controlling the deterioration of the trachyte, and elucidate deterioration processes.

(e) *Assessment of possible interferences of the “cathedral stones”.*

The understanding of the different deterioration processes of the various stones and the interaction of the ascertained parameters within them will contribute to an assessment of the interferences of the cathedral stones. This will help in order to understand the observed negative interferences of the stones in the building context and contribute to preservation planning.

(f) *Development of a selection scheme for replacement stones.*

The long history of the search and usage of replacement materials at Cologne cathedral (Schumacher 2006) implies the need for appropriate replacement stones which are compatible not only with the original stone, which needs to be replaced, but also with all other natural building stones used in the building section. A system for the selection will be developed which comprises the multifactorial aspects of the stones' characteristics as well as their specific deterioration behavior. This will support the evaluation of the compatibility of historic and modern replacement stones within a building and help to assess preservation problems. The multifactorial system contributes to the selection of adequate replacement stones for historic monuments which comprise more than one natural building stone.

In Central Europe in general, mortars are used for the construction of monuments. These play an important part in the deterioration of natural building stones. Mortars may function as a source of alkaline components and contribute to the formation of damaging salts (Grün 1931; Wolff 1972; Arnold 1981, 1992; Bläuer-Böhm 2005; Kraus 2002; Kraus and Droll 2009; Schwiete et al. 1965). Furthermore, due to their different physical properties, e.g., strength, elasticity, density, water absorption, thermal and moisture dilatation, they might display divergent behavior from the stone materials and contribute to their decay, if not cause the deterioration of the natural building stones. This topic is subject to scrutiny and, in general, is discussed in the context of the interferences of construction materials. The present thesis deals with the deterioration and interferences as well as with the replacement of natural building stones; the comprehension of mortars in these assessments is essential, but is beyond the scope of this work.

## **1.2 Deterioration of natural building stone**

Similar to the deterioration of stone in the natural environment, natural building stones deteriorate in the built environment well. The decay of building stones proceeds from an increasing loss of strength to the final collapse of the stone. Deterioration processes are influenced by both intrinsic and extrinsic factors. The first are the physical or chemical characteristics of the stone, such as mineral composition, textural features, petrographic and

petrophysical properties, surface area and defect densities of mineral grains. Extrinsic factors reflect environmental conditions external to the stone, such as climate, the impact of pollution, biological activity, building exposition, interferences with other construction materials (stones and mortars) and pore solution composition (White 2003). In general, deterioration processes are differentiated in chemical, physical and biological deterioration. These different deterioration processes interfere with – and in most cases they enhance – each other and are influenced by anthropogenic impact (Fig. 1.1). As an example, interferences might be the comminution of mineral grains through chemical weathering leading to pore space changes. This entails a different – mostly increased – water uptake, and thus an increase in physical deterioration. Damaging salts – which deteriorate the stone physically – are in many cases formed through the contribution of elements dissolved from the rock-forming minerals by chemical reactions; e.g., gypsum in the case of carbonate stone. Through the chemical decomposition of rock-forming minerals, the cohesion of the rock's matrix decreases, thus leading to a loss of strength and thereby implying vulnerability for physical decay. On the other hand, physical deterioration processes, e.g., salt weathering or freeze-thaw cycles, can severely damage the stone's structure and impair textural features. Thus, the physical impact may result in higher water and pollutant uptake, which again enhances chemical weathering. Physical weathering leading to mechanical decomposition of mineral grains serves as an essential precondition for chemical weathering. Due to the (partial) break down of the stone's structure and minerals, access and the reaction surface are enlarged (White 2003). Biological weathering can be conceived of as a form of two-fold process. On the one hand, microorganisms – e.g., lichen, bacteria, fungi or algae – produce organic acids which serve as  $H^+$  donators, thus leading to chemical weathering (Wierzos and Ascaso 1998; Adamo and Violante 2000; Dornieden and Gorbushina 2000; Jones et al. 2000; Pinna and Salvadori 2000). On the other hand, they may contribute to higher water importation into the stone due to their higher moisture content, thus implying physical deterioration processes (Wihr 1986).

### **1.2.1 Physical deterioration**

In general, physical deterioration consists of physical changes of the stone's structure, usually implied by mechanical stress or load exceeding the mechanical resistance of the stone (Snethlage 1984; Steiger et al. 2011). Deterioration phenomena are many-fold: from fissures and cracks to granular disintegration, flaking and scaling, to spalling, breakouts, crumbling and final fabric collapse. These may result from the poor design of building structures or the impact of higher levels of vegetation, when roots work their way through natural building stone. In addition, fire may cause severe mechanical damage on natural stone. Due to the fact, that stone in general is not a very good heat conductor, fire may lead to significant temperature gradients within the stone (Steiger et al. 2011).



Several processes are addressed as physical deterioration processes: frost and salt weathering, and thermal as well as hydric and hygric dilatation. The main extrinsic factors causing these processes, are temperature and moisture changes and pollution impact; e.g., atmospheric gases and salts. These extrinsic factors often occur in combination; thus, processes interact and in most cases enhance each other – e.g., ice crystallization and salt deterioration, as well as salt crystallization processes and moisture changes (Steiger et al. 2011).

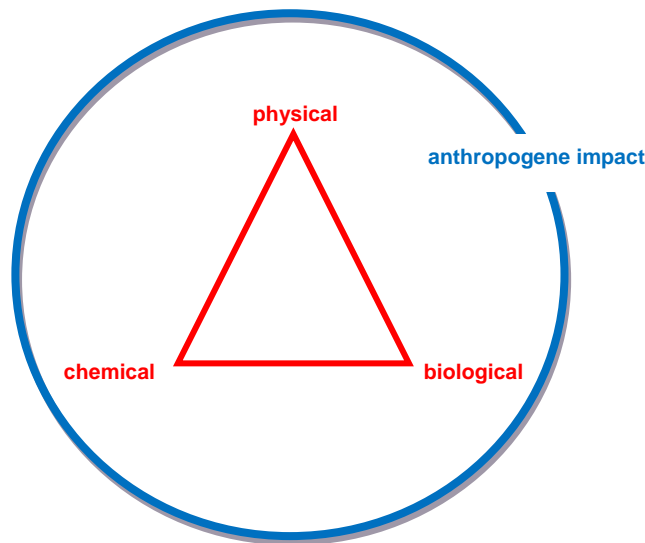


**Figure 1.1** Chemical, physical and biological deterioration affects natural building stone in interactive feedback mechanisms, being influenced overall by the pollution impact of the anthropogenic environment.

Salt deterioration in natural stone has been a subject to research for a long time (Darwin 1839). Salt weathering in natural stone occurs with the crystallization and/or hydration processes of salts contained in the pore solutions. These salts – and in particular the ionic entries – may derive from extrinsic sources transported with capillary water uptake or else water uptake by water vapor absorption as well as with gaseous phases (i.e. atmospheric gases). They may as well be the chemical reaction products of stone immanent components in an acidic attack, e.g., gypsum formation in carbonate-bearing stones. Crystallization processes are mainly controlled by the properties of the salt solution, the properties of the growing salts, climatic conditions and the properties of the natural building stone (Ruedrich and Siegesmund 2006). In general, salt crystallization takes place when the solution is oversaturated. In most cases, salt mixtures are found, which results in a change of crystallization properties from those of pure salt solutions (Steiger et al. 1998). Depending upon the salt solution composition, different mechanisms are discussed, which introduce stress on the stone's microstructure leading to damage (Duttlinger and Knöfel 1993; Charola

2000; Doehne 2002; Ruedrich and Siegesmund 2006). Different models are described for the deterioration mechanisms of salt crystallization in porous materials. Correns and Steinborn (1939) introduced the model of the linear crystal growth pressure for crystal growth from super-saturation solutions. Calculations of crystal growth pressure are often based on very high ratios of the super-saturation of the salt solution (Winkler 1975; Snethlage 1984). Steiger (2005) calculated pressures exceeding the tensile strength of many natural building stones based on a low super-saturated NaCl solution. Another model for salt crystallization within the pore space, states the primarily crystallization of salt in larger pores (Wellmann and Wilson 1965, 1968; Putnis and Mauthe 2001).

A second mechanism leading to salt damage in porous systems is due to the stress caused by the different hydration phases of the salts (Mortensen 1933; Duttlinger and Knöfel 1993). Hydration/dehydration reactions are very complex in the pore space of natural building stones and different hydration stages have been found (Duttlinger and Knöfel 1993; Charola and Weber 1992; Doehne 1994). Especially for salts with hydration phases, it remains a matter of dispute as to which process – crystallization or hydration – is responsible for the strong damage potential (Chatterji et al. 1979; Sperling and Cooke 1980).

Frost weathering in natural stone is due to the stress, which is caused by the growth of ice crystals upon the freezing of the pore water content (Steiger et al. 2011). This is strongly correlated with the water uptake of the stone. Hirschwald (1912) detected a guide value of  $s < 0.9$ , indicating vulnerability to frost damage. This was based on the fact that water upon freezing, undergoes a volume increase of 9%. Thus, stones containing more than 91 vol. % of water by voluntary water uptake are assumed to be extremely susceptible to frost damage. Many stones show saturation degrees in that range, but not necessarily frost damage (Snethlage 1984), while others with a lower saturation degree do (Ruedrich and Siegesmund 2006). Frost deterioration processes are strongly correlated to the pore size distribution. In smaller pores ( $r \leq 0.1 \mu\text{m}$ ), water freezes at lower temperatures (Stockhausen 1981). Thus, the crystallization of ice starts in the larger pores. With the high saturation of the stone and an inappropriate pore size distribution, frost deterioration presumably takes place. On the other hand, when a stone with a higher ratio of smaller pores is only saturated to a minor degree and temperature decreases slowly, the water from the smaller pores may diffuse into the bigger pores where there is enough space for expansion (Snethlage 1984). The model of volume expansion upon ice crystallization as the main deterioration mechanism is debated. Two other models are discussed as being responsible for salt deterioration. Linear crystal growth pressure (Scherer 1999) and capillary pressure (Everett 1961) are also seen as deterioration mechanisms upon ice crystallization. The “Everett-model” explains the aforementioned observations made by Snethlage (1984). However, Everett (1961) assumes

a much higher water supply from smaller to larger pores as being sufficient for crystallization pressure stress. Ruedrich and Siegesmund (2006) draw parallels to the approach of Wellmann and Wilson (1965) of salt crystallization with Everett's model. Steiger (2005) detects super saturation as being the driving force for the capillary pressure model.

At cyclic temperature changes, stone undergoes dimensional changes. Temperature increases and decreases will lead to volume expansion and, in reverse, contraction. An exception to this behavior is observed for marble, where contractions with heat impact can be observed (Siegesmund et al. 1999, 2000; Weiss et al. 2004). Although temperature changes are not very significant, repeated heating and cooling will result in the material fatigue of stones, which may finally lead to the degradation of the stone. This is especially so for the residual stress, which remains within the stone after cooling, and indicates decay potential. It will remain and accumulate over time (Steiger et al. 2011). The thermal dilatation of rocks is due to the thermal behavior and length changes of the rock-forming mineral grains. While most rock-forming minerals show expansion with heat in one direction, calcite shows an expansion in one direction and a contraction in the other (Steiger et al. 2011). Thus, marble is the most susceptible stone to thermal-induced weathering. Thermal cycling leads to the granular decohesion of the stone matrix due to the different thermal expansion coefficients of the rock-forming minerals (Bland and Rolls 1998). The deterioration phenomena described are sanding and, in the case of marble, the so-called "sugaring" (Kessler 1919; Franzini et al. 1983). Granite and especially marble slabs may show specific bowing (Siegesmund et al. 2008; Weiss et al. 2004).

Moisture changes of the ambient condition lead to expansion processes within natural building stones and contribute to their deterioration (Weiss et al. 2004; Ruedrich et al. 2011). Ruedrich et al. (2011) use the term 'moisture expansion' for hygric swelling (when related to RH changes) and hydric swelling (when related to water immersion) (Delgado Rodrigues and Charola 1996), since these describe the conditional terms rather than the mechanisms related to the dilatation. The main processes attributed to moisture expansion are the swelling of clay minerals (Schuh 1987; De la Calle and Suquet 1988; Snethlage et al. 1995; Jimenez Gonzalez and Scherer 2004; Dixon and Weed 1989; Moore and Reynolds 1997) and the development of disjoining pressure (Derjaguin and Obukov 1936; Splittgerber 1976; Stockhausen 1981; Weimann 2001) during wet/dry cycles. The swelling mechanisms of clay minerals within a stone upon wetting are discussed in terms of intra-crystalline (i.e., crystalline) or inter-crystalline (i.e., osmotic) swelling (Heim 1990; Laird 2006). Crystalline swelling occurs in layered clay minerals due to a particular cation exchange or the hydration of the interlayer-cations of the clay mineral (Ruedrich et al. 2011). Osmotic swelling is

attributed to the high negative surface charge of clay minerals, whereby pore water is soaked between the clay minerals by osmosis. The process of the inter-crystalline adsorption of the water, which pushes the clay minerals apart, is known as “osmotic swelling” (Gründer 1980; Madsen and Müller-Vonmoos 1989). The osmotic swelling pressure is much lower than that resulting from the crystalline swelling of the clay minerals (Heim 1990). The different processes leading to the swelling of clay minerals within the built environment is described in detail by Ruedrich et al. (2011).

The difference between the pressure within a water film between two surfaces and the pressure of the bulk water in the pore space of stones is seen as the disjoining pressure (Weinmann 2001). The adsorption of multi-molecular water layers on the mineral surface leads to the reduction of van der Waals energy thus leading to the repulsion of adjacent particles (Splittgerber 1976; Stockhausen 1981; Weinmann 2001). The disjoining pressure is dependent upon the pore radius (Stockhausen 1981).

In general, an increase of hygric swelling is observed in context with a decreasing average pore radius and an increasing microporosity within the stone as well as at ranges of 80 % RH (Ruedrich et al. 2011; Steiger et al. 2011).

The several aspects of hygric expansion – capillary condensation in micropores, disjoining pressure, the development of water surface films and the behavior of bulk water in the range of pore sizes of 0.001–0.1  $\mu\text{m}$ , etc. – are discussed as a matter of controversy (Ruedrich et al. 2011; Steiger et al. 2011).

The wetting-drying cycles of natural building stone introduce stress on the stone matrix and contribute to the weakening of it from the long-term perspective. In the presence of electrolytes, e.g., salts or air pollutants, moisture expansion is enhanced and assumed to lead to residual strain (Snethlage et al. 1995). The deterioration phenomena ascribed to the length changes upon changes of humidity and the impact of water include scaling, flaking, exfoliation, craquelé patterns, fissures, cracks, spalling and differential erosion along fabric discontinuities, e.g., delamination (Rodríguez-Navarro et al. 1997; Sebastián et al. 2008; Ruedrich et al. 2011).

In general, the different extrinsic factors, which provoke physical deterioration processes, are effective at the same time. As mentioned above, moisture expansion is enhanced by the presence of salts as is thermal dilatation (Winkler 1994; Snethlage and Wendler 1997). In the presence of moisture, deterioration through thermal changes is enhanced (Koch and Siegesmund 2004). Changes in frost weathering are discussed where salt electrolytes are involved (Ruedrich and Siegesmund 2006).

Physical deterioration results in the degradation of the stone matrix and mineral bounds, which lead to a loss in the mechanical strength of the stone. Furthermore, the comminution

of the stone's framework entails the enlargement of the reactive surface of the stone, i.e., the minerals liable to chemical weathering.

### 1.2.2 Chemical deterioration

In general, the impact of water, inorganic and organic acids as well as atmospheric gases ( $\text{CO}_2$  and  $\text{O}_2$ ) on rock-forming minerals is viewed as chemical weathering. Through the so called "carbonation weathering", minerals are structurally changed or else dissolved completely (Press and Siever 2003). In comparison to the carbonation weathering of rocks and soils through  $\text{CO}_2$  respectively,  $\text{HCO}_3^-$  diluted in water, the weathering within the built environment is accelerated by anthropogenic components. Through the combustion of fossil fuels, atmospheric gases such as  $\text{SO}_2$  and  $\text{NO}_x$  components are released and enriched in the atmosphere. These react with rain water or the moisture content within the stones and form aggressive acids, which strongly contribute to the chemical weathering. This so called "Rauchgasverwitterung" – or weathering due to the atmospheric acidity (Camuffo 1992) - displays a specific chemical attack in building stones in the form of hydrolysis (Herscovici 1910; Kaiser 1910; Luckat 1984; Kraus 1988). Proton sources are the anthropogenic caused atmospheric gases, such as  $\text{SO}_x$  and  $\text{NO}_x$ , forming acids (White 2003). The annual  $\text{H}^+$  input from sulfuric and nitric/nitrate oxides in Germany is about 3.5 Kg/ha (Pleßow et al. 1997). Furthermore, particulate matter plays an important role in chemical deterioration behavior. Their function as catalysts or reaction nuclei is described (Charola and Ware 2002). Schäfer (1980) ascertained a four to eight times higher oxidation of  $\text{SO}_2$  to  $\text{SO}_4$  in urban areas in comparison with rural environments. In all these processes, water functions as a reactant as well as a transport medium for solutes and particles (Schlabach 2000). The pore space of the stone offers access for the chemical deterioration to the stone's matrix and minerals. As mentioned before, when the pore space is enlarged through other weathering impacts, the reaction surface for chemical weathering increases.

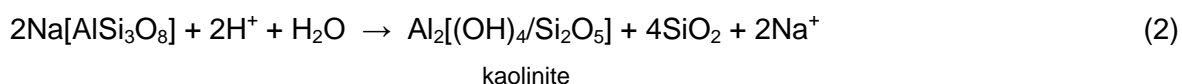
The different rock-forming minerals react differently to the weathering attack. Minerals containing iron, manganese or sulfur in lower oxidation states produce higher oxidation states of these through the oxygen of the water (Kraus 1988). Carbonate rocks, i.e., minerals such as calcite and dolomite, are prone to carbonation weathering as well as to "Rauchgasverwitterung", and generally dissolve. Silicate minerals are less likely to be affected by "Rauchgasverwitterung" (Kraus 1988). The effective acids of the atmospheric deposition are buffered by acidification and hydrolysis reactions of silicates which change the silicate structure (White 2003). The resistivity of the minerals against hydrolysis differs significantly. Olivine shows little resistance, while augite, hornblende, biotite and the various feldspars are more resistant, while muscovite and quartz are barely degrading (Fig. 1.2). Clay minerals are often formed as secondary products from the water containing silicon-oxide-relicts (Kraus 1988).

**Chemical weathering of carbonate rocks**

The weathering of carbonate rocks is so-called solution decomposition. Carbonate components i.e. calcite and dolomite, dissolve and are transported in their ionic form. Typical secondary reaction products are not formed, as it is with silicates (Colman and Dethier 1986). The solution of carbonate rocks in a  $\text{CaCO}_3 - \text{MgCO}_3$ -system is a stoichiometric solution (Wollast 1990). The presence of acidic components through the anthropogenic impact enhances the solution decomposition. Reaction (1) shows the dissolution of calcite within carbonic acid (Okrusch and Matthes 2009).

**Chemical weathering of silicate rocks**

Silicate minerals mainly weather by hydrolysis reactions that consume reactant species – i.e., primary minerals and protons. Weathering products are formed – i.e., solute species and secondary minerals (White 2003). The main representative of the rock-forming minerals of silicate rocks is the feldspar group. Feldspars deteriorate to water-bearing minerals (clay minerals), which may lead to textural impairments within the stone's structure (Press and Siever 2003). Reaction (2) shows the hydrolysis of albite (White 2003).



Silicate weathering is commonly viewed as a ligand exchange process with the metal ions bonded in the mineral structure (Loughnan 1969; White 2003).

Kaiser (1910a) reported the kaolinization of plagioclase in the matrix of Drachenfels trachyte by a hydrolysis reaction through the “Rauchgasverwitterung”. In the experiments conducted with a gas mixture of 10% vol.  $\text{SO}_2$ , 10% vol.  $\text{CO}_2$  und 80% vol. air, the formation of thenardite ( $\text{Na}_2\text{SO}_4$ ) and gypsum ( $\text{CaSO}_4 \cdot 2 \text{H}_2\text{O}$ ) was detected, indicating the release of sodium and calcium.


The experiments performed by Correns and von Engelhardt (1938) showed that the K-feldspar (adularia) does not dilute stoichiometrically. At the beginning, a higher potassium concentration rather than aluminum and silicon concentrations is detected. Potassium is released more easily from the outer zone of the mineral. This leads to the formation of a K-depleted “residual layer” on the surface of the adularia.

Chou and Wollast (1984) investigated the dissolution of albite in different pH. The detected concentrations of sodium, aluminum and silicon suggest the formation of a residual layer on the surface of the feldspar, enriched in Si and Al.

Efes and Lühr (1975) deduce the concentration decrease of  $\text{SiO}_2$ ,  $\text{CaO}$ ,  $\text{Na}_2\text{O}$  and  $\text{K}_2\text{O}$  to the dissolution for feldspars within the weathering horizons of the Drachenfels trachyte.

### Mineral weather resistivity

The weather resistivity of rock-forming minerals is crucial in assessing the weather resistivity of natural stone in the anthropogenic environment. Goldich (1938) observed that the weathering sequence for common igneous rocks in the field was the reverse of Bowen's reaction series, which ranked minerals in the order of crystallization from magma.

increasing weather resistivity											
											
Calcite	Olivine	Anorthite	Augite	Pyroxene	Amphibole	Albite	Biotite	Orthoclase	Muscovite	Clay minerals	Quartz

**Figure 1.2** Mineral weather resistivity (after Press and Siever 2003)

At the lower end of the scale of weather resistivity is calcite, which shows dissolution in chemical weathering. Olivine shows little resistance, followed by anorthite and then Ca-plagioclase. Weather resistivity increases with augite, pyroxene, hornblende, albite – the Na-plagioclase – and biotite. The most weather resistant of the feldspars is the K-feldspar orthoclase. Muscovite and quartz are barely degrading (Fig. 1.2). For clay minerals, the scale of weather resistivity is not to define, since all conversion reactions are reversible. Clay mineral weathering takes place as a  $\text{Me}^+ - \text{H}^+$  exchange towards montmorillonite and, if leaching is extensive, to kaolinite (Loughnan 1969, Snethlage 1984)

### Solute composition, fluid flux, and secondary reaction products

In natural weathering, hydrolyses and other chemical reactions take place. These are mainly complexing or chelating reactions, especially in the presence of organics (White 2003). As mentioned earlier, weathering is influenced by intrinsic and extrinsic factors. In terms of mineral weathering rates, the solute composition has the most direct impact (White 2003). Chemical weathering is ultimately dependent upon the concentration of reactants complexing and detaching the oxygen-bonded metal species from the silicate structure (Casey and Ludwig 1995). Principally, these are hydrogen ions, but complexing agents such as organic

anions can also participate in these processes. In contrast, some solute species, such as aluminum and sodium ions, inhibit experimental weathering rates by interfering and competing with the ligand exchange processes (Oelkers and Schott 1995; Stillings et al. 1996).

Within the pore space of natural building stones, weathering rates are controlled by the mechanisms of moisture transport. For structurally complex minerals undergoing incongruent or stepwise weathering in the natural environment, the relative rates become highly dependent upon specific reaction pathways (White 2003). White et al. (2001) have coupled the weathering rates of granite with the development of secondary permeability. At an initial state of the weathering of fresh granite, the weathering rate of plagioclases is mainly controlled by the low permeability; thus only a little water is transported, which constraints the fluid flux. Thus, the mass of feldspar that can be dissolved is restricted before thermodynamic equilibrium. Under such conditions, weathering is limited by the availability of water and not by the kinetic rate of feldspar weathering. Over time, this transport-limited weathering will lead to a mass loss from the granite with increasing porosity. White (2003) estimates a porosity increase of ~ 50% due to the conversion of plagioclase into kaolinite. The increase of porosity produces higher pore-water flow – i.e., fluid fluxes – which accelerates saturation-limited weathering – “this coupled feedback accelerates plagioclase weathering, which gradually shifts from a transport limited to a kinetic limited reaction” (White 2003, 157). The increasing porosity might be impaired by a certain decrease of permeability due to secondary mineral formation. The rate of K-feldspar weathering shows a comparable transition from transport to kinetic control, but at significant higher flux ratios due to its lower solubility rather than slightly slower reaction kinetics. Concurrent plagioclase dissolution enhances this effect by producing solutes, principally silicon, which further suppress K-feldspar dissolution by increasing the saturation state (White 2003).

Surface reactivity may also be decreased by secondary coatings, i.e., the occlusion by secondary clays and iron and aluminum oxides, the formation of depleted leached layers and the adsorption of organic compounds (Banfield and Barker 1994; Nugent et al. 1998).

In general, clay minerals are the secondary reaction products of feldspar weathering. Very often, mixed-layer minerals are formed with layered structures of illite and montmorillonite with transition to pure swellable montmorillonite (Okrusch and Matthes 2009).

### **1.2.3 Biological deterioration**

Although the impact of biological weathering is not investigated in this study, some general aspects of the influence of microorganisms need to be discussed. In general, the presence of microorganisms – such as algae, lichen, bacteria, and fungi – indicates higher humidity, which may enhance deterioration processes (Wihr 1986). Biological deterioration of microorganisms can be divided into biophysical and biochemical deterioration processes



(Adamo and Violante 2000; Dornieden and Gorbushina 2000; Pinna and Salvadori 2000; Wierzbos and Ascaso 1998). The extent of biological weathering is dependent on qualitative and quantitative distribution of microorganisms and their metabolic products. The different natural building stones constitute various substrates and provide different living conditions for the organisms (Knöfel 1979).

The colonization of microorganisms results in the formation of alteration patinas on stone surfaces, e.g., on marble mainly consisting of calcium oxalate layers (Jones and Wilson 1985), which are linked to biological weathering (Krumbein 1988; Warscheid et al. 1990). Microorganisms produce organic acids, which may function as acids as well as chelating agents (Jones et al. 2000). Besides the acidic solution of minerals, organic acids form metal organic complexes with cations dissolved from the crystal grid of the minerals. Due to these stable complexes, the metal ions remain diluted, whereas as ions they precipitate (Press and Siever 2003). This aspect may enhance the feldspar hydrolytic weathering of silicate rock in general.

Another aspect of biological weathering is colonization with lithotrophic bacteria and fungi. These microorganisms oxidize inorganic substances (Fuchs 2006; Winkler 1975) and may directly support the formation of calcium sulfate dihydrate (Zappia et al. 1998). Out of the lithotrophic bacteria, nitrifying bacteria oxidize nitrous gases ( $\text{NO}_x$ -components) to nitric acid, which again contributes to the deterioration of the stone material (Fuchs 2006). Sulfoxidant organisms are very often connected to crust formation and stone decay (Frediani et al. 1976; Barcellona-Vero and Montesila 1978).

Pohl and Schneider 2005 mention a possible protecting effect of biofilms on carbonate rocks, which in some cases can also be linked to a preservation function on silicate rocks.

These are only a few aspects of biological weathering or the influence of microorganisms. However, the above points clearly indicate the contribution of biological colonization to the deterioration of stone monuments and reveal the broadness and complexity of this topic, which needs further discussion.

### **1.3 The impact of air pollution on stone decay**

The effect of air pollution on stone decay has been a subject in the field of stone deterioration for a long time (Kaiser 1910; Grün 1931; Kieslinger 1932; Winkler 1970; Luckat 1973b, 1984; listed in Charola and Ware 2002). The increasing pollution emission of our industrial society has considerably accelerated the process of weathering of building materials (for discussion see Siegesmund and Snethlage 2011). Generally, the assumption has been that acid-forming sulfur compounds penetrate into the microstructure of the stone and then become neutralized depending upon the rocks' composition. These become concentrated as sulfate-rich salts (especially gypsum enrichment) and are responsible for the many damages

observable (e.g. Knetsch 1952, Kraus 1985a, Kraus 1985b, Kraus and Jasmund 1981). The main pollution-related deterioration processes are gypsum formation and carbonate dissolution (Sabbioni 2003). Most debated is the crust weathering of limestone as a result of the transformation of calcium carbonate into calcium sulfate, due to the impact of air pollutant concentration in the atmosphere and the deposition of anthropogenic sulfur (Henley 1967; Sabbioni 2003). Although SO<sub>2</sub> concentrations have decreased over the last decades, degradation in connection with weathering crusts is still observed. Acid rain, as a result of the contamination of rain water with sulfur, nitrogen oxides and carbon oxides, affects stone material and corrodes rock-forming minerals (Martinez and Martinez 1991). Pollution has changed into a complex multi-pollutant situation with increasing particulate matter, enhancing the acidic impact in terms of dust deposition (Wolff 1986; Charola and Ware 2002; Brimblecombe 2003). The weathering crusts mainly consist of newly formed minerals, e.g., gypsum, with atmospheric particles embedded within. These can be grouped as porous carbonaceous particles (soot), smooth aluminosilicate particles, and metal particles mainly composed of iron (Del Monte et al. 1981; Esbert et al. 1996; Derbez and Lefèvre 1996). These atmospheric particles derive from different sources: fuel oil combustion of domestic heating and power plants, coal combustion and gas oil emission (Sabbioni 1995). Vehicle exhaust (Rodriguez-Navarro and Sebastian 1996) and biomass combustion (Ausset et al. 1992) were also identified as sources.

#### **1.4 Stone deterioration at the Cologne cathedral**

Cologne cathedral is one of the most important cultural monuments of northern Europe and faces severe stone deterioration. The different building stones of the cathedral show a large variety of weathering phenomena. The Drachenfels trachyte, which was the building material of the medieval construction period, shows significant structural deterioration as well as massive formation of gypsum crusts. Cologne is a major city with approximately one million inhabitants. Urban mobile pollution sources, such as automobiles, trucks, railway etc., are the main contributors of air pollution in the city today. Although the emission levels have dropped in the last 30 years, dust pollution is still a major problem. The observed values of air pollution can be correlated with the increased number of chronic respiratory diseases (Wolf 2002). Török et al. (2011) investigated a series of samples from the Cologne cathedral which were collected at about 30 m above the ground from the external walls. Very high concentrations of lead (736 ppm) could be detected in dust samples collected from different areas. The lead also accumulates in the black crust, especially close to the limestone crust interface. This indicates that either the crust exhibits signals of past pollution levels or lead is being mobilized from the surface to deeper zones. Even though the SO<sub>2</sub> content decreased

in the atmosphere, the situation in many industrial countries can be characterized as a “multi-pollutant” setting ( $\text{CO}_2$ ,  $\text{NO}_x$ , VOC (volatile organic compounds), dust, etc.).

The formation of black weathering crusts on different building stones can be seen as a function of pollution impact. The building stones at Cologne cathedral show severe deterioration phenomena, especially the Drachenfels trachyte (Graue et al. 2011). Thin laminar and black framboidal crusts, which incorporate particles from the pollution fluxes, cover the building stones. Weathering crusts also form on the silicate stone and contribute to the degradation of the historic building material. On the Drachenfels trachyte, the crust formation is strongly correlated to the disintegration of the stone. Gypsum is not only found within the crusts but also in deeper zones of disintegrated stone material. The crusts tend to detach, and further structural deterioration follows. Contour scaling, flaking and exfoliation are characteristic decay features on the Drachenfels trachyte, leading to granular disintegration and crumbling. On the Obernkirchen sandstone and on the Stenzelberg latite, weathering crusts form in very thin scales, 2–3 mm thick, which tend to detach from the stone. The Schlaitdorf sandstone shows thick black weathering crusts, which are frequently accompanied by severe contour scaling several centimeters thick, as well as pronounced granular disintegration. On the Krenshiem Muschelkalk, the crusts seem to temporarily stabilize the stone surface (see Siegesmund et al. 2007). On surfaces exposed to rain, solution phenomena can be observed, e.g., microkarst (Graue et al. 2011).

Since 1820, when the construction work and first repair work resumed, the building stones of the Cologne cathedral and their deterioration behavior have been the subject of scientific scrutiny. Starting with the observation of an ongoing decay of the building's structure, the aim of these investigations has always been the search for suitable replacement stone material.

Since the middle of the 19<sup>th</sup> century, a number of investigations for suitable building materials for the Cologne cathedral existed. Von Lasaulx (1882) broached the subject of weathering resistance in the implementation of building stones. During the period under the supervision of master builder Hertel (1903 - 1927), a first systematic survey of the deterioration behavior of the building stones of the Cologne cathedral took place (Hertel 1927). Besides the works of Kaiser (1910; 1910a; 1910b), Hirschwald (1910; 1912) was substantially involved in the development of constructional investigations and the analyses of building stones. He also laid the foundation for geoscientific analyses in the preservation of cultural monuments.

Grün (1931; 1933) showed that the condition of the different building stones at the Cologne cathedral varied widely (Grün 1931; 1933; Rathgen and Koch 1934). The mortars used were considered as a potential source for the deterioration and Grün (1931) explicitly addressed the environmental influences as deterioration factors.

Beginning with Knetsch (1952) emphasis was placed on the geological and climatic context. The influence of air pollutants and especially of flue gas on the deterioration of natural

building stones was detected in a program in the 1970's and potential preventive conservation treatments were tested (Luckat 1973a; 1974; 1975; 1977; 1984; Wolff and Luckat 1973; Wolff 1986; Mirwald et al. 1988). Efes and Lühr (1976) accentuated the influence of environmental pollutants as a significant factor for the stone decay. Further studies dealt with the different deterioration processes in several natural building stones from the Cologne cathedral (Kraus 1980; 1985; 1985a; Kraus and Jasmund 1981; Mirwald et al. 1987; Knacke-Loy 1988; 1989).

### **1.5 Interferences of adjacent stones**

Kraus (1985a, b) and von Plehwe-Leisen et al. (2007) describe the negative interferences between the original building stone, the Drachenfels trachyte and the Krensheim Muschelkalk at Cologne cathedral. Stronger flaking and exfoliation are observed on the Drachenfels trachyte ashlar placed next to carbonate stone. Wolff (1992) reported on the negative interferences between the Schlaitdorf sandstone and Londorf basalt lava, which mainly deteriorates the sandstone and, with it, the neo-gothic building structure. These interactions of the different construction materials (stones and mortars) need to be investigated in terms of chemical and physical interferences in the context with specific building physical situations, climate and environmental conditions. The insights gained need to be considered in terms of assessments for preservation strategies (Garrecht 2005). They will contribute to the compilation of requirements for replacement stones.

### **1.6 Cultural heritage preservation needs for adequate replacement stones**

The observations of severe stone deterioration as a function of pollution impact and the negative interferences between different natural building stones imply the question for heritage preservation and conservation needs. Besides conservation measures, the replacement of severely degraded building stones is important for the static safety of buildings. The selection of an appropriate replacement material is a crucial decision. The observed negative interactions of the Schlaitdorf sandstone and the Londorf basalt lava, as well as the Drachenfels trachyte and the Krensheim Muschelkalk, raise the question again as to which stone material with comparable mineralogical, physical and technical properties is suitable as a replacement material for the different stones used at Cologne cathedral. The preservation of the Cologne cathedral is determined by the appropriate choice of a replacement stone as well as the development of conservation treatments and materials. Potential solutions were drawn for the conservation of the Drachenfels trachyte (Dombauhütte Köln 2006; von Plehwe-Leisen et al. 2007). Until now, the discussion about the preservation and conservation of the stone materials used for the Cologne cathedral remains in progress.

### **1.7 History of the selection of replacement stones for the Drachenfels trachyte**

The regularly recurring search for a compatible replacement material at Cologne cathedral reveals the basic problem, namely that the question of stone procurement and preservation could not be solved, or if so then only temporarily. Since 1846, Schlaitdorf sandstone has been used. This stone was favored due to its good weathering resistivity, as observed Ulm minster and in Southern Germany. After a short period, this sandstone showed severe damage in Cologne cathedral. This indicates that the different climate and environment determine the deterioration behavior of the stone. In the climatic and environmental conditions of the industrialized area of Cologne, the sandstone showed severe damage very early on. Thus, it was no longer used and instead Obernkirchen sandstone was implemented from the 1890s onwards (Scheuren 2004; Schumacher 2004).

Between 1918 and 1940, Krenshiem Muschelkalk was *en vogue*; thus, it was used for Cologne cathedral. After WWII, the extremely weather-resistant Londorf basalt lava was solely used. This gray stone resembled well the dark weathered surface of the Drachenfels trachyte and the other stones in the Cologne cathedral. Since the 1980s, the goal was to use replacement materials, which are the main constituent of the respective building sections. The procurement faced severe, and partly insurmountable, difficulties. Currently, the search for replacement stones focuses on stones which are similar in their optical properties but which do not show the disadvantages of the original stone. Since 2001, Bozanov sandstone from the Czech Republic has been used for renovation work within the sandstones. Since 2005, a trachyte from Italy, the Montemerlo trachyte, replaces the severely deteriorated Drachenfels trachyte (Scheuren 2004; Schumacher 2004).

In the beginning, the choice of a replacement material was determined by economic aspects and optical properties. Since the middle of the 19<sup>th</sup> century, when the aspect of “weather resistivity” found its way into the search, stones that were expected to be highly weather resistant were focused upon. Nowadays, the selection mainly ensues based upon mineralogical and petrophysical comparability, as well as upon geologically allied formations and optical similarity (Schumacher 2004). A high accordance is objected to only with the stone this replaced. Possible negative interferences of the newly inserted material with other stones used in the building section in question are not considered so far.

### **1.8 Requirements for replacement stones**

The preservation at Cologne cathedral is determined through the selection of an adequate replacement stone as well as upon the development of conservation measures. The project for the “conservation of the medieval Drachenfels trachyte”, from 2004 until 2006, showed new solution processes. In terms of stone exchange, the first choice for a replacement stone

would be the original stone material. This option is significantly restricted by the fact that the historic stones are not always available, as is the case for the Drachenfels trachyte.

In the 19<sup>th</sup> century, economic aspects have been the determining factor for the selection of replacement stones. In the 20<sup>th</sup> century, optical properties and weather resistivity became more important. Nowadays, the selection of a replacement stones is more differentiated and the requirements are described in more detail. Intrinsic (mineralogical composition, textural features, and petrophysical properties) and extrinsic material parameters are distinguished. So far, these parameters are regarded in terms of the original stone as a basis, i.e., in the replacement material, these parameters are adjusted only to the material which ought to be replaced. In the literature, guidelines can be found indicating the boundary values of the single parameters (i.e., mineral composition, porosity, water absorption and saturation, drying characteristics, moisture and thermal dilatation, strength properties, etc.) (Snethlage 2005). Optical and mineralogical criteria as well as petrophysical properties are also important. Besides these general criteria for replacement stones, it is substantial to ascertain which stones are available in a sufficiently large amount and in constant quality over longer periods of time. The just mentioned general criteria only refer to the one original stone, which ought to be replaced. In many historic buildings, a number of different stones are used, as is the case at Cologne cathedral. In this instance, it is essential that a replacement stone is not only comparable with the original stone - which is replaced – but is compatible with all other stones used in the masonry bond.

At Cologne cathedral, the different building stones used show a diverse petrography and mineralogical composition as well as a broad variety of petrophysical properties. The comparison with valid guidelines reveals the broad spectrum of the materials used. The strong divergence of the ascertained parameters of the stones shows that the constraints for a replacement material make it almost impossible to find an ideal stone. It is important to evaluate the parameter and to determine those which specifically characterize the stone. At this point, the specific petrophysical properties as well as the typical deterioration behavior have to be included.

## 2 The cathedrals – construction history of the Cologne, Xanten and Altenberg cathedrals

This study concerns both the utilization and deterioration of natural building stone employed in the construction of Cologne cathedral. Built during the middle ages at the same time as the Cologne cathedral, the cathedrals at Xanten and Altenberg reveal the use of comparative natural building stone not only at the time of their original construction but also during later building and restoration/conservation work. The following text considers correlations between these cathedrals and examines the stone used and the building histories, i.e. construction, reconstruction and repair work, for all three cathedrals.



**Figure 2.1** South elevation of the Cologne cathedral

Cologne cathedral (Fig. 2.1) represents the archdiocese of Cologne. Its present day form stems from 1248 following the demolition and burning of parts of the original cathedral.



Already in 1164 there was a pressing need for the building of a new cathedral due to the donation of the relics of the Holy Three Kings combined with an increase to the number of pilgrims (Schock-Werner et al. 2011). The new building work was commenced in 1248 under the authority of the first master cathedral builder and mason "Meister Gerhard" (Wolff 2005), the building's principal and the financier comprised the cathedral chapter (Beuckers 2005). The laying of the foundation stone by Archbishop Konrad von Hochstaden took place on the fifteenth of August of that year.



**Figure 2.2** Xanten cathedral from the South East (Schubert, Dombauhütte Xanten).

Xanten cathedral (Fig. 2.2), which in 1263 succeeded various Carolingian and Ottoman-Roman predecessors, is the gothic ecclesiastical building of the canonical foundations in Xanten that prevailed in the eighth century (Bader 1964). Having been begun by "Meister Jakobus" and with contributions from 1396 to circa 1406 by a "Meister Gerhard" of Cologne (Hilger 1995), the cathedral was finally completed after a three hundred year construction period in the sixteenth century (Bader 1949). The new gothic style, employed in the building of the Cologne cathedral, encountered in many other churches and cathedrals at that time with their five delineated spaces and column figures in the main choir, acted as a model for the building of the Xanten cathedral (Bader 1949). The gothic construction integrated the grand west front, which had only been built fifty years previously in the Staufer era. Though the architectural arrangements of Xanten cathedral's southern portal exhibit a late gothic interpretation of Cologne cathedral's "Petersportal", the chancel area in particular demonstrates distant architectural fundamentals (Hilger 1995). The financing of the collegiate



church was sourced through the assets of the chapter of canon and from the sale of letters of indulgence (Bader 1964). The laying of the foundation stone by Friedrich von Hochstaden, the provost of the Xanten canonical establishment, occurred in 1263.



**Figure 2.3** Altenberg cathedral, as seen from the East. (©Heidemarie Wolf, Odenthal)

Begun a mere eleven years after the commencement of building work to the cathedral in Cologne, Altenberg cathedral (Fig. 2.3) is a Cistercian church that had financial contributions from the von Berg counts. Undoubtedly, this was a situation very agreeable for both parties. Through participation in the expansion of the cloister the noble sponsor could consolidate a territorial and political sphere of influence and profit from an increase in agronomic authority. Also the cloister embodies a suitable site for the interment for the representative of the sovereign powers. In turn the cloister enjoys protection as well as the security provided by the rich proceeds resulting from generous donations and profits generated through use of the cloister. The Altenberg cathedral's master builder, having been employed at the Cologne building site, must have been extremely familiar with Cologne cathedral's construction. The blueprints of the Cologne cathedral chancel as a basis for the chancel area at Altenberg were improved by reference to older differing calculations from Amiens and Beauvais. (Lepsky and Nußbaum 2005; Heydasch-Lehmann et al. 2008)

The proximity in time between the start of the specific building projects of the three houses of god is remarkable. They reflect the enormous building activity of the twelfth and thirteenth centuries in the Rhine-Maas-region (Beukers 2005). Autonomous building projects were the result of the individual architectural arrangements, the different specific used formats of

natural stone ashlars at the three sites and the distinct building organizations as well as the specific standalone building consortiums comprising the Cathedral Chapter, Chapter of canon or Noble sponsorship (Graue et al. 2013b).

Drachenfels trachyte was the singular building material employed at all three sites during the construction phase of the Middle Ages. This natural building stone had been popular since Roman times due to its balanced degree of strength, which would expect a good workability verses and a relative adequate resistance to weathering (Berres 1996; Scheuren 2004).

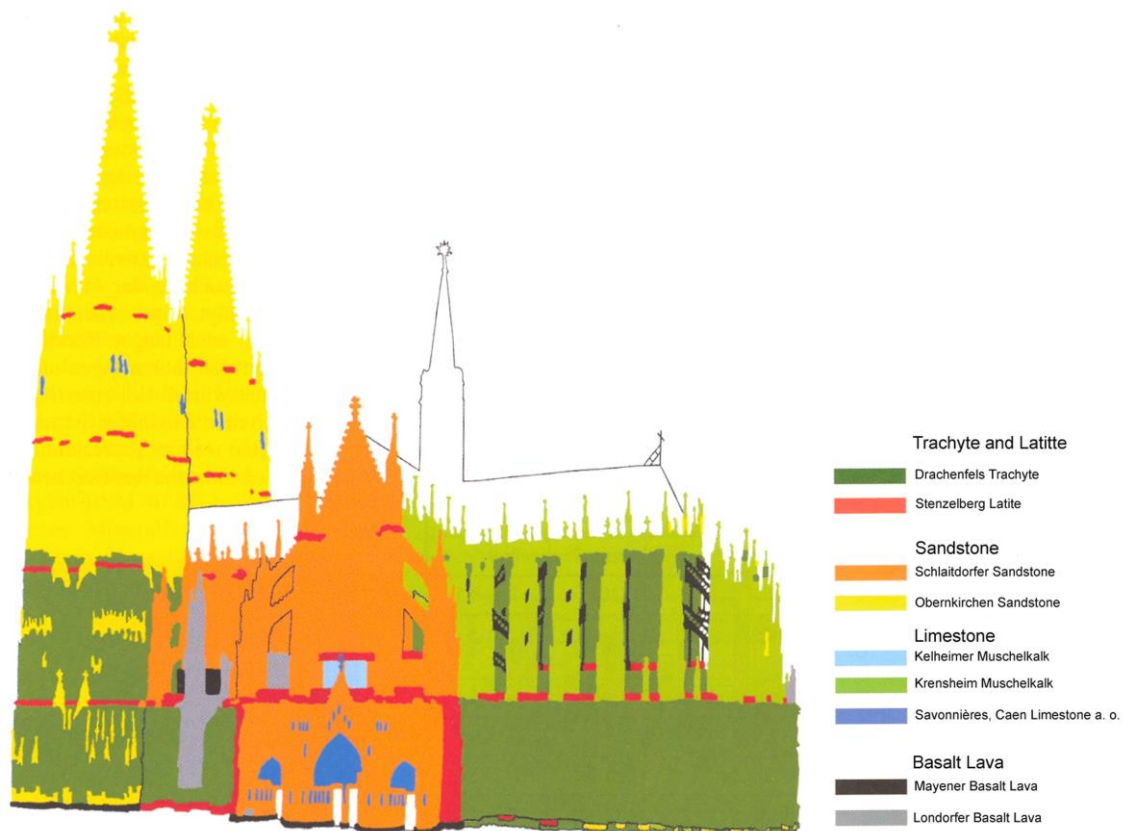


**Figure 2.4** Lithological map of the south elevation of the Cologne cathedral (Windscheid (2004) after Wolff and Luckat 1973)

The construction of the Cologne cathedral began in 1248. The medieval part of the cathedral was built of Drachenfels trachyte from the nearby quarry at the Siebengebirge. The construction was halted at the beginning of the sixteenth century and then recommenced during the nineteenth at which time Drachenfels trachyte was no longer available. At the beginning of the nineteenth century efforts to obtain Drachenfels trachyte reached a conclusion in 1829 with the expropriation proceedings by the Prussian king Friedrich Wilhelm the third. As a reason was quoted the danger posed from uncontrolled rockslides. A much more important inducement would have been the desire to protect the middle age ruins at the Drachenfels, and the victory monument from 1814 commemorating the end of Napoleon's reign, and also because Drachenfels had by this time become a tourist attraction of

international renown. This prohibition of further stone mining can be seen as one of the first measures of monument and landscape protection (Berres 1996 ; Scheuren 2004).

In the 1820ies, when first repair works started and the construction of the cathedral resumed, local stone available from the Siebengebirge was the primary choice as a replacement material. Initial renovations were conducted using latite obtained from the “Stenzelberg” and a few supplementary materials from the quarries of the Siebengebirge. After a short period it was apparent, that the Stenzelberg latite was a very time intensive and therefore cost consuming building material and that other stones from the quarries at the Siebengebirge were of minor quality (Schumacher 2004).

**Table 2.1** Main construction phases and used building material at the Cologne, Xanten and Altenberg cathedrals.

CONSTRUCTION PHASE	BUILDING STONES
<b>Cologne cathedral</b>	
First construction phase 1248 – 1520/30	<b>Drachenfels trachyte,</b> Weiben tuff
Resumption of the work, first repair works 1820-30	Wolkenburg latite <b>Stenzelberg latite,</b> Heilbronn sandstone
Second construction phase >sandstone-period< 1842 – 1860	<b>Schlaitdorf sandstone</b>
since 1864	<b>Obernkirchen sandstone</b>
Restoration works I >limestone period < 1903 – 1945	<b>Krensheim Muschelkalk</b> (1918 – 1940) Caen, Savonnières
Restoration works II since 1952 since 2001 since 2005	<b>Londorf basalt lava</b> <b>Bozanov sandstone</b> <b>Montemerlo trachyte</b>
<b>Xanten cathedral</b>	
First construction phase 1263 – 1529	<b>Drachenfels trachyte,</b> Eifel-tuff
First reconstruction phase 1857 – 68	Weiben tuff, Udelfangen sandstone
Second reconstruction phase 1947 – 1966	Baumbergen sandstone, basalt, several limestone, <b>Krensheim Muschelkalk</b>
<b>Altenberg cathedral</b>	
First construction phase 1259 – 1400	<b>Drachenfels trachyte,</b> tuff, graywacke
First reconstruction phase 1815 – 1847	graywacke, Eifel-tuff, Eifel basalt lava
Second reconstruction phase 1894 – 1915	graywacke, several sandstone, basalt lava, tuff, <b>Stenzelberg latite, Krensheim Muschelkalk</b>
Restoration works 1995 – 2006	<b>Krensheim Muschelkalk</b>

In the middle of the 19<sup>th</sup> century the second construction phase used sandstone from “Schlaitdorf” in southern Germany. Later with the establishment of the railway connection linking Cologne and Minden, it was possible to transport the “Obernkirchen” sandstone from Lower Saxony. The so called third construction phase, comprising restoration works, started in 1903 and lasted until WWII, during which time the “Krensheim Muschelkalk” was the

typical stone utilized. In the 1950's, the decay resistant basalt lava from "Londorf" was used. At the present time, the trachyte from "Montemerlo" in Italy is being used to replace the deteriorated Drachenfels trachyte and a sandstone from "Bozanov" in the Czech Republic for the weathered Schlaitdorf sandstone (Fig. 2.4; Tab. 2.1) (Scheuren 2004; Schumacher 2004).

### 3 The cathedrals' environments

#### 3.1 Industrial, urban and rural environment

The three buildings are located in very different environmental settings (Fig. 3.1). Cologne cathedral (53 m above *NN*) is located in a metropolitan center with one million inhabitants next to the river Rhine. Xanten cathedral (22 m above *NN*) is the Catholic church of a small city on the Lower Rhine with 18,000 inhabitants and with smaller industrial effects (Arnhem, NL), while Altenberg cathedral (149 m above *NN*) is situated in a greenfield setting surrounded by forested mountains in the “Bergisches Land”.



**Figure 3.1** The cathedrals and their environmental settings: a. Cologne, b. Xanten, c. Altenberg.

Middle Europe, belonging to the mid-latitudes, has a damp, cool temperate climate. The western German climate shows a maritime influence due to its geographical proximity to the North Sea and the Atlantic, and therefore the Gulf Stream has an impact through the West Wind Drift (Lauer and Bendix 2004). This geographic position provides mild winters and moderate summers. Temperature, relative humidity, and rainfall differ only a little at the three locations (Tab. 3.1). The mean annual temperature is 11.4°C in Cologne, 10.6°C in Xanten and 7.1°C in Altenberg. The warmest months are July and August; the coldest months are January and December, with temperatures around –10 to +30°C and relative humidity ranging between 65 and 95%. The relative humidity shows highest annual values of 90–95% in winter (November to February) and lowest annual values for April to August from 65 to 75% (Tab. 3.1).

**Tab. 3.1:** Climate and annual mean concentration of air pollutants for Cologne, Xanten and Altenberg, 1987-2012 (data compilation from LANUV 2010, WMO-UN 2012)

Parameter	Cologne	Xanten	Altenberg
Mean annual temperature	11.4 °C	10.6 °C	7.1 °C
Mean daily temperature (min. /max.)	-10.8 /29.9 °C	-14.6 /29.0 °C	-17.3 /27.4
Annual precipitation	520-850 mm	490-890 mm	920-1690 mm
Warmest/ coldest month	July /Jan	July /Dec	July /Dec



The buildings are exposed to ubiquitous air pollutants of anthropogenic origin. These are mainly gaseous pollutants like  $\text{SO}_2$  and  $\text{NO}_x$ . Concentrations of both of these have decreased over the last decades, causing an increase in precipitation pH (Fig. 3.2). The effect of particulate matter in the form of settling dust shows continuously steady values.  $\text{SO}_2$  shows highest annual values in the winter months (December to March) and lowest annual values in August.

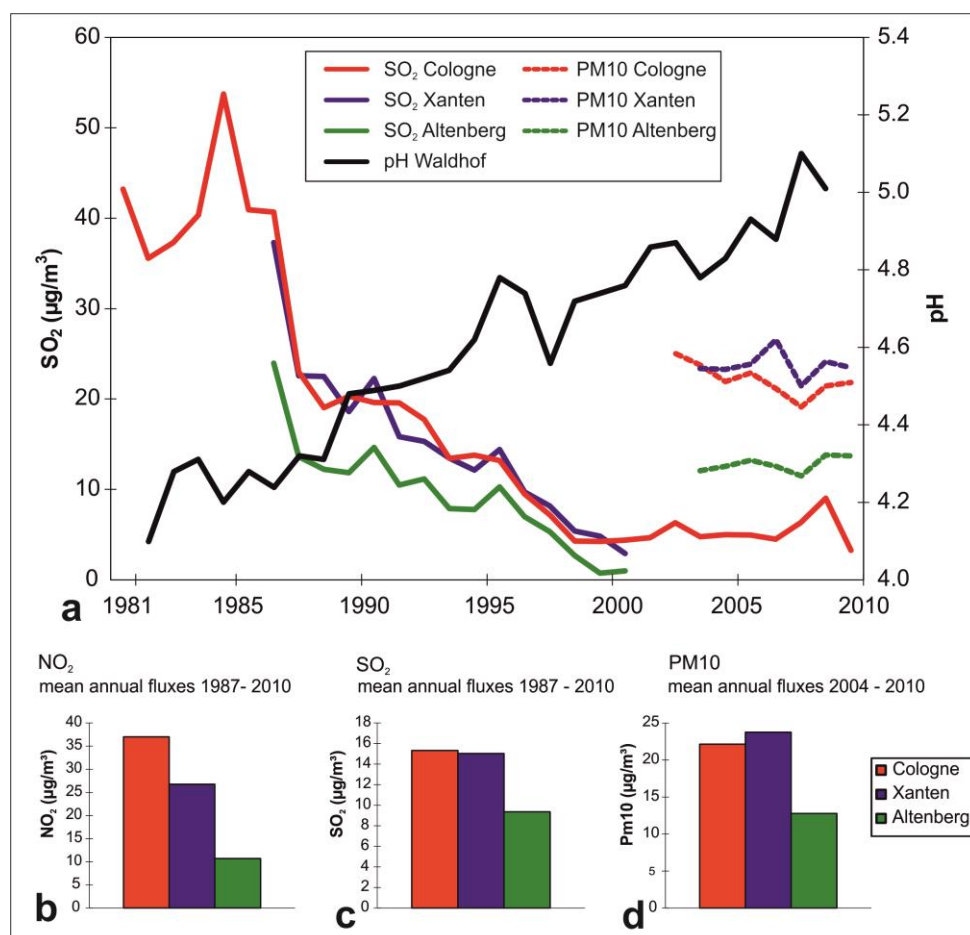


**Figure 3.2** (a)  $\text{SO}_2$  and PM10 fluxes of industrial (Cologne), urban (Xanten) and rural (Altenberg) locations versus pH precipitation (Waldhof), 1981–2010 (mean annual fluxes) (LANUV 2010; UBA 2011); (b-d) Mean annual fluxes from industrial, urban and rural environment: (b)  $\text{NO}_2$  from 1987 to 2010; (c)  $\text{SO}_2$  from 1987 to 2010; (d) PM10 from 2004 to 2010. Data are based on measuring stations from LANUV (Landesamt für Umwelt, Natur und Verbraucherschutz Nordrhein-Westfalen). For Cologne the data were acquired from the LANUV station in Cologne-Rodenkirchen at a distance of 6 km from the cathedral. For Xanten local data were available from the LANUV station in Wesel at about 13 km distance from Xanten cathedral on the other side (east bank) of the river Rhine. For Altenberg the data of several LANUV stations were compared and the data of Netphen in the Rothaargebirge (70 km east from Altenberg, also in a rural hilly and forested region) showed similar values.

Data for the  $\text{SO}_2$ -fluxes show a strong decrease over the past 30 years, with a similar impact for Cologne and Xanten and a lower influence in Altenberg. The particulate matter (PM10) has been monitored since 2003/2004 and shows the highest values for Xanten and the lowest for Altenberg. The relatively high values for Xanten in comparison to Cologne may be explained by a certain pollution impact from the bigger city of Arnhem, NL, from which

pollution fluxes are transported with west winds. Altenberg is also subject to west winds and therefore to a certain impact by the pollution fluxes of the industrial area of Cologne, Leverkusen and Düsseldorf. In general, the comparably low values for Altenberg reflect the arborous, rural surrounding area. The Cologne cathedral is located in the city center next to the main railway station, which has served as an active traffic interchange since the industrial era. Within the city of Cologne there are four power plants, and 15 kilometers south-west of Cologne is a larger coal-fired power plant.

### **3.2 Material temperature and moisture balance in the building stones**

Apart from the assessment of the environmental situations, further data relevant to building climate will be acquired. Long-term measurements of temperature and humidity inside the different building stones at Cologne cathedral are conducted. Varying gradients of moisture content are detected within the different natural building stones *in situ*. Correlations of the material depth, the outdoor climate, and the exposition of the stone are obtained for the individual natural stones. The influence of exposition (the cardinal direction, the height, and the architectural structure of the building section in question) on the near-surface will be ascertained, as well as the building climate. Data on the moisture distribution and temperature within the stones will be collated with observed decay phenomena to help explain interactions of moisture, temperature, and deterioration processes. The impact of climate situation on the deterioration of the stones, and on possible interferences of the stones with each other, will also be discussed.

#### **3.2.1 Material and methods**

A number of publications discuss potential methods for measuring moisture in capillary-porous materials in building construction (Altmann 1970; Vos 1970; Kaspar 1978; Berliner 1980; Neue 1986; WTA 1992; Arendt 1993; Fischer 1993; Rachow-Seemann et al. 1995; Weber 1995; Kupfer 1997; Leschnik 1999; WTA 2004). The constraints within the planned measurements – easy handling, low cost, long-term and outdoor measurements of physically bound water in historical building stones *in situ* – determined the choice of the measuring method with capacitive sensors. The measurements should run over a long period of time and not be too labor-intensive. The sensors must be outdoor-proofed and of small size, since they are to be placed inside historical stones. Deterioration processes in natural building stones are water-driven. Thus, it is the measurement of physically bound water content that is of interest, rather than that of chemically bound water (WTA 2004).

The capacitive method in this case delivers data of relative humidity (RH) from a hollow space within the pore space of the natural building stone. The measured values for temperature and RH are the parameters of the air in the porous system, which is in

equilibrium with the moisture content of the natural building stone. This is not necessarily the same humidity as at the same time and temperature in smaller pores of the stone, but relative measurements are achievable (Weber 1995). Regarding the hysteresis of the sorption isotherms (curve of the correlation of material moisture to the humidity of the air) the moisture content of the material can be deduced from the RH (Fischer 1993). These have to be calibrated with complementary laboratory testing. Further, the presence of electrolytes in the material has to be considered, because the attuned humidity equilibrium very much depends on the concentration of hygroscopic salts (Fischer 1993).

At Cologne cathedral temperature and relative humidity were measured within four different building stones (Drachenfels trachyte, Obernkirchen and Schlaitdorf sandstone, Krensheim Muschelkalk) in four monitoring fields at similar height and facing the four cardinal directions (Fig. 3.3).

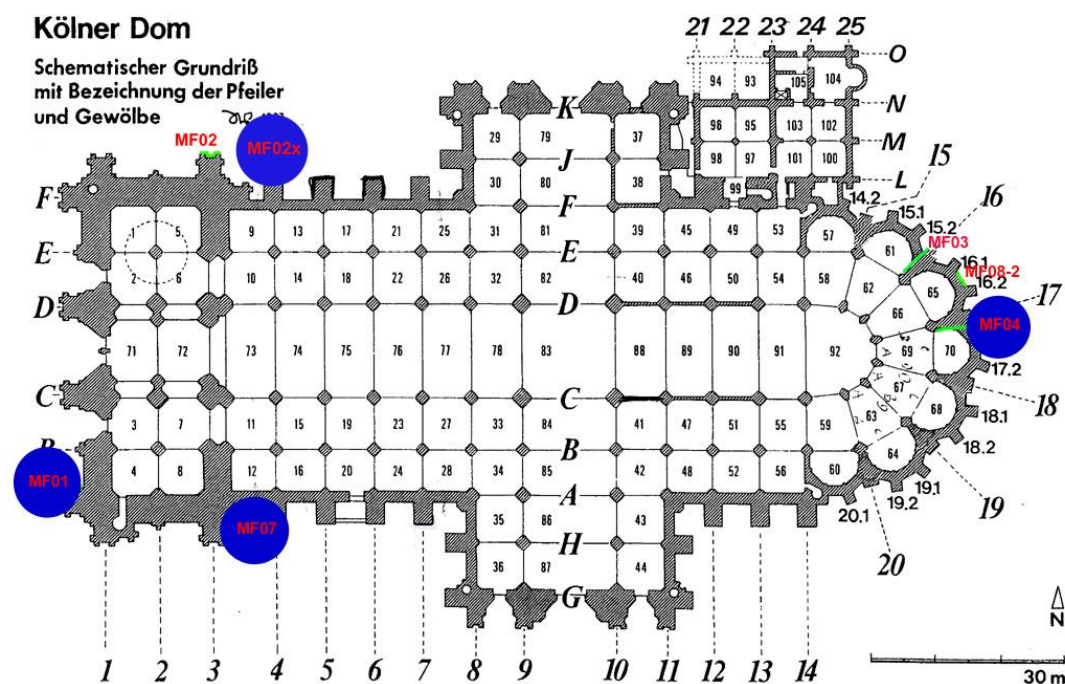


**Figure 3.3** Monitoring fields at Cologne cathedral (marked in blue).

Temperature and RH were measured in the stones at different depths and at different distances to the adjacent stones or joints. Capacitive sensors of diameter 8 mm were placed in appropriately sized drill holes (see Weber 1995). Temperature and RH were taken within these spaces in the stones, sealed from the outside with silicon. Continuously high RH can cause condensation within these cavities, which may lead to errors in measurement. This error is inherent in the measurement technique and is caused by a break-up of electrical potential. The capacitive measurement of humidity detects changes in the voltage field, that



is, the change of capacity at the condenser, i.e., capacitor. In the case of moisture penetration over extended periods of time, the voltage field fails and therefore false data is collected (see Weber 1995). After drying, the device functions again and the measurement is continued automatically. The false data differ significantly from actual data in the range of 1–100% RH, and correction during data processing is possible. If these irregularities occur more often, they may also impair the durability of the devices and lead to inaccuracies in long-term measurements. For the present period of measurement, this aspect was not relevant.

A further problem was in relation to the hardware: when the first devices were installed, the cables were too short; adapters therefore had to be placed outside. This weakness in the installation led to the failure of the outdoor plugs and to sectional data dropout.

### 3.2.2 In situ-measurements

Monitoring field MF01 is located at the western façade oriented towards the North. Two sensors were placed in the Drachenfels trachyte and two in the Obernkirchen sandstone. One sensor in each stone was placed at a depth of 18 mm, the other at a depth of 32 mm. A surface temperature detector was fixed on the surfaces of each stone. One sensor, shielded from direct rain, was placed to measure outside humidity and temperature (Fig. 3.4 and 3.5). Measuring parameters are shown in Table A3.1 (see Appendix); a selection of the measured data is shown in Fig. 3.12.



**Figure 3.4** Installation of the sensors in MF01 in Drachenfels trachyte and Obernkirchen sandstone

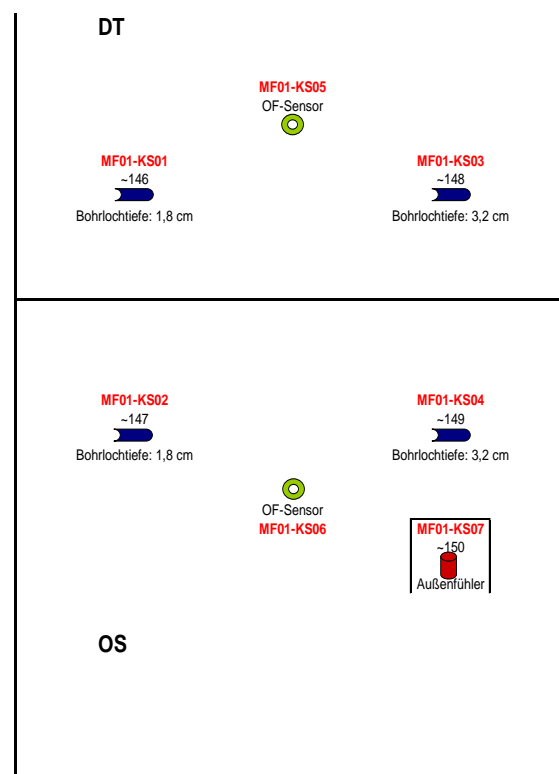


**Figure 3.5** Scheme of the installation of the sensors (KS) in MF01 in Drachenfels trachyte (DT) and Obernkirchen sandstone (OS)

Monitoring field MF02x is located at the northern façade oriented towards the North. Two sensors were placed in the Drachenfels trachyte and two in the Schlaitdorf sandstone. One sensor in each stone was placed at a depth of 23 mm, the other at a depth of 37 mm. A surface temperature detector was fixed on the surfaces of each stone. One sensor, shielded from direct rain, was placed to measure outside humidity and temperature (Figs. 3.6 and 3.7). Measuring parameters are shown in Table A3.2 (see Appendix); a selection of measured data is shown in Fig. 3.13.



**Figure 3.6** Installation of the sensors in MF02x in Drachenfels trachyte and Schlaitdorf sandstone

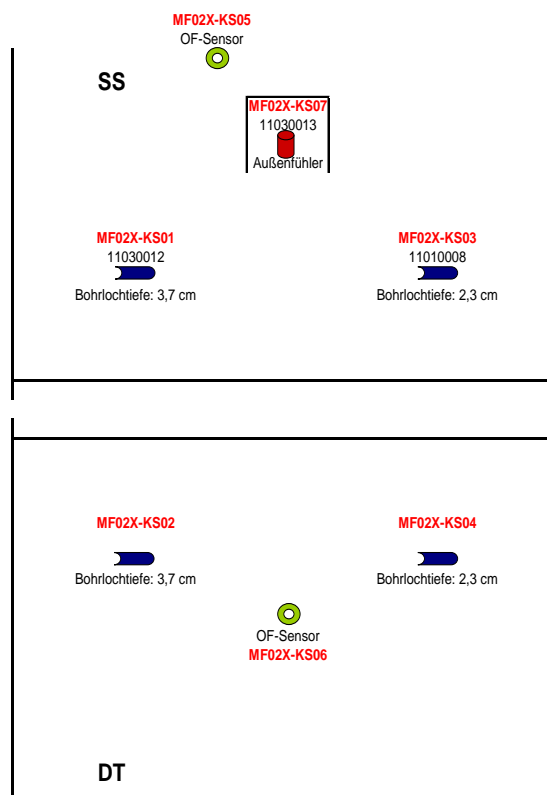


**Figure 3.7** Scheme of the installation of the sensors (KS) in MF02x in Drachenfels trachyte (DT) and Schlaitdorf sandstone (SS)

Monitoring field MF04 is located at choir buttresses at the eastern façade oriented towards the South-East. Two sensors were placed in the Drachenfels trachyte and two in the Obernkirchen sandstone, and four more were placed in the Krensheim Muschelkalk. The sensors were all placed at a depth of 23 mm. The arrangement of the sensors followed the orientation of the stones in relation to each other. In this monitoring field Drachenfels trachyte (DT) is placed next to the Obernkirchen sandstone (OS). In the overlying row, the Krensheim Muschelkalk (KM) is placed (Figs. 3.8 and 3.9). Two pairs of sensors (KM–OS and KM–DT) were placed at two different distances to each other. Additionally, two pairs of sensors (OS–DT) were placed at the same distances to each other, but at varying distance to the overlying Krensheimer Muschelkalk. The different distances of the sensors to each other not only mark the distance to the adjacent stone, but also the distance to the joints in between. A surface

temperature detector was fixed on the surfaces of each of the three stones. One sensor, shielded from direct rain, was placed to measure outside humidity and temperature (Figs. 3.8 and 3.9). Measuring parameters are shown in Table A3.3 (see Appendix); a selection of measured data is shown in Fig. 3.14.



**Figure 3.8** Installation of the sensors in MF04 in Drachenfels trachyte, Obernkirchen sandstone and Krensheim Muschelkalk

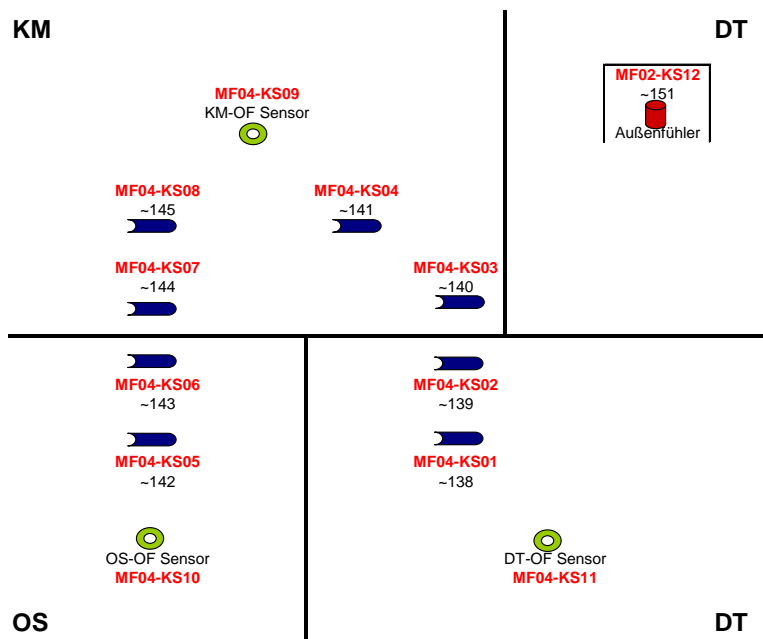


**Figure 3.9** Scheme of the installation of the sensors (KS) in MF04 in Drachenfels trachyte (DT) and Obernkirchen sandstone (OS) and Krensheim Muschelkalk (KM)

Monitoring field MF07 is located at the southern façade oriented towards the South. Two sensors were placed in the Drachenfels trachyte and two in the Obernkirchen sandstone. One sensor in each stone was placed at a depth of 18 mm, the other one at a depth of 30 mm. A surface temperature detector was fixed on the surfaces of each stone. One sensor, shielded from direct rain, was placed to measure outside humidity and temperature (Figs. 3.10 and 3.11). Measuring parameters are shown in Table A3.4 (see Appendix); a selection of measured data is shown in Fig. 3.15.

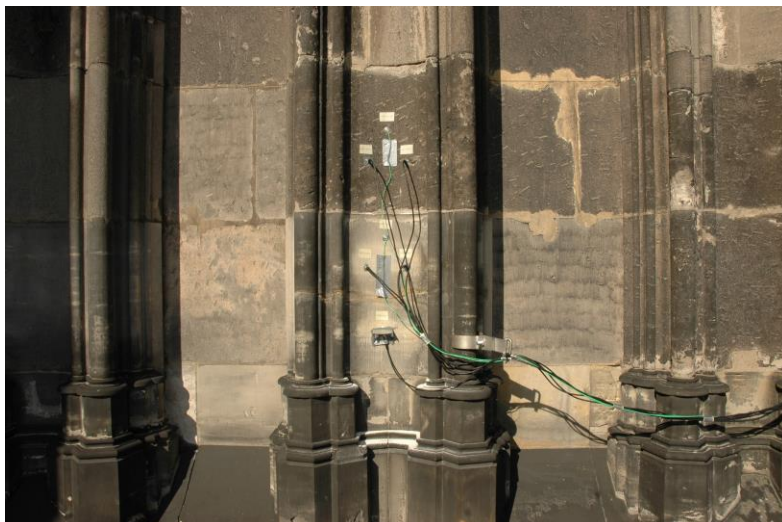


**Figure 3.10** Installation of the sensors in MF07 in Drachenfels trachyte and Obernkirchen sandstone

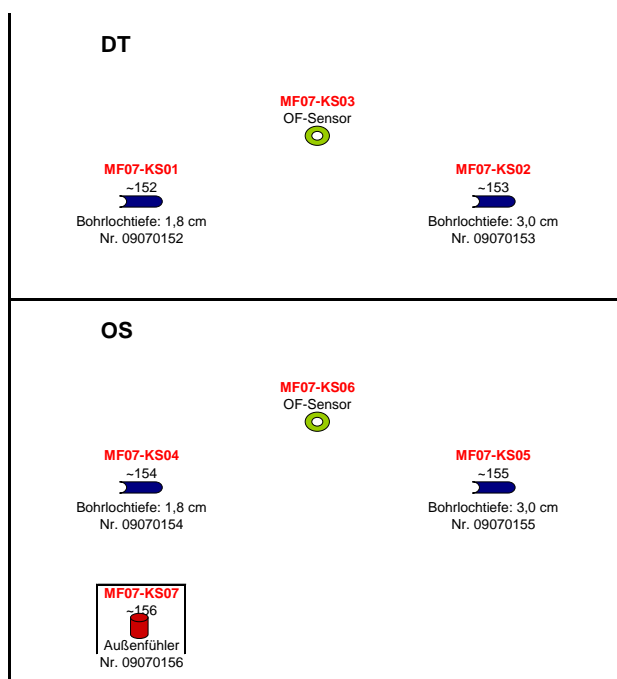


**Figure 3.11** Scheme of the installation of the sensors (KS) in MF07 in Drachenfels trachyte (DT) and Obernkirchen sandstone (OS)

### 3.2.3 Acquired data

The following shows representative measurements.

#### MF01 (western façade)

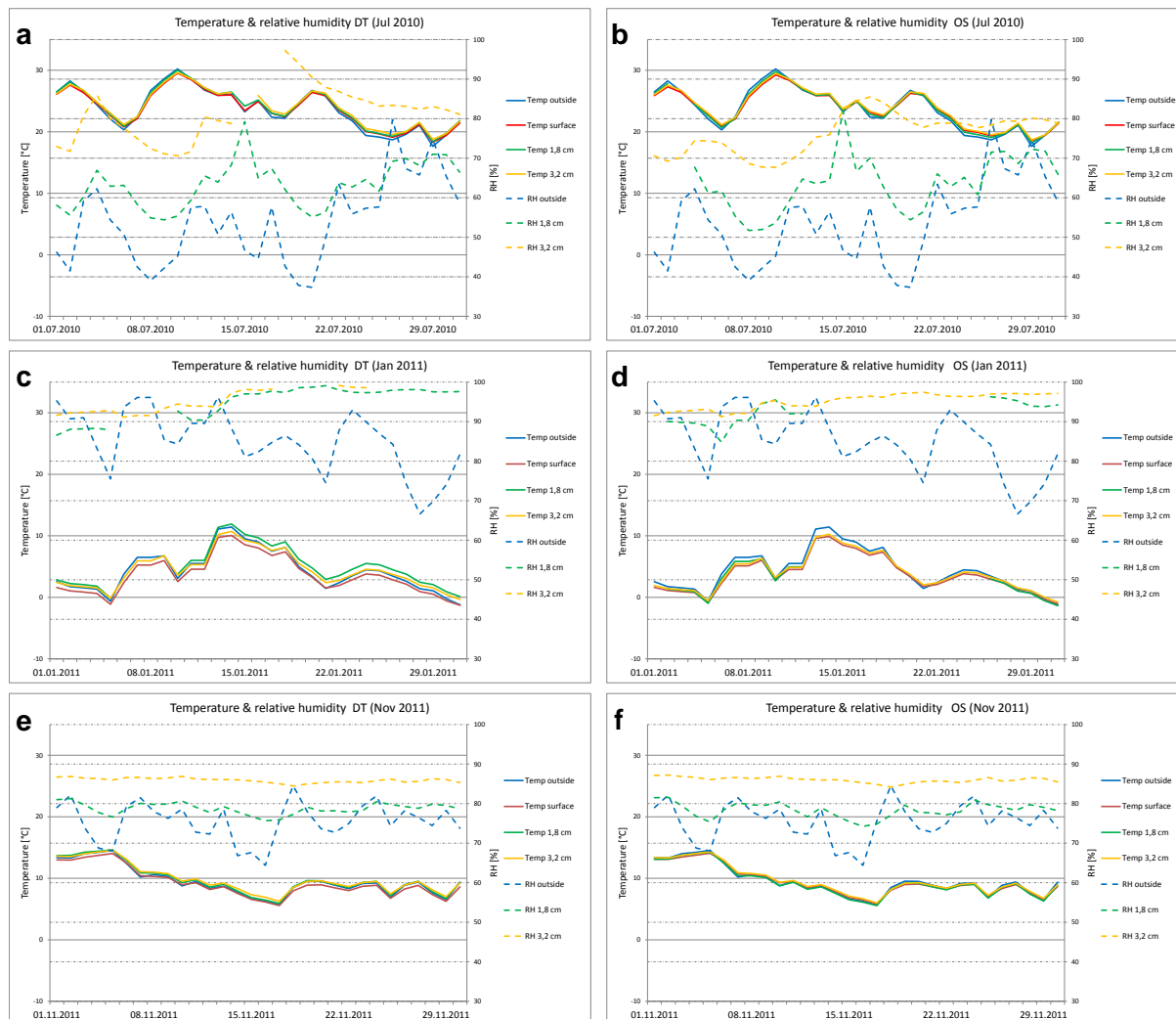


**Figure 3.12 (a-f)** Temperature and relative humidity (RH) monitoring in the monitoring field MF01. **(a, c, e)** outside temperature and RH (blue), Drachenfels trachyte (DT) temperature and RH at a depth of 18 mm (green) and at a depth of 32 mm (yellow) as well as surface temperature (red): **(a)** July 2010; **(c)** January 2011; **(e)** November 2011; **(b, d, f)** outside temperature and RH (blue), Obernkirchen sandstone (OS) temperature and RH at a depth of 18 mm (green) and at a depth of 32 mm (yellow) as well as surface temperature (red), **(b)** July 2010; **(d)** January 2011; **(f)** November 2011



### MF02x (northern façade)

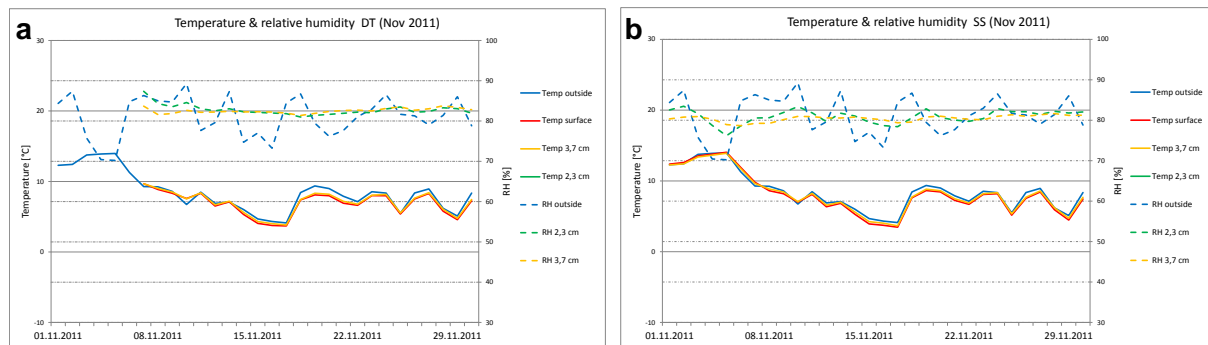


**Figure 3.13** Temperature and relative humidity (RH) monitoring in the monitoring field MF02x. **(a)** outside temperature and RH (blue), Drachenfels trachyte (DT) temperature and RH at a depth of 23 mm (green) and at a depth of 37 mm (yellow) as well as surface temperature (red), November 2011; **(b)** outside temperature and RH (blue), Schlaitdorf sandstone (SS) temperature and RH at a depth of 23 mm (green) and at a depth of 37 mm (yellow) as well as surface temperature (red), November 2011

## MF04 (eastern façade)

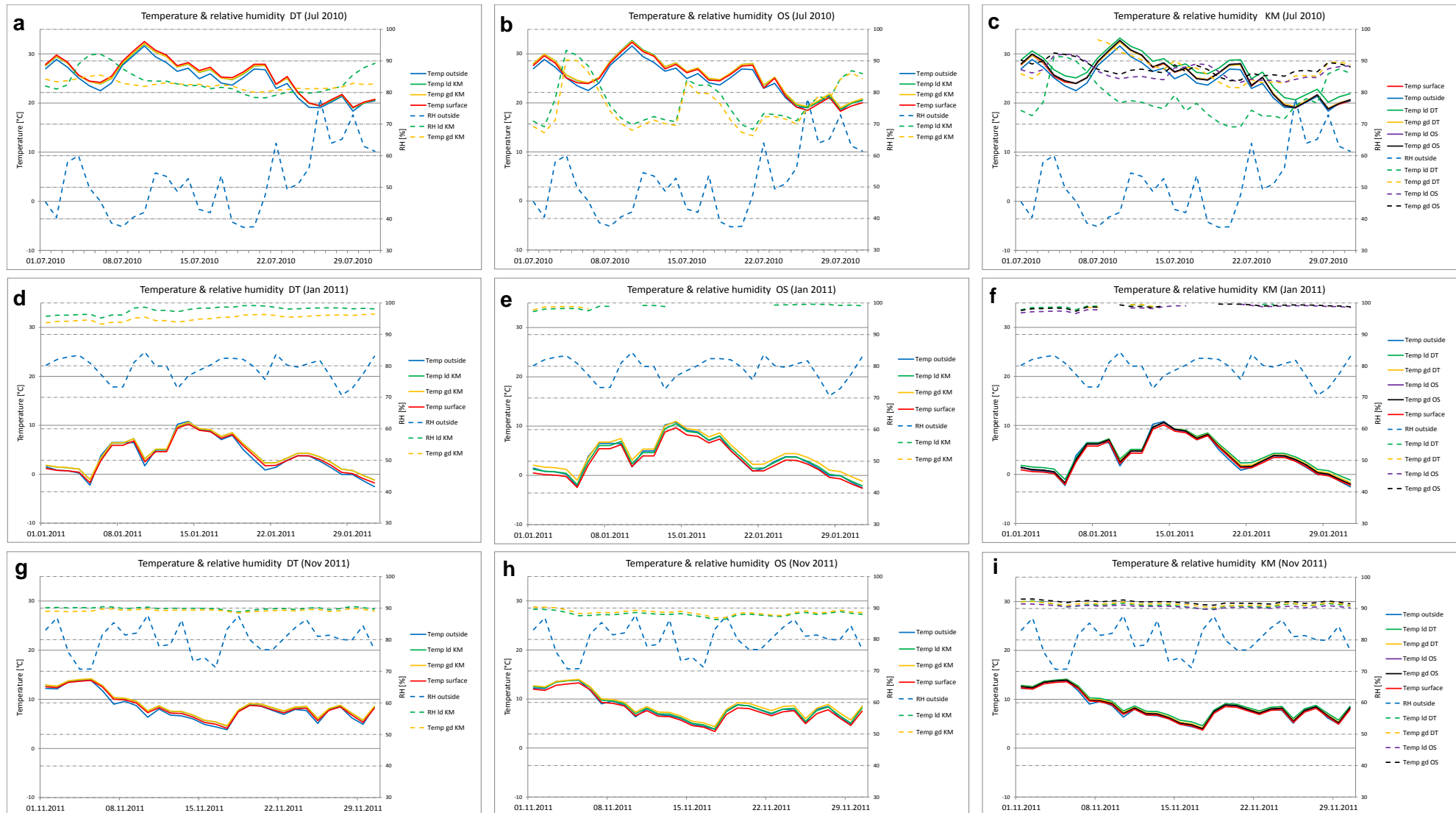


**Figure 3.14 (a-i)** (previous page) Temperature and relative humidity (RH) monitoring in the monitoring field MF04. **(a, d, g)** outside temperature and RH (blue), Drachenfels trachyte (DT) temperature and RH with little distance to Krensheim Muschelkalk (KM) (green) and with greater distance to KM (yellow) as well as surface temperature DT (red): **(a)** July 2010; **(d)** January 2011; **(g)** November 2011; **(b, e, h)** outside temperature and RH (blue), Obernkirchen sandstone (OS) temperature and RH with little distance to Krensheim Muschelkalk (KM) (green) and with greater distance to KM (yellow) as well as surface temperature OS (red), **(b)** July 2010; **(e)** January 2011; **(h)** November 2011; **(c, f, i)** outside temperature and RH (blue), Krensheim Muschelkalk (KM) temperature and RH with little distance to Drachenfels trachyte (DT) (green) and with greater distance to DT (yellow), Krensheim Muschelkalk (KM) temperature and RH with little distance to Obernkirchen sandstone (OS) (violet) and with greater distance to OS (black) as well as surface temperature KM (red), **(c)** July 2010; **(f)** January 2011; **(i)** November 2011

### MF07 (southern façade)

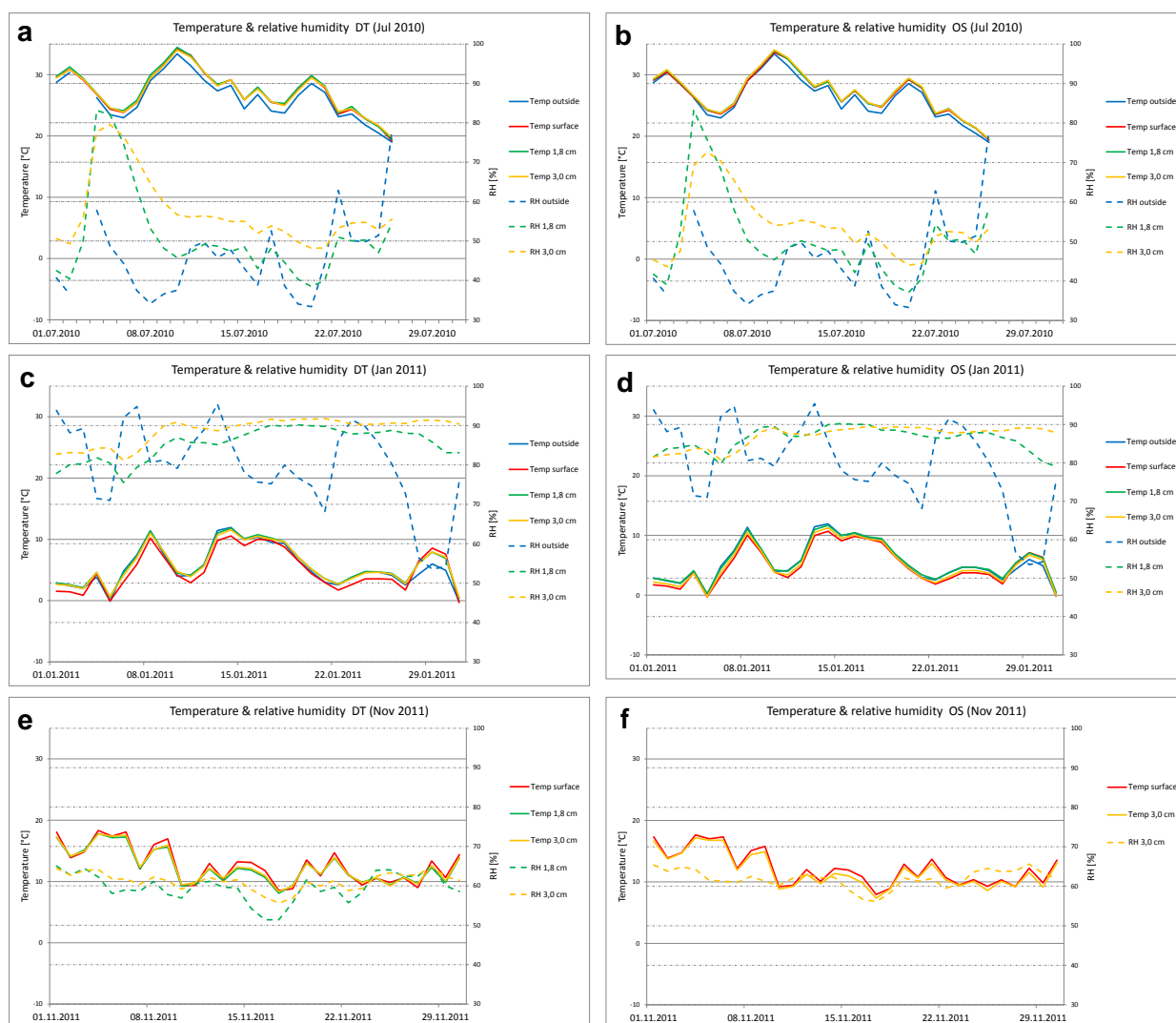


**Figure 3.15 (a-f)** Temperature and relative humidity (RH) monitoring in the monitoring field MF07. **(a, c, e)** outside temperature and RH (blue), Drachenfels trachyte (DT) temperature and RH at a depth of 18 mm (green) and at a depth of 30 mm (yellow) as well as surface temperature (red): **(a)** July 2010; **(c)** January 2011; **(e)** November 2011; **(b, d, f)** outside temperature and RH (blue), Obernkirchen sandstone (OS) temperature and RH at a depth of 18 mm (green) and at a depth of 30 mm (yellow) as well as surface temperature (red), **(b)** July 2010; **(d)** January 2011; **(f)** November 2011



### 3.3 Conclusions

An influence of environmental climate on the temperature and humidity distribution in the different building stones was detected. The measurements taken show the moisture balance and temperature of the stones in comparison to each other. They show clear gradients of relative humidity (RH) and temperature in the ashlar of different stone materials at various depths at identical exposure areas. The correlation of these gradients to the outside conditions is depth-specific. Variations can be seen according to the exposition of the building section. Relative moisture distribution is detected by measurements of relative humidity and temperature. A conversion to absolute and material-relative moisture contents would be the next step of the evaluation, which needs further comparative “thermo gravimetric” analyses and laboratory testing (see Fischer 1993).

The measured temperature values show only small variations between the outside and the material temperature inside the stone. The highest differences – of about 2°C – are observed for the northern façade (MF02) and the southern façade (MF07) in March/April 2011. The sensor in the Krensheim Muschelkalk oriented towards the East (MF04; sensor close to the adjacent Drachenfels trachyte – A-KS03) shows values with a constant degree of variance of about 3–4°C; this might be a question of a malfunctioning sensor. The almost uniform courses of the curves show slight retardations at temperature increases or decreases. In the cold winter months (October to March) the temperatures inside the stone are lower than the outside temperature. In the warmer summer months this is reversed – the temperature inside the stones is higher than the outside temperature. This is observable for the western façade (MF01), the northern façade (MF02x), and also on the eastern façade (MF04), though not as significantly. At the southern façade (MF07), the temperature inside the stones is higher throughout than the outside temperature. As expected, a clear trend of higher temperatures is observed for the southern façade (MF07; Fig. 3.15 e) in comparison to the northern (MF02x; Fig. 1.13 a), western (MF01; Fig. 3.13 e), and eastern sides (MF04; Fig. 3.14 g). This is paralleled by lower RH values, which correlate with temperature.

In terms of the relative humidity, clear gradients are detectable. The deeper inside the stone the sensor is, the flatter – more amplitude-reduced – the course of the curve. This indicates a decreasing direct impact of the outside humidity on the inside moisture. This may reflect to a certain degree the hysteresis of the sorption isotherms (see Fischer 1993); much more than this, however, it indicates a separate “stone climate” (see Schuh 1988).

At the western façade (MF01), where the sensor is placed deeper inside the stone, a tendency of higher relative humidity can be observed. The lower the outdoor RH, the

difference is higher. This indicates that an almost constant moisture content of 85–95% RH is established at a depth of 32 mm. This decreases in very warm summer months down to 70% RH.

In the eastern-oriented measuring field (MF04), the sensors are all placed at the same depth inside the stones but at different distances to the joints or the adjacent stones. The RH curves of the sensors inside the ashlar are highly amplitude-reduced. In the winter months, RH in the Drachenfels trachyte is around 95–100%; in the Krensheim Muschelkalk, RH values range between 90–100%. In respect of several days with minus temperatures, frost action inside the stones can be assumed. In the warmer months (April to September/October), RH ranges are lower, at an average of around 80% with the lowest values around 70%. The stone climate differs very much from the outside climate. RH shows higher values than the outside humidity.

It is noticeable that, in this monitoring field, the sensors in the Drachenfels trachyte show different values in correlation to the distance to the adjacent stone. It still has to be ascertained whether this is due to a certain moisture impact by the joints, or whether the relatively higher RH values of the Krensheimer Muschelkalk are responsible. Regarding the four sensors inside the Krensheim Muschelkalk, the two placed closer to the Drachenfels trachyte and Obernkirchen sandstone show lower RH values than the two sensors in the Krensheim Muschelkalk. A generally higher water balance inside the Krensheimer Muschelkalk can be concluded. From this, a feedback mechanism can be deduced of adjacent stones, leading to a higher moisture load into the stone with the originally lower water balance, i.e., a higher load from the Krensheimer Muschelkalk to the Drachenfels trachyte and from the Krensheim Muschelkalk to the Obernkirchen sandstone.

On the northern façade (MF02x), only a small amount of data could be collected due to several problems with the installation of the sensors. The curves of the sensors inside the stone are amplitude-reduced and run in an average range of the outside humidity. The sensor at 37 mm depth reveals a tendency of higher RH in comparison to the sensor at 23 mm depth. Similar observations can be made for MF07 at the southern façade with relatively higher temperatures and correspondingly lower RH values.

As expected, a correlation of the stone climate to the cardinal direction can be seen. An amplitude-delayed behavior of RH inside the stones is observed. Furthermore, the measurements show a general tendency of continuously higher relative humidity at deeper sensors compared to those placed closer to the surface of the respective stone. Thirdly, in one and the same stone different RH values were measured according to distance to the joints or adjacent stones, indicating interference from the water balance and moisture contents of neighboring natural building stone ashlar.

Time- and amplitude-delayed behavior of humidity measurements in sandstone over the course of a day was first detected by Schuh (1988). The moisture content inside the sandstone (11 mm depth) shows less variance (low amplitude) than the outside and surface sensors. The humidity inside the stone is generally higher except in heavy rainfall, when outside humidity increases rapidly to high values (90–100% RH). Thus, Schuh 1988 refers to an individual “stone climate”.

The collected data show tendencies of moisture balance inside different building stones. Different gradients of moisture content are ascertained in the different building stones – higher-resolution measurements would be a great help here. The reliability of the recorded data still has to be confirmed by further measurements; the choice of method also has to be evaluated. For example, the behavior of the sensors after a condensation event should be further investigated. Numerous publications exist concerning technical moisture-measuring in porous material for comparable single measurements (see above). However, technical requirements of devices, i.e., sensors and data collectors, need to be formulated to improve devices and installation, and thus reproducible measurements. The chosen method allows low-invasive long-term measurements.



## 4 Stone decay at the cathedrals

### 4.1 Decay features of the “cathedral stones”

At the cathedrals a large number of different stone materials was used (Tab. 2.1). At Cologne cathedral the increasing deterioration of the building materials from the historic and more recent construction history has endangered the building's structure. Construction scaffolding, which is nowadays always present as a permanent installation indicates that preservation work is continuous at the Cologne cathedral.

The increasing pollution emission of our industrial society has considerably accelerated the process of weathering of building materials. Generally, the assumption has been that acid-forming sulfur compounds penetrate into the microstructure of the stone and then become neutralized depending upon the rocks' composition. These become concentrated as sulfate-rich salts (especially gypsum enrichment) and are responsible for the many damages observable (e.g. Knetsch 1952, Kraus 1985a, 1985b, Kraus and Jasmund 1981). Cologne is a major city with approximately one million inhabitants. Urban mobile pollution sources, such as automobiles, trucks, railway etc., are the main contributors of air pollution in the city today. Although the emission levels have dropped in the last 30 years, dust pollution is still a major problem. The observed values of air pollution can be correlated with the increased number of chronic respiratory diseases (Wolf 2002). Török et al. (2011) investigated a series of samples from the Cologne cathedral which were collected at about 30 m above the ground from the external walls. Very high concentrations of lead (736 ppm) could be detected in dust samples collected from different areas. The lead also accumulates in the black crust, especially close to the limestone-crust-interface. This indicates that either the crust exhibits signals of past pollution levels or lead is being mobilized from the surface to deeper zones. Even though the SO<sub>2</sub> content decreased in the atmosphere, the situation in many industrial countries can be characterized as a “multi-pollutant” setting (CO<sub>2</sub>, NO<sub>x</sub>, VOC (volatile organic compounds), dust, etc.).

The different building stones of the Cologne cathedral show a large variation of weathering phenomena. On two representative survey areas (Fig. 4.1 and 4.2), the building material and the deterioration phenomena have been mapped in accordance with the classification by Fitzner et al. (1995) and Siedel et al. 2011. Typical decay phenomena consisting of erosion, surface recession, scaling, structural disintegration, flaking and depositions are illustrated in Figures 4.3 and 4.4. The individual deterioration phenomena are assigned to the different building stones and described in detail.

The detailed map of Figure 4.1 shows a section of the northern pillar of the North Tower, i.e. the medieval part built with Drachenfels trachyte and the modern construction phase from the

19<sup>th</sup> century, when Obernkirchen sandstone was employed. The amount of Drachenfels trachyte used in the mapped area is about 71%, Obernkirchen sandstone was used approximately 27% as well as a minor percentage (~2%) of Schlaitdorf sandstone (Fig. 4.1a). While the complete surfaces of all stones show a more or less distinctive deposition of dust and aerosols, microbiological growth can only be observed in the lower areas at the cornice. The localizations of the deterioration phenomena are shown in the map presented in Figure 4.1.

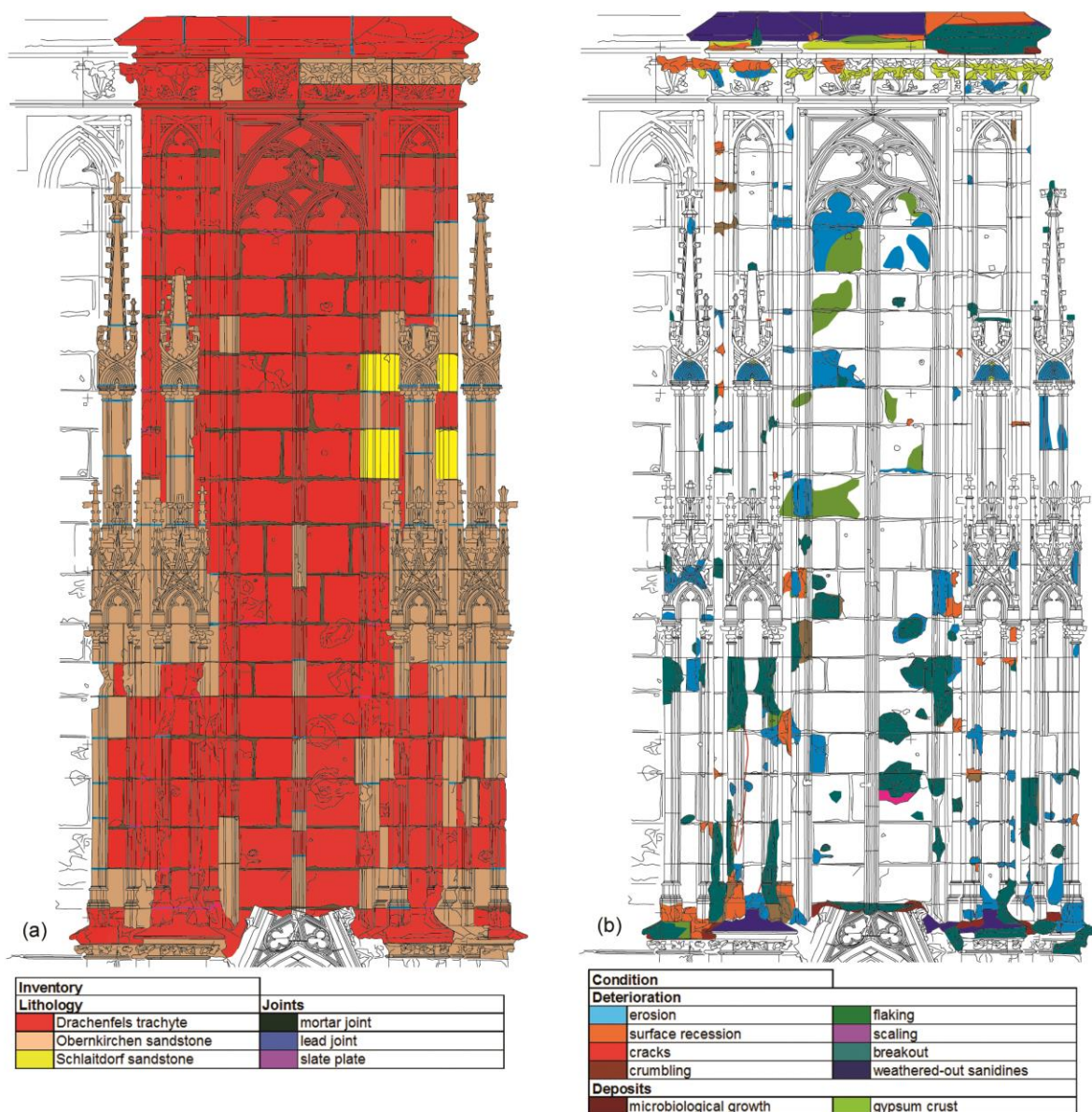


**Figure 4.1** Map illustrating the northern pillar of the North Tower at the Cologne cathedral. **(a)** Stone distribution: 71% Drachenfels trachyte (red), 27% Obernkirchen sandstone (beige), ~2% Schlaitdorf sandstone (yellow). Joints: mortar joints (brown), lead joints (light blue), slate plates (pink). **(b)** The main deterioration phenomena are: erosion (light blue), flaking (green), surface recession (orange), scaling (pink), cracks (red), breakouts (dark turquoise), crumbling (brown), weathered-out sandstones (dark blue), microbiological growth (dark red), gypsum crusts (light green)

The detailed map illustrated in Fig. 4.2 shows a section on the northern pillar of the flying buttresses of the choir, indicating that the major deterioration is on the Drachenfels trachyte. The building material and the deterioration phenomena – erosion, gypsum crusts, scaling, flaking, cracks and depositions – have been mapped, displaying their distribution within the selected wall area.

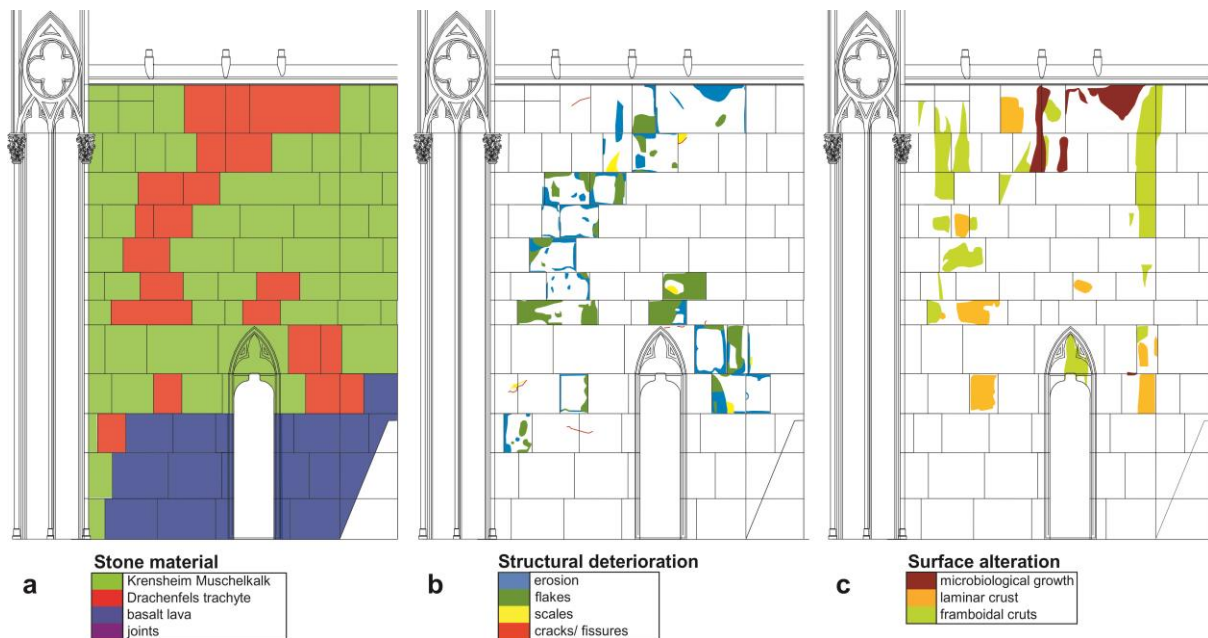


**Figure 4.2** Mapping of a flying buttress of the choir at Cologne cathedral: **a.** lithology: Drachenfels trachyte (red), Krenshelm Muschelkalk (green), basalt lava (blue), joints (purple); **b.** structural deterioration: erosion (light blue), flaking (green), scaling (yellow), cracks (red); **c.** surface alteration: microbiological infestation (dark red), laminar crusts (orange), framboidal crusts (light green).

The different building stones of the Cologne cathedral show a large variation of weathering phenomena. In particular, the Drachenfels trachyte shows severe deterioration. The main deterioration phenomena observable in the Drachenfels trachyte are erosion and surface recession (Fig. 4.3) coexisting with flaking (Fig. 4.3f), exfoliation and structural disintegration to crumbling (Fig. 4.3d) and the massive formation of gypsum crusts (Fig. 4.4a). Surface recession areas often display stronger further decay in terms of microcracks, crumbling to total collapse. Scaling is observable and very often shows a granular disintegrated zone on the reverse side whereas the original stone surface generally still exists (Fig. 4.3b). Formation of cracks and fissures may also propagate many centimeters in depth into the stone. The Drachenfels trachyte is characterized by large crystals of sanidines – up to 7 cm in length. These may cause a different weathering behavior between the matrix and the phenocrysts. In the mapped area the sanidines are weathered-out (Fig. 4.3g), but only in the areas of the cornices. The flow direction of the Drachenfels trachyte, which is indicated by the orientation of these large crystals of sanidine, has a certain impact onto the weathering behavior of the stone. In the Drachenfels trachyte the deterioration is more intense when the



flow fabric is parallel to the visible surface of the building stone (Fig. 4.3e), e.g. the preferred orientation of sanidines is surface parallel. Sanidine crystals and the groundmass matrix often show a different weathering behavior depending on the mounting direction of the building stone. The large crystals are either weathered-out or are protrudent due to the loss of the surrounding matrix. A third variation is the surface parallel weathering of components, matrix and phenocrysts (surface parallel oriented show a simultaneous surface recession. A number of breakouts can be observed in the Drachenfels trachyte, which are a result of the mechanical impact of bombing during WW II. Plehwe-Leisen et al. (2007) have reported that flaking and scaling is often observed. The flaking can occur in a very pronounced fashion, which eventually leads to structural disintegration and total fabric collapse. There are strong indications that the decay phenomenon in the Drachenfels trachyte is especially critical in the direct neighborhood of carbonate replacement stones (Kraus 1985a; Plehwe-Leisen et al. 2007). In many places the decay starts from the joints, which is indicated by gypsum crusts, flaking, exfoliation and scaling (Fig. 4.5a).

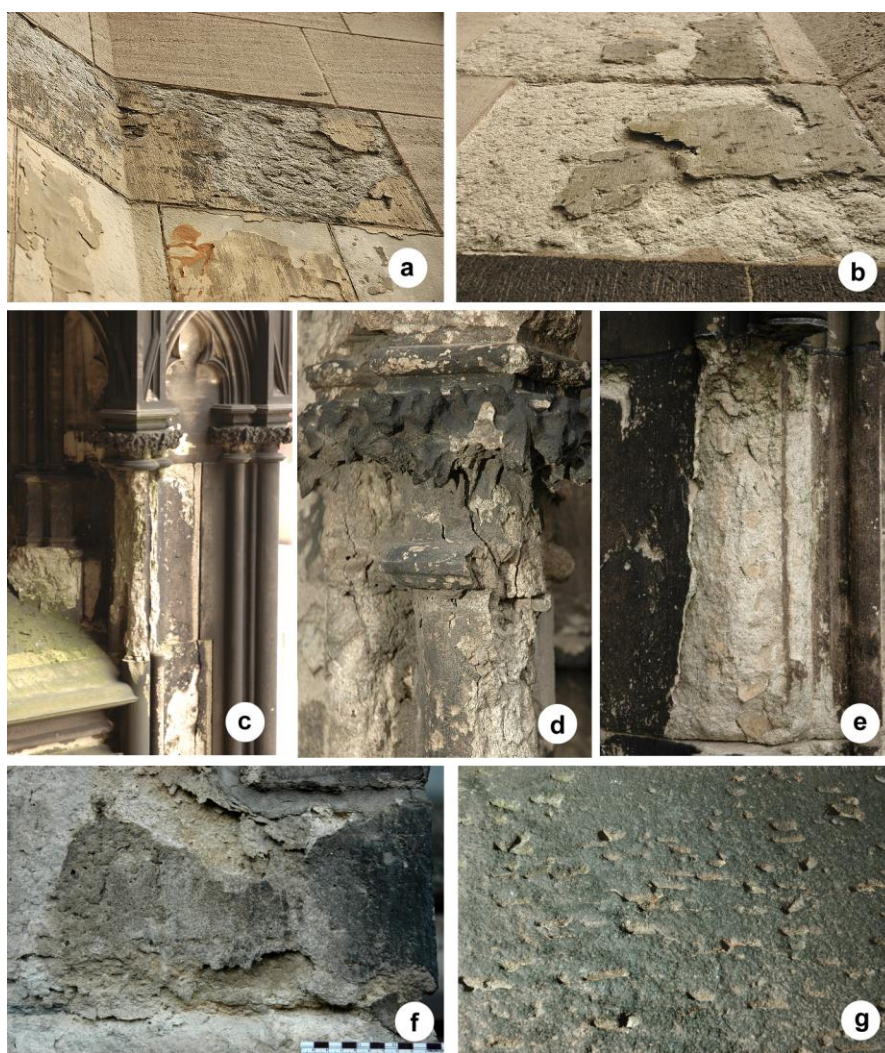


**Figure 4.3** Deterioration phenomena: **(a)** overview: scaling and flaking of Drachenfels trachyte (center); scaling of Obernkirchen sandstone due to surface treatment (lower part); and Krenshelm Muschelkalk (upper part); **(b)** Drachenfels trachyte: scaling; **(c)** Drachenfels trachyte: surface recession and structural disintegration (deteriorated pilaster strip); **(d)** Drachenfels trachyte: pronounced decay in form of microcracks, crumbling to total collapse; **(e)** Drachenfels trachyte: pronounced erosion due to the placement direction with surface planar sanidines; **(f)** Drachenfels trachyte: flaking; **(g)** Drachenfels trachyte: weathering out of sanidines

On the Drachenfels trachyte the formation of thin laminar crusts as well as thick framboidal crusts is observed (Fig. 4.4). Black framboidal crusts tend to bulge out and detach from the



stone surface. The stone structure in the background of these crusts is strongly weakened and disintegrates in form of multiple flaking, exfoliations and further crumbling. Thin laminar crusts often built on structural intact stone surfaces but contour scaling is often accompanied. These surface parallel scales show a thickness of a few millimeters to 1-2 centimeters with the formation of a brittle disaggregated zone on the back.

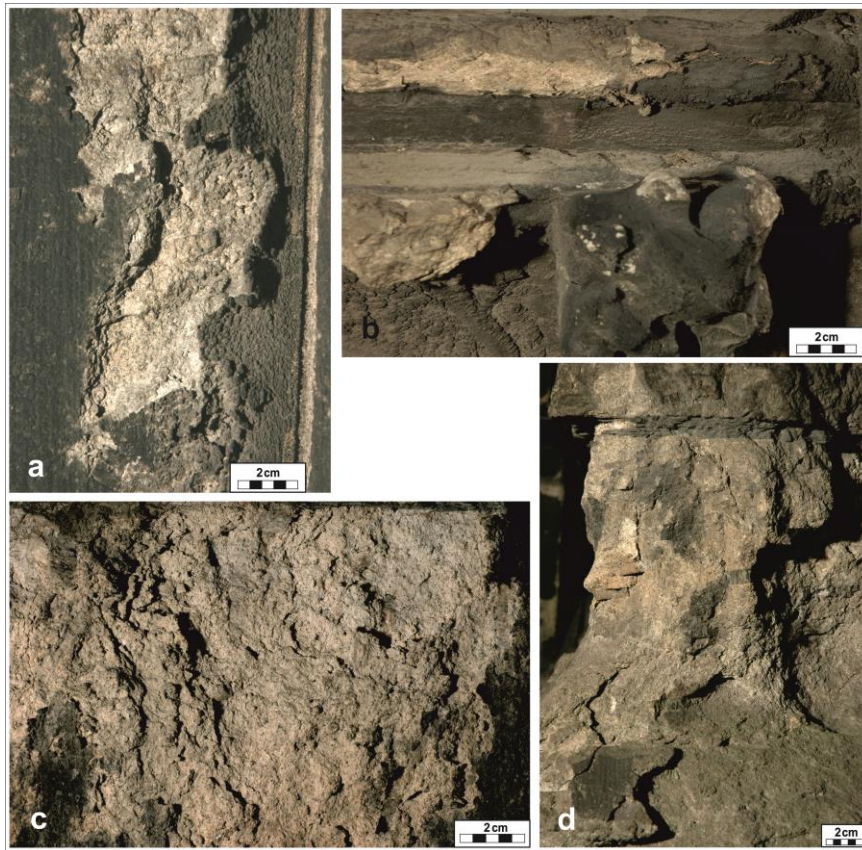


**Figure 4.4** Weathering forms of Drachenfels trachyte. **(a)** framboidal weathering crust, showing bulging and flaking of the rock underneath; **(b)** weathering crust, bulging and flaking in decorated part; **(c)** erosion and flaking; **(d)** structural disintegration and crumbling to total fabric collapse.

In general Obernkirchen sandstone is a very deterioration resistant stone material (Grimm 1990). In the area of the north tower the main deterioration phenomenon is the deposition of dust, forming grayish to black crusts as well as the formation of gypsum crusts in posterior areas (Fig. 4.5b). At the Cologne cathedral in some areas the Obernkirchen sandstone was painted to color adjust the stone to the Krensheim Muschelkalk, which was used for reinstatement work in the 1930-ies. In connection with this paint layer a surface parallel scaling of very thin scales (thickness of 1 – 2 mm) can be observed (Fig. 4.3a). Further severe damage is visible along joints, where the sandstone shows breakouts due to spalling, especially on the decorative parts, e.g. pilaster strips (Fig. 4.5c).

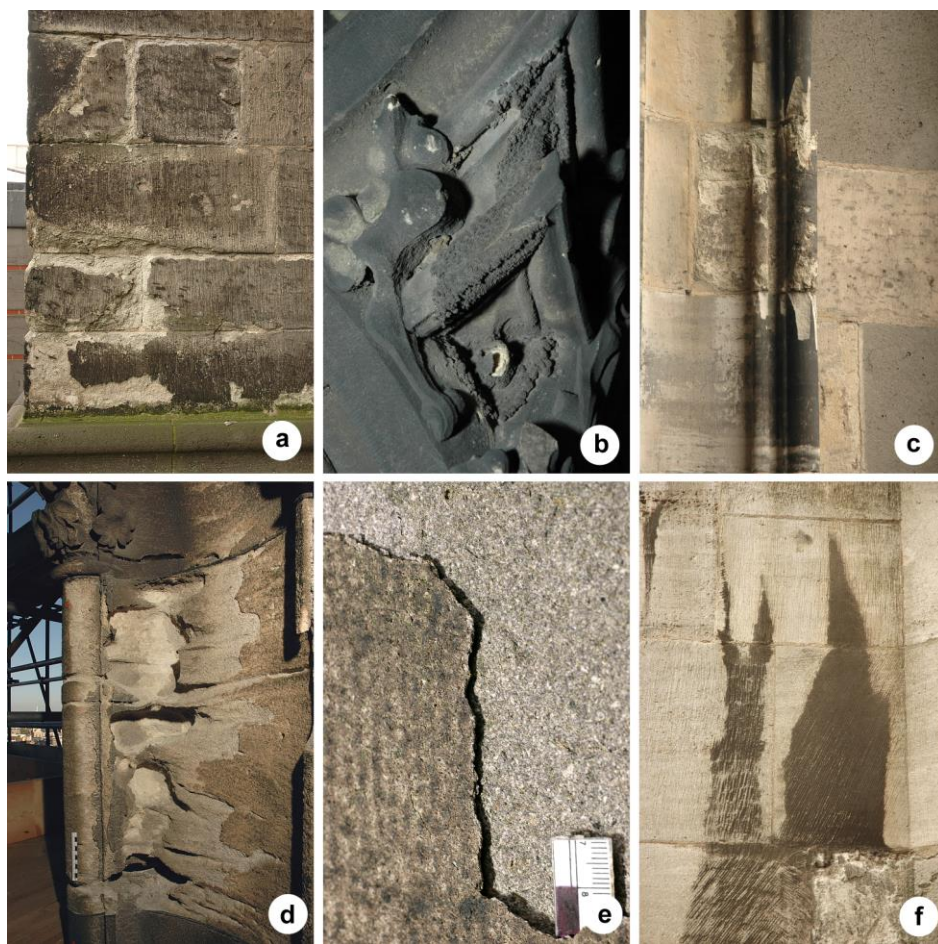


**Figure 4.5** Deterioration phenomena: **(a)** Drachenfels trachyte: deterioration starting from the joint; **(b)** Obernkirchen sandstone: black dirt and gypsum crusts; **(c)** Obernkirchen sandstone: break-outs due to spalling along joints; **(d)** Schlaitdorf sandstone: scaling, granular disintegration to sand and relief due to rounding and notching; **(e)** Stenzelberg latite: scaling; **(f)** Krensheim Muschelkalk: black gypsum crusts

Schlaitdorf sandstone is a very problematic stone at the Cologne cathedral. Kraus (1985) and Grimm (1990) report that this stone characteristically disintegrates. The carbonate cement (app. 14 wt. %) causes the problem, whereby gypsum formation occurs that leads to massive scaling and flaking phenomena as well as granular disintegration. Moreover, another very typical deterioration phenomenon for the Schlaitdorf sandstone is rounding and notching together with granular disintegration (Fig. 4.5d).

At present little is known about the deterioration behavior of the Montemerlo trachyte at the Cologne cathedral, since this stone has only been implemented in recent years. Very often intensive orange-brown discoloration of the Montemerlo trachyte can be observed when it is used as a replacement stone. These iron discolorations have a negative aesthetic effect, but no structural impact. However, Lazzarini et al. (2008) report exfoliation and flaking, powdering and alveolic weathering for the Montemerlo trachyte.

Stenzelberg latite and Londorf basalt lava are very resistant against weathering. Due to the high porosity, the Londorf basalt lava is susceptible to microbiological action. The main deterioration phenomenon of Stenzelberg latite is a typical formation of scales with a

thickness of 2 – 3 mm (Fig. 4.5e). Furthermore Grimm (1990) observed exfoliation and contour-scaling, granular disintegration into grus as well as powder, and breakout of mafic mineral nests.

Bozanov sandstone shows spalling along edges when mounted, which is problematic for masonry works. Přikryl et al. (2010) reported on granular disintegration, scaling, flaking, crust formation as well as blistering, fracturing, salt efflorescences and alveoli formation for the medium grained Bozanov sandstone.

In principal the Krensheim Muschelkalk is a deterioration resistant stone. This carbonate building stone shows massive gypsum crust formations as a result of acid rain (Fig. 4.5f). This is visible in rain protected areas, while on surfaces exposed to rain, solution phenomena can be observed e.g. microkarst. In these situations the blocks express a surface roughness and it leads to a loss of shape or form in detailed and decorative figural areas.

Joints are primarily filled with lime mortar, which often have inserted slate plates. These are randomly visible due to the weathered mortar. The present findings indicate that these slate plates are used to cover the entire contact surface of the building stones (Nußbaum and Lepsky 2010). The majority of the joints have been redone several times with modern mortars during the different restoration phases.

The building stones are covered by black laminar and framboidal crusts. On the Drachenfels trachyte the crust formation is strongly correlated to the disintegration of the stone. The crusts tend to detach, and further structural deterioration follows. Contour scaling, flaking and exfoliation are characteristic decay features on the Drachenfels trachyte, leading to granular disintegration and crumbling (Fig. 4.4). On the Obernkirchen sandstone and on the Stenzelberg latite weathering crust form very thin scales, 2 – 3 mm thick, which tend to detach from the stone. The Schlaitdorf sandstone shows thick black weathering crusts which are regularly accompanied by severe contour scaling of several centimeter thicknesses and pronounced granular disintegration. On the Krensheim Muschelkalk the crusts seem to temporarily stabilize the stone surface (see Siegesmund et al. 2007). On surfaces exposed to rain, solution phenomena can be observed, e.g. microkarst (Graue et al. 2011).

## **4.2 Comparison of the decay at the three different locations**

At Xanten cathedral, the main deterioration phenomena of the Drachenfels trachyte are scaling and flaking, as well as crack formation. Surface deposition and black weathering crusts are found on many ashlar. These are mainly laminar crusts on intact stone surfaces and partially framboidal weathering crusts, which show detachment and disintegrated stone material underneath. In some places break-outs are observable, as well as exfoliation and stronger disintegration due to flaking (Dombauhütte Köln 2006). The severe crumbling to total fabric collapse, which is ascertained in Cologne cathedral, is not detected in Xanten.



Similarly to Cologne, Xanten also shows varying weathering behavior in sanidine phenocrysts, which can be seen as weathered-out or as protruding due to the loss of the matrix. Partially orange-red or brownish-orange discolorations can be seen. The latter are often seen in context with disintegrated stone. Very often these orange-red discolorations can be observed underneath black weathering crusts, but may also occur on the surface (Fig. 4.6 and b) (Dombauhütte Köln 2006).



**Figure 4.6** (a) Orange-red discoloration underneath a removed black weathering crust with intensive discoloration on the sanidine (Dombauhütte Köln 2006); (b) brownish-orange discoloration on the surface of the Drachenfels trachyte

The tuff only shows a small amount of deterioration. Black weathering crusts can be seen as well as powdering surfaces in some spots; very rarely, crack formation and scaling is also detected. The sandstones (Baumberger and Udelfanger) are generally in good condition; only partially flaking and sanding surfaces can be observed, and occasionally significant crust formation is found, especially in protected areas. The limestone used shows microkarst phenomena. In the basalt lava no deterioration phenomena are detected. (Knapp and Dungs 2004)

At the Altenberg cathedral only a very little structural deterioration is observed in the Drachenfels trachyte. The main deterioration phenomena are scaling and flaking, which can only be found to a minor extent. Laminar crusts are often accompanied by microbiological contamination. In isolated spots, detachment of the crusts is detectable. Reddish discolorations on the Drachenfels trachyte do not occur in conjunction with structural impairment. Break-outs and cracks are not very distinct. Before the restoration measures started in the 1990s, several deterioration phenomena were surveyed (IBS 1990). The Stenzelberg latite showed scaling, but to a very small degree. The tuff showed the most significant deterioration compared to other stones used in the Altenberg cathedral. Black weathering crusts were detected, which were often detached and found in context with

granular disintegration, as well as scaling and flaking and occasionally crumbling. Greywacke ashlar showed delamination along geologically pre-existing joints, as well as sanding, surface recession and crumbling. In the limestone, crust formation and microkarst were detected to a minor degree. The different stones showed crust formation, sanding, exfoliation and break-outs. In the basalt lava no deterioration phenomena were detected. (IBS 1990)

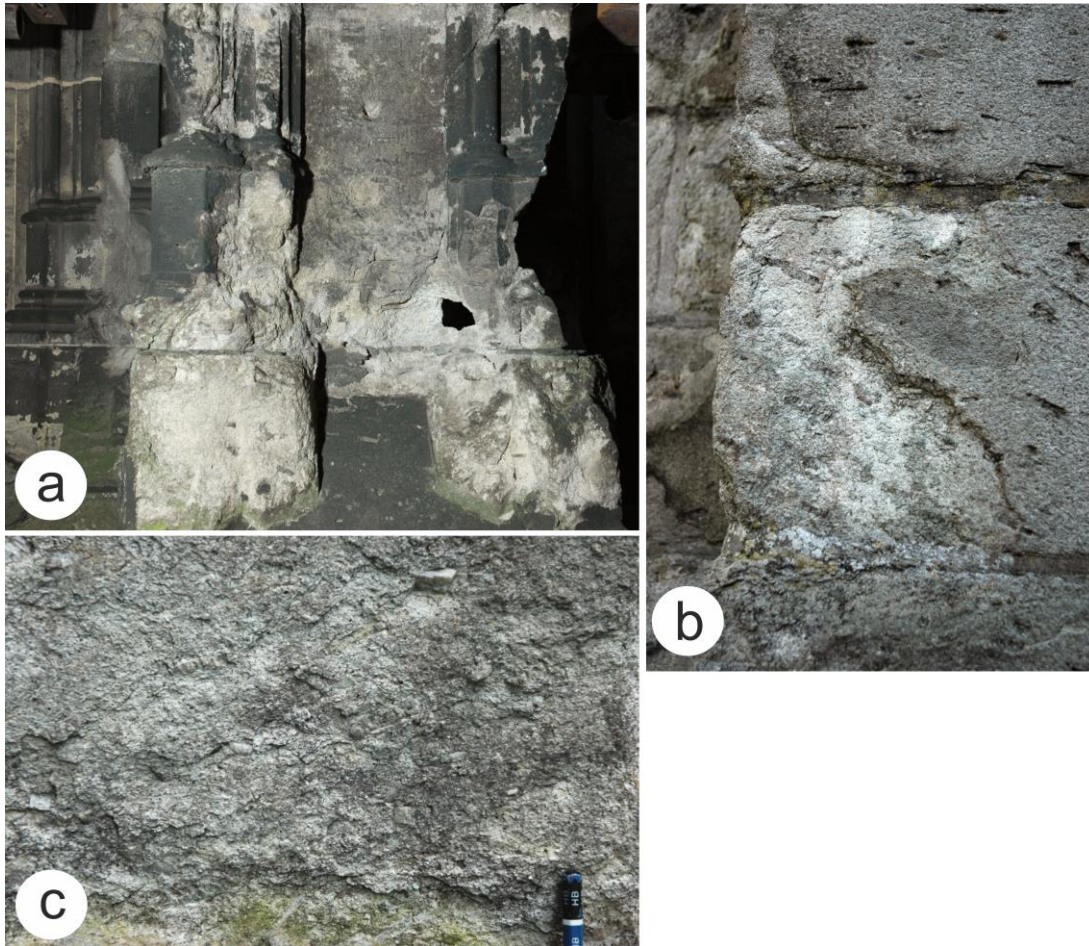


**Figure 4.7** (a) Crumbling and total fabric collapse observed at Cologne cathedral; (b) scaling at Xanten cathedral; (c) flaking at Altenberg cathedral

Comparing the three locations with each other, clear gradients are detected regarding the different kinds of damage and their intensity (Graue et al. 2013b). The strong deterioration of the Drachenfels trachyte, which is observed at the Cologne cathedral in the form of crumbling to complete fabric failure leading to static impairments, is not detected at the Xanten or the Altenberg cathedrals. At all three locations, scaling and flaking are ascertained as the main deterioration phenomena in the Drachenfels trachyte. These are not as significant at Xanten and Altenberg as they are at Cologne; the same is true of surface depositions and formation of black weathering crusts (Graue et al. 2013a). Black weathering crusts at Cologne cathedral are mostly manifested as thick framboidal crusts with disintegrated stone material underneath, or as laminar crusts on the surface of detached

scales. At Xanten cathedral, weathering crusts are most likely to occur as laminar crusts or surface deposition on mostly intact stone substrates. At Altenberg, laminar crusts can partially be observed. Very often these are accompanied by significant microbiological contamination.

## 5 The building stones of the Cologne cathedral

### 5.1 Geology at the Cologne cathedral

Of the investigated stones at the Cologne cathedral the oldest natural building stone in geological terms is the Krensheim Muschelkalk. It formed in the Middle Triassic period during the Upper Muschelkalk, when the region of the today's Federal Republic of Germany was dominated by a broad inland sea. This fossil-rich carbonate stone was deposited in a warm-marine milieu (Grimm 1990). The fine porous limestone comes from quarries at Grünsfeld-Krensheim in Baden-Württemberg (Lukas 1990).

When the Muschelkalk Sea withdrew from the Germanic Basin and the region became dry land, the sedimentation of the Schlaitdorf sandstone took place about 210-220 Ma ago during the Keuper (Upper Triassic). This sandstone, also called Stubensandstein, forms the highest layer of the Keuper-Schichtstufe along the river Baar (Renz et al. 2013). From 1842 to 1868 this sandstone of the Middle Keuper (Gips- und Sandsteinkeuper) was purchased for the construction of Cologne cathedral from the Schönbuch quarries near Schlaitdorf in Baden-Württemberg (Grimm 1990; Schumacher 2004). Until today this coarse, mainly dolomitic-kaolinite cemented sandstone is quarried at Pliezhausen (Lukas 1990; notice: Lauster Steinbau, Stuttgart 2013).

During the Jura epoch, the German Basin was divided into a Northern-German and Southern-German shallow sea due to the lifting of the Middle-German land bridge (Grimm 1990). In the Lower Cretaceous the Lower Saxony Basin subsided and collected detritus from the Middle German land bridge. In shallow delta areas the Wealden-sandstones of the Lower Cretaceous were deposited in a brackish-limnic environment (Grimm 1990). The well-known Obernkirchen sandstone belongs to this Wealden-sequence (Grimm 1990). With the completion of the Cologne – Minden railway in 1847 the possibility of an economic transport of this sandstone from quarries at the Bückeberge to Cologne was given (Schumacher 2004).

The Bozanov sandstone is found in the northern part of the Intra-Sudeten Basin at the border of Poland and the Czech Republic. The center of the basin is filled with Upper Cretaceous marine sandstones, which transgressively lay on the Rotliegend and Variscan basement rocks of the Bohemian Massif (Lehr 2008). The sandstones are found from the Cenomanium up to the Santonium strata (Ehling 2007). The Bozanov quarry lies on the Polish-Czech border. In Poland, where this stone is quarried as well, it is known as Radkov sandstone (Graniteland 2013). During the Cenomanian transgression, i.e., at the time of the deposition of the Radkov-Bozanov sandstones significant tectonic movements took place. As a consequence, the transport of coarse-grained clastic material increased. The deposition of these coarse clastic fluvial storm-sediments took place along fault zones. At steep,

tectonically controlled synclines, the sediments deposited in shelf environment along the coast line (Lehr 2008). The stone material shows significant inhomogeneities at outcrop scale (Ehling and Siedel 2011). Thus, the blocks for the replacement works at the Cologne cathedral have to be individually chosen.

The Montemerlo trachyte comes from the Euganean hills in Northern Italy. The eruption that formed these hills started during the Eocene with basaltic magma. A later eruption phase during the Lower Oligocene is characterized by a series of complex magma compositions. Si-rich magmas solidified to form compact effusive domes or kryptodomes underneath sediment layers. The volcanic eruptions at the Oligocene took place in a sub-aqueous environment (Colombra s a). The trachytes of the Colli Euganei appear in closely neighbored domes and form a major part of the eruptive features (Koch 2006). The quarries at the Colli Euganei host important deposits of natural building stones, which have been used as early as in Roman times until today (Koch 2006).

The Drachenfels trachyte, the Stenzelberg latite and the Londorf basalt lava are Neogene volcanic rocks mainly formed in the Miocene (Grimm 1990). Thus, the earliest used building stone at Cologne cathedral belongs to the youngest ones in geological terms.

The first construction material of the Cologne cathedral was the Drachenfels trachyte from the nearby Siebengebirge. It formed during the Tertiary related to the so-called “mittelrheinischen Vulkanismus” also known as “Siebengebirgsvulkanismus” at 28 to 6 Ma BP. The basement of these rocks are well consolidated Devonian sediments, which are strongly overprinted by Variscian folding, subsequent erosion, and later on through bloc faulting and volcanism. At the beginning of the Tertiary, the “Rheinisches Schiefergebirge” lifted and at the same time the “Kölner Bucht” subsided. Because of this subsidence of the “Kölner Bucht” the North Sea ingressed as far as to the southern tip of the triangle shaped bay. The sediments of the Oligocene form the basement rocks of the volcanic strata. In the Miocene the North Sea gradually regressed to the North. The fracture zones related to the bloc faulting partly controlled the volcanic events. The Drachenfels was formed during the late Oligocene as a steep walled volcano with domed top (krypto-dome) underneath the overlaying tuff by the extrusion of viscous non-depleted magma. (Berres 1996)

From the shape-preferred orientation of the large sanidine phenocrysts the formation as a krypto-dome can be deduced, which grew from inside underneath a tuff cover (Cloos und Cloos 1927). Later on, the uppermost layers of this tuff (80 m) were eroded (Berres 1996).

Slightly younger than the Drachenfels trachyte is the Stenzelberg latite, which can be found partially as extrusive rocks transsecting in the trachyte. The Stenzelberg latite is a tertiary volcanic rocks belonging to the Miocene (24-5 Ma) (Berres 1996). The trachyte is assigned to a second eruption phase, whereas the latite is related to a third eruption phase (Grimm 1990).



The outcrop area of the Londorf basalt lava is located at the western border of the Vogelsberg, which is with ca. 2,500 km<sup>2</sup> one of the biggest continuous basalt region of Middle Europe. Strong tectonic movements during the late Oligocene, the uplift of the Central German Uplands associated with the formation of graben structures caused an intensive basaltic volcanism in the late Tertiary – mainly in the Miocene but as well until the Pliocene. Along the related fault zones magma could ascent and effuse. The Londorf basalt lava is a porous volcanic rock which is cropped until today.

## **5.2 Petrography of the “cathedral stones”**

The Drachenfels trachyte is a light gray, partially pale yellowish or reddish, porous, porphyritic rock with phenocrysts of sanidine up to 7 cm in size (Fig. 5.1a) (Simper 1990). The fabric of the trachyte can be divided into three different elements: first, the above mentioned large phenocrysts of sanidine. Secondly, a micro- to cryptocrystalline groundmass consisting mainly of feldspar laths and xenomorphic quartz. Thirdly, altered volcanic glass fractions as interstitial material between the small feldspar laths of the groundmass form a mesostasis. These interstitial areas of recrystallized glass are strongly fractured with a high and distinct porosity (Fig. 5.2a). The large phenocrysts in the Drachenfels trachyte are embedded in a very fine groundmass with flow fabric. The sanidine phenocrysts show a preferred orientation, tracing the flow fabric. The small lath-shaped feldspars of plagioclase and sanidine and show a local flow fabric around the large idiomorphic sanidine crystals, with the result that several textural domains with shape-preferred orientation of the feldspar laths exist within the groundmass (Fig. 5.2b). The sanidine as well as the plagioclase phenocrysts show significant crack formation, which can be considered as a secondary porosity. This probably traces back to geological relaxation processes during the cooling (thermal contraction) of the volcanic rock.

Grimm (1990) classifies the rock as quartz-trachyte. The Drachenfels trachyte mainly consists of sanidine (50 wt. %), plagioclase (24 wt. %) and quartz (13 wt. %). Other components are augite (5 wt. %) and biotite (5 wt. %) and common accessory minerals are ore (2 wt. %) and apatite, zircon and sphene (1 wt. %) (Vieten 1961; Koch 2006). The sanidine phenocrysts often show Carlsbad twins and growth zones. Biotite shows strong pleochroism and is often strongly altered. The micro- to cryptocrystalline groundmass (64%) mainly consists of feldspars and quartz (Simper 1990). Plagioclase phenocrysts (mean grain size is 0.8 mm) are observed as well. They show growth zoning and contain about 30 mol % anorthite (Ab<sub>70</sub>An<sub>30</sub>) (Kraus 1985a; Grimm 1990). Apatite and sphene often form large, idiomorphic crystals (Grimm 1990). The interstitial volcanic glass fractions are often recrystallized and altered to montmorillonite (Koch 2006) (Fig. 5.2c). Vieten (1961) detected 1-5 wt. % montmorillonite in samples from different outcrops at the Drachenfels. Clay mineral

analyses with X-ray fluorescence and cation exchange capacity (Dohrmann and Kaufhold 2009) reveal concentrations of 3–5 wt. % of montmorillonite within the Drachenfels trachyte. The clay minerals are not only found within the interstitial areas but in the entire pore space and as crystal coating. In places, calcite occurs in contiguity with Fe-oxides (Fig. 5.2d) indicating alteration processes. In some cavities pyrite and aggregates of pyrite-hematite (limonite?) can be found (Koch 2006).

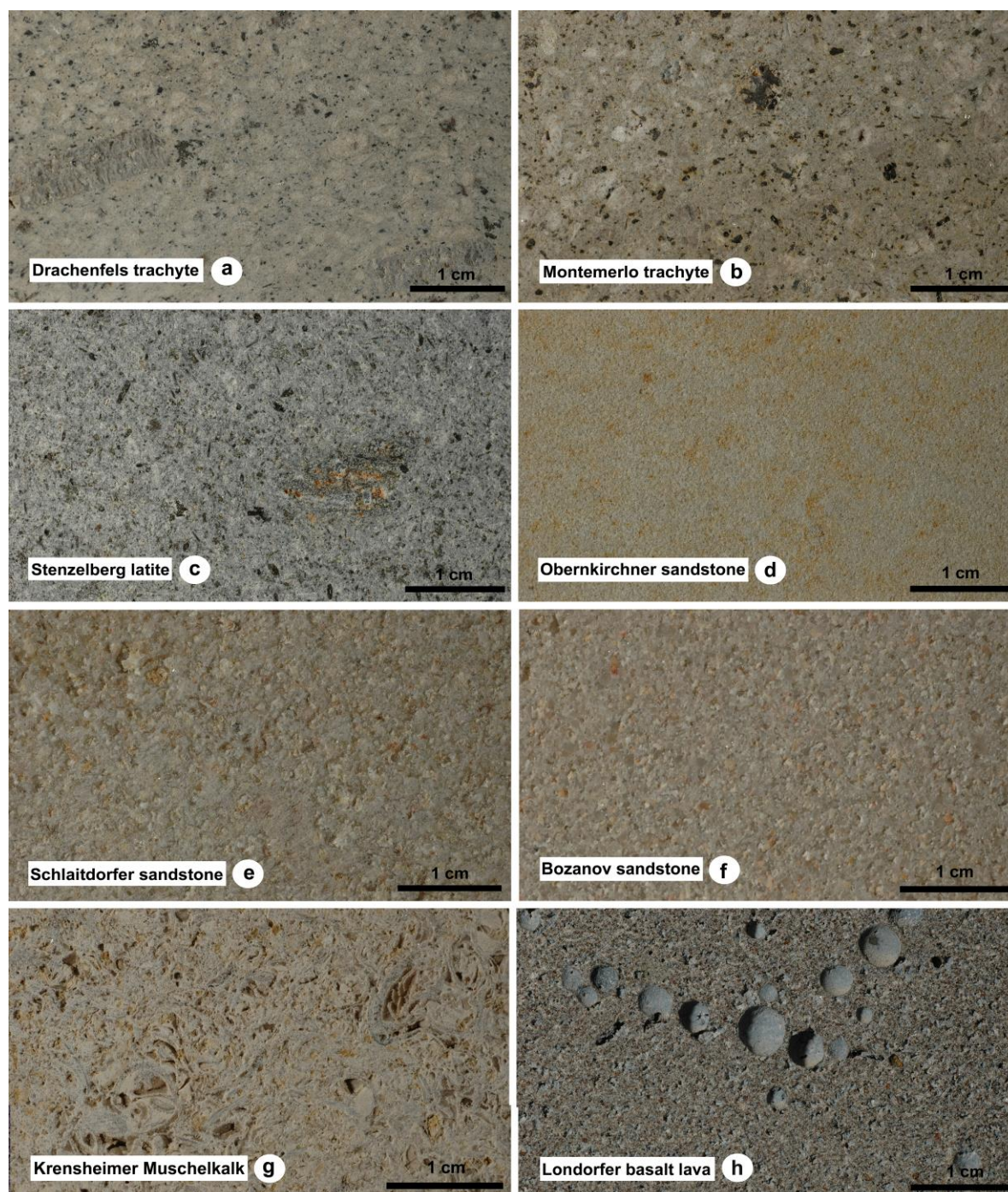


**Figure 5.1** Cut sections of the investigated stones from Cologne cathedral (a) Drachenfels trachyte, (b) Montemerlo trachyte, (c) Stenzelberg latite, (d) Obernkirchen sandstone, (e) Schlaitdorf sandstone, (f) Bozanov sandstone, (g) Krensheim Muschelkalk and (h) Londorf basalt lava



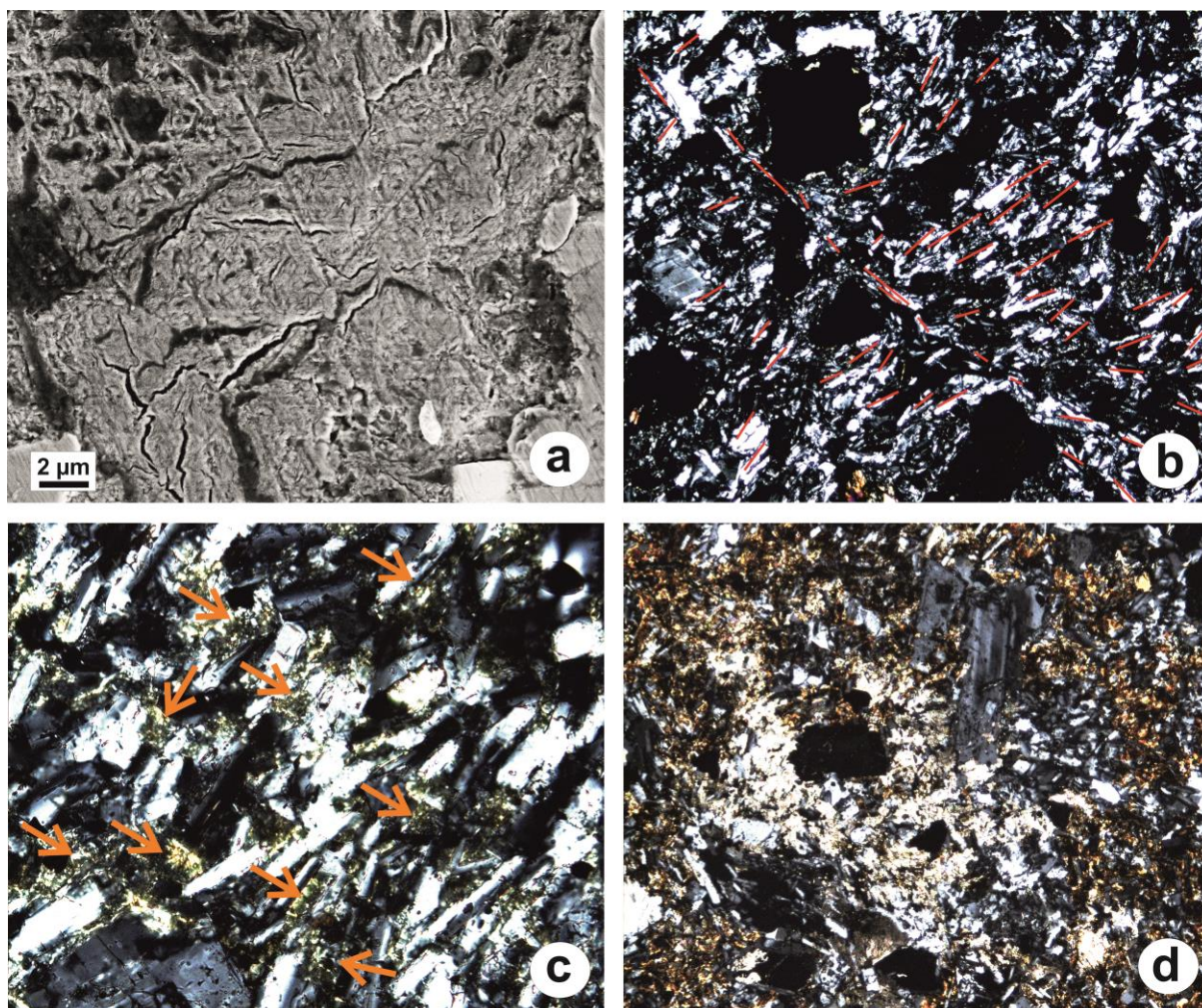


**Figure 5.2** (a) Secondary electron picture of Drachenfels trachyte – altered volcanic glass fractions in the interstitial areas are much fractured, showing a very distinct porosity; (b) the fluidal structure of the groundmass produces several textural domains with preferred orientation of the groundmass feldspar laths (marked with red lines) (crossed polars; image width 1.68 mm); (c) recrystallized and altered volcanic glass fractions in an unweathered rock sample, showing high interferences in crossed polars (marked with arrows; image width 0.42 mm); (d) accumulation of calcite and Fe-oxides as a result of alteration processes (crossed polars; image width 1.68 mm).

The trachyte of Montemerlo shows an isotropic and homogenous fabric (Fig. 5.1b). In some cases, the rock exhibits a holocrystalline fabric with a weak parallel texture, where millimeter to centimeter large white feldspar crystals, black biotite and dark, prismatic amphiboles float in a gray, weakly yellow groundmass. Feldspar crystals can attain sizes ranging from 0.5 mm to 10 mm. Biotites are smaller than 2 mm. The composition was determined by Koch (2006) as follows: K-feldspar (53%), plagioclase (15%), quartz (8%), amphibole (8%), biotite (5%), pyrite (7%) and calcite (4%). The phenocrysts can constitute about 40% of the total rock. Accessory minerals are zircon, apatite and sphene. The groundmass is microcrystalline and mostly consists of anorthoclase, sanidine, plagioclase and seldom quartz. Plagioclase occurs as euhedral and subhedral, zoned and twinned phenocrysts up to 6 mm in size as well as in the groundmass. Alkali-feldspars are predominantly anorthoclase and seldom occur as sanidine. (Koch 2006)

The Stenzelberg latite is a medium gray, porphyritic, and in part porous quartz-latite (Fig. 5.1c). The micro- to cryptocrystalline matrix (77%) is mainly composed of plagioclase and sanidine. Plagioclase, hornblende with individual grain sizes up to 10 cm, augite, and biotite occur as phenocrysts. Accessory minerals are apatite, sphene, zircon and ore minerals. The mafic minerals are often accumulated in clusters. (Grimm 1990) The normative mineral content is 39 % plagioclase, 37% sanidine, 9 % hornblende, 7 % quartz, 3 % ore minerals, 2 % augite, 2 % biotite and 1 % apatite, zircon and sphene (Vieten 1961). Feldspar laths define the flow fabric. The Stenzelberg latite has a low porosity (8.5%), showing mainly intra- and minor inter-particle pores with heterogeneous pore sizes (Grimm 1990).

The Obernkirchen sandstone is a medium-grained, moderately to well-sorted quartz arenite showing a white to orange color (Fig. 5.1d). The color is derived from iron oxide and hydroxide. The detrital fraction (maximum grain size 300 microns) is composed of monocrystalline quartz (98 %), muscovite, zircon, tourmaline, rutile and opaque minerals. Grains are rounded, spherical and rod-shaped with an aspect ratio up to four (Morales Demarco et al. 2007). Most of the grain contacts are concave-convex and sutured. The fabric is grain-supported. The matrix (ca. 5%) is composed of aggregates consisting of authigenic kaolinite showing the characteristic booklet structure. The cement consists of rare silica (probably syntaxial overgrowths) and iron oxide patches. Obernkirchen represents a pure quartz sandstone with a small amount of kaolinite (Dienemann and Burre 1929; Grimm 1990).

The Schlaitdorf sandstone is a whitish to yellowish coarse-grained, well-sorted often parallel, angular and cross-bedded rock (Fig. 5.1e). The detrital fraction (65%) is represented by quartz (72%), rock fragments (12%), feldspar (2%) and cement (14%). The feldspar is often more intensely weathered. The cement consists of coarse-grained dolomite, in parts silica and rarely illite and kaolinite, which show a dispersed distribution. The main accessories (< 1%) are apatite, zircon, tourmaline and opaque minerals. Variegated marly clay is mostly accumulated in layers and occurs parallel to the bedding. Grain contacts are mainly along the long axes of the grains and they are often narrowly intergrown (Grimm1990).

The Bozanov sandstone is a coarse- to medium-grained arkosic sandstone (Fig. 5.1f). It is only weakly cemented and shows a light gray to yellow color. Sporadically clay cement participates in grain cementation as a clay mineral seam or as a crack and gusset pore infilling (smectite). Many grains display an initial interlocking grain boundary with concave-convex grain contacts. The mineralogical composition is given by quartz (79%), rock fragments (10%), feldspar (5%), clay minerals (smectite, kaolinite, around 5%) and accessories like biotite, zircon and opaque minerals. Very typical are cross-bedding, gradations and shell-shaped cavities and impressions. The feldspar content and its

decoration by hematite crystals are very characteristic features. The rock is poorly-sorted (Koch 2000; 2001; Přikryl et al. 2010).

The Krensheim Muschelkalk is a light, brownish-grayish fine porous limestone consisting of shell fragments (Fig. 5.1g). It is classified as a grainstone according to Dunham (1962) or as a densely packed bio(micro)sparite after Folk (1962). Mussel- and brachiopod shells of 5-7 mm sized are densely packed in a fine calcite matrix; pores are partially filled with calcite or often filled with residual material. The components are oriented parallel to the bedding, showing a moderate sorting. The composition consists of 75% biogenic components mainly with micritic rendering, 5% cement and 20% pores. The cement is sparitic and partially micro-sparitic. The pore space is characterized by gusset pores, particle solution pores and mould pores. The fabric is grain supported with mainly long and point contacts (Grimm 1990; Siegesmund et al. 2010).

The Londorf basalt lava is a brownish to bluish gray basalt (Fig. 5.1h). Orange-brownish olivine crystals of 1-2 mm give the rock a weakly porphyritic appearance. The fabric is fine- to medium-grained and around the vesicles hyaloophitic. The rock is composed of plagioclase (47%), augite (26%), olivine (14%) and ore minerals (ilmenite and magnetite around 10%). Accessories of a cryptocrystalline nature (3 %) and partially glass (up to 50%) also occur. The rock is highly porous. Besides generally smaller pores, a less frequent pore type of up to 6 mm in diameter is characteristic. The pores are often coated by light-gray bluish secondary zeolites. Inclusions of quartzite and claystone fragments up to 5 cm can be observed (Grimm 1990; Steindlberger 2003).

### 5.2.1 Density, porosity, pore size distribution

Analyses were carried out to determine density, porosity and pore size distribution (PSD) on non-deteriorated samples from eight of the natural building stones used at the Cologne cathedral. Density was measured by buoyancy weighing on cubic samples (65 mm). The dry mass, the water saturation and the mass of the samples immersed in water were measured to obtain information concerning the porosity (DIN 52102). Furthermore, the pore size distribution was determined by using mercury intrusion porosimetry (MIP) on cylindrical samples ( $\varnothing$  12.5 mm) (Brakel et al. 1981; Siegesmund and Dürrast 2011).

The investigated stones show medium porosities from 11.8% (Montemerlo trachyte) to 19.9% (Schlaitdorf sandstone), except the Stenzelberg latite, which belongs to low porosity stones with a porosity of 8.5% (Tab. 5.1).

The stones investigated in this study have densities from 2.10 g/cm<sup>3</sup> to 2.52 g/cm<sup>3</sup> and can be grouped according to the density. The three sandstones have lower densities. Krensheim Muschelkalk and the trachytes have slightly higher densities. The highest density shows the basalt lava (2.52 g/cm<sup>3</sup>) (Tab. 5.1).

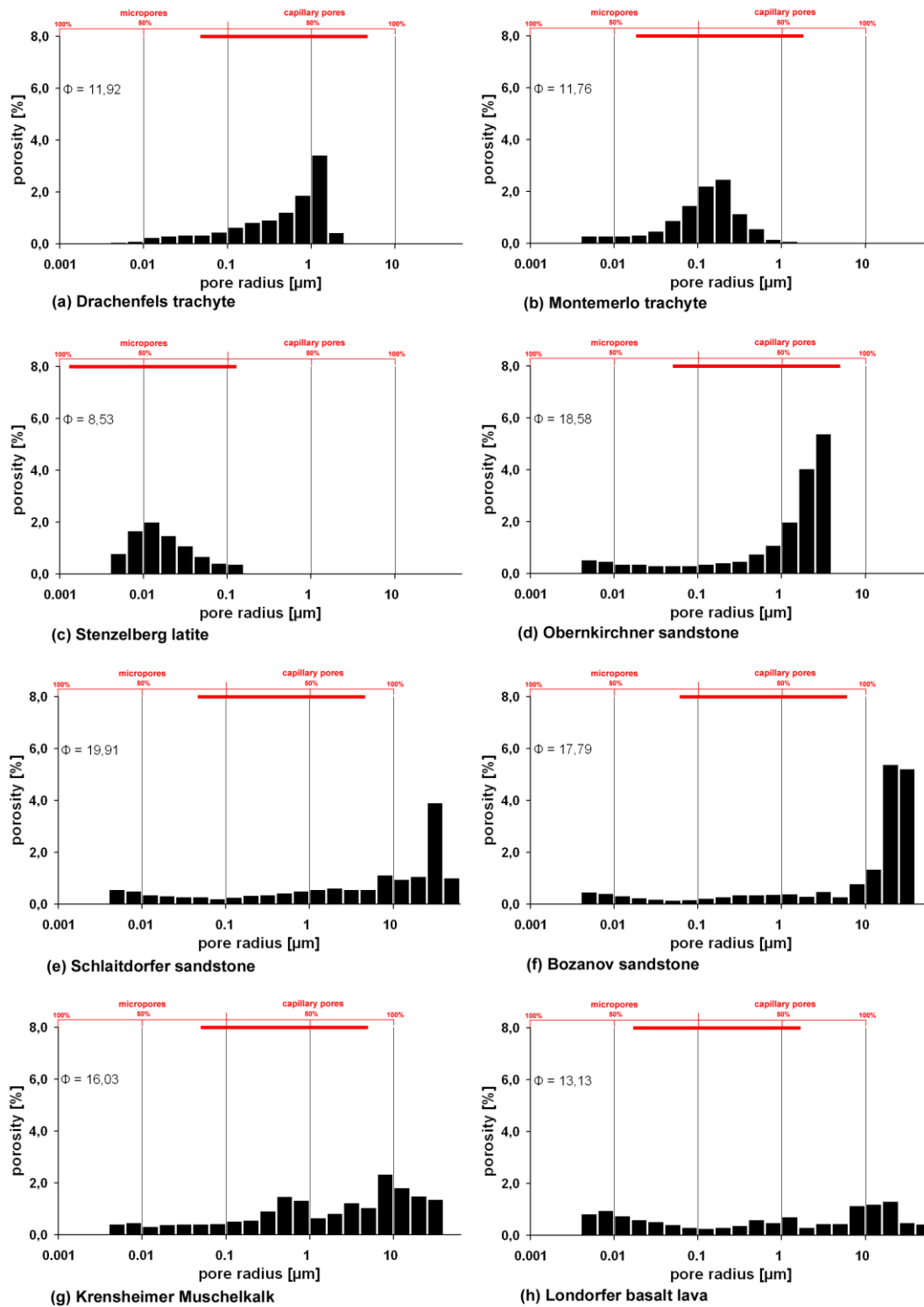


**Figure 5.3** Pore size distribution of the investigated natural building stones ( $\Phi$  = porosity) determined by means of mercury porosimetry. The red bar indicates the percentage of micro- and capillary pores.

**Table 5.1** Bulk and matrix density, porosity, mean and mode pore radius, capillary water uptake, saturation coefficient, vapor diffusion resistance and sorption.

Rock type	Bulk density (g cm <sup>-3</sup> )	Matrix density (g cm <sup>-3</sup> )	Effective porosity (vol.-%)	Mean pore radius (µm)	Mode pore radius (µm)	Capillary water uptake (w-value) (kg/m <sup>2</sup> √h)	Saturation degree (S-value)	Water vapor diffusion resistance (µ)		Sorption at 95% RH (wt-%)
								Z	X	
Drachenfels trachyte	2.33	2.64	11.92	0.414	1.334	0.55	0.74	37.38	17.91	1.88
Montemerlo trachyte	2.35	2.66	11.76	0.108	0.211	0.99	0.71	40.49	31.82	1.11
Stenzelberg latite	2.46	2.69	8.53	0.017	0.013	0.30	0.76	56.39	50.20	2.78
Obernkirchen sandstone	2.16	2.65	18.58	0.821	3.350	1.26	0.64	15.89	14.95	0.72
Schlaitdorf sandstone	2.10	2.63	19.91	2.891	33.497	6.68	0.64	20.56	16.93	0.38
Bozanov sandstone	2.17	2.63	17.79	5.953	21.135	6.90	0.65	16.51	19.69	0.75
Krensheim Muschelkalk	2.25	2.68	16.03	-	0.64 / 8.2 *	1.30	0.59	69.45	51.25	0.29
Londorf basalt lava	2.52	2.92	13.13	-	0.0082 / 28 *	0.39	0.59	37.78	38.60	1.62

\* bimodal PSD



Analogous to the classification by Rüdrieh and Siegesmund 2006 the pore size distributions (PSD) of the investigated stones – except of the Krensheim Muschelkalk and Londorf basalt bava – show a unimodal distribution. Schlaitdorf and Bozanov sandstones have a broader distribution of pores ranging from 0.0064 – 82  $\mu\text{m}$  with a clear peak of pores at > 10  $\mu\text{m}$  (Fig. 5.3e & f). Obernkirchen sandstone has a narrower distribution (0.0064 – 64  $\mu\text{m}$ ) (Fig. 5.3d) and Drachenfels trachyte even closer (0.0082 – 28  $\mu\text{m}$ ) (Fig. 5.3a). Even stronger limited is the PSD of the Montemerlo trachyte from 0.0064 – 1  $\mu\text{m}$  (Fig. 5.3b) and the Stenzelberg latite with a PSD from 0.0064 – 0.28  $\mu\text{m}$  (Fig. 5.3c) with a relatively narrowed pore radii maximum. Krensheim Muschelkalk and Londorf basalt lava show a bimodal PSD (Fig. 5.3g & h).

Figure 5.4 shows the correlation of mean pore radius and porosity. In general it can be remarked, that with a higher porosity the mean pore radius is also high. An exception is the Obernkirchen sandstone, which has a high porosity of 18.6% and a relatively small mean pore radius of 0.82  $\mu\text{m}$ .

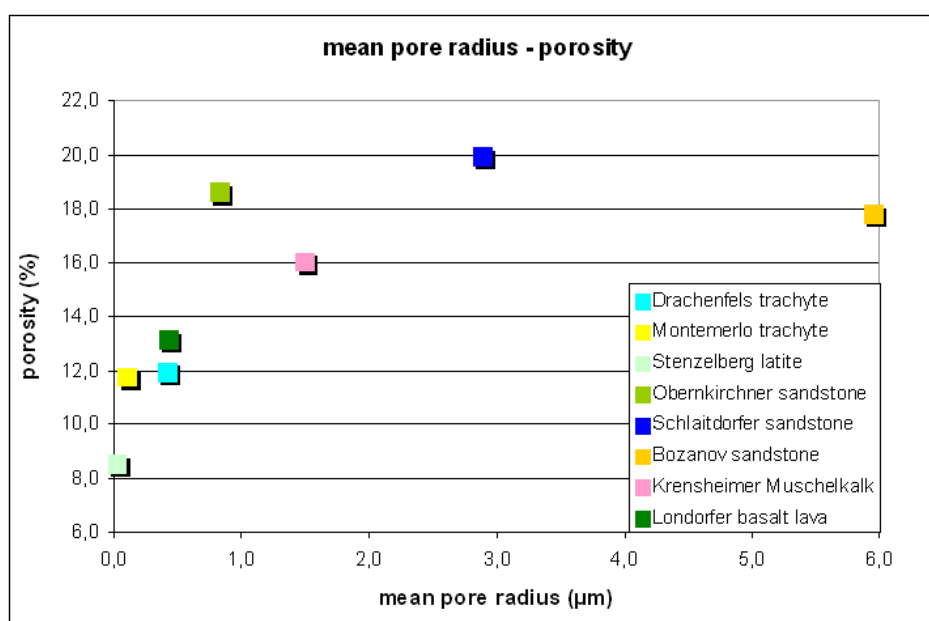


**Figure 5.4** The investigated natural building stones show a tendency of higher porosity correlated to a higher mean pore radius

### 5.3 Moisture properties

#### 5.3.1 Capillary water absorption

Capillary water absorption was measured according to the standard EN 1925 on cubic samples (65 mm). The measurements were done in two directions parallel and perpendicular to the bedding of the stone. The w-value is the amount of water taken up per area by the stone with the square root of time (Wesche 1996).



The Drachenfels trachyte, Stenzelberg latite and Londorf basalt lava show low capillary water absorption values ( $w < 0.5 \text{ kg/m}^2\sqrt{\text{h}}$ ). Montemerlo trachyte, Obernkirchen sandstone and Krensheim Muschelkalk have a medium value ( $1 - 1.5 \text{ kg/m}^2\sqrt{\text{h}}$ ); Schlaitdorf and Bozanov sandstones show a high capillary water absorption value ( $6.5 - 7 \text{ kg/m}^2\sqrt{\text{h}}$ ) (Snethlage 2005; Siegesmund and Dürrast 2011). The values are listed in Table 5.1.

The Drachenfels and the Montemerlo trachyte show a mode pore radius – the pore radius corresponding to the region of the steepest slope (Aligizaki 2006) – in the range of  $0.1 - 1 \text{ }\mu\text{m}$  (Fig. 5.3a & 5.3b; Tab. 5.1), which is the lower range of capillary active pores according to Klopfer (1985). These two rocks absorb water slowly with a low to medium  $w$ -value. The mode pore radius class of the Obernkirchen sandstone ranges from  $1 - 6.4 \text{ }\mu\text{m}$ , which is within the medium range of capillary active pore size (Fig. 5.3d; Tab. 5.1). This sandstone shows slow but continuous water suction with a medium  $w$ -value. The Schlaitdorf and Bozanov sandstones show mode pore sizes in the range of  $10 - 100 \text{ }\mu\text{m}$  (Fig. 5.3e & 5.3f; Tab. 2). These two rocks soak water rapidly and have a high  $w$ -value. Krensheim Muschelkalk has a bimodal distribution and two peaks at  $0.64 \text{ }\mu\text{m}$  and  $8.2 \text{ }\mu\text{m}$  (Fig. 5.3g; Tab. 5.1). Although 84% of the porosity belongs to the capillary active pores, the  $w$ -value is not high, because of the low connectivity of the pore space (Kraus 1985a). Stenzelberg latite and Londorf basalt lava show extremely slow water suction with low  $w$ -values. Ninety-five percent of the pores in the latite are micropores ( $< 0.1 \text{ }\mu\text{m}$ ) (Fig. 5.3c). Londorf basalt lava consists of about 34% micropores (Fig. 5.3h).

Based on the measured data, the stones can be divided into three groups (Snethlage 2005): 1) Stenzelberg latite, Londorf basalt lava and Drachenfels trachyte have low mean pore radii and low capillary water absorptions ( $w$ -values); 2) Montemerlo trachyte, Krensheim Muschelkalk and Obernkirchen sandstone have mean pore radii in the lower to medium range of capillary active pore sizes and medium capillary water absorptions; 3) Schlaitdorf and Bozanov sandstones with high mean pore radii have high water absorbing coefficients ( $w$ -values).

### 5.3.2 Water saturation coefficient

The values for water uptake under vacuum and atmospheric pressure were also determined as well as the degree of saturation ( $s = W_{\text{atm}}/W_{\text{vac}}$ ). Porosity is equivalent to the water uptake under vacuum in vol.-% relative to the total volume of the rock. The saturation coefficient ( $s$ -value) was measured according to the standard DIN 52103. It represents the ratio of the pore space, which fills up with water under normal atmospheric pressure conditions. The closer the water saturation coefficient comes to 1, the higher the proportion of pore spaces filled with water under atmospheric pressure. The values for the water saturation of the investigated stones range from  $0.59 - 0.76$  (Tab. 5.1). The Krensheim Muschelkalk and Londorf basalt lava show the lowest  $s$ -values. The Schlaitdorf, Obernkirchen and Bozanov

sandstones are in a medium range. The Drachenfels and Montemerlo trachytes as well as Stenzelberg latite are rocks with higher s-values.

### 5.3.3 Sorption/ Desorption

To measure the hygroscopic water adsorption, the equilibrated sample weight was measured with ascending and descending relative humidity in steps of 10% from 15% to 95% and 95% to 15% at 30°C on cylindrical samples ( $\varnothing$  20 mm, 50 mm in length) according to the standard DIN 66138. At the hygroscopic level the water adsorption of a rock is regulated by the humidity of the air and it is separated into sorption (moisture adsorption) and desorption (moisture release). In the hygroscopic range of 0 to 95% relative humidity, moisture content of the rocks increases with rising humidity along so-called sorption isotherms.

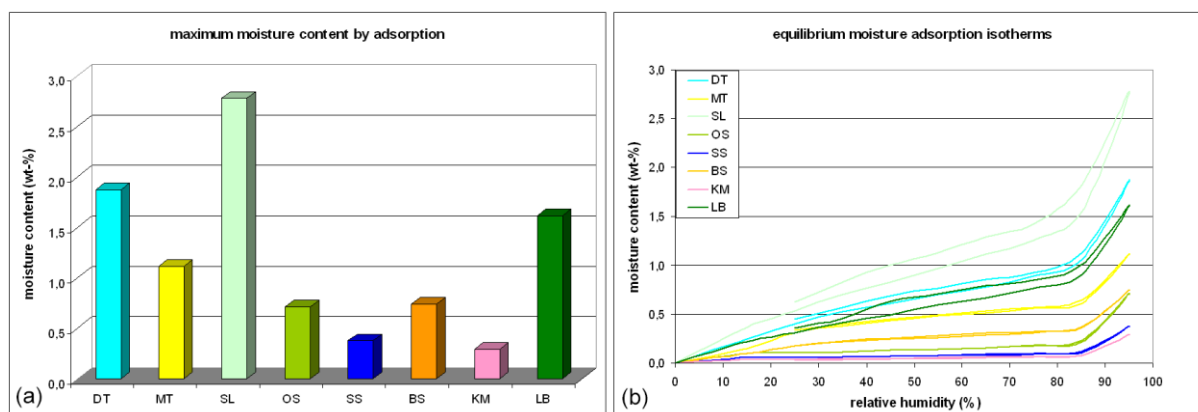


**Figure 5.5 (a)** The diagram shows the moisture content of the stones by moisture adsorption (sorption) at 95% relative humidity. **(b)** Equilibrium moisture sorption isotherms, showing a significant increase at relative humidity levels > 85% reflecting capillary condensation. Drachenfels trachyte (DT), Montemerlo trachyte (MT), Stenzelberg latite (SL), Obernkirchen sandstone (OS), Schlaitdorf sandstone (SS), Bozanov sandstone (BS), Krensheim Muschelkalk (KM) and Londorf basalt lava

The highest mass increase (at 95% RH) is shown by the Stenzelberg latite with a value of 2.78 wt. %, whereas the lowest value was determined for the Krensheim Muschelkalk (0.29 wt. %) (Tab. 5.1; Fig. 5.5a). The Drachenfels trachyte and Londorf basalt lava also show a relatively high water adsorption, whereas the Montemerlo trachyte, Obernkirchen and Bozanov sandstones have a medium water adsorption. Schlaitdorf sandstone only shows a small mass increase. Stenzelberg latite, Londorf basalt lava and Drachenfels trachyte show a hysteresis in their sorption-desorption-behavior: The decrease of mass is less than the increase; indicating that the stone material dries slower with descending relative humidity and still contains a residue of moisture as a possible indication of capillary condensation (Fig. 5.5b). Stenzelberg latite probably shows the effect of capillary condensation, whereas the Montemerlo trachyte and Londorf basalt lava may possibly show little effect as well.

### 5.3.4 Water vapor diffusion resistance

The water vapor diffusion resistance is defined by the vapor diffusion resistance coefficient ( $\mu$ -value). It was measured at 20°C by using the wet cup-method on disk-shaped stone samples (Ø 50 mm, 10 mm in thickness) according to the standard EN ISO 12572. The water vapor diffusion resistance value indicates to what extent the transport resistance of the water vapor is higher in rock than in air. With the help of the wet-cup method, the  $\mu$ -value is determined at 50 and 95% relative humidity (RH). This range represents the central European climate.

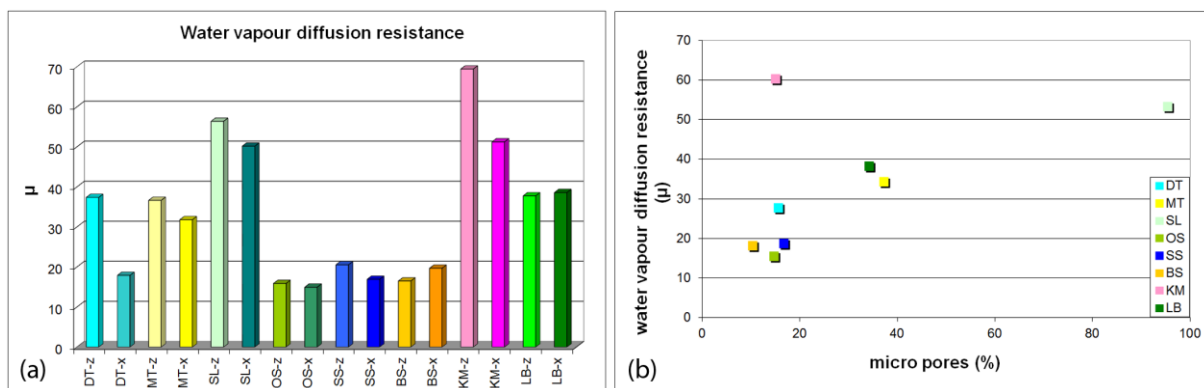


**Figure 5.6 (a)** Water vapor diffusion resistance ( $\mu$ ) of the investigated stones, perpendicular (z) and parallel (x) to the bedding of the stones; **(b)** average water vapor diffusion resistance in correlation with the percentage of micropores of the investigated stones. The diagrams indicate the diversity of the stone properties and show a correlation of higher water vapor diffusion resistance due to a higher amount of micropores. Drachenfels trachyte (DT), Montemerlo trachyte (MT), Stenzelberg latite (SL), Obernkirchen sandstone (OS), Schlaitdorf sandstone (SS), Bozanov sandstone (BS), Krensheim Muschelkalk (KM) and Londorf basalt lava

Of the investigated stones the Krensheim Muschelkalk and Stenzelberg latite have a high resistance to water vapor diffusion. Drachenfels and Montemerlo trachyte as well as the basalt lava show a medium resistance, respectively. The sandstones have the highest permeability of the investigated stones (Tab. 5.1; Fig. 5.6a). The Drachenfels trachyte shows a remarkable directional dependence of water vapor diffusion resistance which could mainly be controlled by the flow fabric (Tab. 5.1). A higher resistance correlates with a higher amount of micropores (Fig. 5.6b): capillary condensation takes place in micropores, which holds back water due to solvent water diffusion. This leads to capillary suction (retention), which is much slower than water vapor diffusion (Snethlage 1984). Only the Krensheim Muschelkalk does not fit this correlation.

### 5.3.5 Hydric and hygric dilatation

The length and volume increase and decrease of rocks with changes of moisture is well-known as hygric (in the range between 0% and 95% RH) and hydric (water saturated) expansion and contraction (Delgado Rodrigues and Charola 1996; Weiss et al. 2004; Ruedrich et al. 2010). Hydric dilatation is measured on cylindrical stone samples (Ø 20 mm,

50 mm in length) completely immersed in water. An overview of the hygric dilatation on the different stone materials is given in Table 5.2. In general, hygric dilatation is low. The highest dilatation is determined at the Montemerlo trachyte with a value of 0.316 mm/m perpendicular to the bedding. High hygric swelling was measured in the Drachenfels trachyte, Stenzelberg latite and Londorf basalt lava. The Obernkirchen sandstone has medium hygric swelling, whereas the other two sandstones, Schlaitdorf and Bozanov sandstone have low hygric dilatation. The length change of the Krensheim Muschelkalk is within the accuracy of measuring (Tab. 5.2).

**Table 5.2** Thermal expansion coefficient and hygric dilatation.

Rock type	Thermal dilatation coefficient (expansion)			Hygric dilatation	
	x-( $10^{-6}K^{-1}$ )	z-( $10^{-6}K^{-1}$ )	anisotropy (%)	x - (mm/m)	z – (mm/m)
Drachenfels trachyte	5.32	6.05	12.0	0.253	0.236
Montemerlo trachyte	6.25	4.65	25.5	0.291	0.316
Stenzelberg latite	9.41	7.36	21.7	0.196	0.230
Obernkirchen sandstone	11.60	12.17	4.6	0.089	0.060
Schlaitdorf sandstone	9.65	11.96	19.3	0.025	0.025
Bozanov sandstone	8.78	8.65	1.5	0.027	0.013
Krensheim Muschelkalk	4.75	6.82	30.3	0.000	0.005
Londorf basalt lava	5.32	5.78	8.0	0.226	0.186

Generally hygric dilatation is anisotropic in nature and values for anisotropy of about 50% are reported in the literature (Rüdrich et al. 2005). With respect to the rocks from the Cologne cathedral, only the Bozanov and Obernkirchen sandstones show a medium anisotropy. Furthermore, the expansion of the different stones is time dependent: Londorf basalt lava, Drachenfels trachyte, Bozanov and Schlaitdorf sandstones, have already reached over 50% of their maximum expansion perpendicular to the bedding in the first 30 minutes. Montemerlo trachyte attained 88% of the total expansion in that time. Obernkirchen sandstone already expanded to its whole extent after five minutes. Stenzelberg latite has only reached 13% in the first 30 minutes. This time dependence is ascribed to different pore space properties. Where stones with well interconnected pores and relatively high porosities show a fast expansion, stones with a less well interconnected pore space have a slower expansion (Rüdrich et al. 2005).

Hygric dilatation processes occur with changes of the relative humidity. The measured hygric expansion differs from hygric expansion. Low hygric dilatation values are shown by the Schlaitdorf (0.063 mm/m) and the Bozanov (0.010 mm/m) sandstones. Moisture expansion in the Krensheim Muschelkalk is negligible (0.001 mm/m). Obernkirchen sandstone has a somewhat higher expansion result (0.065 mm/m). Stenzelberg latite shows high hygric expansion with dilatation in the z-direction (perpendicular to bedding) of 0.231 mm/m. The

Londorf basalt lava also has a high hygric expansion (0.185 mm/m). Hygric dilatation in the Montemerlo trachyte (0.142 mm/m) is slightly higher than that of the Drachenfels trachyte (0.110 mm/m). With increasing relative humidity a sharper increase of hygric expansion can be observed at around 80 - 85% relative humidity (Fig. 5.7).

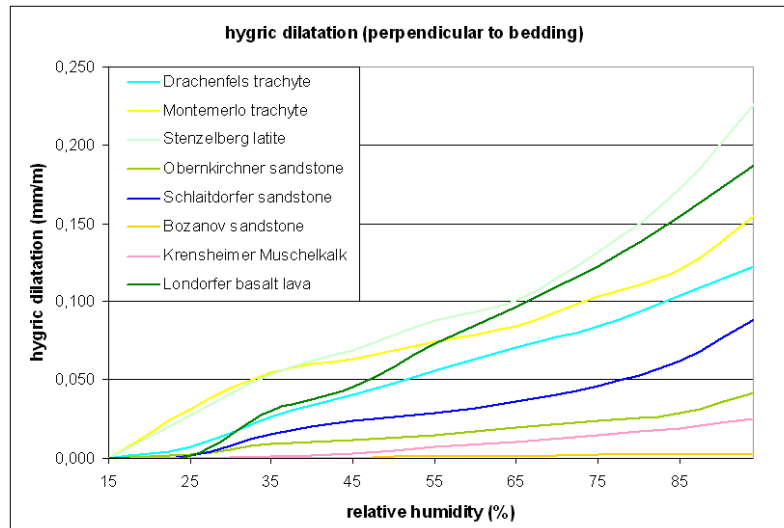


**Figure 5.7** Hygric dilatation perpendicular to the bedding of the stones with relative humidity ranging of 15–95%

## 5.4 Thermal Dilatation

Thermal expansion was measured on cylindrical samples ( $\varnothing$  15 mm, 50 mm in length) within five consecutive heating cycles from 20°C to 95°C. The length variation (resolution  $< 1 \mu\text{m}$ ) was determined as a function of temperature and was measured in two directions: perpendicular (z-direction) and parallel (x-direction) to the bedding. The thermal expansion coefficient was calculated ( $\alpha = \Delta l / l \times \Delta T$ ) as well as the residual strain ( $\epsilon_{rs} = \Delta l_{rt} / l$ ) after one heating cycle (Zeisig et al. 2002; Koch and Siegesmund 2001). Anisotropy was determined by the difference of the expansion coefficients in both directions.

Drachenfels trachyte and Londorf basalt lava show low thermal expansion coefficients and only little anisotropy. Montemerlo trachyte and Krensheim Muschelkalk display low expansion values and pronounced anisotropy. Bozanov sandstone has a medium coefficient but no anisotropy. Stenzelberg latite has a medium thermal expansion coefficient and anisotropy of about 21%. Obernkirchen and Schlaitdorf sandstones show high thermal expansion coefficients, only the latter displays an anisotropy of about 19% (Tab. 5.2). No residual strain was observed for the investigated stones.

## 5.5 Mechanical properties

### 5.5.1 Uniaxial compressive strength

The uniaxial compressive strength was measured in two directions (z-direction: perpendicular and x-direction: parallel to the bedding of the rock) on planar cylindrical samples ( $\varnothing$  50 mm, 50 mm in length;  $r/d = 1$ ) according to the standard DIN EN 1926. Based on the scale<sup>3</sup> effect the compressive strength ratio may differ up to 20% higher by measuring samples with  $r/d$ -ratio of 1 instead of  $r/d$ -ratio of 2 (Peschel 1983). The load was applied with a strain rate of 1000 N/s until failure. The compressive strength varies between 45.1 N/mm<sup>2</sup> and 126.4 N/mm<sup>2</sup> (Tab. 5.3). The Stenzelberg latite has the highest compressive strength (126.4 N/mm<sup>2</sup>), while the strength values for the Krensheim Muschelkalk, Schlaitdorf and Bozanov sandstones are less than 50 N/mm<sup>2</sup>. Only the Stenzelberg latite belongs to the high strength rocks, while rocks with compressive strength values between 55 N/mm<sup>2</sup> and 70 N/mm<sup>2</sup> belong to the low strength rocks, as there are the Drachenfels trachyte and Londorf basalt lava (Mosch 2008). Obernkirchen sandstone and Montemerlo trachyte display higher uniaxial compressive strength values. Except for the Obernkirchen sandstone and the Montemerlo trachyte a directional dependence of the compressive strength is less pronounced in the other samples (Tab. 5.3).

**Table 5.3** Uniaxial compressive strength, tensile strength and flexural strength of the investigated rocks in non-weathered condition.

Rock type	Uniaxial compressive strength (N/mm <sup>2</sup> )		Tensile strength (N/mm <sup>2</sup> )		Flexural strength (N/mm <sup>2</sup> )	
	Z	X	Z	X	Z	X
Drachenfels trachyte	65.54	66.59	3.087	3.674	5.999	6.100
Montemerlo trachyte	75.53	84.75	3.439	3.680	6.725	8.195
Stenzelberg latite	126.41	120.02	9.735	8.621	15.707	9.881
Obernkirchen sandstone	86.72	76.29	4.594	4.669	7.992	6.825
Schlaitdorf sandstone	47.59	51.44	3.256	3.343	6.492	5.733
Bozanov sandstone	45.10	52.08	3.462	3.343	3.975	4.410
Krensheim Muschelkalk	48.35	52.74	4.498	4.544	8.467	6.763
Londorf basalt lava	63.10	72.18	5.099	5.921	12.567	12.749

### 5.5.2 Flexural strength

Flexural strength is an important mechanical property for natural building stones. Failures due to bending stress are more common than those caused by compressive or shear stresses. The flexural strength values are usually lower than the compressive strength values for a rock. Mosch (2008) mentions a correlation of 10 : 1 for the compressive to the flexural strength. Flexural strength (one point bending) was measured according to the standard DIN EN 12372 on oblong samples (150 mm, 40 mm, 25 mm) in two direction (perpendicular and parallel to the bedding of the rock). The flexural strength values of the investigated rocks

cover the range between  $4.0 \text{ N/mm}^2$  (Bozanov sandstone) and  $15.7 \text{ N/mm}^2$  (Stenzelberg latite) (Tab. 5.3). Londorf basalt lava has a high flexural strength, whereas the Schlaitdorf sandstone, the Drachenfels and Montemerlo trachytes show medium flexural strength values. The Obernkirchen sandstone and the Krensheim Muschelkalk display somewhat higher flexural strength values. The values are listed in Table 5.3.

### **5.5.3 Tensile strength**

In order to obtain the values of the tensile strength, measurements were made using the Brazilian Test according to the standard DIN 22024. Investigations were performed on disk-shaped specimens ( $\varnothing 40 \text{ mm}$ ,  $20 \text{ mm}$  in thickness). The load was applied with a strain rate of  $30 \text{ N/s}$ . Measurements were applied in two directions (perpendicular and parallel to the bedding of the rock). The tensile strength varies between  $3.1 \text{ N/mm}^2$  (Drachenfels trachyte) and  $9.7 \text{ N/mm}^2$  (Stenzelberg latite), depending on the sample and direction of load with respect to the rock fabric. Of the investigated stones Londorf basalt lava has a medium tensile strength. Obernkirchen, Schlaitdorf and Bozanov sandstones, Krensheim Muschelkalk and Montemerlo trachyte have a lower tensile strength (Tab. 5.3). Many rocks show the smallest tensile strength perpendicular to the bedding. In the case of the samples investigated, the heterogeneity may also play an important role in explaining the observed data (Tab. 5.3). However, the anisotropy of all the rocks is not very well pronounced.

## **5.6 Deterioration phenomena and physical decay processes**

Due to its building history many different building stones were implemented at the Cologne cathedral, which show different deterioration behavior. These stones differ not only in their genesis, but also in their visual appearance, their mineralogical composition as well as in their porosity features and rock fabric, and therefore also in their petrophysical properties, which again determine the deterioration behavior. Furthermore, exposition, climatic situation, industrial-based pollution and building physics play a major role (for further discussions see Siegesmund and Snethlage 2011).

A high porosity in connection with a high water uptake is considered as having a high damage potential. High water uptake values (w-value) combined with a high saturation coefficient (s-value) are the first indicators for a possible susceptibility to weathering, or in other words, pollutant transport, hygric and hydric expansion, frost damage and salt crystallization in the pore spaces, etc. Along with the capillary water uptake, an important role is also played by the sorption (water derived from the absorbed humidity) and desorption (water released in relation to the relative humidity). This determines, among others the drying behavior, which is influenced by the capillary transport, the water vapor diffusion and the critical moisture of the stone.

The capillary absorption capacity of a porous stone is defined by its water uptake coefficient (w-value). This is a process driven by the capillary forces that originate in the micro- and capillary pores (Klopfer 1985). Rocks with a high amount of capillary pores are expected to have a high w-value, which means they have the capacity to rapidly absorb water by capillary uptake in the pore spaces. Stones with low capillary absorption (suction) have a w-value of  $< 0.5 \text{ kg/m}^2 \cdot \sqrt{\text{h}}$ , those with medium absorption range from  $0.5 \text{ kg/m}^2 \cdot \sqrt{\text{h}}$  to  $3.0 \text{ kg/m}^2 \cdot \sqrt{\text{h}}$  and stones showing strong water suction have w-values  $> 3.0 \text{ kg/m}^2 \cdot \sqrt{\text{h}}$  (Snethlage 2005). A w-value of  $> 3.0 \text{ kg/m}^2 \cdot \sqrt{\text{h}}$  suggests a sufficient uptake of water in the pore spaces to keep the stone moist for a long time and to mobilize any salts present. The importance of this parameter cannot be underestimated, since a strong absorption capacity simultaneously means that a high pollutant uptake and distribution occurs in the pore spaces. This is the reason why dense building stones will sometimes weather on the surface, whereas those with a good absorption capacity will deteriorate at depth.

The water saturation coefficient (s-value) gives an approximate value for the frost resistance of natural building stones. Hirschwald (1912) proposed the following guideline values using the saturation coefficient: when  $s < 0.80$  the rock is weathering and frost resistant; for values ranging between 0.80 and 0.90 it is uncertain and further investigations are necessary; and when  $s > 0.90$  the rock is not frost resistant. Similar limitations are given by the standard DIN 52103: a rock with  $s < 0.75$  is considered weathering resistant and susceptible to weathering when  $s > 0.9$ . A s-value  $> 0.75$  indicates that if the water supply is high enough, the pore space is filled with water to a higher degree and frost action could happen.

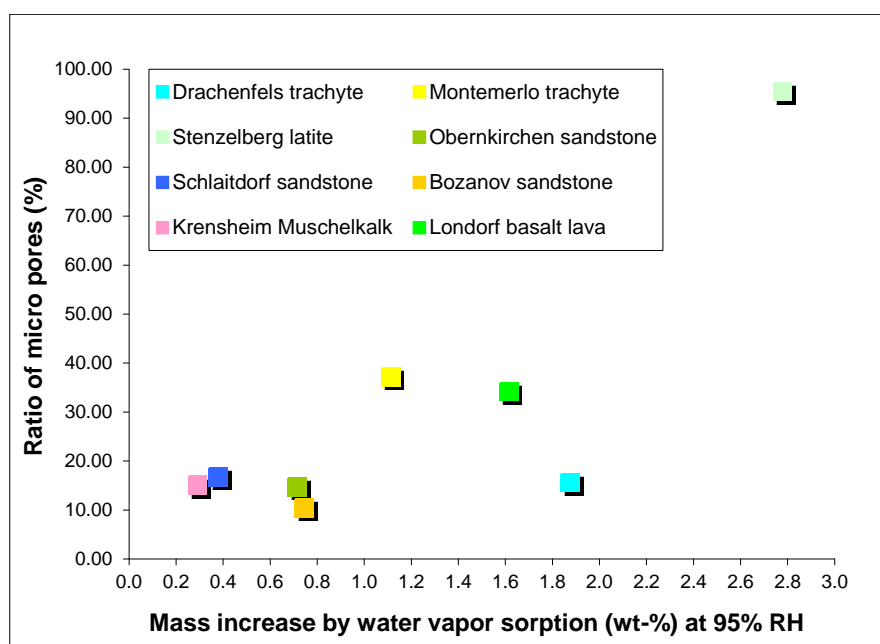


**Figure 5.8** The investigated stones of the Cologne cathedral show a tendency towards a higher percentage of micropores correlated to a higher water adsorption due to capillary condensation. However, the ratio of micropores in the Drachenfels trachyte would suggest a lower sorption.



Sorption is the adsorptive addition of water from the air. This occurs under isothermic conditions in two steps: 1. Adsorption of molecular water films on the inner surface of the stone material, and 2. Capillary condensation in pores  $< 0.1 \mu\text{m}$  in size (Kraus 1985a). The pore size distribution gives a clue to the water uptake by adsorption: with an increasing amount of micropores the sorption increases as well due to capillary condensation, assuming the pore space communicates well (Fig. 5.8).

Pore size distribution and porosity of a rock are responsible for water and moisture uptakes as well as water transport. Generally, pores are divided due to their size into different classes: micropores ( $< 0.1\mu\text{m}$ ), capillary pores ( $0.1\mu\text{m} - 1\text{mm}$ ) and macropores ( $>1\text{mm}$ ) (Klopfer 1985). When capillary pores are present, water can be taken up and rises by capillary action. Fluid and capillary transport mechanisms are the main driving factor. On the other hand, micropores adsorptively accumulate water from the air at their inner surface (capillary condensation). Surface and solution diffusion are the main transport mechanisms (Siegesmund and Dürst 2011).

The drying of natural building stones is a function of the capillary transport, the water vapor diffusion and the critical moisture of the stone. According to Kraus (1985), when a water-saturated rock dries, the relative rapidly absorbed water from precipitation is by comparison released at a slower rate. This lengthy process is due to the capillary absorbed water being released to a large extent by vapor diffusion. The first stage in the drying of a stone occurs over the rock surface, as an evaporation surface, provided that the capillary water is replenished from the deeper parts of the rock. When this capillary thread tears off (critical moisture), water vapor diffusion transport starts. Thus, low critical moisture indicates a faster drying natural stone. In this case, the capillary transport forces are much stronger. At a value less than the critical moisture, the significant determining factor for the drying process is the water vapor conductivity. When a stone has a high water vapor diffusion resistance, the water release becomes progressively slower. This can be correlated to the pore size distribution, whereby a high resistance can be expected as a result of a large proportion of micropores. Since the capillary water is condensed and bound, the evaporation of any water from the stone material is very difficult (Snethlage 1984). Furthermore the connectivity of the pore space plays a certain role. The process of drying in this second phase diminishes more and more, because the distances of water vapor diffusion transportation become greater until moisture reaches equilibrium with the surrounding air. Besides water vapor diffusion also surface and solution diffusion takes place (Kraus 1985a). Therefore the length of the first drying phase is mainly determined by the percentage of capillary active pores, besides external climatic factors, e.g. wind, temperature and insolation etc., which have major impact, the second phase is determined by water vapor diffusion properties; considering the general water uptake and saturation properties (w- and s-values) and the connectivity of the

pore space. Furthermore Kraus (1985a) mentions, that with a capillary active and well communicating pore system, water may even be transported further into deeper zones of the stone, although the active water supply already ended.

Moisture expansion (hydric and hygric dilatation) describes the length or volume change, which most natural building stones undergo by wetting in correspondence to climatic factors of the environment. The processes responsible are not yet ultimately defined; the volume change may be attributed to the swelling of clay minerals as well as to disjoining pressure. This latter effect is relevant for all minerals, and significant moisture expansion is correlated to a large amount of micropores ( $< 0.1 \mu\text{m}$ ) (Ruedrich et al. 2010). According to Ruedrich et al. (2005) hygric dilatation is essentially a reversible process, i.e. no residual strain is ascertained after reducing relative humidity back to the starting value. This only applies for demineralized water, which means by the presence of damaging salts in building stones, these processes might be affected remarkably.

A number of deterioration phenomena can be traced back to the volume increase of natural building stones by moisture expansion, e.g. scaling, flaking and granular disintegration. In most cases, building stones show an irregular moisture distribution, whereby moisture gradients diverge leading to a build-up of strain and resulting decay.

Rocks show volume changes due to changing moisture contents, as well they undergo length or volume changes due to changes of temperature. This process is determined by the individual properties of the mineral content and composition but also by the structure and the rock fabric of the natural building stone. The volume change does not necessarily increase linearly to the temperature, which means that the linear thermal expansion coefficient is often only valid for a certain temperature interval (Siegesmund and Dürrast 2011). The residual strain is of pronounced relevance in terms of deterioration resistance. A permanent length change of building stones after returning back to the initial temperature can be traced to microcracking and thus indicates potential decay (Ruedrich et al. 2011).

Strength properties such as compressive, flexural and tensile strengths are rock parameters, which also limit the durability of dimension stones. Material failure occurs, when stresses induced by mechanical weathering processes exceed the strength of the material. In respect of frost and salt deterioration resistance, damage occurs when the stresses due to salt and ice crystallization exceed the tensile strength (Ruedrich et al. 2005). The strength properties correlate to the grain fabric cohesion. Important fabric parameters for the strength are the porosity, the pore size distribution, the grain size, the grain contacts, the type and state of cementation as well as a preferred grain boundary orientation.

Drachenfels trachyte has a medium porosity, a low capillary water uptake and a high *s*-value, which might suggest certain sensitivity to frost-related weathering. Luckat (1973a) demonstrated that the Drachenfels trachyte is especially sensitive to salt weathering processes. Flaking and scaling can be pronounced, especially in the direct neighborhood of carbonate replacement stones (Kraus 1985a; von Plehwe-Leisen et al. 2007). Flaking and scaling are often noticeable as a predecessor for further accelerated decay by fissures, cracks, crumbling and material loss.

The water uptake by adsorption of the building stone is in a medium range, moisture expansion is relatively high, and with 84% the percentage of capillary active pores is quite high. In terms of drying of the Drachenfels trachyte, water vapor diffusion transport mechanisms already start at relatively high water content ( $> 3$  wt-%) of the stone (Kraus 1985a). In respect of its water vapor diffusion resistance a long drying time is observed, showing after 15 days no complete drying (Kraus 1985a). Furthermore, Kraus (1985a) mentioned, that building stones exposed to the natural environment experience a rewetting before they might dry out completely. While uniaxial compressive strength is in the medium range of the investigated stones, tensile and flexural strength are low. For the Drachenfels Trachyte a continuous high water content, and therefore sufficient water supply as “support” for deterioration mechanisms exists, which presumably are due to the high *s*-value, water uptake by adsorption, vapor diffusion resistance and retarded drying. Here different moisture gradients are assumed, whereby hydric dilatation has an effect to a certain extent. In the context of electrolytes i.e. ions dissolved from other carbonate stones nearby for example, salt deterioration processes might be enhanced in addition to pollution. The low strength values, especially for the tensile strength, indicate a modest resistance against weathering.

Montemerlo trachyte has been used at the Cologne cathedral since 2005 and still does not exhibit any structural damage. However, Lazzarini et al. (2008) reported on exfoliation and flaking, powdering and alveolic weathering for the Montemerlo trachyte in Venice (Italy) mainly related to salt deterioration. The relatively low water uptake only allows a certain uptake of pollutants but porosity and pore size distribution assume a prolonged drying time. Therefore crystallization of salts can occur and due to the low tensile strength, damage is possible.

The typical deterioration phenomenon of the Stenzelberg latite is a scaling of 2-3 mm thick scales (Fig. 4.5e). Stenzelberg latite may have a low capillary water uptake, but also a high water saturation (76%), which indicates a certain liability to frost-related decay. Sorption is slow, but shows high values and hysteresis, which implies a decelerated moisture release. The high percentage of micropores underlines the slow moisture uptake and also release. A further retardation and especially zoning of these processes is to be expected due to the technical surface treatment and the material compaction involved. Thereby gradients of

moisture, material consistency and strength are evolved, which could lead to surface parallel detached material layers of a few millimeter in thickness due to frost shattering. Hydric dilatation might have a certain but minor impact.

Obernkirchen sandstone is mentioned as a building stone with a high resistance against weathering. It mainly shows superficial deterioration phenomena, which does not have a severe structural impact, except of the gypsum crusts (Fig. 4.5b). The formation of these crusts indicates a strong pollution imission at the Cologne cathedral in the past. Due to the application of a coat of paint, to color adjust to the Krensheim Muschelkalk, applied in the 1930's, surface parallel scaling of approximately 1-2 mm occurs. Spalling along edges near to joints (Fig. 4.5c) is presumably due to mechanical impact of strain, caused by the joint fill material. However, Morales Demarco et al. (2007) determined a strength loss due to water saturation of about 14% for the Obernkirchen sandstone.

Schlaitdorf sandstone shows characteristic deterioration in the form of rounding and notching in context with scaling and granular disintegration to sand (Fig. 4.5d). Kraus (1985) describes the decay of Schlaitdorf sandstone due to loss of cementation through the formation of damaging salts, i.e. gypsum due to high SO<sub>2</sub>-immision. The Schlaitdorf sandstone has a high porosity and a high w-value, which determines the high water uptake. The formation of gypsum in the pores leads to accumulation of damaging salts and thereby to scaling and surface recession. Efes (1980) observed an increase of smaller pores near the surface and a reduction of water vapor diffusion up to 50%, leading to retarded moisture release. With a saturation coefficient of 0.64 the Schlaitdorf sandstone is not vulnerable to frost attack. Kraus 1985a detected in the Schlaitdorf sandstone a second drying phase by water vapor diffusion, which starts at a water content of < 2 wt-%. During this drying phase by water vapor diffusion, a pronounced accumulation of not readily soluble gypsum salts exists in the pore space.

At present the Bozanov sandstone shows little evidence of decay except spalling along the edges, which may occur during the mounting of the wettened building stones. This stone has only been implemented at the Cologne cathedral since 2001. Přikryl et al. (2010) have reported on sanding, scaling, flaking, crust formation, blistering, fracturing, salt efflorescence, alveoli formation for the medium-grained Bozanov sandstone. They detected a high amount of water soluble salts responsible for blistering, granular disintegration, scaling and flaking. Other weathering processes described are: cyclical wetting and drying, freeze-thaw cycles, a different thermal expansion of insulated stone surfaces and less heated interior areas of the stone. The petrophysical data of the present investigations support these observations. Although Bozanov sandstone does not have a very high water saturation degree, the capillary water uptake is high. Thus, water supply is high, promoting frost-related weathering as well as possible high loads of damaging salts leading to salt deterioration phenomena.

Since strength values are low, these decay processes may propagate to a vast extent. The thermal dilatation coefficient supports the assumption of structural deterioration due to different temperature gradients.

Krensheim Muschelkalk and Londorf basalt lava are building stones with a high resistance against weathering. The main deterioration phenomenon of the Krensheim Muschelkalk at the Cologne cathedral is black surface crusts, which occur solely in rain protected areas (Fig. 4.5f). Due to the decrease of SO<sub>2</sub>-emission over the last several years, this decay probably will regress as well (Siegesmund et al. 2007; Török et al. 2011). The accumulated pollution of the past certainly affects historical monuments in the present but also in the future. Krensheim Muschelkalk shows microkarst phenomena, which are typical for carbonate stones and are also related to an acidic environmental impact.

Londorf basalt lava only is affected by pronounced microbiological growth, which is associated with a great number of large pores (Grimm 1990).



## 6 Aspects of physical weathering

As described in the introduction, the deterioration of natural building stones is controlled by physical, chemical and biological processes. In the following chapter experiments and tests are described to determine the behavior of the building stones towards extrinsic physical impacts: namely, drying behavior, frost resistance and salt weathering sensitivity.

The drying of a porous stone is very much dependent upon the extrinsic environmental conditions and is controlled by intrinsic properties, such as pore space characteristics as well as mineralogical composition. The drying behavior itself has an influence on the general weathering behavior of a stone because, in general, the deterioration processes of natural building stones are moisture correlated. Thus, the resistances to freeze-thaw cycles and cyclic salt load are also governed by the drying behavior of the porous material. Major physical deterioration processes are ascribed to salt and ice crystallizations in the pore spaces of natural building stones. The deterioration phenomena assigned to these physical damage processes are flaking, scaling, exfoliation and disintegration, as well as sanding and granular disintegration (Rüdrieh et al. 2005).

Salt-Weathering tests and freeze-thaw cycles comprise two laboratory experiments indicating the resistance of the un-weathered stone material towards the impact of salt and frost.

### 6.1 Drying properties

Generally, the process of the moisture release of porous materials is divided into two phases (Vos 1978; Snethlage 1984; Klopfer 1985; Kraus 1985a). The first phase displays a period of rapid drying and is dominated by the capillary transport of water from the inner sections of the stone towards the stone surface where moisture evaporates. This phase continues as long as the capillary water supply of liquid water towards the stone surface equals the surface evaporation rate. The evaporation rate correlates to the gradient of the water vapor partial pressure at the stone surface and the environment. Thus, this first phase predominantly depends upon the environmental conditions (temperature, relative humidity and air turbulences) (Kraus 1985a; Snethlage 1984). The point at which the material moisture content does not allow any further capillary transport to the surface is called the “critical moisture content” (Vos and Tammes 1968). Larger pores have a reduced capillary suction than smaller pores; thus, the capillary transport – the *capillary thread* – towards the stone surface is cut after a relatively short time (Klopfer 1974; Kraus 1985a). Franzen and Mirwald (2004) observed an increase in the drying rate in rough stones due to the enlarged evaporation surface.

In the second drying phase, the release of moisture decelerates continuously and is dominated by water vapor transport and surface solution diffusion transport within the pore

space towards the surface of the stone. This phase mainly depends on intrinsic parameters, such as water vapor diffusion transport – namely the resistance to it, the pore size distribution, the interconnectivity of the pores and the surface tension.

These two main phases can be subdivided: the first phase is divided into two segments (Franzen and Mirwald 2004); the segment *a* shows a steep decrease in the drying rate. Franzen (2002) described it as a laboratory artifact. It may also resemble the first minutes of the drying of a natural building stone after a heavy rain fall. In segment *b*, the drying rate increases and the curve shows an almost linear progression, indicating a steady moisture release of the stone. On rough stones, the drying rate may even increase (Franzen and Mirwald 2004). Segment *b* is the period of drying ascribed to the capillary transport mechanisms from the inner areas of the stone towards the surface, when the water supply from inside balances the evaporation rate at the surface of the stone (Snethlage 1984; Kraus 1985a; Poschlod 1990; Tournier et al. 2000; Franzen and Mirwald 2004). This ends when the critical moisture is reached (Vos 1978); the drying rate decreases significantly and the second main drying phase starts. Tournier et al. (2000) and Franzen and Mirwald (2004) divided this second phase into two sub-segments: the first is indicated by a sharper decrease of the drying rate, when drying is controlled by solution diffusion transport and water vapor diffusion transport. In the last segment, the curve tapers off along an asymptotic course, when vapor transport mechanisms are dominant. Drying ends when the moisture content in the stone is at equilibrium with the ambient air.

For the present measurement of drying, i.e., the moisture release under atmospheric conditions, cubic samples (65 mm) of the investigated stones were water saturated (analogous DIN 52102:2006-02) and, afterwards, dried under laboratory conditions (drying over 6 sides, no air turbulences in a closed cabinet, 23°C, app. 80-85 % RH). The weight loss was measured continuously.

The results of the drying tests of the eight investigated stones are shown in figure 6.1. For each sample, two curves are plotted: the continuous line displays the decrease of water content over time and the dashed line shows the drying rate, which is the first derivation of the weight loss in respect to time (Franzen 2002; Franzen and Mirwald 2004).

The four stages of drying are shown in the curves of the investigated stones except for Stenzelberg latite and the Londorf basalt lava (Fig. 6.1). With the curves of the latter, segment *a* can be discerned whereas the other segments of the drying process cannot be distinguished. Due to the high ratio of micropores in the Stenzelberg latite (95 %) and the lack of connectivity of the pore space in the Londorf basalt lava (Kraus 1985a), these stones are more characterized by vapor and solution diffusion transport mechanisms than by capillary transport mechanisms, as indicated by the low *w*-values (Tab. 5.1).



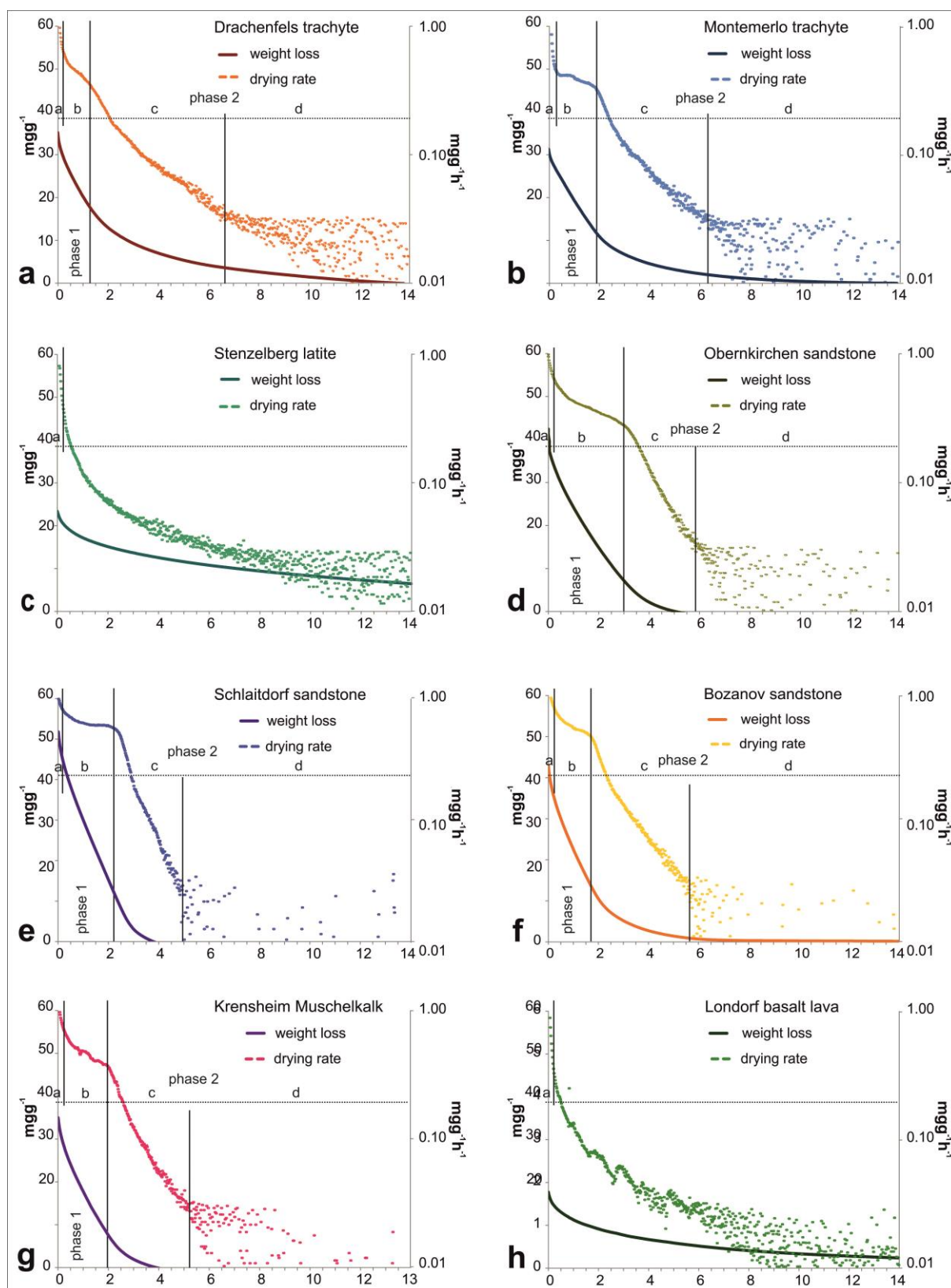


**Figure 6.1** Drying curves of the investigated stones: a Drachenfels trachyte; b Montemerlo trachyte; c Stenzelberg latite; d Obernkirchen sandstone; e Schlaitdorf sandstone; f Bozanov sandstone; g Krenshelm Muschelkalk; h Londorf basalt lava. The continuous line displays the decrease of water content over time and the dashed line shows the drying rate (note log-scale in right y-axis). Drying phases 1 and 2 as well as the four segments a – d are shown.

The curves of the other six investigated stones clearly show the four different stages of drying (Fig. 6.1). In the Drachenfels trachyte, the end of the first drying phase is not as significant as in the other stones. Similar to the Montemerlo trachyte, the Drachenfels trachyte released about 50% of its water content at the point when water vapor transport controlled drying began (Fig. 6.1a and b). The Krensheim Muschelkalk lost about 60% of its water content by the end of the first drying phase (Fig. 6.1g). Comparing the three sandstones, the Obernkirchen released already app. 85%, the Schlaitdorf app. 75% and the Bozanov sandstone app. 70 % of its water content when the capillary supported drying ended (Fig. 6.1d-f).

If the duration for the first drying phase of the investigated stones – i.e., until *critical moisture content* is reached – is compared with the data given in the literature, the present test shows longer durations. For the Drachenfels trachyte, 1.3 days; for the Montemerlo trachyte, 1.9 days; for the Obernkirchen, 3 days; for the Schlaitdorf sandstone, 2.2 days; for the Bozanov sandstone, 1.7 days; and for the Krensheim Muschelkalk, 2 days were measured. Kraus (1985a) ascertained a first drying phase of 0.6 days for the Drachenfels trachyte; for the Schlaitdorf sandstone, 0.85 days, and for the Obernkirchen sandstone, 0.75 days. For the latter, Franzen (2002) measured 0.4 days until end of the first drying phase.

These different durations are very much dependent upon the ambient conditions. As mentioned earlier, this first phase depends upon environmental conditions (temperature, relative humidity and air turbulences). The moisture release of Obernkirchner sandstone was tested at different environmental conditions (Snethlage 1984). At 20°C and 40% relative humidity, drying accelerates with the increasing velocity of wind: at a calm, the critical moisture content is reached after 10 h; with a wind velocity of 2 m/s after 4 h, and with a 4 m/s velocity after 1 h. Snethlage (1984) also showed the correlation of the evaporation surface with the drying rate. For the Obernkirchner sandstone - as an example - it was shown that the drying over five sides of the stone sample almost doubled the drying rate in comparison with the drying over one side until *critical moisture content* was reached (Snethlage 1984). As shown, the various *critical moisture contents* are reached by different drying rates at different times, indicating that this material parameter is more dependent upon the surrounding conditions. Thus, for drying measurements the experimental conditions were sought to be monitored. In terms of the drying behavior of natural building stone in the built environment, the release of moisture is very sensitive to building-physical and microclimatic condition changes.



**Figure 6.2** Drying was measured in a closed cabinet

In the present experiment, the drying was measured in a closed cabinet (Fig. 6.2). Despite a relatively high temperature (23°C) and the drying over six sides of the cubic sample, the relative humidity was high (80-85%), indicating a low water vapor partial pressure gradient; thus, the evaporation rate was very low.

The drying measurements show high residual moisture contents for the Stenzelberg latite (18.5%) and the Londorf basalt lava (13.2%), indicating that the stone does not dry completely. The residual water is available for potential moisture-related deterioration processes. The elevated residual water content can be ascribed to increased water vapor diffusion resistance due to the elevated ratio of the micropores of these stones and a lack of interconnectivity of the pore space. As mentioned before, the experimental conditions included a high RH; thus, the equilibrium water content at the end of the measured drying process is reflected. This correlates well to the ascertained data of the relatively high water adsorption of these four stones (Tab. 5.1).

If the drying behavior of the two trachytes is compared and correlated with the petrophysical properties, the two stones show similar curves (Fig. 6.1a and b). The more linear course of the curve in segment *b* correlates well with the ascertained *w*-values (Tab. 5.1), indicating less capillary activity for the Drachenfels trachyte.

The drying behavior of the three sandstones shows a pronounced first drying phase and a significant linear curve for segment *b* (Fig. 6.1c and d). The rough stone surface of the Schlaitdorf sandstone may contribute to a slightly elevated drying rate in this segment (Fig. 6.1c). The saturation degree of the three stones is similar but the capillary water uptake is

much higher in the Schlaitdorf and Bozanov sandstone (Tab. 5.1), which is reflected in the linear course of the curve in segment *b* indicating the capillary activity. The fourth segment *d* of the drying process becomes very irregular, probably due to the smaller content of micropores within the stones and inconstant water vapor and surface solution diffusion transport mechanisms.

The Krensheim Muschelkalk stays somewhat in the mid-field of the investigated stones. The four segments of the drying can clearly be divided. The knee at the point of critical moisture content is significant, indicating a steep decrease of moisture release from there onwards. This might be explained by a relatively good capillary transport in segment *b* – reflected by a medium *w*-value. Moreover, in segment *c* water release becomes increasingly hindered due to underrepresented water vapor transport mechanisms. This is reflected by the low sorption and high water vapor diffusion resistance (Tab. 5.1).

Stenzelberg latite has a low capillary water uptake, a high ratio of micropores and a significant sorption together with high water vapor transport resistance. As the drying curve shows, the stone will stay moist at equilibrium with a residual content of almost a fifth of its adsorbed water. As mentioned before, water transport within this stone is almost exclusively controlled by water vapor transport mechanisms - the stone is not capable of releasing the capillary uptaken water by vapor transport.

Similar drying behavior can be addressed with regard to the Londorf basalt lava. With a slightly higher porosity but a lower *s*-value, a similar *w*-value and a lower vapor resistance compared to the Stenzelberg latite (Tab. 5.1), in general, the water balance of this stone is at a very low level, which is reflected in its high weather resistance.

The experiments show that the drying behavior is highly dependent upon the environmental conditions. It can also be seen that a high capillary water uptake is not necessarily the main factor controlling drying properties. Much more important are pore space properties - e.g., the ratio of micro-pores.

## **6.2 Freeze–thaw weathering tests**

Frost weathering is discussed as one major physical deterioration process. During winter, most damage in natural building stones is ascribed to alternating freeze and thaw cycles. Ruedrich et al. (2011) report over 30 freeze–thaw cycles per year in Munich, which implies high impact rates.

The formation of ice from a solution such as ice crystallization differs from that of pure water in terms of the freezing point. Ruedrich et al. (2011) ascertain that, due to a certain salt content and smaller pore sizes, the freezing point decreases. In smaller pores, the freezing takes place at increasingly lower temperatures, whereas in larger pores the water crystallizes at temperatures closer to 0°C. This leads to a heterogeneous freezing - i.e., crystallization in

the pore space. Furthermore, pore space properties - e.g. the pore shapes (Hirschwald 1908) - and the interconnection of pores (Stockhausen 1981; Weiss 1992) are of major importance.

Different mechanisms are held responsible for the stress resulting from ice crystallization in the pore space of the rock leading to the disintegration damage of the natural building stone. Hirschwald (1908) addressed the damage to the volumetric expansion of freezing water. Capillary (Everett 1961) and hydraulic pressure (Powers and Helmuth 1953; Setzer 1999) due to the redistribution of water molecules in the pore space and the linear growth pressure (Correns and Steinborn 1939; Steiger 2005) were discussed as the main processes leading to stress on the natural stone. The main precondition for the damage on the stone is that stress introduced by ice freezing exceeds the strength of the stone (Winkler 1968).

On the eight investigated natural building stones, laboratory freeze–thaw tests were performed to verify the sensitivity of the rocks to freezing. Rock prisms with a dimension of 40 x 40 x 160 mm were subjected to 35 freeze–thaw cycles. Four specimens for each rock-type were tested. One cycle encompasses, firstly, the immersion of the samples in water at a temperature of 20°C for 2 h, followed by the storage of the samples at -20°C for 16 h in air. After every 5<sup>th</sup> cycle, the samples were dried to weight constancy at 60°C in a drying chamber. The material deterioration was examined by weight measurements and the measurements of the ultrasonic waves parallel to the long axis of the sample perpendicular to the bedding/foliation (Z-direction) (Rentsch and Krompholz 1961). With the latter, the compressive wave velocities ( $V_p$ ) and the dynamic Young's modulus ( $dE$ ) are evaluated.

The results of the loss of weight, the change of ultrasonic velocity ( $V_p$ ) and Young's modulus are shown in figure 6.3.

For the Drachenfels trachyte, almost no changes of weight are observable (Fig. 6.3a-c). After 35 cycles, only a 0.6% loss in weight was detectable. The samples exhibit only a very light decrease of the  $V_p$  and the Young's modulus. The  $V_p$  was reduced from 3.2 to 3.0 km/s. The Young's modulus decreased from 21.3 to 18.7 kN/mm<sup>2</sup>. No damage was observed in the sample, which correlates with the constant weight.

The sample of the Montemerlo trachyte stays more or less unaffected during the freeze–thaw test (Fig. 6.3d-f). In terms of the elastic properties, only the Young's modulus showed a slight decrease, from 15.7 to 13.3 kN/mm<sup>2</sup>. The  $V_p$  decreased from 2.6 to 2.4 km/s. No macroscopic damage occurred.

The Obernkirchen sandstone samples show no loss of weight (Fig. 6.3g-i). The elastic properties showed variances of 3%. Macroscopic damage was not observed.

For the Schlaitdorf sandstone, no loss of weight is detected (Fig. 6.3j-l). For the elastic properties, a slight decrease is measured: the Young's modulus reduced from 28.5 to 26.3 kN/mm<sup>2</sup>; the Vp was reduced from 3.8 to 3.6 km/s. No macroscopic damage occurred.

At to the sample of the Bozanov sandstone, no loss of weight was measured (Fig. 6.3m-o). The elastic properties showed a decrease of 2% for the Vp and 6% for the Young's modulus. Macroscopic damage was not observed.

The Krenshiem Muschelkalk is the only stone sample of the tested stones that showed a slightly more pronounced change after 35 freeze-thaw cycles in terms of its elastic properties (Fig. 6.3p-r). The Vp decreased from 5.0 to 4.4 km/s. The Young's modulus displayed a decrease from 45.7 to 36.1 kN/mm<sup>2</sup>. A loss of weight cannot be detected, which corresponds with the stable condition of the sample without any occurrence of damage.

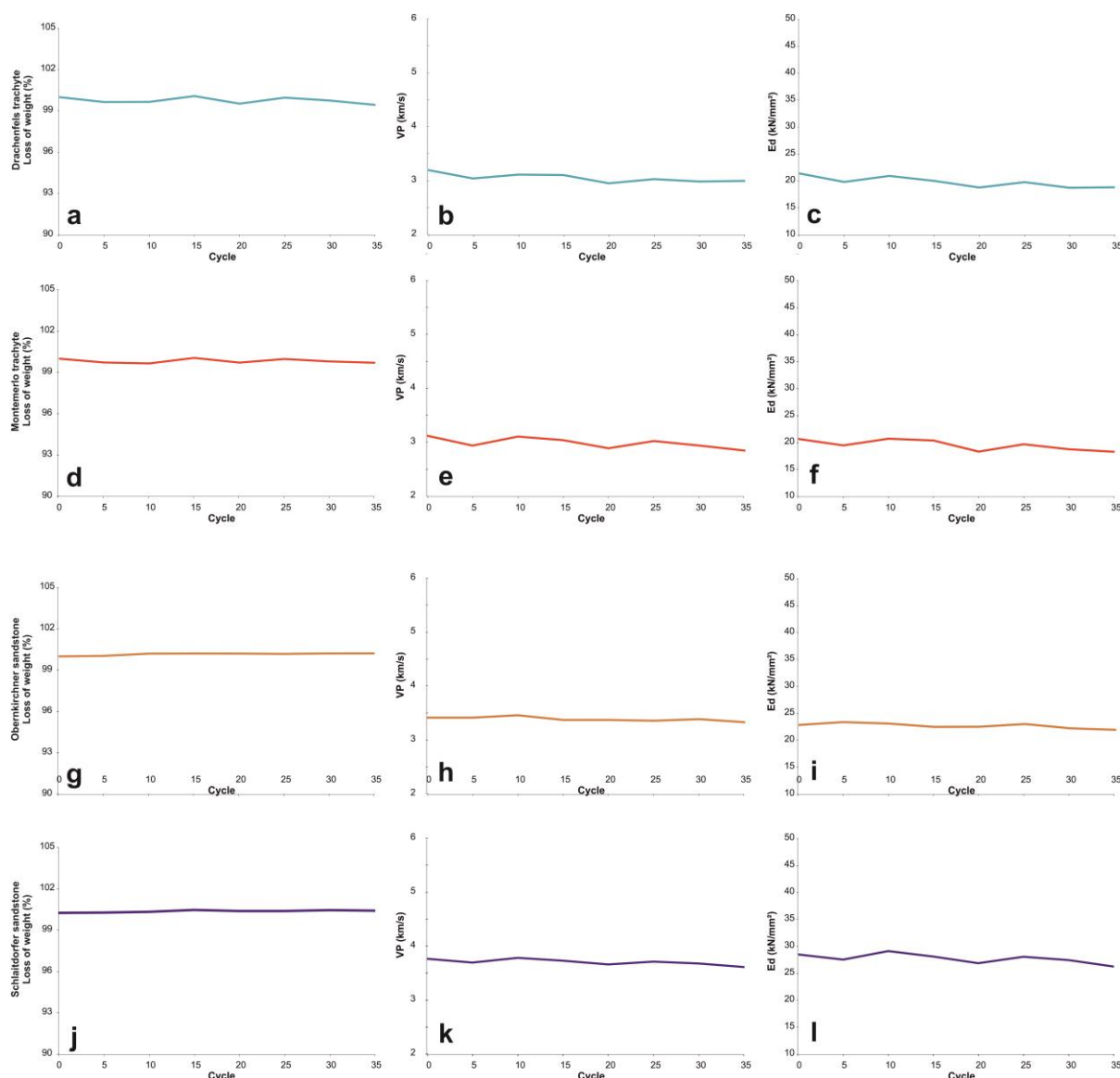


**Figure 6.3** Freeze-thaw test: The graphs show the changes in the weight loss, the compressional wave velocities (Vp) and the dynamic Young's modulus (dE) of the eight stones investigated

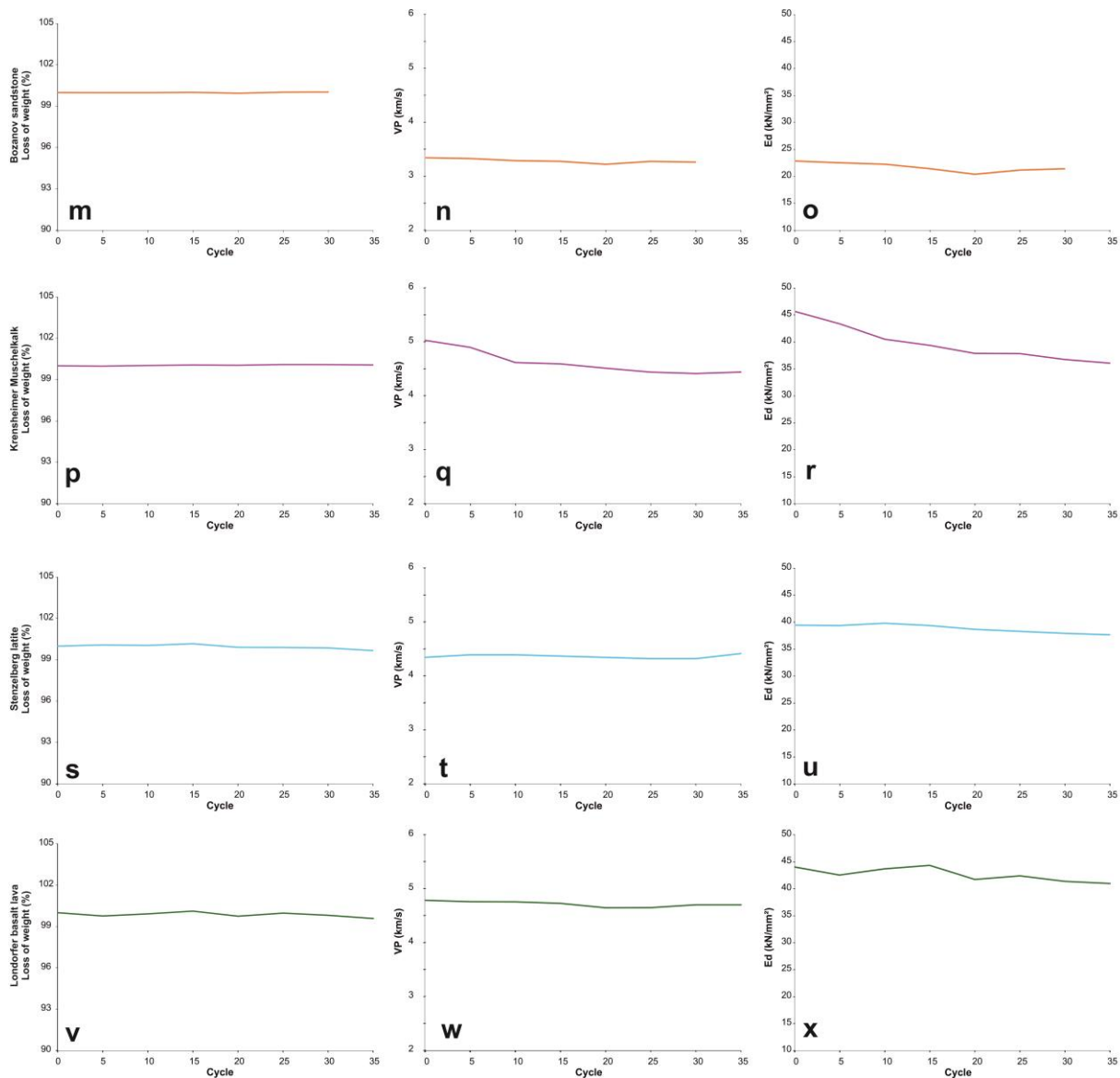


**Figure 6.3** continued. Freeze-thaw test: The graphs show the changes in the weight loss, the compressional wave velocities (Vp) and the dynamic Young's modulus (dE) of the eight stones investigated

The samples of the Stenzelberg latite are more or less unaffected during the freeze test (Fig. 6.3s-u). Weight loss is not detected and the elastic properties vary only between 2–5%. The Young's modulus decreased from 39.4 to 37.7 kN/mm<sup>2</sup>. Damage in the sample cannot be detected.

For the Londorf basalt lava, almost no changes of weight were observed (Fig. 6.3v-x). After 35 cycles, only 0.4% loss in weight was detectable. The Vp showed an decrease of 2% and the Young's modulus was reduced from 44.1 to 41.0 kN/mm<sup>2</sup>. No damage was observed in the sample.

The detection of loss of weight and changes in elastic properties as well as macroscopic damage in the investigated stones indicate that for all of them there was a minor impact within 35 freezing-thaw cycles. Ruedrich et al. (2011) stated that only after more than 50

cycles is there a clear tendency where the deterioration develops to fabric collapse, or where only the elastic properties are slightly reduced. This could be one explanation of the minor changes among the stones. According to the radius freeze point relation of Stockhausen (1981), ice crystallization in the pore space would be expected for all of the investigated stones. In pores larger than  $0.006\text{ }\mu\text{m}$ , water freezes at temperatures below  $-20^{\circ}\text{C}$ .

The Drachenfels trachyte has a very low capillary water uptake (Tab. 5.1). According to the radius freeze point relation of Stockhausen (1981), the water in the pores will freeze at almost the same temperature, from app.  $-1$  to  $-5^{\circ}\text{C}$ . Even though the strength properties are not very high due to the small amount of water uptaken and the short crystallization range, the stress induced by the freeze-thaw cycles will not lead to material failure. The reduction of the elastic properties may indicate that, in respect of long-term stress due to freeze-thaw cycles, the material cohesion might decrease, resulting in pore space changes - e.g., the opening of pore space - and thus different crystallization conditions.

A similar scenario can be drawn for the Montemerlo trachyte, since its fabric is as inhomogeneous as that of the Drachenfels trachyte with a similar PSD but a slightly higher capillary water uptake (Fig. 5.4 and Tab. 5.1). The strength properties of the Montemerlo trachyte are higher than those of the Drachenfels trachyte (Tab. 5.3).

The Obernkirchen sandstone has a low saturation coefficient (0.64), a unimodal PSD with no pore  $>0.006\text{ }\mu\text{m}$  (Fig. 5.4) and high strength properties. These values indicate a high resistance against frost weathering.

Schaitdorf and Bozanov sandstone both have high capillary water uptake, but their saturation coefficients are similar to that of the Obernkirchner sandstone. Both stones show a wider distribution of their pore sizes with a higher number of larger pores. For both stones, a slight decrease of the elastic properties is ascertained, which might have a particular impact due to the strength properties, which are not very high (Tab. 5.3).

The Krensheim Muschelkalk has a medium porosity and a medium capillary water uptake, a low saturation coefficient and a bimodal PSD with two peaks – at  $0.64$  and  $8.2\text{ }\mu\text{m}$ . These petrophysical parameters are not expected to be sensitive to frost, but the detection of the elastic properties within the freeze-thaw weathering test show a clear decrease. Ruedrich et al. (2011) address these decohesion processes of the materials in relation to the temperature sensitivity of the calcite stone. They detected a pronounced residual strain for a Kuaker limestone after five dry and ten wet heating cycles ( $20$ – $90^{\circ}\text{C}$ ). This grain displacement and loss of material cohesion is explained by the strong anisotropic dilatation behavior of the calcite single crystal. Similar behavior has been seen in marble (Siegesmund and Kirchner 2003; Siegesmund et al. 2008; Siegesmund and Ruedrich 2008).



The Stenzelberg latite shows a low capillary water uptake, very narrow PSD with 95% micropores ( $<0.1 \mu\text{m}$ ) and high strength properties. Within this stone, all the water freezes in a very short range of temperature in almost all the pores. Thus, only a very small quantity of water from smaller pores might function as a reservoir of water for further crystal growth in larger pores. The strength values indicate a resistance against stresses from ice crystallization.

Londorf basalt lava has a very low capillary water uptake and low saturation coefficient, as well as high strength properties. This might assume any frost sensitivity. However, Young's modulus is reduced, indicating the decohesion processes of the material. The PSD of the Londorfer basalt lava shows a bimodal distribution with two peaks – at  $0.0082$  and  $28 \mu\text{m}$ . The numerousness of smaller pores between  $0.006$  and  $0.028 \mu\text{m}$  might serve as a fluid reservoir for further crystallization processes in larger pores.

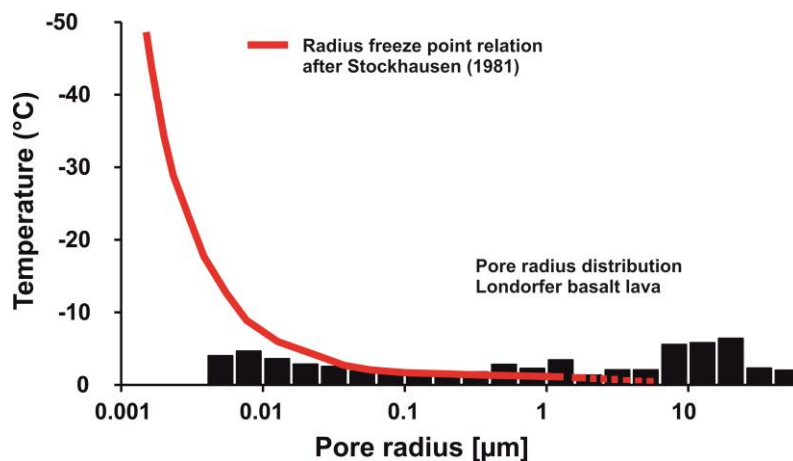


**Figure 6.4** The radius freeze point relation, following Stockhausen (1981)

The test does not reveal a high frost sensitivity for the cathedral stones. However, the slight decreases of the elastic properties observed are noticeable and might indicate a long-term sustainability in relation to frost weathering. As discussed earlier, the relevance of laboratory tests for the weathering of natural building stones has to be relativized (Ruedrich et al. 2011; Siegesmund and Kirchner 2003). With regard to the environmental impact, it is not just the frequency of the freeze-thaw cycles that important. The frost intensity matters more: how long and to what extent do temperatures fall below  $0^{\circ}\text{C}$ . Most of any potential damage is assumed for a temperature range between  $-4$  and  $-15^{\circ}\text{C}$  (Walder and Hallet 1985). External temperatures causing these temperature ranges within natural building stones are not often reached in Central Europe (Ruedrich et al. 2011). Climate calculations impose a decrease of the frequency of freeze-thaw events for Central Europe (Grossi et al. 2007).

As to ice crystallization in the pore space, water has to be abundant in the pores. Thus, the moisture content of the rocks is crucial for freeze-thaw events *in situ*. In the test, the samples are water saturated and supercooling took place in air. For building stones it is different in

most cases: since the building's rain flow or melting snow, which happens above 0 °C, serves as source for the capillary water uptake (Ruedrich et al. 2011). However, material moisture measurements undertaken in four test fields at Cologne cathedral reveal temperatures within the different building stones of Drachenfels trachyte, Obernkirchen and Schlaitdorf sandstone as well as Krensheim Muschelkalk below -4 °C at a depth of 1.8 cm (chapter 3.2). This occurs with relatively regularity in December and February, when the moisture content of the stones is also high (70 to 95 % RH). At first sight, this seems to meet the conditions for a damage scenario involving freeze-thaw cycling. However, the parallel measurements of water vapor content show very little content (2.5 g/kg water in air), which resembles  $3.85 \cdot 10^{-7}$ % vol. of water in the Drachenfels trachyte. This would imply that at these temperatures the water within the stone mainly occurs as a surface film. The water content, namely the water vapor content, is calculated from the measured data within a hollow space 8 mm in diameter, which stays at equilibrium with the humidity and temperature of the pore space of the stone, but does not display the same physical behavior (chapter 3.2). Even at low temperatures, pores <0.1 µm are expected to be filled with water due to capillary condensation in these micropores at higher RH ranges (Siegesmund and Dürrast 2011). Especially in the range of 85–95% RH, the detected mass increase through water vapor absorption is significant (Fig. 5.6) and correlates to the higher ratio of micropores within the stones (Fig. 5.9). At 95% RH and 30 °C, a mass increase of 1.88% wt. is detected for the Drachenfels trachyte. This resembles a volume increase of 4.38% vol. in the stone and an increase of 36.5% vol. with respect to the pore space. In correlation with the pore size distribution, pores ≤0.64 µm will be filled at 95% RH and 30 °C. In the Obernkirchen sandstone, 13% vol. of the pore space will be filled with water at 95% RH and 30 °C. This indicates a water saturation of pores ≤0.064 µm. For the Krensheim Muschelkalk, a mass increase of 0.29% wt. is detected at 95% RH and 30 °C, indicating that only a minor percentage (0.75% vol.) of pores >0.01 µm will be filled with water. Although the data measured at a temperature of 30 °C cannot be quantitatively correlated with the situation at 0 °C - or even -4 °C - they indicate the impact of micropores and capillary condensation at higher RH.

Correlating the pore size distributions of the investigated stones with the radius freeze point relation, following Stockhausen (1981) (Fig. 6.5 green line), at a temperature of -4 °C the pores with pore sizes <0.01 µm (on the left of the blue marking line) will not contribute to frost action if filled with water due to the lower deviation of the radius freeze point relation curve (Fig. 6.5). Pores with sizes >0.01 µm (on the right of the blue marking line) would have to be filled with water for frost action to take place. Regarding the collected data of the measurements and testing, it can be assumed that pores >0.1 µm are probably not filled with water or only to a minor percentage at a measured temperature of -4 °C and 70-95% RH.

Thus, in terms of frost damage, the critical range of pore sizes at  $-4\text{ }^{\circ}\text{C}$  would be within the range of  $0.01\text{--}0.1\text{ }\mu\text{m}$ .

Regarding the pore size distributions of the eight investigated stones and the ratio of pores within the range of  $0.01\text{--}0.1\text{ }\mu\text{m}$ , a certain susceptibility on the part of the Drachenfels and the Montemerlo trachyte, as well as the Stenzelberg latite, can be presumed (Fig. 6.5). As to the Stenzelberg latite, the observed deterioration phenomena of the formation of thin scales ( $2\text{--}3\text{ mm}$  of thickness) may be attributed to frost deterioration.

In another case, with high water importation into the stone - e.g., heavy rain fall and subsequent rapidly falling temperatures - damage due to frost action can be imagined. Additionally, structurally disturbed material – where decohesion started – displays changed petrophysical properties which might promote frost weathering. In contrast to this, the freezing point gets reduced due to the salt content of the pore water, which is generally the case in building stones.

This discussion elucidates once again the significance of the correlation of intrinsic properties - e.g., pore size distribution - and extrinsic properties - e.g., outside temperature and humidity as well as fluid water supply - in appraising deterioration processes.

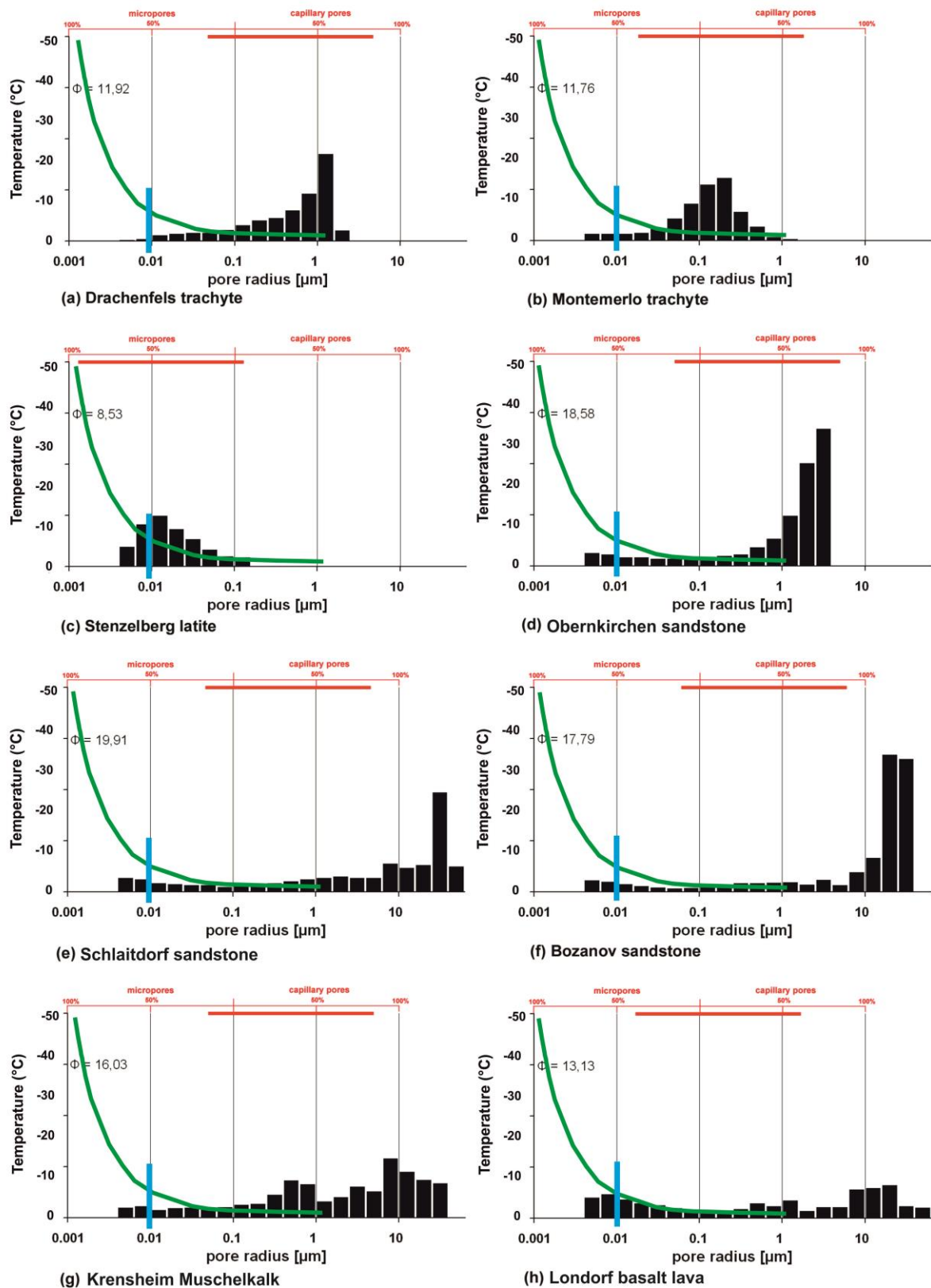


**Figure 6.5** correlation of the pore size distributions (PSD) and the radius freeze point relation after Stockhausen (1981) (green line) and the measured moisture and temperature conditions on site at Cologne cathedral indicating the ratios of pores, in which ice crystallization may occur (marked blue).

### 6.3 Salt-weathering tests

The different models for salt deterioration mechanisms, the individual mechanisms of how salts crystallize from solutions and how salt crystallization causes stress in a porous system, have been outlined in the introduction.

To assess the salt weathering sensitivity of the natural building stones investigated in this work, a salt-weathering test according to standard DIN EN 12370 was performed. Two cubic specimens (65 mm edge lengths) of each stone were salt loaded in succeeding cycles. Each cycle comprised a 4h period of imbibition in a sodium sulfate solution (10%), followed by a 16 h drying period in a drying chamber at 60°C. After a cooling phase of 2 h, the samples were weight controlled.

The resistance is evaluated by weight loss, visible changes and the macroscopic damage of the samples recorded after each cycle. The test is carried out until a 40% weight loss or until the complete breakdown of the samples; alternatively until 75 cycles. Sodium sulfate is a commonly occurring and extremely destructive masonry salt (Doehne 1994; Rodriguez-Navarro et al. 2000); thus, this test exposes the samples to extreme stresses. Depending upon the ambient conditions (temperature and relative humidity), sodium sulfate occurs in several hydration phases. Two stable phases are known: the water free-phase thenardite ( $\text{Na}_2\text{SO}_4$  (V)) and the hydrate phase mirabilite ( $\text{Na}_2\text{SO}_4 \cdot 10\text{H}_2\text{O}$ ). Two other phases have been identified as well: the heptahydrate phase ( $\text{Na}_2\text{SO}_4 \cdot 7\text{H}_2\text{O}$ ) and the meta-stable water-free phase ( $\text{Na}_2\text{SO}_4$  (III)) (Steiger 2009). The transition between these phases takes place at temperature and humidity ranges often found in buildings in Central Europe (Steiger et al. 1998). The hydration from thenardite to mirabilite is associated with a volume increase of 300% (Price and Brimblecombe 1994).

Depending upon the temperature the phase transition occurs at different relative humidity, e.g. at 20 °C hydration from thenardite ( $\text{Na}_2\text{SO}_4$  (V)) to mirabilite ( $\text{Na}_2\text{SO}_4 \cdot 10\text{H}_2\text{O}$ ) takes place at 75% relative humidity. At the same temperature and slightly differing RH (71–72 %) the meta-stable triad water-free phase makes a transition to mirabilite and at a RH of ca. 82 % the heptahydrate can be formed. This indicates that the RH ranges in which the different hydrate phases form are very narrow and may be traversed several times per day (Fig. 6.6).

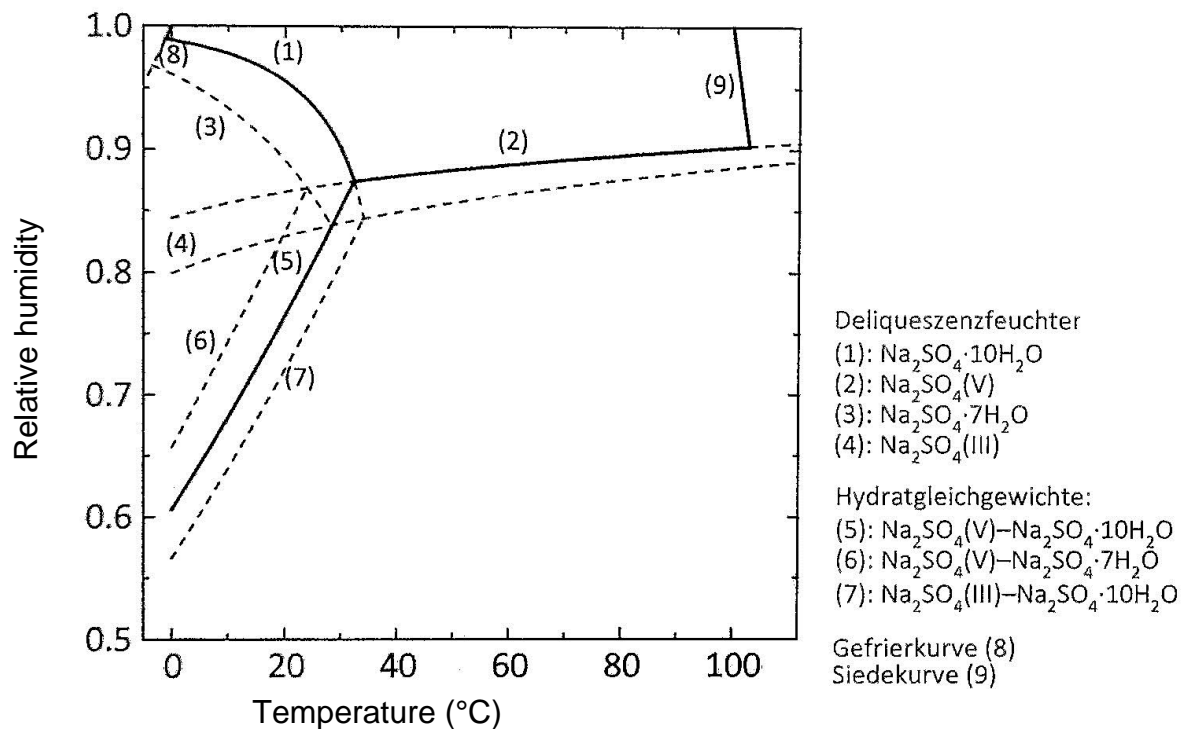


**Figure 6.6** Deliquescence humidities of the system  $\text{Na}_2\text{SO}_4 - \text{H}_2\text{O}$ , stable equilibrium: solid line; metastable equilibrium: dashed line (from Steiger 2009)

### Results of laboratory salt-weathering tests

The different building stones investigated here show very different salt-weathering stabilities (Fig. 6.7). The Montemerlo trachyte, the Krensheim Muschelkalk and the Bozanov sandstone show little resistance to salt deterioration experiments. They lose 10 % of their weight after 18 cycles, followed by the Drachenfels trachyte with 26 cycles (Fig. 6.7). The weight loss and weathering of the two Drachenfels trachyte specimens vary significantly. These four stones show a minor salt weathering stability. The Schlaitdorf is in the middle of the range. The Obernkirchen sandstone shows a strong divergence of its two samples: sample *a* stays unweathered until the end of the test (Fig. 6.7), whereas sample *b* loses 10% of its weight after just 18 cycles. The Stenzelberg latite and the Londorf basalt lava are more or less unaffected (Fig. 6.7).

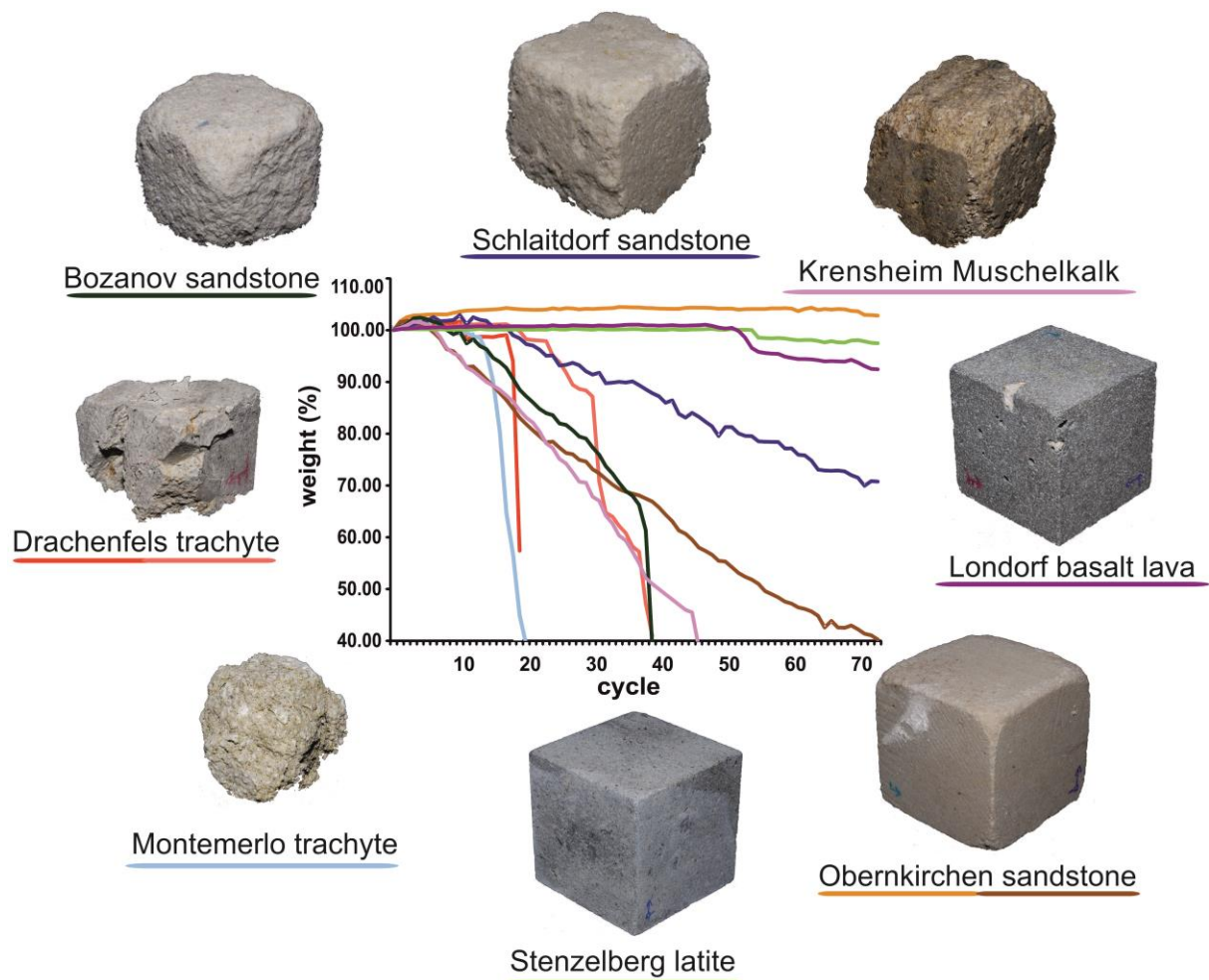


**Figure 6.7** Salt deterioration tests with sodium sulfate. The Montemerlo trachyte (MT) shows minimum salt weathering resistance. The Drachenfels trachyte (DT), Krensheim Muschelkalk (KM) and Bozanov sandstone (BS) also show little resistance. The Schlaitdorf sandstone (SS) presents a weight loss of 70% after 70 cycles. The Obernkirchen sandstone (OS) displays varying medium-to-high salt-weathering resistance. The Londorf basalt lava (LB) and the Stenzelberg latite show a minimum weight loss within this experiment.

The forms of damage and material loss behavior of the stones are very distinct. The form of damage of the Drachenfels trachyte is unique and it very much resembles the crumbling observable *in situ* at Cologne cathedral. The disintegration does not start from the outer surface moving subsequently towards the “inner core” as is observable for the sandstones. The Drachenfels trachyte shows fissures and crack formation, leading to a fragmentation of the sample resulting in crumbling, disintegration and the spalling off of fragments, which in many cases still show the unaffected surface. The crack formation is not necessarily bound to the large phenocrysts; it runs through the matrix as well (Fig. 6.8). Efflorescence is not observed.

The Montemerlo trachyte shows a very different form of damage. This rock sample subsequently weathers from the outer surface to the inside, leaving a flaking surface. Crack formation is not as pronounced as it is in the Drachenfels trachyte (Fig. 6.7).

The Krensheim Muschelkalk shows a somewhat visually comparable form of damage as that of the Montemerlo trachyte. The components are subsequently weathered. Efflorescence is not observed.



**Figure 6.8** Salt-weathering test: Deterioration in the Drachenfels trachyte sample showing fissures and crack formation alongside large phenocrysts and in the matrix as well.

The three sandstones show similar damage progress: a granular sanding and disintegration from the surface towards the core of the sample. The Bozanov sandstone shows significantly more deterioration and its surface recession is not as regular as it is in the Schlaitdorf or the one sample of Obernkirchen sandstone.

In the salt-weathering test, the Stenzelberg latite and the Londorf basalt lava lose less than 10 % of their weight. The form of damage in the Stenzelberg latite resembles the phenomena observed *in situ* at Cologne cathedral: the detachment of scales of 1–2 mm thickness (Fig. 6.7). The Londorf basalt lava shows crack formation and scaling (Fig. 6.7). These deterioration phenomena are not well known for this building stone, indicating the highly destructive power of the salt-weathering test.

## Discussion

The salt-weathering test illustrates well the deterioration phenomena observed *in situ*. Especially for the Drachenfels trachyte, it is shown that this stone does not show even surface recession, instead showing crack formation and crumbling. As described earlier, the salt used in the test is a very destructive one; thus, pronounced damage with the samples is expected. In the deterioration samples from Cologne cathedral, gypsum is detected in the form of crusts on the stone surfaces as well as in the disintegrated zones of the stone material (Graue et al. 2013a). Even though gypsum is the least soluble of the soluble damage salts (Charola et al. 2007), it tends to accumulate and thus provoke severe damage



of the stone material (see chapter 8.5). Although the crystallization processes of these two salts vary significantly, the deterioration they cause can be compared.

The Schlaitdorf sandstone shows a moderate resistance to salt deterioration. The main deterioration phenomena observed for this stone at the Cologne cathedral are formation of massive gypsum crusts, scaling and flaking, as well as granular disintegration, rounding and notching. In the deterioration samples of the Schlaitdorf sandstone from Cologne cathedral, Kraus (1985a) detected gypsum concentrations of up to 23.2 wt. %. The formation of gypsum is due to the acidic environmental attack on the carbonate cement of the stone (app. 14 wt. %). To these high concentrations of damaging salts, the Schlaitdorf sandstone is able to oppose a certain resistance, but with recurring wetting and drying cycles due to the climate impact the stone deteriorates significantly.

Obernkirchen sandstone, Londorf basalt lava and Stenzelberg latite can be generally addressed as being salt-weathering resistant natural building stones. However, the scaling observable on the Stenzelberg latite can to be seen in context with salt deterioration processes.

The low resistances of Montemerlo trachyte, Bozanov sandstone and Krensheim Muschelkalk are significant. For the Montemerlo trachyte, salt-weathering sensitivity is reported for Venice, Italy (Lazzarini et al. 2008). Přikryl et al. (2010) report severe deterioration due to the salt-weathering of the Bozanov sandstone at the Charles Bridge in Prague. As to the Krensheim Muschelkalk, a general weathering resistance is assigned. If at all, solution-weathering and microkarst phenomena are mentioned (Grimm 1990).

The salt-weathering behavior of natural building stones is dependent upon their fabric properties and petrophysical parameters. Crucial parameters include the pore space properties, such as effective porosity, pore size distribution, pore shape and pore interconnectivity (Ruedrich and Siegesmund 2006). The mineral composition, the rock fabric, drying properties and the tensile strength of the stone are important parameters as well for the determination of salt-weathering processes.

For sandstones, a high porosity together with a high capillary water uptake and low tensile strength are held as being primarily responsible for salt decay. In terms of the distribution of pore sizes, a wider range of pore sizes with a higher ratio of micropores and even bimodal PSD are held as being responsible in promoting salt deterioration. For sandstones, in general, slow drying is correlated with scaling deterioration and faster drying to granular disintegration (Ruedrich and Siegesmund 2006).

If the petrophysical properties of the investigated stones are correlated with the observed damage within the test, then for the Stenzelberg latite and the Londorf basalt lava a high

resistibility is ascertained due to low porosity, a low capillary water uptake and the high tensile strength of these stones. The scaling of the Stenzelberg latite has to be seen with its drying properties and high critical moisture as being due to the large content of the micropores, leading to a zone of maximum moisture, where salts precipitate and cause the disintegration of the stone material (Kraus 1985a; Ruedrich and Siegesmund 2006; Snethlage and Wendler 1997).

Obernkirchen sandstone is not affected very much by the salt test. This stone has a low  $w$ -value, high strength properties and a narrow range of pore sizes, as well as good grain contacts and good drying properties.

Schlaitdorf sandstone and Bozanov sandstone have high porosities, high capillary water uptake and a wide range of pore sizes, which are clearly more pronounced with regard to larger pores. Their tensile strength is similar; drying behavior in the Bozanov sandstone is slightly retarded. These characteristics would lead us to expect an almost similar salt-weathering resistibility, but the test results show a significantly higher sensitivity for the Bozanov sandstone. This might be due to the longer drying duration in conjunction with the clay mineral content. Besides the salt weathering processes caused by salt crystallization in the pore space, the swelling of clay minerals has to be considered as well, which becomes significantly intensified by the presence of salts.

The higher salt weathering sensitivity of the Montemerlo trachyte in comparison to the Drachenfels trachyte may be explained by the slightly higher capillary activity and higher water vapor diffusion resistance, due to the higher number of pores with pore sizes  $< 0.01 \mu\text{m}$ . The higher salt uptake and retarded drying might promote better salt crystal growth, and thus have a greater impact upon salt deterioration.

## **7 Aspects of chemical weathering**

### **Laboratory tests of the chemical weathering of the investigated natural building stones**

The chemical weathering of natural building stones described at the outset is mainly due to an acidic attack through atmospheric gases ( $\text{SO}_x$ - und  $\text{NO}_x$ -) dissolved and oxidized in rainwater forming anorganic acids. As well contribute water and organic acids to the deterioration of building stones. The different natural building stones react through the corrosion of their rock-forming minerals (e.g., silicate stones) or their dilution/solution (e.g., carbonate stones), which eventually leads to the formation of harmful substances (e.g. salts). The following data were available for the evaluation of the chemical resistance of the different stones against acidic attack and the behavior of the stones in varying pH to estimate chemical deterioration process of the eight investigated stones in an anthropogenic environment. Data come from acid buffering capacity tests and leaching experiments.

#### **7.1 Acid buffering capacity**

To evaluate the acid sensibility of the various stones, acid capacity buffering tests were conducted. The prepared stone material was titrated with hydrochloric acid ( $\text{HCl}$  – 0.01mol/l, and 1 mol/l for Krenshelm Muschelkalk) until steady pH 4 was achieved. The ion equivalent detects the quantity of acid-soluble ions in the different stones at pH 4.

##### **7.1.1 Material and methods**

Suspensions were prepared with a 1 g powder fraction of the various stones and 25 ml of distilled water. Hydrochloric acid ( $\text{HCl}$ ) was successively added to the stone suspensions until pH 4 was established. The concentration of added  $\text{HCl}$  0.01mol/l was evaluated potentiometrically. The concentrations correlated with the different stones, indicated by the titration curves of the stone suspensions (Fig. 7.1). The concentration of the added  $\text{HCl}$  solution (mol) gives a rate for the acid buffering capacity (Table 7.1; Fig. 7.2).

##### **7.1.2 Results**

The highest buffering capacity showed the carbonate rock. A high capacity was shown by the Schlaitdorf sandstone as well. The four volcanic rocks (Drachenfels and Montemerlo trachyte, Stenzelberg latite and Londorf basalt lava) had comparable values, whereas in the two sandstones (Bozanov and Obernkirchen sandstone) the lowest acid buffering capacities were detected (Table 7.1; Fig. 7.2).

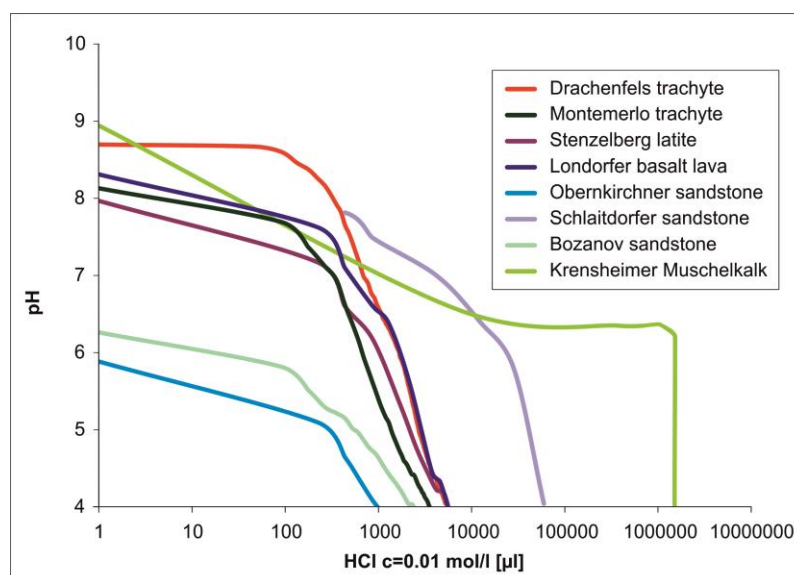


**Figure 7.1** Titration curves of the eight investigated stones with HCl. Please note the logarithmic scale of the x-axis as well.

### 7.1.3 Discussion

Due to the high calcite content of the Krensheim Muschelkalk it is expected that it buffers a high concentration of added HCl over a long period of time. A similar behavior was ascertained for the Schlaitdorf Sandstein with a carbonate cement (appr. 14 %). The extremely high acid buffering capacity of the Krensheim Muschelkalk indicates that this stone shows the highest vulnerability to acidic attack since it will dissolve. In general, the acidic environmental impact is caused to a large extent by sulfuric components. Thus, limestone generally forms gypsum crusts as a result of transformation from  $\text{CaCO}_3$  into  $\text{CaSO}_4 \cdot 2 \text{H}_2\text{O}$  (see chapter 8.3.1). Török et al. (2006) observed the protective role of weathering crusts for the limestone, at least to a certain extent.

The Schlaitdorf sandstone shows a long buffering capacity as well due to its carbonate cement. This indicates a high vulnerability to chemical environmental acidic impacts. These results correlate strongly with the observed damage of the exposed building stones. The Schlaitdorf sandstone deteriorates and forms gypsum. To a large part the decay of the Schlaitdorf sandstone is due to the loss of cementation through the formation of damaging salts, i.e., gypsum due to high  $\text{SO}_2$ -immision (Kraus 1985a).

For silicate rocks, it can generally be noted that the feldspars – here, mainly plagioclases – and certain accessory components show a reduced acid resistance compared to quartz (Loughnan 1969). The lowest buffering capacity was shown by the Obernkirchen sandstone. This stone is a quartz-arenite with 95-98 % monocline quartz. Thus, it contains only a few compounds, that are affected by acidic impacts and so it indicates a high chemical resistivity. In addition, the Bozanov sandstone shows a relatively low buffering capacity. The slightly higher capacity is due to the higher content of stone fragments and feldspars in comparison with the Obernkirchen sandstone.

**Table 7.1** Quantity in ml of added hydrochloric acid (0.01 mol/l) and the corresponding ion-equivalent until pH 4 is reached

	0,01 M HCl (ml)	equivalent HCl (mol)
KM	2,050.00	$2.05 \cdot 10^{-2}$
SS	75.00	$7.5 \cdot 10^{-4}$
OS	1.00	$1.0 \cdot 10^{-5}$
BS	2.70	$2.7 \cdot 10^{-5}$
DT	6.30	$6.3 \cdot 10^{-5}$
MT	4.20	$4.2 \cdot 10^{-5}$
SL	7.00	$7.0 \cdot 10^{-5}$
LB	7.50	$7.5 \cdot 10^{-5}$

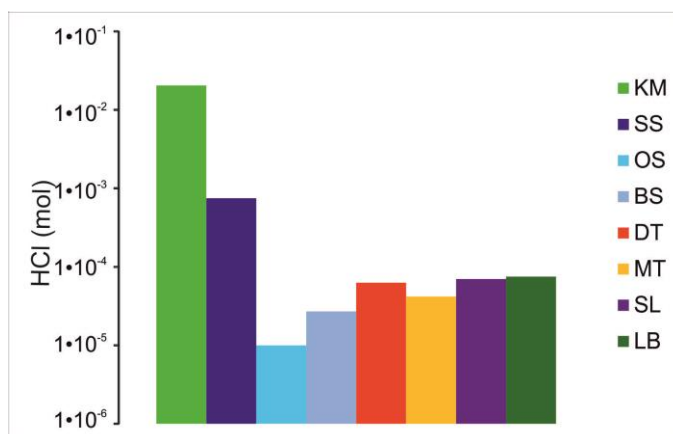


**Figure 7.2** Ion equivalent of the acid buffering capacity of 1 g stone powder of the investigated stones in HCl (please note the logarithmic scale of the y-axis); KM = Krenshelm Muschelkalk, SS = Schlaidorf sandstone, OS = Obernkirchen sandstone, BS = Bozanov sandstone, DT = Drachenfels trachyte, MT = Montemerlo trachyte, SL = Stenzelberg latite, LB = Londorf basalt lava

Compared to these two sandstones, the volcanic rocks show a higher acid buffering capacity due to their broad mineral composition. In the Drachenfels trachyte plagioclase (24 %) and to a lesser degree, the biotite (5 %), sanidine (50 %), apatite (< 1 %), and accessory calcite might also contribute to the acid buffering. The Montemerlo trachyte contains calcite (4 %), which is highly soluble, but in addition plagioclase (15 %), biotite (5 %) and amphibole (8 %) might be dissolved and buffer the acid impact. To a lesser extent, the contents of sanidine (53 %) might be involved. For the Stenzelberg latite a corrosion of plagioclase (39 %) and hornblende (9 %) is expected as well as for biotite (2 %) and sanidine (37 %). In the Londorf basalt lava olivine (14 %) and plagioclase (47 %) are attacked by the acid impact.

## 7.2 Leaching with methane-sulfonic-acid at pH 4

In a second experiment, the powdered stone fractions were leached in methane-sulfonic-acid (MSA). The various concentrations of the MSA were at ion-equivalent concentrations as the applied HCl to achieve pH 4. Leached fractions were then qualitatively and quantitatively analyzed.

### 7.2.1 Material and methods

A powdered fraction (1 g) of each stone was dispersed in 25 ml of ion-equivalent concentrations of MSA as a leachant at pH 4 over 24 hours (see Tab. A7.0 in the appendix). The pH was controlled after 24 hours. Afterwards, anions and cations in the eluates were measured by ion chromatography analyses. Major cations were analyzed on a DIONEX 320 using electrochemically suppressed conductivity detection with ion separation achieved on a

CS16 column using methane sulfonic acid as an eluent. The major anions were analyzed on a DIONEX 500 using electrochemically suppressed conductivity detection with ion separation achieved on an AS11-HC column using potassium hydroxide as eluent. The calibration ranges were the following: chloride: 1–20 mg/l; sulfate: 20–200 mg/l; nitrate: 1–40 mg/l; ammonium: 0.5–20 mg/l; sodium/potassium/magnesium: 2–20 mg/l; lithium: 0.25–2.5 mg/l. The aluminum was analyzed with ICP-OES on an Optima 3300 DV.

## 7.2.2 Results

The experiment shows a much higher concentration of leached cations in comparison with anions. In what follows, the cation yields of aluminium, sodium, potassium, magnesium and calcium are discussed. The concentrations of the leached fractions from Krensheim Muschelkalk (MK), Schlaitdorf sandstone (SS), Obernkirchen sandstone (OS), Bozanov sandstone (BS), Drachenfels trachyte (DT), Montemerlo trachyte (MT), Stenzelberg latite (SL), and Londorf basalt lava (LB) in MSA pH4 over 24 hours differed significantly (Tab. 7.2; Fig. 7.3).

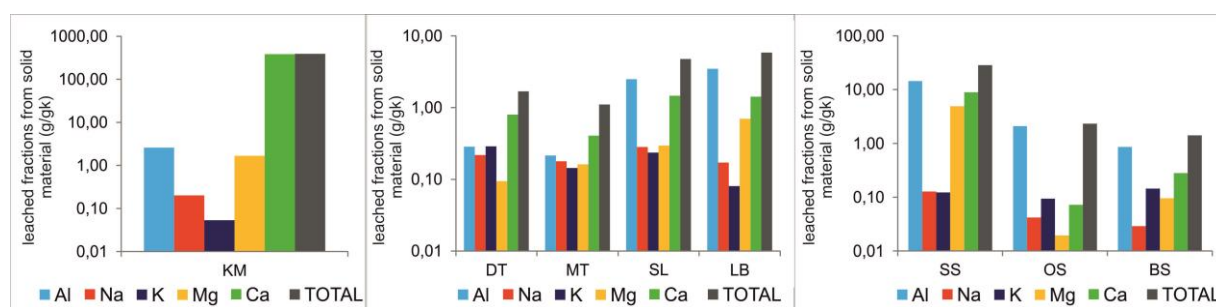


**Figure 7.3** Concentrations (g/kg) of the leached fractions relative to the solid material from the investigated stones in MSA at pH 4 (please note the logarithmic scale of the y-axes) (a) from Krensheim Muschelkalk; (b) from Schlaitdorf sandstone (SS), Obernkirchen sandstone (OS), Bozanov sandstone (BS); (c) from Drachenfels trachyte (DT), Montemerlo trachyte (MT), Stenzelberg latite (SL), and Londorf basalt lava (LB)

**Table 7.2** Concentration of the leached fractions

	Al g/kg	Na g/kg	K g/kg	Mg g/kg	Ca g/kg	TOTAL g/kg
KM	2.60	0.20	0.05	1.68	385.99	390.53
SS	14.37	0.13	0.12	4.90	8.94	28.45
OS	2.09	0.04	0.09	0.02	0.07	2.32
BS	0.86	0.03	0.14	0.10	0.28	1.41
DT	0.29	0.22	0.29	0.09	0.80	1.68
MT	0.22	0.18	0.14	0.16	0.41	1.11
SL	2.49	0.28	0.24	0.30	1.47	4.77
LB	3.48	0.17	0.08	0.70	1.42	5.85

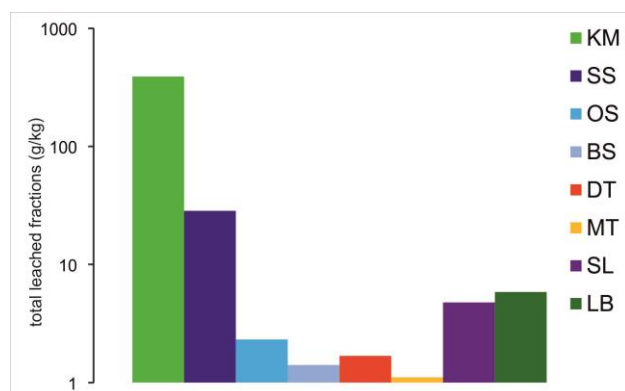


**Figure 7.4** Concentration (g/kg) of the total leached fractions from the investigated stones in MSA at pH 4 (please note the logarithmic scale of the y-axis)

In correlating the concentration of the leached fractions to the element concentration in the host rock (Tab. 7.3) the proportion (percentages of the total content) of the elements

leachable by MSA at pH 4 from the powdered stone fractions are given (White 2003). These percentages indicate the “leachability” of the element from the natural building stone in the specific leachant (Tab. 7.4; Fig. 7.5) (Snäll and Lilijefors 2000). The complete data set of the XRF analyses of the host rocks are found in the appendix (A.5.1).

**Table 7.3** Element concentration in the host rock (XRF analysis)

	Al	Na	K	Mg	Ca	TOTAL
	g/kg	g/kg	g/kg	g/kg	g/kg	g/kg
<b>KM</b>	8.04	5.19	0.42	2.71	373.43	389.80
<b>SS</b>	25.83	0.52	0.83	5.25	9.36	41.79
<b>OS</b>	20.69	5.93	1.41	0.30	0.21	28.56
<b>BS</b>	22.97	2.45	13.45	0.54	0.64	40.05
<b>DT</b>	92.41	32.94	46.32	4.70	17.15	193.52
<b>MT</b>	96.32	38.50	39.27	6.63	15.15	195.88
<b>SL</b>	96.85	30.94	33.62	8.86	35.38	205.65
<b>LB</b>	75.95	24.48	10.96	49.45	58.82	219.66

**Table 7.4** Leachability (% of total wt. %) of Al, Na, K, Mg, Ca from the investigated stones in MSA pH4

	Al	Na	K	Mg	Ca
	%	%	%	%	%
<b>KM</b>	32,4	3,9	12,9	61,9	100,0
<b>SS</b>	55,6	24,5	14,8	93,3	95,4
<b>OS</b>	10,1	0,7	6,7	6,5	33,7
<b>BS</b>	3,7	1,2	1,1	17,7	43,6
<b>DT</b>	0,3	0,7	0,6	2,0	4,6
<b>MT</b>	0,2	0,5	0,4	2,4	2,7
<b>SL</b>	2,6	0,9	0,7	3,3	4,1
<b>LB</b>	4,6	0,7	0,7	1,4	2,4

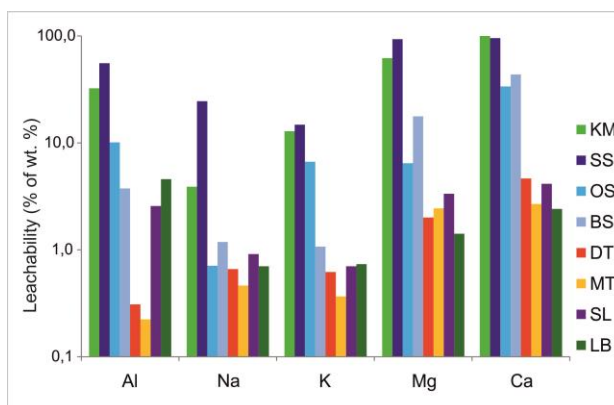


**Figure 7.5** Leachability (% of total wt. %) of Al, Na, K, Mg, and Ca from the different building stones in MSA at pH 4 (KM: Krensheim Muschelkalk; SS: Schlaitdorf sandstone; OS: Obernkirchen sandstone; BS: Bozanov sandstone; DT: Drachenfels trachyte; MT: Montemerlo trachyte; SL: Stenzelberg latite; LB: Londorf basalt lava)

## 7.2.3 Discussion

The diagram in figure 7.1 shows that the eluates of the stones maintain a relatively high pH for a certain duration, then the pH increases significantly. This is reflected by the concentrations of cations diluted (Tab. 7.3). The quality and the quantity of the leached fractions are correlated with the mineral composition of the different stones (Tab. 7.4; Fig. 7.5). Thus, the content of the different minerals of the various stones is discussed in terms of the minerals' weather resistance – namely, their acid resistivity – analogous to Goldich (1938). An attempt is made to qualitatively and semi-quantitatively correlate the leached fractions with the various minerals of each natural building stone.

In the Drachenfels trachyte plagioclase (24 wt. %), apatite (< 1 wt. %), biotite (5 wt. %), and sanidine (50 wt. %) are found (Vieten 1961; Koch 2006; see chapter 5.2), which show a

certain solubility. Partially found calcite – in the Drachenfels trachyte an alteration product of anorthite content in the plagioclases (Ab<sub>70</sub>/An<sub>30</sub>) (Grimm 1990) – dissolves in acid solution. The content of clay minerals – up to 5 % montmorillonite (Vieten 1961; Dohrmann 2013) – has to be taken into account in terms of mineral weathering. Sphene (< 1 wt. %), quartz (13 wt. %) and augite (5 wt. %) as well as accessory ore minerals (2 wt. %) and zircon (1 wt. %) (Vieten 1961; Koch 2006) are more weather resistance minerals and show lower solubility.

The calcite – although an accessory component – weathers easily and releases calcium. In comparing the weather resistance of plagioclases and orthoclases, the latter show a much higher resistivity. Out of the plagioclases, the calcium-rich anorthite shows higher solubility than the sodium-rich albite (White and Brantley 1995; Brantley 2003). The cations released from these rock-forming minerals are Ca<sup>2+</sup>, Na<sup>+</sup> and K<sup>+</sup> ions (Tab. 7.2). Apatite is soluble in the common acids (HCl, HNO<sub>3</sub>, H<sub>2</sub>SO<sub>4</sub>) (Strübel and Zimmer 1991). This mineral possibly releases calcium ions due to the acidic impact. Potassium is released from the interlayer of biotite under deterioration impact (Loughnan 1969; Steiger et al. 2011). The loss of potassium from biotite correlates progressively with increasing weathering intensity (White 2003). The Kali-feldspar sanidine releases potassium-ions. This occurs in significantly lower ratios in relation to plagioclases (Loughnan 1969). The weathering of montmorillonite to kaolinite is associated with the release of magnesium ions (Altschuler et al. 1963; Heydemann 1966). Biotite releases magnesium as well (Steiger et al. 2011).

In the Drachenfels trachyte, the leached calcium and sodium fractions can be attributed to the dissolution of calcite and the corrosion of plagioclases and apatite. The released potassium can be correlated with a certain biotite and sanidine solution. The magnesium content in the eluate may derive from montmorillonite and biotite weathering. The release of the aluminum is due to the corrosion of the silicates in general (White 2003).

The concentration of leached calcium and magnesium fractions relative to the concentration in the untreated Drachenfels trachyte is significantly higher than the concentration of sodium, potassium, and aluminum (Fig. 7.5), assuming a preferred plagioclase and clay mineral weathering. The relatively high calcium concentration is not just ascribed to the solution of the calcite content in the host rock. Thus, it may be attributed to the vast cryptocrystalline matrix with a major ratio of plagioclases with an anorthite content of 30 mol % (Kraus 1985a). During the process of the chemical weathering of plagioclase phenocrysts with calcic cores surrounded by more sodic rims, the plagioclase cores weather more rapidly, producing a preferential release of solute calcium relative to sodium (Clayton 1986). This process of an incongruent dissolution has been invoked to explain the excess solute calcium to sodium ratios relative to what would be expected from the bulk plagioclase stoichiometry (Stauffer 1990; White 2003).



In the Montemerlo trachyte 4 wt. % of calcite is found, which solutes readily in its ions in pH 4. Besides plagioclase (15 wt. %) and amphibole (8 wt. %), biotite (5 wt. %) and sanidine (wt. 53 %) are found in the Montemerlo trachyte (Koch 2006).

Although the concentration of calcite is relatively low in the Montemerlo trachyte compared with the other rock-forming minerals (Tab. 7.2; Fig. 7.3c), its solubility is very high and in pH 4 it will be completely dissolved, thereby providing calcium. As described for the Drachenfels trachyte, the leached calcium, sodium and potassium fractions on the one hand derive from the solution of the feldspars. On the other hand, biotite provides a certain amount of potassium and the amphibole group contributes to a minor grade to the concentration of all five leached fractions. Again, the released aluminium can be ascribed to silicate corrosion in general. Noticeable in the Montemerlo trachyte is the high concentration of leached magnesium. This may be ascribed to a certain biotite solution as well as to the weathering of the clay mineral content. Koch (2006) mentioned relatively high clay mineral concentrations in the Montemerlo trachyte.

The Stenzelberg latite contains a high ratio of plagioclase (39 wt. %) besides hornblende (9 wt. %), biotite (2 wt. %) and sanidine (37 wt. %). Calcium, magnesium and aluminium show significant leachabilities in this stone (Tab. 7.4; Fig. 7.5). The released calcium ions can be partially attributed to the corrosion of the plagioclase, as well as to the hornblende and – to a lesser degree – to the apatite. The leached magnesium and aluminum fractions might rather be ascribed to the hornblende and the biotite solution, rather than to the corrosion of other rock-forming minerals in the Stenzelberg latite.

In the Londorf basalt lava olivine (14 wt. %) and plagioclases (47 wt. %) can be addressed as contributing to the leached fractions of aluminium, calcium and magnesium ions (Tab. 7.2; Fig. 7.3c). The acid resistivity of olivine is relatively low (Strübel and Zimmer 1991) and the release of magnesium is expected (Loughnan 1969). Grimm (1990) and Steindlberger (2003) describe accessories of a cryptocrystalline nature (3 wt. %) and partially glass (up to 50%). The components might contribute to the relatively high leachabilities of aluminium, calcium and magnesium.

The leachabilities of the ions in the Krenshiem Muschelkalk clearly indicate the decomposition of the carbonate rock (Tab. 7.4). The content of calcium is released completely. The minor content of other leached fractions show high leachabilities as well due to the complete dissolution of the rock.

The Schlaitdorf sandstone is characterized by a high content of dolomite, partially illite and kaolinite, cement of 14 wt. % (Grimm 1990). The quartz content (72 wt. %) is barely affected by the solution. Rock fragments (12 wt. %) and feldspar (2 wt. %) might contribute to the concentration of the leached fractions. The high yields of diluted calcium, magnesium and aluminum can be ascribed to the cement of the rock (Tab. 7.2; Fig. 7.3b).

The Obernkirchen sandstone represents pure quartz sandstone with a small amount of kaolinite within its matrix (5 wt. %) (Dienemann and Burre 1929; Grimm 1990). A significant concentration of aluminium can be detected in comparison with the other leached elements. This can be addressed to the kaolinite degradation, since quartz is barely affected.

The Bozanov sandstone is composed of quartz (79 wt. %), rock fragments (10 wt. %), feldspar (5 wt. %), and clay minerals (smectite, kaolinite; around 5 wt. %), besides accessories (Koch 2000; 2001; Přikryl et al. 2010). Relatively higher concentrations of aluminium and calcium are leached (Tab. 7.2; Fig. 7.3b). The aluminium concentration is probably leached from kaolinite decomposition. For the sedimentation of the Bozanov sandstone, a fast transport of coarse-grained clastic material is reported (Lehr 2008). Thus, rock fragments are constituent of the sandstone and are very inhomogeneous. The yield of calcium, potassium and magnesium may be attributed to the weathering of these rock fragments, feldspars and the clay minerals as well.

### **7.3 Leaching experiments**

The deterioration attack on natural building stone in an anthropogenic environment is many-fold. Through the extrinsic factors of dry and wet deposition of air pollutants and atmospheric gases as well as the impact of microbiological contamination and moisture import into the porous material through rain and humidity, solutions in the pore space of natural building stones are formed, which show varying compositions, concentrations and pH values. Natural building stones deteriorate chemically due to a corrosion of their rock-forming minerals through these pore solutions (Loughnan 1969; Kraus 1985; Colman and Dethier 1986; Pielow 1997; Schlösser 1991). The solubility of rock-forming minerals is very much pH-dependent (McBride 1994; White 2003). The chemical breakdown of silicate minerals proceeds through the solution or partial solution of some of the constituent cations of the mineral (Loughnan 1969; Holdren and Speyer 1986).

In the following experiment, the reaction of the investigated building stones to the impact of different pH solutions was considered. Two different grain size fractions (coarse and fine sample fractions) from the various stones at different pHs over various periods of time were tested. The pH values of the eluates and leached fractions were detected. The Krensheim Muschelkalk – being a carbonate rock – was excluded from these leaching experiments.

#### **7.3.1 Material and methods**

The fine sample fraction of the investigated stones (Tab. 7.5) is a fine powder of the stones; the coarse fraction has grain sizes of 4–10 mm (Fig. 7.6a and b). The leachants were demineralized water, a Kolthoff-buffer at pH 3.4, a Palitzsch-buffer at pH 7 and pH 8.4, and a

saturated gypsum solution (Tab. 7.6). The preparation of the leachants is described in the appendix (Tab. A7.1).

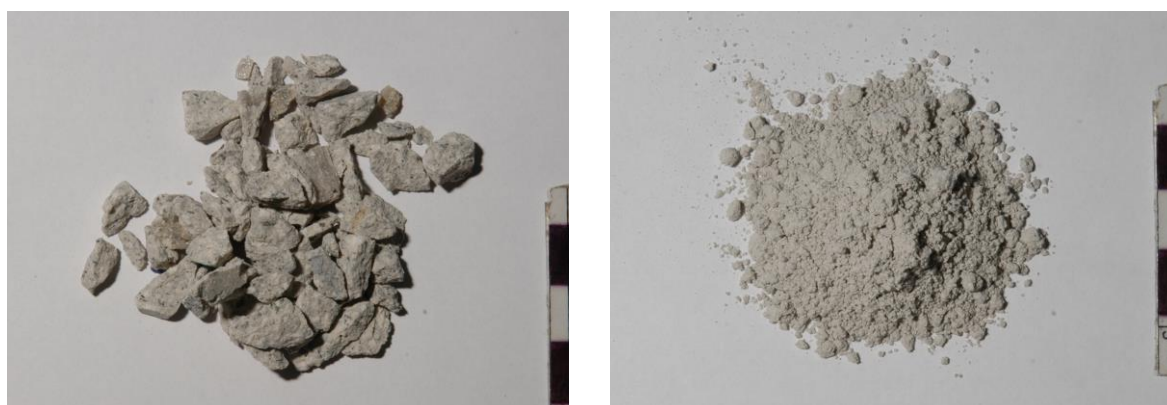
**Table 7.5:** Investigated stones

DT	Drachenfels trachyte
MT	Montemerlo trachyte
SL	Stenzelberg latite
OS	Obernkirchen sandstone
SS	Schlaitdorf sandstone
BS	Bozanov sandstone
LB	Londorf basalt lava

**Table 7.6:** Leachants

1	Demineralized water
2	pH 3,4 (analogous Kolthoff )
3	pH 7,0 (analogous Palitzsch)
4	pH 8,4 (analogous Palitzsch)
5	saturated gypsum solution

sample SS was not eluted in pH 3.4

**Figure 7.6** (a) coarse sample fraction (4–10 mm) (b) fine sample fraction (stone powder)

From the fine sample fraction about 3 g of material, and from the coarse fraction about 9 g (mass was checked individually) were eluted in 25 ml of the different leachants. Samples were continuously tempered in a water bath (35°C) and agitated daily. After the various leaching periods, the pH was measured. From the eluates of the three consecutive one-week leaching periods of charge 1 (Ch1Wo1, Ch1Wo2, Ch1Wo3), and from the first four-week leaching period of charge 2 (Ch2Wo4), leached fractions were analyzed ion chromatographically (see 7.2 Materials and methods).

**Table 7.7** Leaching periods: charge 1: three consecutive one-week leaching periods; charge: two consecutive four weeks periods; charge 3: one twelve-week leaching period

charge 1			charge 2		charge 3
week 1	week 2	week 3	week 4	week 8	week 12
Ch1Wo1	Ch1Wo2	Ch1Wo3	Ch2Wo4	Ch2Wo8	Ch3Wo12

The leaching periods were divided in three charges: charge 1 consists of three consecutive one-week periods, where the eluates were charged from one and the same stone fraction; at charge 2, the eluates were changed after a four-week period until eight weeks in total had passed; charge 3 was left sitting over the complete twelve-week leaching period (Tab. 7.7).

### 7.3.2 Detection of pH changes

The complete data for the detected pH values is in the appendix (Tab. A7.2). The measurements show a strong increase in all the leachants. In the pH 3.4, the values rise to pH 6.5 (Obernkirchen sandstone) and to pH 8.0 (Stenzelberg latite and Londorf basalt lava) in the first week (Fig. 7.7). This indicates that the cations are readily soluble and that the buffer is not sufficient to maintain a steady pH. At the various new fillings the increase of pH values was less significant. In the consecutive one-week leaching periods, the pH continues to increase (except for the Obernkirchen sandstone), but not as much. Comparing the one-week with the twelve-week leaching period, the increase of the pH during the longer leaching period is more significant for the sandstones (Fig. 7.8). For the Stenzelberg latite and the Londorf basalt lava, slightly lower values are detected (Fig. 7.8).

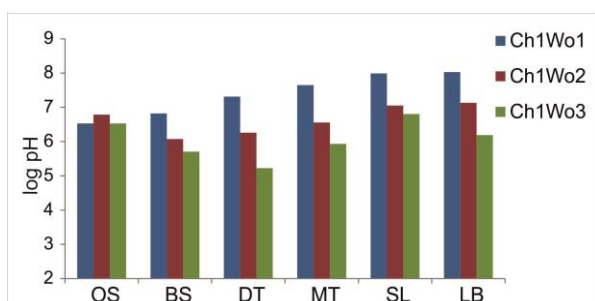


**Figure 7.7** The pH values of the eluates of charge 1 of three consecutive one-week leaching periods in leachant pH 3.4; fine sample fraction of the investigated stones

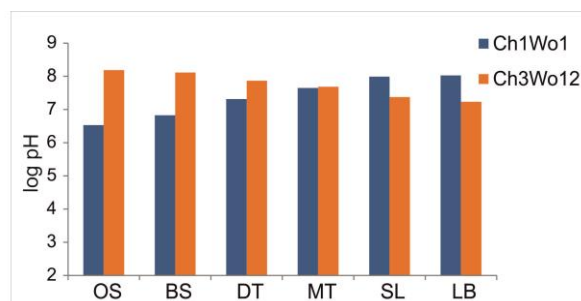


**Figure 7.8** The pH values of the eluates comparing the one-week with the twelve-week leaching period in leachant pH 3.4; fine sample fraction of the investigated stones

### 7.3.3 Leached fractions

#### Schlaitdorf sandstone

The concentrations (g/kg) of the individual leached fractions from the Schlaitdorf sandstone (fine and coarse grain sizes) in the different leachants (demineralized water, pH 7, pH 8, and saturated gypsum solution) are shown in figure 7.9; and figure A7.1 as well as in table A7.3 in the appendix. The leachabilities of the individual leached fractions (% of wt. %) from the Schlaitdorf sandstone (fine and coarse grain sizes) in the different leachants (demineralized water, pH 7, pH 8, and saturated gypsum solution) are shown in table A7.4 in the appendix. Due to a measuring error, data for the third one-week elution period (Ch1Wo3) in pH 7 is missing.

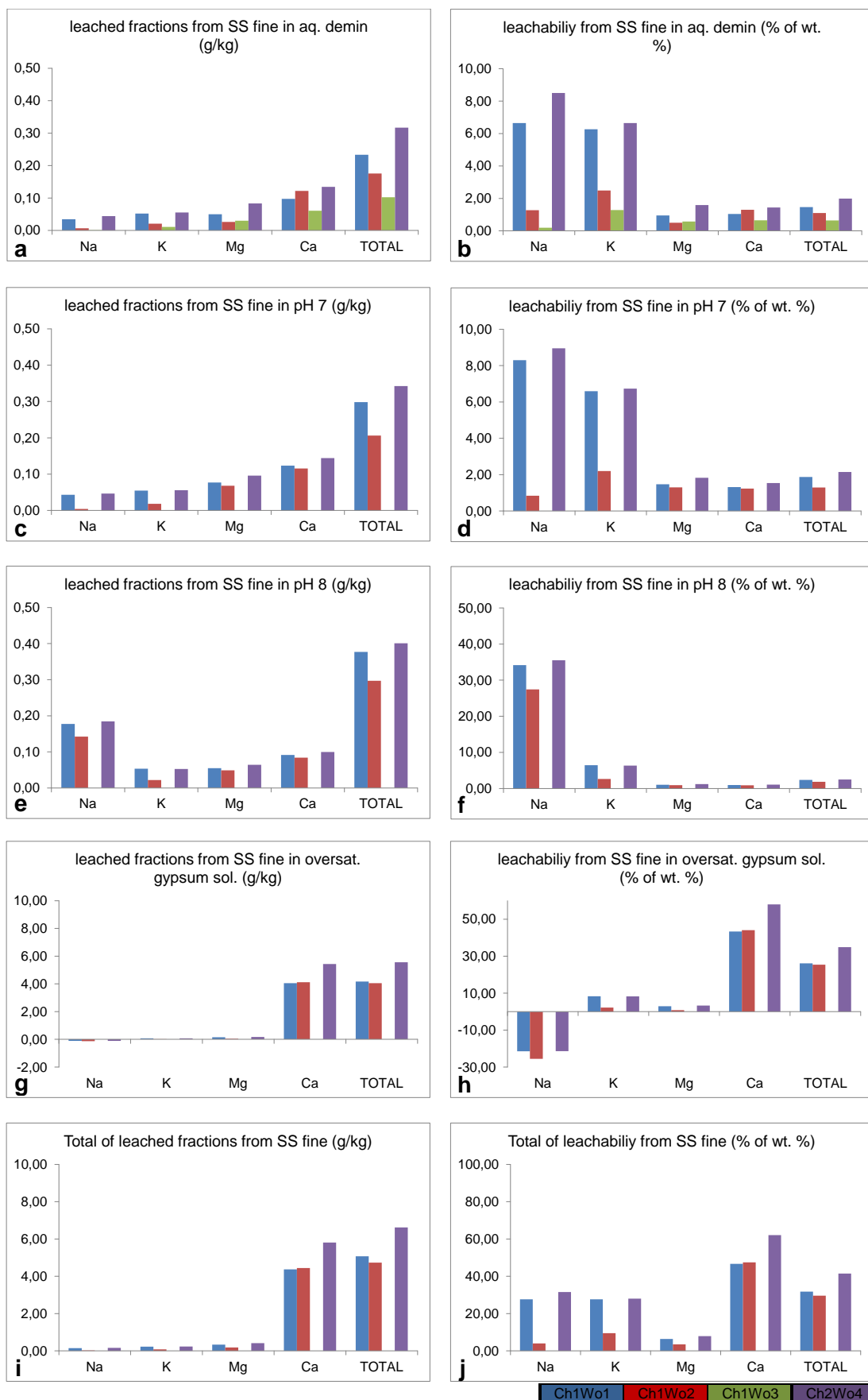


**Figure 7.9** Concentrations (g/kg) and leachabilities (% of wt. %) of the leached elements from the fine sample fraction from the Schlaitdorf sandstone (please note the different scales).

Comparing the concentrations of the leached fractions from the fine sample fractions from the Schlaitdorf sandstone in the different leachants, calcium is the most leached fraction except in pH 8, in which sodium shows the highest concentrations. (Fig. 7.9 a,c,e,g,i). Comparing the leachabilities of the different fractions in the various leachants, sodium and potassium show high leachabilities in demineralized water, pH 7 and pH 8 (Fig. 7.9 b, d, f). In the saturated gypsum solution the calcium fraction shows a significantly higher leachability (Fig. 7.9 h; Tab. A7.4 in the appendix). In the saturated gypsum solution highest concentrations of leached fractions are detectable (Fig. 7.9 g). In the other three leachants, the concentration of the total leached fractions differs insignificantly (Fig. 7.9 a, c, e). In general, the calcium fraction shows highest concentrations as well the highest leachability from the Schlaitdorf sandstone (Fig. 7.9 i and j).

The high sodium concentration in pH 8 as well as the high calcium concentrations in the saturated gypsum solution might indicate cation exchange processes. In the buffers of pH 3.4, pH 7 and pH 8.4 borax ( $\text{Na}_2\text{B}_4\text{O}_7 \cdot 10 \text{H}_2\text{O}$ ) is contained (see buffer preparation in the appendix Tab. A7.1). Here the sodium ions, and in the gypsum solution the calcium ions, of the salts might be replaced by cations leached from the Schlaitdorf sandstone. This assumption is underlined by the higher yield of calcium ions in the four week elution period (Ch2Wo4) in comparison with the first one-week elution period (Ch1Wo1) (Fig. 7.9 g). Cation exchange is a time dependent process. Thus, over longer leaching periods more ions can be exchanged.

However, the high yields of calcium associated as a total with high leachability indicate the major impact of the dissolution of the carbonate cement in the Schlaitdorf sandstone.

As expected, the concentrations of the leached fractions are much lower in the coarse sample fractions from Schlaitdorf sandstone compared with the fine sample fractions due to the smaller reactive surfaces of the former (Tab. 7.8a). Noticeable are the relatively high sodium concentrations as well as the leachabilities in demineralized water, pH 7 and pH 8 (Fig. A7.1 a, c, e in the appendix). Higher concentrations as well as higher leachabilities would have been expected for the calcium and also for the magnesium fraction. These two derive from the dolomite cement of the stone, which is relatively soluble in the fine as well as in the coarse sample fractions. High element yields in the coarse sample fractions are assumed to come from smaller grain sizes in the natural stone. The high yields of sodium might be explained by a cation exchange process with borax. This readily soluble salt forms other salts with magnesium and calcium (boracite and colemanite) which show lower solubility compared with borax. Thus, magnesium as well as calcium ions from the dolomite cement, are “caught” by the  $\text{BO}_3^{3-}$  anion and sodium is released. Noticeable as well is the high concentration of calcium in the saturated gypsum solution. A possible explanation could be cation exchange processes.

## leached concentrations

		<b>fine</b>	<b>coarse</b>	
<b>SS</b>	<b>Na</b>	0,06	0,02	
	<b>K</b>	0,03	0,01	
	<b>Mg</b>	0,05	0,01	
	<b>Ca</b>	0,10	0,02	
	<b>SS</b>	<b>0,25</b>	<b>0,05</b>	<b>4,5</b>

<b>DT</b>	<b>Na</b>	0,07	0,01	
	<b>K</b>	0,08	0,03	
	<b>Mg</b>	0,01	0,00	
	<b>Ca</b>	0,10	0,03	
	<b>DT</b>	<b>0,25</b>	<b>0,07</b>	<b>3,7</b>

<b>MT</b>	<b>Na</b>	0,03	0,00	
	<b>K</b>	0,02	0,01	
	<b>Mg</b>	0,03	0,03	
	<b>Ca</b>	0,13	0,05	
	<b>MT</b>	<b>0,21</b>	<b>0,09</b>	<b>2,3</b>

<b>OS</b>	<b>Na</b>	0,02	0,01	
	<b>K</b>	0,00	0,00	
	<b>Mg</b>	0,00	0,00	
	<b>Ca</b>	0,03	0,01	
	<b>OS</b>	<b>0,05</b>	<b>0,02</b>	<b>3,4</b>

<b>BS</b>	<b>Na</b>	-0,01	-0,01	
	<b>K</b>	0,03	0,00	
	<b>Mg</b>	0,00	0,00	
	<b>Ca</b>	0,00	0,00	
	<b>BS</b>	<b>0,02</b>	<b>-0,01</b>	<b>-3,0</b>

<b>SL</b>	<b>Na</b>	0,09	0,03	
	<b>K</b>	0,04	0,00	
	<b>Mg</b>	0,01	0,00	
	<b>Ca</b>	0,02	0,01	
	<b>SL</b>	<b>0,16</b>	<b>0,04</b>	<b>4,0</b>

<b>LB</b>	<b>Na</b>	0,05	0,00	
	<b>K</b>	0,01	0,00	
	<b>Mg</b>	0,03	0,00	
	<b>Ca</b>	0,05	0,01	
	<b>LB</b>	<b>0,15</b>	<b>0,02</b>	<b>9,6</b>

**a**

## leachabilities

		<b>fine</b>	<b>coarse</b>	
<b>SS</b>	<b>Na</b>	11,02	3,62	
	<b>K</b>	4,18	1,01	
	<b>Mg</b>	1,05	0,26	
	<b>Ca</b>	1,06	0,18	
	<b>SS</b>	<b>4,33</b>	<b>1,26</b>	<b>3,4</b>

<b>DT</b>	<b>Na</b>	0,20	0,03	
	<b>K</b>	0,17	0,06	
	<b>Mg</b>	0,22	0,04	
	<b>Ca</b>	0,59	0,17	
	<b>DT</b>	<b>0,29</b>	<b>0,08</b>	<b>3,9</b>

<b>MT</b>	<b>Na</b>	0,15	0,01	
	<b>K</b>	0,08	0,01	
	<b>Mg</b>	0,24	0,13	
	<b>Ca</b>	0,20	0,21	
	<b>MT</b>	<b>0,17</b>	<b>0,09</b>	<b>1,8</b>

<b>OS</b>	<b>Na</b>	0,03	0,03	
	<b>K</b>	1,68	0,43	
	<b>Mg</b>	0,34	0,05	
	<b>Ca</b>	0,33	0,28	
	<b>OS</b>	<b>0,59</b>	<b>0,20</b>	<b>3,0</b>

<b>BS</b>	<b>Na</b>	-0,27	-0,38	
	<b>K</b>	0,20	0,01	
	<b>Mg</b>	0,35	0,03	
	<b>Ca</b>	0,45	0,02	
	<b>BS</b>	<b>0,18</b>	<b>-0,08</b>	<b>-2,2</b>

<b>SL</b>	<b>Na</b>	0,29	0,08	
	<b>K</b>	0,11	0,02	
	<b>Mg</b>	0,09	0,02	
	<b>Ca</b>	0,06	0,02	
	<b>SL</b>	<b>0,14</b>	<b>0,04</b>	<b>3,8</b>

<b>LB</b>	<b>Na</b>	0,22	0,00	
	<b>K</b>	0,12	0,01	
	<b>Mg</b>	0,07	0,01	
	<b>Ca</b>	0,08	0,02	
	<b>LB</b>	<b>0,12</b>	<b>0,01</b>	<b>12,7</b>

**b**

**Table 7.8 (a)** Average concentrations (g/kg) and total concentrations (g/kg) of leached elements from the fine and coarse sample fractions from the different stones in demineralized water, pH 3.4, pH 7 and pH 8.4; **(b)** average leachabilities (% of wt. %) and total leachabilities (% of wt. %) of leached elements from the fine and coarse sample fractions from the different stones in demineralized water, pH 3.4, pH 7 and pH 8.4

**Drachenfels trachyte**

The concentrations (g/kg) of the individual leached fractions from the Drachenfels trachyte (fine and coarse grain sizes) in the different leachants (demineralized water, pH 3.4, pH 7, pH 8, and saturated gypsum solution) and the respective totals are shown in figure 7.10; and figure A7.2 and table A7.5 in the appendix. The leachabilities of the individual leached fractions (% of wt. %) from the Drachenfels trachyte (fine and coarse grain sizes) in the different leachants (demineralized water, pH 3.4, pH 7, pH 8, and saturated gypsum solution) are shown in table A7.6 in the appendix.

Comparing the concentrations of the leached fractions from the fine sample fractions from the Drachenfels trachyte, a continuous decrease can be observed for consecutive elution periods (Ch1Wo1 to Ch1Wo3) (Fig. 7.10 a, c, e, g, i). Sodium and potassium fractions show relatively regular values of around 0.1 to 0.2 g/kg in all the leachants (Fig. 7.10 a, c, e, g, i). Calcium shows higher concentrations in the pH 3.4 leachant (Fig. 7.10 c). The highest concentrations of leached fractions are given in the pH 3.4 leachant (Fig. 7.10 c). The total concentration of leached fractions is about double compared to the other leachants. The highest yields in concentration in total are given by sodium and potassium (Fig. 7.10 k). The highest leachability in total as the percentage of leached fractions relative to the element concentration in the host rock gives magnesium (Fig. 7.10 l). In the demineralized water sodium shows the highest leachability (Fig. 7.10 b). In the other leachants (pH 3.4, pH 7, and pH 8), calcium shows the highest leachability (Fig. 7.10 d, f, h). In the saturated gypsum solution a decrease of calcium concentration is detected (Fig. 7.10 i). The highest leachability in the saturated gypsum solution shows magnesium (Fig. 7.10 j). The highest concentrations of leached fractions are detectable in the pH 3.4 leachant with calcium being the main supplier (Fig. 7.10 c). In the coarse sample fractions from the Drachenfels trachyte, the concentrations of leached fractions and leachabilities are much lower compared to the fine sample fractions (Fig. A.7.2 in the appendix). The overall relative tendencies are comparable, except for slightly higher concentrations of the calcium fraction in the demineralized water, pH 3.4 and pH 8 for the longer elution period of four weeks (Ch2Wo4) (Fig. A.7.2 a, c, g in the appendix).



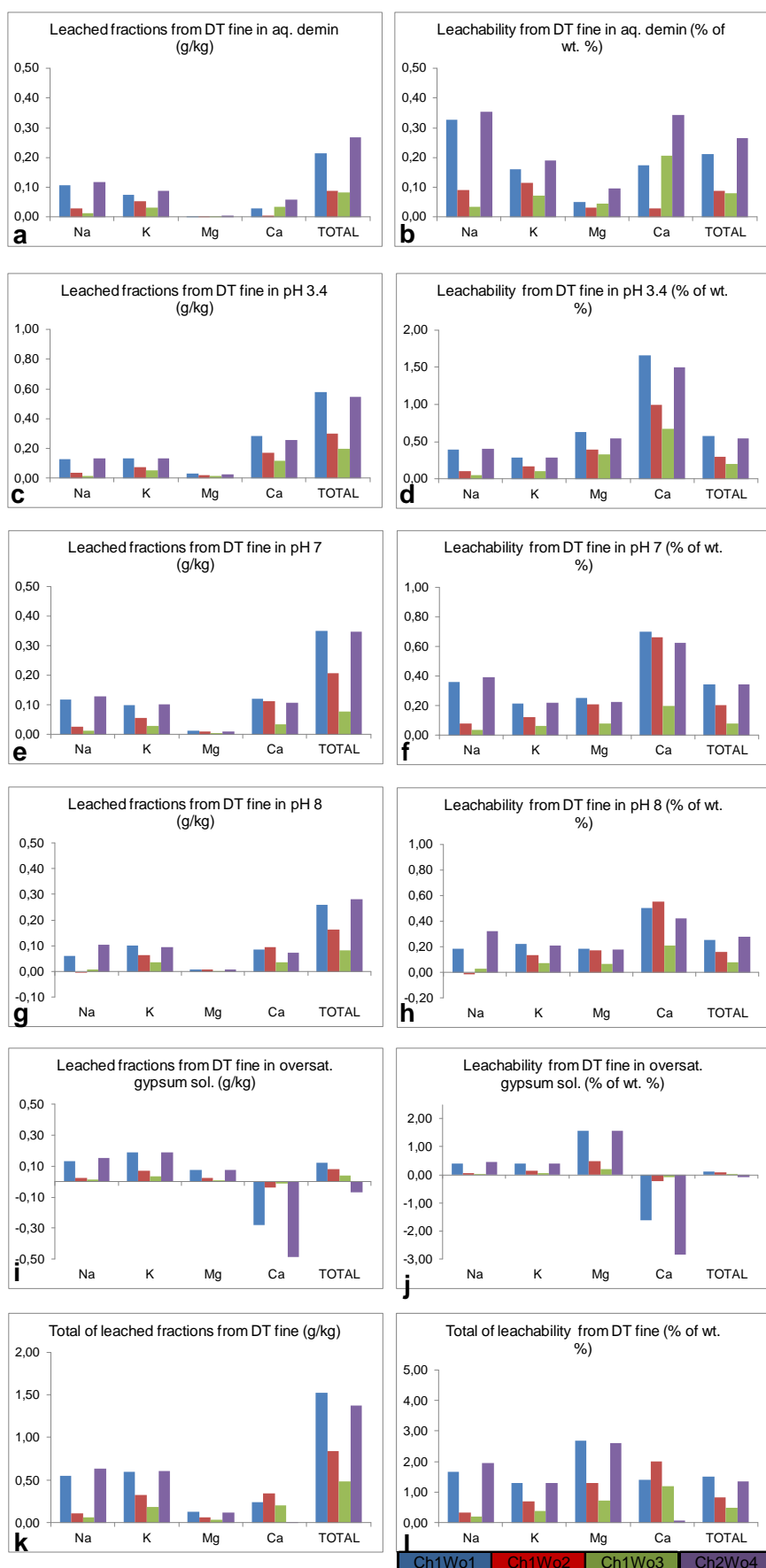


**Figure 7.10** Concentrations (g/kg) and leachabilities (% of wt. %) of the leached elements from the fine sample fraction from the Drachenfels trachyte (please note the different scales).

The data shows a more or less steady release of sodium and potassium, with very regular values in all the leachants in terms of concentration and leachability. This might be attributed to the corrosion of the high plagioclase and sanidine content in the cryptocrystalline matrix of the host rock. As for acidic impact, higher calcium yields are found in terms of concentration as well as in terms of leachability. This indicates a higher acid sensitivity of the minerals. The calcium content may derive from the weathering of the anorthite content in the plagioclases, from the minor content of apatite and from the accessory calcite. The higher leachabilities – but low concentrations – in the demineralized water, pH 7 and pH 8 in the fine sample fraction, as well as the slightly higher concentrations in the coarse sample fraction over longer elution periods may indicate calcite content. This mineral shows higher solubility than the silicate minerals; thus, higher leachability is detected. Since calcite is ascertained in the Drachenfels trachyte only in minor concentrations, only small quantities of leached calcium are achieved. The high magnesium leachability and the reduced calcium concentration in the saturated gypsum solution may indicate a cation exchange process from the clay mineral content in the Drachenfels trachyte.

### **Montemerlo trachyte**

The concentrations (g/kg) of the individual leached fractions from the Montemerlo trachyte (fine and coarse grain sizes) in the different leachants (demineralized water, pH 3.4, pH 7, pH 8, and saturated gypsum solution) and the respective totals are shown in figure 7.11; and figure A7.3 as well as in table A7.7 in the appendix. The leachabilities of the individual leached fractions (% of wt. %) from the Montemerlo trachyte (fine and coarse grain sizes) in the different leachants (demineralized water, pH 3.4, pH 7, pH 8, and saturated gypsum solution) are shown in table A7.8 in the appendix.

Comparing the concentrations of the leached fractions from the fine sample fractions from the Montemerlo trachyte, a continuous decrease can be observed for consecutive elution periods (Ch1Wo1 to Ch1Wo3) (Fig. 7.11 a, c, e, g, i). The sodium fraction shows the highest values, except for in the saturated gypsum solution (Fig. 7.11 i). The calcium concentration is pronounced in the pH 3.4 leachant (Fig. 7.11 c). The highest concentrations of leached fractions are given in the pH 3.4 leachant (Fig. 7.11 c). The Magnesium concentration in pH 3.4 is noticeable, as it is in the saturated gypsum solution (Fig. 7.11 c and i).

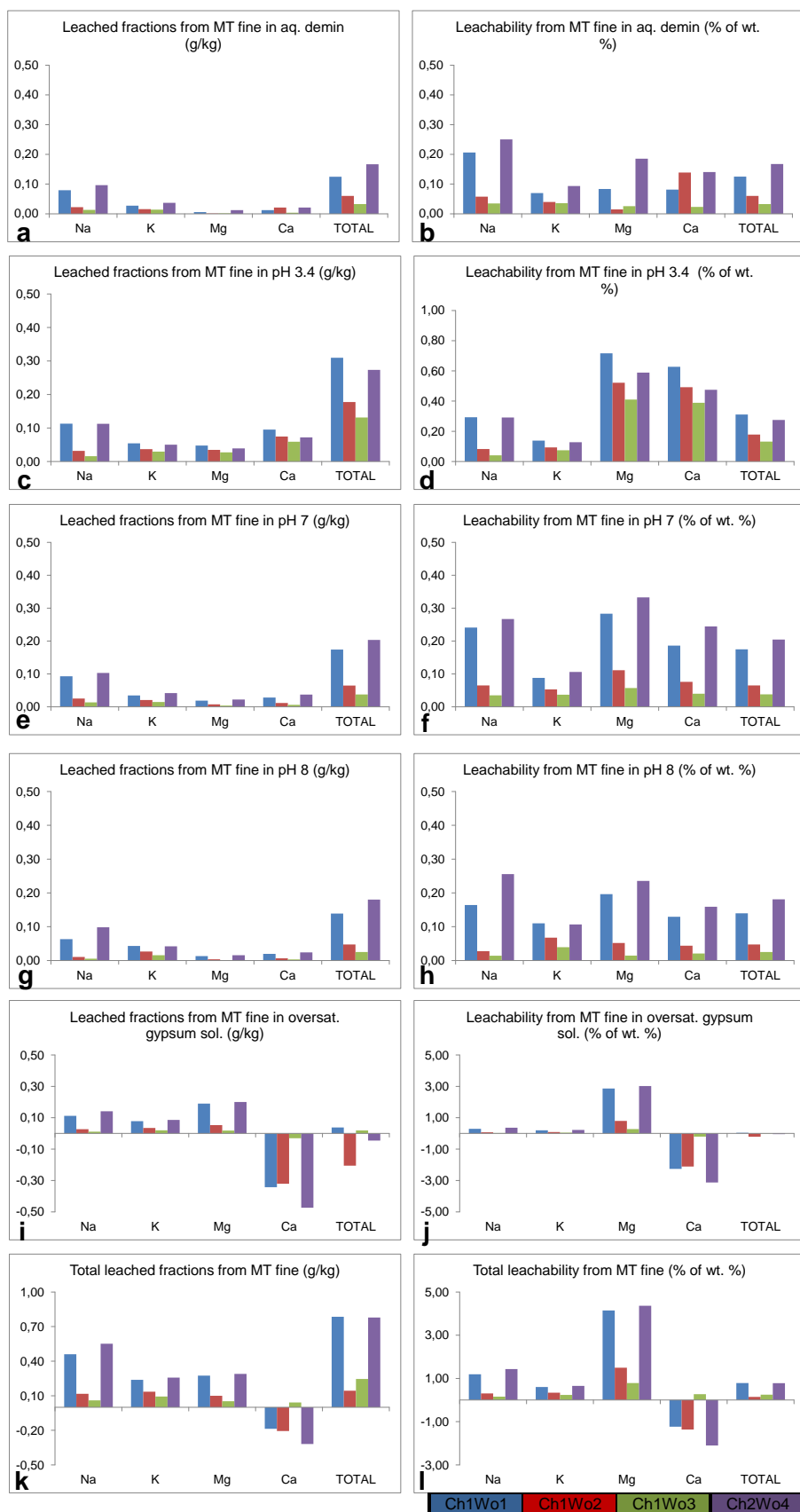


**Figure 7.11** Concentrations (g/kg) and leachabilities (% of wt. %) of the leached elements from the fine sample fraction from the Montemerlo trachyte (please note the different scales).

The highest yields in concentration in total are given by sodium and magnesium (Fig. 7.11 k). The leachability for magnesium is always relatively high (Fig. 7.11 d, f, h, j); thus, the total for the magnesium is significant (Fig. 7.11 l). In the saturated gypsum solution, a decrease of calcium concentration is detected as being associated with a strong increase in magnesium concentration (Fig. 7.11 i). The highest leachability in the saturated gypsum solution shows magnesium (Fig. 7.11 j).

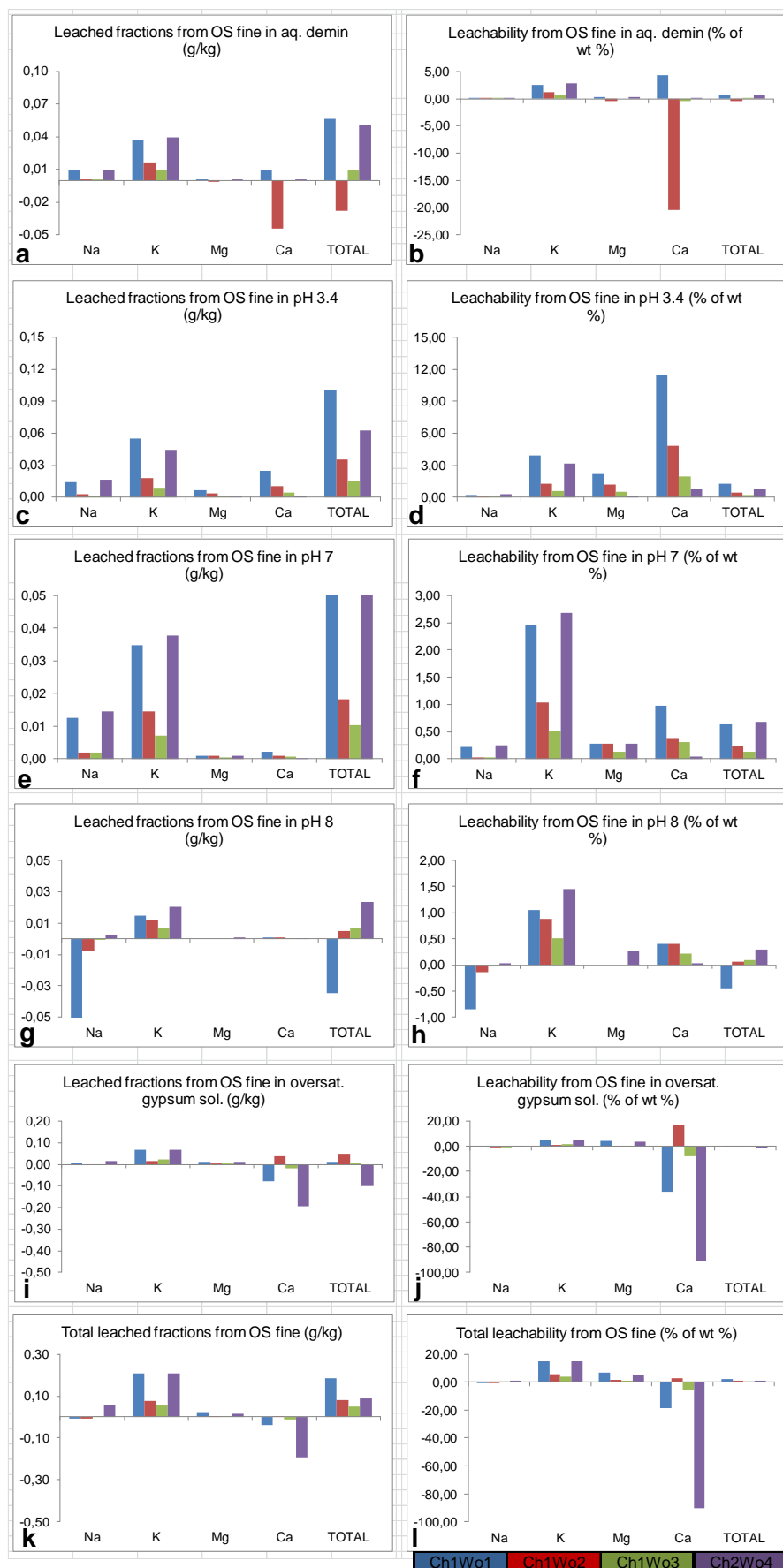
Comparing the different total yields of leached fractions, the highest values are detected for the pH 3.4 leachant with all four elements being the major supplier (Fig. 7.11 c).

In the coarse sample fractions from the Montemerlo trachyte, the concentrations of leached fractions and leachabilities are much lower compared with the fine sample fractions (Fig. A7.3 in the appendix). Noticeable are the high calcium yields in the demineralized water and pH 3.4, as well as in pH 8 (Fig. A7.3 a, c, g in the appendix).

Compared with the Drachenfels trachyte, the leached concentrations have a higher variance in the Montemerlo trachyte. The potassium concentration is significantly lower in the Montemerlo trachyte. A part of the leached sodium, potassium and calcium fractions might derive from the feldspar corrosion. The relatively high calcium yields especially in the coarse sample fraction of the Montemerlo trachyte can be attributed to the calcite content in the host rock. The potassium and the pronounced magnesium concentrations and leachabilities, which are significant in the pH 3.4 leachant from the fine grained sample as well as in the demineralized water, pH 3.4 and pH 8 leachants from the coarse grained sample, indicate a biotite and a certain clay mineral weathering. The high magnesium concentrations associated with a strong decrease in concentration of calcium in the saturated gypsum solution may indicate cation exchange processes from the clay minerals contained in the Montemerlo trachyte.

### **Obernkirchen and Bozanov sandstone**

The concentrations (g/kg) of the individual leached fractions from the Obernkirchen sandstone (fine and coarse grain sizes) in the different leachants (demineralized water, pH 3.4, pH 7, pH 8, and saturated gypsum solution) and the respective totals are shown in figure 7.12; and figure A7.4 as well as in table A7.9 in the appendix. The leachabilities of the individual leached fractions (% of wt. %) from the Obernkirchen sandstone (fine and coarse grain sizes) in the different leachants (demineralized water, pH 3.4, pH 7, pH 8, and saturated gypsum solution) are shown in table A7.10 in the appendix.



The concentrations (g/kg) of the individual leached fractions from the Bozanov sandstone (fine and coarse grain sizes) in the different leachants (demineralized water, pH 3.4, pH 7, pH 8, and saturated gypsum solution) and the respective totals are shown in figure 7.13; and figure A7.5 as well as in table A7.11 in the appendix. The leachabilities of the individual leached fractions (% of wt. %) from the Obernkirchen sandstone (fine and coarse grain sizes) in the different leachants (demineralized water, pH 3.4, pH 7, pH 8, and saturated gypsum solution) are shown in table A7.12 in the appendix.

Comparing the concentrations of the leached fractions from the fine sample fractions from the Obernkirchen and Bozanov sandstones, a continuous decrease can be observed for consecutive elution period (Ch1Wo1 to Ch1Wo3). Obernkirchen and Bozanov sandstone show comparable concentrations of leached fractions from their fine grained samples, with potassium showing the highest yields (Fig. 7.12 and 7.13). In the saturated gypsum solution the concentrations of magnesium and potassium are higher from the Bozanov sandstone than from the Obernkirchen sandstone. This is associated with a significant decrease in calcium, indicating cation exchange processes.

The leachabilities of the various elements from the two sandstones differ: in the Obernkirchen sandstone, potassium shows significantly higher leachability. Although the concentrations are very small, this is easily understandable since the leachability reflects the percentage of leached fraction relative to the initial element content in the host rock. The leached potassium fraction may originate from accessory muscovite components. From the Bozanov sandstone, similar concentrations of potassium are leached, but the leachability is less. This indicates that the Obernkirchen sandstone is a pure arenite sandstone with minor amounts of other minerals, whereas for the Bozanov sandstone rock fragments and feldspar components as well as a certain clay mineral content are reported (Koch 2006; Přikryl et al. 2010).

Comparing the fine sample fraction from Obernkirchen sandstone with the coarse sample fraction, leached concentrations are about three times higher in the fine grained sample (Tab. 7.8a). Looking at the total concentration of leached elements from the Bozanov sandstone the difference seems to be within the measurement accuracy (Tab. 7.8a). If the single leachants are regarded, it is obvious that the yield from the fine sample fraction is much higher than that from the coarse sample fraction. The strong depletion of sodium in pH 8 (Tab. A7.5g in the appendix) changes the value of the total. .

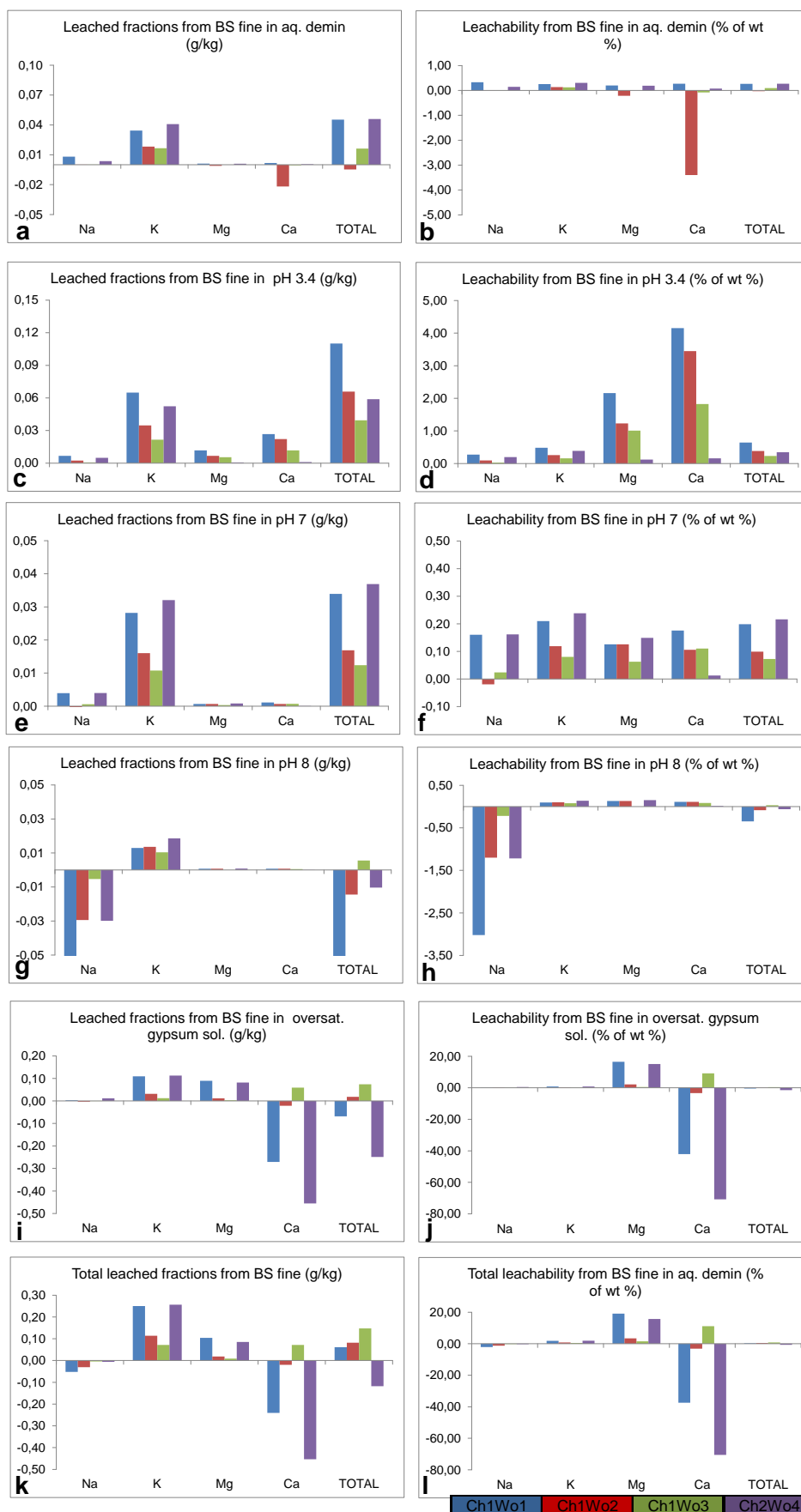


**Figure 7.13** Concentrations (g/kg) and leachabilities (% of wt. %) of the leached elements from the fine sample fraction from the Obernkirchen sandstone (please note the different scales).

### 7.3.4 Discussion

Comparing the pH values from the first to the third one-week leaching periods of charge 1 (Fig. 7.7), a decrease is obvious. This is reflected by the total concentration of leached elements from the various stones (see Fig. 7.10–7.13 diagram c).

The concentrations of the leached elements differ from leachant to leachant, but a tendency for a primary leached fraction can be observed for each stone: from the Schlaitdorf sandstone this is calcium; from the Drachenfels trachyte, potassium; from the Montemerlo trachyte, the highest yields are given by sodium and magnesium; from the Obernkirchen sandstone, the highest concentrations of potassium are detected; from the Bozanov sandstone, potassium and magnesium; from Stenzelberg latite, the highest yields are found for sodium; and from Londorf basalt lava, this is magnesium and sodium. The highest yields are generally found in the pH 3.4 leachant.

The negative values found for the calcium fraction in the saturated gypsum solution seems to be confusing at first sight. They can be explained by cation exchange processes. In rocks containing clay minerals, the cation exchange should preferably take place with the clay mineral content of the various host rocks; e.g., Drachenfels and Montemerlo trachyte as well as Bozanov sandstone. Thus, they may function as a sort of indicator for the clay mineral content. In the Stenzelberg latite and in the Londorf basalt lava, where strong decreases in calcium and significantly higher concentrations of magnesium are found (Tab. A7.13–A716 in the appendix), this might involve tracing back to the hornblende and the olivine weathering. This points to how the cation exchange process with the calcium ions from gypsum cannot be ascribed to a specific mineral. In saturated gypsum solution, an only slightly increased solubility of K-feldspar is detected in comparison with demineralized water (Snethlage 1984). Therefore, a minor impact is deduced on the feldspar dissolution by gypsum within the pore space of sandstones.

## 7.4 Leaching processes in natural building stone

Snäll and Liljefors (2000) conducted leaching experiments on different rock-forming minerals in different strong acidic solutions. They determined the leachability of the element as the proportions (percentages of the total content) of elements soluble by the leachant. For the various elements, varying leachabilities were detected depending upon the type of leachant, leachant concentration, leaching time, temperature, grain size and mineralogical composition of the sample, as well as the experimental conditions.

Looking at the leachability of the elements from a rock rather than from a separated mineral, several points have to be considered. First, natural building stone is a highly inhomogeneous, porous material composed of various rock-forming minerals. The leachability of the elements from the various minerals depends upon different aspects; e.g.,



the mineralogy and the chemical composition of the mineral. The solubility of the mineral is dependent upon its grain size, indicating the major importance of textural features within the natural stone itself. In addition, the characteristics of the pore space in terms of the means of transport and accessibility are crucial. The pore space contains pore fillings and other artifacts, which are relatively ready-soluble in general. Thus, the experiments described are an approximation towards the leachability of different natural building stones in comparison with one another. However, from these experiments tendencies and conclusions can be drawn in terms of the correlation of leachability, grain size, and leachant. The interaction of several chemical reactions in correspondence with the different leachants and their specific implications for some of the rock-forming minerals is highlighted.

#### 7.4.1 Correlation of leachability, grain size and leachant

A higher leachability indicates a more ready release of the element from the respective minerals in the host rock. Thus, the mineral can be addressed as less weather resistant and more easily degradable. Meanwhile, low leachabilities show that the element is barely leached from the respective mineral in the host rock. Thus, the mineral shows higher weather resistance and corrodes less. With smaller grain sizes of the mineral within the host rock, the leachability increases due to the higher reaction surface.

The high leachability of an element from a coarse sample fraction from natural stone may indicate the leachability from a mineral with a low weather resistance and/or a large reaction surface, whereas a low leachability of the same element from a coarse sample fraction from the stone may indicate a higher weather resistance of the mineral or a larger mineral grain size. Thus, a physical comminution of the stone sample – i.e., the mineral grain – would yield higher leachabilities.

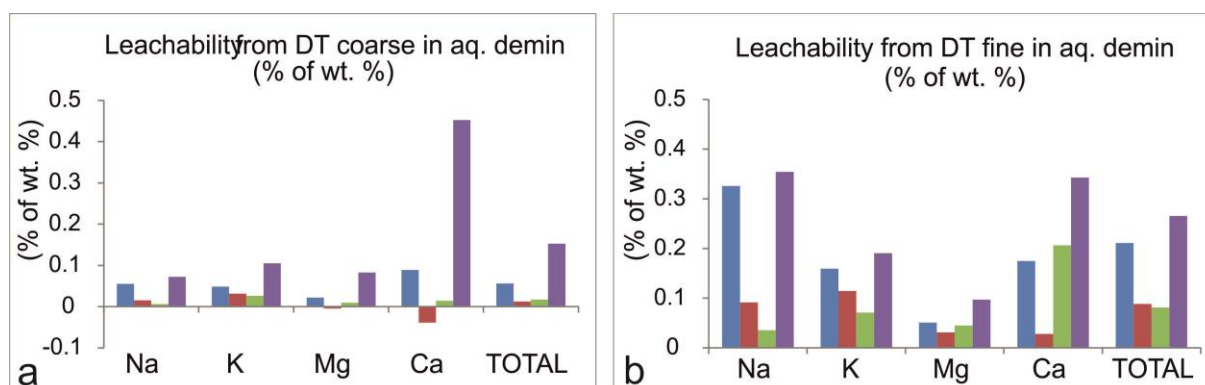


**Figure 7.14 (a)** Leachability (% of wt. %) from the fine sample fraction from the Drachenfels trachyte; **(b)** leachability (% of wt. %) from the coarse sample fraction from the Drachenfels trachyte

With regard to the different grain size samples of the various rocks used in the experiment just mentioned; in general, the higher leachabilities of elements are reached in the finer sample fractions. As an example, the high leachability of calcium from the coarse sample

fraction from the Drachenfels trachyte may indicate a certain leached concentration of ready-soluble calcite (Fig. 7.14a). Additionally, the high amount of plagioclases ( $\text{Ab}_{70}\text{An}_{30}$ ) in the cryptocrystalline groundmass displays a large reaction surface for calcium to be leached. In the fine sample fraction, the leachabilities of the other elements converge somewhat on the leachability of calcium. This indicates a comminution of minerals, which originally show lower leachabilities within the texture of the host rock.

#### 7.4.2 Dependency upon the leachant

In comparing the test for acid buffering capacity, the leaching experiment with MSA, and the leaching in demineralized water, the concentrations of leached fractions differ very much depending upon the leachant. If the total concentration of leached elements in demineralized water from the fine sample fraction from the investigated stones of one and four weeks (Fig. 7.15) is compared to that with MSA over 24 hours (Fig. 7.4) and with the ion equivalent of the acid buffering capacity with HCl (Fig. 7.2) strong divergences are noticeable.

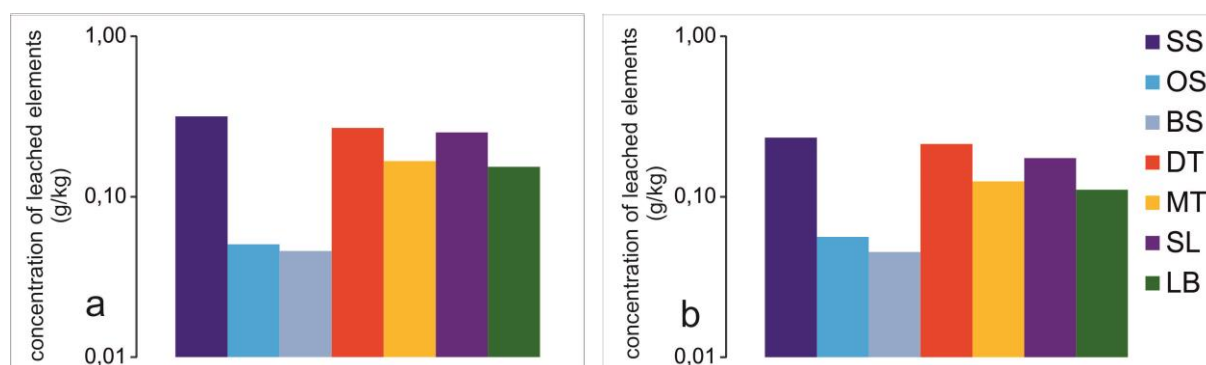


**Figure 7.15** Total concentrations (g/kg) of the leached elements from the fine sample fraction from the investigated stones in demineralized water **(a)** after a one-week leaching period; **(b)** after a four-week leaching period

The acid buffering capacity shows high capacities for Krensheim Muschelkalk and Schlaitdorf sandstone, a medium capacity for the volcanic rocks and the lowest for the Obernkirchen arenite sandstone. This is reflected by a close proximity within the leaching in demineralized water (Fig. 7.15). The results of the leaching in MSA show very different results: Montemerlo trachyte is the least leachable, whereas Stenzelberg latite and Londorf basalt lava yield high concentrations of leached elements (Fig. 7.4). The determinative factor for the overall results in the MSA seems to be the high concentrations of leached aluminium from Obernkirchen sandstone, Stenzelberg latite and Londorf basalt lava (Tab. 7.2). These results are comparable, are only to a certain extent, with the results from the leaching in demineralized water, since from the latter the aluminum was not analyzed. However, HCl can be expected to release all possible cations in terms of a protolysis, as well the aluminum ions. Thus, the results of total concentrations and the acid buffering capacity should be comparable. However, the question arises as to where, through the leachant MSA, a specific selectivity in

terms of aluminum leaching exits; e.g. chelating etc. This not necessarily be related to the feldspar solution, but it may affect kaolinite (5 % in the Obernkirchen sandstone) and hornblende (9 % in the Stenzelberg latite). As to the Londorf basalt lava, the total of aluminum arrives from the plagioclases. In summary, it confirms the assessment of Snäll and Lilijefors (2000), namely that leachability is very much dependent upon the leachant.

Kraus (1983) conducted leaching experiments on cubic samples (20 x 20 x 5–10 mm) of Schlaitdorf and Obernkirchen sandstone, Drachenfels trachyte, Londorf basalt lava and Krenshiem Muschelkalk in sulfuric and sulfurous acid, tartaric acid, demineralized water, and a solution of calcium hydroxide and sulfuric acid. A correlation was observed for the loss of weight of the samples with the pH of the leachant, the carbonate concentration and pore size distribution, all indicating higher weight losses at lower pH, higher carbonate content and larger pore sizes. In the cubic samples, textural changes were detected. The change in water uptake could not be correlated with the aforementioned context of weight loss. Thus, a number of different chemical reactions are assumed, leading to a diversity of reaction products and changes in the pore space of the sample. The pH values detected in the experiments from Kraus (1983) show similarities with the pH values in the experiments described within (Tab.7.9). This might indicate a typical pH value specific for the various stones that is thus controlled by the chemical composition of the stones (Kraus 1983).

**Table 7.9:** The pH values in different leachants from the experiments conducted by Kraus (1983) and in the aforementioned experiments

	SS	OS	DT	LB
H <sub>2</sub> O pH 6 °	7.5	7.2	6.8	6.8
H <sub>2</sub> O pH 6 *	7.9	6.9	7.2	6.9
H <sub>2</sub> SO <sub>4</sub> pH 4 °	7.5	7.3	6.6	6.8
Kolthoff-buffer pH 3.4 *	X	7.1	7.3	7.0
Ca(OH) <sub>2</sub> /H <sub>2</sub> SO <sub>4</sub> solution pH 8.5 °	7.6	7.5	6.9	7.0
saturated gypsum sol. pH 4.8 *	7.3	6.0	7.1	6.6

° Kraus (1983); \* coarse sample fraction Ch3Wo12

Comparing the totals of the leached calcium fractions from both experiments, similarities cannot be found (Tab. 7.10). This again indicates the dependencies ascertained by Snäll and Lilijefors (2000). Moreover, Kraus (1983) detected a significantly increased weight loss of the Drachenfels trachyte and the Londorf basalt lava in the tartaric acid leachant. This resembles the high solubility of feldspars in strongly chelating organic acids (Huang and Keller 1970), which might also be assumed for the leaching results in the pH 3.4 leachant of the experiments containing succinic acid mentioned earlier.

**Table 7.10:** Concentrations of leached calcium in different leachants from the experiments conducted by Kraus (1983) and in the aforementioned experiments

		SS	OS	DT	LB
H <sub>2</sub> O pH 6 °	g/kg	1.7•10 <sup>-3</sup>	8.8•10 <sup>-4</sup>	1.9•10 <sup>-4</sup>	4.2•10 <sup>-4</sup>
H <sub>2</sub> O pH 6 *	g/kg	0.03	n.d.	0.02	0.01
H <sub>2</sub> SO <sub>4</sub> pH 4 °	g/kg	1.85•10 <sup>-3</sup>	1.31•10 <sup>-3</sup>	3.80•10 <sup>-4</sup>	6.57•10 <sup>-4</sup>
Kolthoff-buffer pH 3.4 *	g/kg	X	n.d.	0,04	0.02
Ca(OH) <sub>2</sub> /H <sub>2</sub> SO <sub>4</sub> solution pH 8.5 °	g/kg	1.68•10 <sup>-3</sup>	1.62•10 <sup>-3</sup>	3.33•10 <sup>-4</sup>	6.31•10 <sup>-4</sup>
saturated gypsum sol. pH 4.8 *	g/kg	1.5	- 0.01	- 0.12	- 0.27

° after Kraus (1983); \* coarse sample fraction Ch1Wo1

### 7.4.3 Interaction of weathering reactions

In the conducted experiments, several chemical reactions are apparent. In HCl, the main interaction with the minerals is protolysis. Additionally, HCl is a strong acid (pKs-value: –6). Affected by protolysis are all those rock-forming minerals analogous to Goldich (1938).

With MSA as a leachant, protolysis is probably the main reaction with the minerals. As an organic acid, MSA displays a relatively strong acidity of pKs –0.6 (Brownstein and Stillman 1959) to –1.9 (Paul et al. 1970). Since MSA is an organic acid and displays a sufficient electron density (min. one free pair of electrons), it may function as a complex-ligand (Rozas and Weaver 1996). The formation of chelates is very much pH-dependent.

Feldspar corrosion proceeds as the incongruent dissolution of the feldspars in a proteolyse reaction where alkali and earth alkali cations are leached and replaced by H<sup>+</sup> (Correns 1962; Loughnan 1969; Chou and Wollast 1984; White and Brantley 1995; White 2003). At a certain state of equilibrium an aluminum hydroxide layer forms on the mineral surface, acting as a protective layer (Chou and Wollast 1984). This layer has a certain stability in relation to neutral pH values. At higher or lower pH, feldspar corrosion proceeds. In the presence of organic acids, this sensitive equilibrium might be disturbed by the chelating effects of the organic acid on the aluminum ion. Thus, the “protective layer” might be affected and feldspar corrosion thereby enhanced (McBride 1994).

Within the Kolthoff-buffer at pH 3.4 and the Palitzsch-buffers at pH 7 and pH 8.4 – both containing organic acids and readily soluble salts – further reactions might be possible. For the Schlaitdorf sandstone, a cation exchange with borax and salt formation is considered.

A stronger, noticeable cation exchange process is seen in the saturated gypsum solution. The calcium ions from the gypsum interact with the clay minerals contained in some of the stones, as well as with hornblende, olivine and – possibly – biotite. Potassium and magnesium ions from the interlayer of these minerals are presumably exchanged by calcium

ions. This would explain the higher potassium and magnesium yields paired with a strong decrease in calcium. These reciprocal concentrations could advert to a particular clay mineral content within the stone. This would only be qualitatively indicated, since concentrations of leached elements might be controlled by the other aforementioned reactions as well.

As to the very complex situation of these elutes with various leachants – which show several possible weathering reactions – and the inhomogeneous natural building stones, the single reactions cannot be determined quantitatively. However, some mineral specific-reactions can be deduced.

#### **7.4.4 Comparison of experimental and natural weathering rates**

Weathering rates are dependent on a number of factors that can be classified as either intrinsic or extrinsic to a specific mineral (White and Brantley 2003). Intrinsic properties are physical or chemical characteristics, such as mineral composition, surface area and defect densities. Extrinsic features reflect environmental conditions external to the silicate phase that impact chemical weathering, such as solution composition, climate and biological activity. These processes are dependent upon external environmental conditions that are difficult to recreate fully under laboratory simulations. Out of these factors, solute compositions have the most direct impact on mineral weathering rates (White 2003).

In natural environments, changes in acidic impact are not directly reflected by weathering rates. This indicates that, besides hydrolysis (hydrolytic cleavage and ion exchange with hydrogen ions), other processes sometime overcome the expected results for natural weathering (White 2003). In general, the experimental rates of silicate dissolution decrease as solutions approach thermodynamic equilibrium (Burch et al. 1993, Taylor et al. 2000). White (1995) found that the apparent thermodynamic supersaturation of silicate minerals in the “natural environment” (soil pore waters) resulted from excessive values for the total dissolved aluminum. In reality, much of this aluminum is complexed with dissolved organics in shallow soils and does not contribute to the thermodynamic saturation state of silicate minerals. This indicates that, natural weathering rates are much stronger than experimental ones due to the complexing of aluminum hindering the supersaturation (White 2003).

As mentioned in chapter 1, weathering rates in the natural environment are significantly dependent upon fluid flux or water transport mechanisms controlling the saturation of pore solutions. The experimental data shows, that under neutral to acidic pH conditions, the rates of sodic plagioclase and K-feldspar dissolution were essentially the same (Blum and Stillings 1995). However, K-feldspar is commonly much more resistant to weathering than is plagioclase during natural weathering (Nesbitt et al., 1997). White (2003) detected a pronounced kaolinization of plagioclase. In contrast to that, “K-feldspar in the immediate proximity of plagioclase grains remains pristine and unaffected by weathering” (White 2003,

156). This is explained by their different thermodynamic saturation states, where the pore water is saturated with K-feldspar but undersaturated with more soluble plagioclase.

#### **7.4.5 Conclusion**

The experiments reflect relatively well the many-faceted situation of the impact of environmental deterioration, where different leachants affect natural building stone. Thus, several weathering reactions are expected which may enhance or hinder one another. Protolysis is not the only aspect operating as the major chemical reaction taking place in mineral corrosion. Chelating effects and cation exchange processes are expected to affect rock-forming minerals as well. White 2003 states that the interpretation of rock weathering based on solute concentrations is complicated by the fact that individual solute species (i.e., Na, K, Ca, Mg) are commonly produced by more than one weathering reaction. A spreadsheet approach (Garrels and Mackenzie 1967) is usually incorporated to calculate mineral masses, which commonly generates non-unique results that require independent confirmation of the actual weathering reactions (Parkhurst and Plummer 1993).

Furthermore, secondary reaction products may influence weathering reactions: “weathering acts on mineral surfaces by decreasing the overall surface free energy by selectively dissolving more soluble components and attacking structural defects and dislocations” (White 2003, 154). Weathering rates may decrease with continued weathering due to a decrease of overall surface free energy and due to secondary coatings (i.e., the occlusion by secondary clays and iron and aluminium oxides), the formation of depleted leached layers and the adsorption of organic compounds (Banfield and Barker 1994; Nugent et al. 1998).

The different tested grain sizes of the samples elucidate the impact of physical weathering on chemical deterioration processes. The mineral comminution through physical weathering leads to smaller mineral grain sizes and, thus, larger reactive surface and overall surface free energy, which potentiate chemical weathering. Additionally, physical deterioration processes texturally modify the fabric of the stone and change the pore space properties thus, creating new passages and pathways for chemical reaction fluids. On the other hand, through mineral weathering and the formation of deterioration layers of secondary weathering products, the cohesion of the mineral compound is weakened. This textural impairment promotes physical weathering.

The experiments elucidate fluid–mineral interactions. They illustrate possible reaction mechanisms and the deterioration processes of chemical weathering. The experimental studies are correlated with results in the literature and the weathering processes are related to reaction mechanisms, helping with the understanding of how natural building stone weathering will behave under various environmental conditions. As to any future work, the various components of rain water detected, causing the chemical deterioration of natural building stones and the composition of the resulting pore fluids might be detected, and their

leaching effects on the stones as well as on their single rock-forming minerals might be investigated separately. Here, different sample fractions – including cubic samples – might be compared.





## 8 The effect of air pollution on stone decay

As outlined in the introduction, the deterioration of natural building stone can be described by physical, chemical and biological deterioration processes. Through the experiments and tests described in chapter 6 and 7 several relevant physical and chemical processes could be specified. Even more, it is apparent that natural stone decay is distinctively complex and entails multi-factorial dependences and causalities. The interaction of environmental pollution impact and building stone decay is to be covered in the following chapter.

Severe stone deterioration is evident at the Cologne cathedral. In particular, the “Drachenfels” trachyte, which was the building material of the medieval construction period, shows significant structural deterioration as well as massive formation of gypsum crusts.

In the following, crust formation on limestone, sandstone and volcanic rock from the Cologne cathedral, as well as from the Xanten and Altenberg cathedrals are investigated. These three buildings, showing varying degrees of deterioration, are located in different areas and exposed to varying industrial, urban, and rural pollution. Thin laminar and black framboidal crusts form on calcareous as well as silicate stone. The lack of a significant intrinsic calcium and sulfur source for the formation of the gypsum crusts on the Drachenfels trachyte indicates major extrinsic environmental impact: a sufficient offer of  $\text{SO}_x$  from pollutant fluxes as well as external calcium sources (e.g., pollution, mortars, and neighboring calcite stones). Chemical analyses reveal strong gypsum enrichment within the crusts as well as higher concentrations of lead and other pollutants (arsenic, antimony, bismuth, tin, etc.), which generally can be linked to traffic and industry. The formation of weathering crusts in an industrial environment is clearly distinguishable from that in rural areas. Scanning electron microscopy observations confirm that the total amount of pollution is less at the Altenberg cathedral than at the Cologne and Xanten cathedrals. XRF analyses show that the formation of gypsum occurs in lower amounts at Altenberg. This correlates well with the measured  $\text{SO}_2$  content and the intensity of the decay at the different locations. Furthermore, the different types of crusts, e.g., framboidal and laminar crusts can be differentiated and assigned to the different locations. The black weathering crusts on the silicate Drachenfels trachyte contribute to the degradation of the historic building material. They enhance mechanical moisture-related deterioration processes and the decay by chemical corrosion of rock-forming minerals. Although  $\text{SO}_2$  concentrations in air have shown a strong decrease over the past 30 years, degradation in connection with weathering crusts is still observed. This indicates that not only contemporary or recent emissions, but also past pollutant concentrations have to be considered.

The formation of black weathering crusts as a function of pollution on different building stones in three different environmental settings is discussed. Crust formation on the Drachenfels trachyte, a volcanic rock, in the Cologne Cathedral as well as in the Xanten and

Altenberg Cathedrals, is investigated and compared to crust formation on limestone. Data are compared to those from other sites, including monuments in Hungary, confirming the weathering gradient of natural building stones from a rural to an urban environment.

The cathedrals in Cologne, Xanten, and Altenberg are three major gothic buildings of the Rhineland region, built during the thirteenth and fourteenth centuries using the same construction materials. Construction started in Cologne in 1248, in Xanten in 1263, and in Altenberg in 1259. The main construction material of the medieval building period was Drachenfels trachyte from the quarries of the “Siebengebirge”. Later restoration and reconstruction phases mainly in the nineteenth century employed similar building materials at all three monuments: “Stenzelberg” latite, “Obernkichen” and “Schlaitdorf” sandstone, and “Krensheim Muschelkalk” as well as “Londorf” basalt lava. Mortars employed were lime mortars in the medieval period, in the nineteenth century customary cement mortars were in use. (see chapter 2)

The building stones show severe deterioration phenomena, especially the Drachenfels trachyte (Graue et al. 2011). Thin laminar and black framboidal crusts, which incorporate particles from the pollution fluxes, cover the building stones. Weathering crusts also form on the silicate stone and contribute to the degradation of the historic building material. On the Drachenfels trachyte, the crust formation is strongly correlated to the disintegration of the stone. Gypsum is not only found within the crusts but also in deeper zones of disintegrated stone material. The crusts tend to detach, and further structural deterioration follows. Contour scaling, flaking and exfoliation are characteristic decay features on the Drachenfels trachyte, leading to granular disintegration and crumbling. On the Obernkirchen sandstone and on the Stenzelberg latite, weathering crusts form in very thin scales, 2–3 mm thick, which tend to detach from the stone. The Schlaitdorf sandstone shows thick black weathering crusts, which are frequently accompanied by severe contour scaling several centimeters thick, as well as pronounced granular disintegration. On the Krensheim Muschelkalk, the crusts seem to temporarily stabilize the stone surface (see Siegesmund et al. 2007). On surfaces exposed to rain, solution phenomena can be observed, e.g., microkarst (Graue et al. 2011).

The present investigation aims to access the problem of stone deterioration due to weathering crusts related to atmospheric pollution. Mineralogical and geochemical methods are combined: optical microscopy, X-ray diffraction (XRD) and fluorescence (XRF), as well as scanning electron microscopy (SEM), coupled with energy-dispersive X-ray spectroscopy (SEM-EDX) and wavelength dispersive microprobe analyses (WDS). Furthermore, laser ablation inductively coupled plasma mass spectrometry (La-ICP-MS) and inductively coupled plasma optical emission spectrometry (ICP-OES), as well as ion chromatography analyses with spectroscopy (IC), are used to address the issue. Polycyclic aromatic hydrocarbons

(PAH) are determined by microwave-accelerated extraction and subsequent gas chromatography with mass spectrometric detection (MAE-GC-MS).

## 8.1 Material and methods

To understand the context of building stone diversity and the different deterioration features, a sample field at Cologne cathedral was mapped, analogous to the system developed by Fitzner et al. (1995) (Fig. 4.1 and 4.2). Samples from crusts and dust as well as unweathered and weathered rock samples were collected from the Cologne, Xanten and Altenberg cathedrals from the different building stones (Drachenfels trachyte, Obernkirchen sandstone, Krenshiem Muschelkalk). The index of analyzed samples is found in Tab. A8.1 in the appendix.

Sample preparation and sample analyses were performed on the different sample types using overlapping techniques in mineralogical and geochemical analyses whenever possible. Thin sections perpendicular to the exposed surface of the rock were prepared and textural analysis of thin sections was performed by polarizing microscopy. The chemical data presented focus on the C, Na, Mg, Si, S, K, Ca, Al, Ti, Mn, Fe, Zn, As, Sb, Pb, and Bi contents of the host rocks and crusts.

The chemical composition was obtained by X-ray fluorescence spectroscopy. Major element oxides and the trace elements Ba, Cr, Ga, Nb, Ni, Rb, Sr, V, Y, Zn and Zr were analyzed by XRF on 105 °C-dried samples, prepared as fused disks of lithium tetraborate-metaborate (FLUXANA FX-X65, sample-to-flux ratio 1:6). A PANalytical Axios Advanced wavelength-dispersive spectrometer and matrix correction programs were used to calculate concentrations.  $\text{H}_2\text{O}^+$  and  $\text{CO}_2$  were determined using a Vario EL III (Elementar Analysensysteme GmbH, Hanau/Germany). An ELTRA CS 2000 (ELTRA GmbH Neuss) is used for measuring sulfur.

The mineralogical composition of the samples (black crusts and dust) was determined by X-ray diffraction (XRD). Powder X-ray patterns were obtained using a PANalytical Empyrean powder diffractometer with Cu  $\text{K}\alpha$  radiation, automatic divergent and antiscatter slits, and a PIXcel<sup>3D</sup> detector. The diffraction data were recorded from 5° to 85° 2 $\theta$  via a continuous scan with a step-size of 0.013 and a scan time of 60 s per step. The generator settings were 40 kV and 40 mA. The Rietveld algorithm BGMN was used for quantitative analysis (Bergmann et al. 1998).

LA-ICP-MS (laser ablation inductively coupled plasma mass spectrometry) analyses were performed on thin slices of the samples. The laser used was a Compex 110 Excimer (ArF 193 nm) by Lambda Physik (Goettingen, Germany), a GeoLas optical bench by MikroLas (Goettingen, Germany), a small volume sample chamber, an ablation pit with a diameter of 120  $\mu\text{m}$ , a 10 Hz repetition rate for the laser pulses and about 3 J/cm<sup>2</sup> available energy. The

mass spectrometer was a Perkin Elmer DRC II (Siex, Canada). Calibration was done using NBS610 (NIST, USA), internal Standard  $^{43}\text{Ca}$ , dwell time 10 ms/isotope, 0.925 s per sweep, and a total of 250 sweeps giving a total measurement time of 3:50 min. Measured isotopes were:  $\text{Li}^7$ ,  $\text{Na}^{23}$ ,  $\text{Mg}^{24}$ ,  $\text{Mg}^{25}$ ,  $\text{Al}^{27}$ ,  $\text{Si}^{29}$ ,  $\text{P}^{31}$ ,  $\text{S}^{34}$ ,  $\text{Cl}^{35}$ ,  $\text{K}^{39}$ ,  $\text{Ca}^{43}$ ,  $\text{Sc}^{45}$ ,  $\text{Ti}^{47}$ ,  $\text{Ti}^{49}$ ,  $\text{V}^{51}$ ,  $\text{Cr}^{53}$ ,  $\text{Mn}^{55}$ ,  $\text{Fe}^{57}$ ,  $\text{Co}^{59}$ ,  $\text{Ni}^{60}$ ,  $\text{Cu}^{63}$ ,  $\text{Cu}^{65}$ ,  $\text{Zn}^{66}$ ,  $\text{Ga}^{71}$ ,  $\text{Ge}^{73}$ ,  $\text{As}^{75}$ ,  $\text{Rb}^{85}$ ,  $\text{Sr}^{88}$ ,  $\text{Y}^{89}$ ,  $\text{Zr}^{90}$ ,  $\text{Nb}^{93}$ ,  $\text{Mo}^9$ .

To visualize the microfabric of the crust and the host rock, and to detect elemental-mineralogical composition of samples, SEM-EDX techniques were applied on thin sections as well as on small fragment samples (LEO GEMINI SEM 1530 and LEO 1455 Gemini, as well as AMRAY 1630). EDX-analyses were performed on a Quantra 200F (Fei) with a field emission cathode with an initial voltage of 20 kV (Department of Crystallography, Geoscience Center University of Goettingen, Germany).

Wavelength dispersive microprobe analyses were performed with a JEOL JXA 8900 RL instrument (Department of Geochemistry, Geoscience Center University of Goettingen, Germany). For quantitative measurements, 15 kV acceleration voltage, 15 nA beam current on the Faraday cup, a defocused beam of 3.5  $\mu\text{m}$  and counting times between 15 s on the peak for Na, Mg, Al, Si, K, Ca and Fe and 30 s for P, S, Ti and Ba were chosen. Data processing was done with the CITZAF routine in the JEOL software, which is based on the  $\Phi(\rho Z)$  correction method (Armstrong 1991, 1995). The following standards were used for the analysis: Albite for Na, MgO (synthetic) for Mg, anorthite for Al, wollastonite for Si and Ca, sanidine for K, apatite for P, baryte for S,  $\text{TiO}_2$  (synthetic) for Ti, rhodonite for Mn, hematite for Fe and celsian for Ba. Detection limits are calculated from the error propagation of the two measurements of the background signals of each X-ray line and are given as a 2-sigma value. The element distribution of Mg, Al, K, Ca, Fe (WDS) and S, Si (EDS) was mapped using an acceleration voltage of 15 kV and beam current of 30 nA. The acquisition time was set to 50 ms per step. The scan grid was spaced at 0.5  $\mu\text{m}$  per step, covering in total 400 x 400 steps. Simultaneous acquisition of the backscatter signal in composition mode was performed.

For PAH analysis the pulverized rock samples (1g) were weighted into Teflon vessels, internal standards (acenaphthen D 10, phenanthren D 10, pyren D 10, chrysen D 12, perylen D 12, and bBenzo(g,h,i)perylene D 12) and 5 mL iso hexane/ acetone (3:1 v:v) were added and subsequently extracted on a MARS XPRESS microwave system at 130 °C for 20 min. After cooling, the supernatant was removed and transferred into purging vials. After the addition of 500  $\mu\text{L}$  toluene, it was purged in a gentle stream of nitrogen until dry. The remains were re-dissolved into 500  $\mu\text{L}$  toluene, transferred into autosampler vials and centrifuged at 5000 rpm for 10 min. They were then immediately analyzed on a GC-MS (Agilent 7890A, 5975E). Separation of the analytes was achieved using a Varian VF5-ms column

(30x250x0.25) and a steady temperature gradient of 6 °/min up to a final temperature of 325 °C. Data were recorded in single ion monitoring mode (quantifier in parenthesis) with a dwell time of at least 50 ms per amu for the following analytes: acenaphthylen (152), fluorene (166), phenanthrene (178), anthracene (178), pyrene (202), 7H-benzo-fluorene (216), cyclopenta(c,d)-pyrene (226), benzo(a)anthracene (228), chrysene (228), 5-methyl-chrysene (242), benzo(b,j,k) fluoranthene (252), benzo(a)pyrene (276), indeno(1,2,3-cd)-pyren (278), dibenzo(a,h)-anthracene (276), benzo(g,h,i)-perylene (302), dibenzo(a,l)-pyrene (302), dibenzo(a,e)-pyrene (302), dibenzo(a,i)-pyrene (302), dibenzo(a,h)-pyrene (302). Quality was assured by simultaneous monitoring, scanning 50 350 amu. The method quantitation limit was 1 µg/kg.

## 8.2 Black weathering crusts on the natural building stones

### 8.2.1 Crust classification

The deposition of airborne particulates and the formation of crusts can be observed on surfaces over the entirety of Cologne Cathedral. These surface deterioration features appear in different manifestations, from patina-like grayish black surface depositions and soiling to thin black laminar crusts and thick framboidal or cauliflower-like black crusts. Especially with framboidal crusts, surface detachment and loss as well as further disintegration is observed (Fig. 8.1a). These cauliflower-like weathering crusts vary extremely in thickness from 2 to 15 and even 30 millimeters (Török et al. 2011). Their specific morphology also describes them as dendritic (Török et al. 2011), globular (Bonazza et al. 2007), rosey (Antill and Viles 1999) or framboidal (Török 2003, 2008). They display globular or rosette-like formations of gypsum crystals. Calcareous and also quartz particles cover the stone surface, and organic as well as inorganic particles from the pollution fluxes are incorporated into the crusts. Framboidal crusts generally build up in sheltered to moderately exposed areas as well as in cavities on vertical stone surfaces. They are often observed at different sites and for different building stones (Amoroso and Fassina 1983; Camuffo 1995; Sabbioni 1995; Bonazza et al. 2004, 2007b).

Thin laminar black crusts trace the stone surface and may cover complete sections of the building's structure, not necessarily preferring protected sites (Fig. 8.1b). This kind of crust does not change the morphology of the stone surface (Fitzner et al. 1995) and seems to have very strong bonds with the stone surface (Török et al. 2011; Siegesmund et al. 2007). Scaling is often observed with laminar crusts.

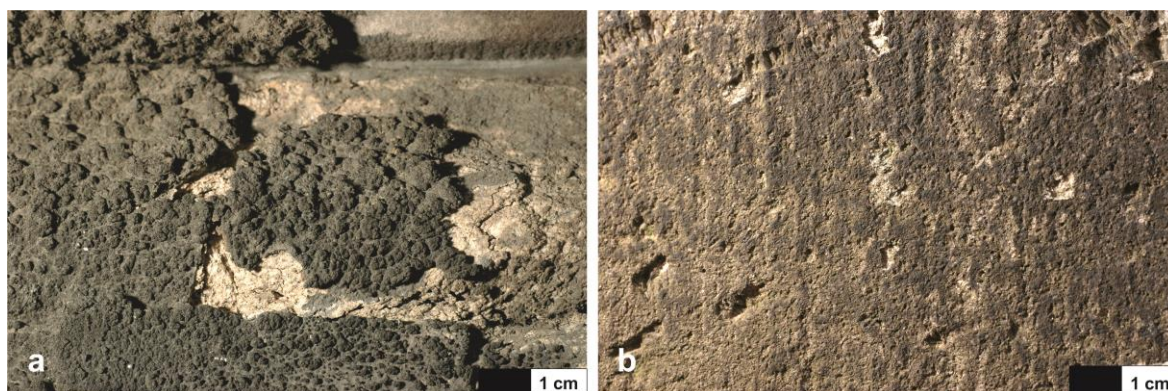


**Figure 8.1** a. Cauliflower-like or framboidal crust on Drachenfels trachyte contributing to the disintegration of the stone and leading to flaking and material loss; b. laminar crust on Drachenfels trachyte tracing the stone surface, where working traces are still visible.

Other investigated building stones of Cologne cathedral also show crust formation. On the Schlaitdorf sandstone, massive gypsum crusts build up due to the carbonate cement (app. 14%) leading to characteristic disintegration in the form of scaling, flaking and granular disintegration into sand (Lukas 1990). The main deterioration phenomenon of Stenzelberg latite is a typical formation of scales with a thickness of 2–3 mm (Graue et al. 2011). Obernkirchen sandstone has a high weather resistance, but shows black crusts and the formation of gypsum crusts in posterior and sheltered areas. Krensheim Muschelkalk as a carbonate building stone shows massive gypsum crust formations. This is visible in rain-protected areas, while on surfaces exposed to rain, solution phenomena can be observed e.g., microkarst. Unlike the Drachenfels trachyte, the limestone shows no structural disintegration with crust formation. At first it has almost a consolidating or inhibiting function.

In order to describe the variations of the different building stones and the specific deterioration features, a representative survey area has been mapped in accordance with the classification by Fitzner et al. (1995) (Fig. 4.1 and 4.2). The building material and the deterioration phenomena – erosion, gypsum crusts, scaling, flaking, cracks and depositions – have been mapped, displaying their distribution within the selected wall area.

If the three cathedrals from the industrial (Cologne), urban (Xanten) and rural (Altenberg) locations are compared, they show clear differences in terms of deterioration gradients and crust formation. While Altenberg cathedral shows only very little stone deterioration, in Xanten and especially in Cologne the decay is significant. At Cologne cathedral, severe damage can be observed entailing static disturbances. At all three cathedrals, scaling and flaking are the main deterioration features, though the observed effect is less at Xanten and Altenberg. As the mapping shows (Fig. 4.2), scaling and flaking are mainly concentrated in the Drachenfels trachyte. At Xanten und Altenberg cathedrals, the deterioration is often located in superficial areas of the building stones of Drachenfels trachyte, reaching only several centimeters in depth. Here it seldom reaches such a significant depth where the

structural disintegration comprises crumbling and total fabric collapse, as seen at Cologne Cathedral. The same can be ascertained for the intensity of surface soiling and weathering crusts. At Cologne Cathedral weathering crusts on building stones become apparent, whether as dark brownish-black surfaces of a mostly already detached stone surface or as framboidal crusts with a disintegrated stone matrix underneath (see Fig. 8.1). In Xanten, weathering crusts are more to be addressed as thin laminar crusts or soiling on a mostly structurally intact original building stone surface. The current condition of Altenberg cathedral reflects the extensive restoration and repair works carried out since the 1990s. Nevertheless, previous investigations only detected black weathering crusts to a minor degree (IBS 1990).

### **8.2.2 Mineralogy and fabric of black weathering crusts**

Microscopic observation reveals high porosity of the framboidal crusts (Fig. 8.2a) and very small (10–50 µm) and evenly spread acicular gypsum crystals (Fig. 8.2b). Cavities within the crystals cause the high porosity of the crust. The crust contains a significant amount of widely spread organic matter (black opaque particles). The crust formation on the Drachenfels trachyte is characterized by a thin, dense black layer on the surface of the host rock (10–20 µm), mainly consisting of organic material or carbonaceous particles (containing elemental and organic carbon) (Saiz-Jimenez 1993; Turpin and Huntzicker 1995), which may function as a catalyst for the formation of gypsum (Amoroso and Fassina 1983; Rodriguez-Navarro and Sebastian 1996; Ausset et al. 1992). On this surface layer, a porous framboidal crust builds with finely distributed gypsum crystals and crystal aggregates, together with quartz and feldspar particles (<0.1 mm) (Fig. 8.2d). The brownish tanning derives from iron-oxides/hydroxides (Do 2000). Framboidal black crusts on Drachenfels trachyte can be described as a porous mixture of gypsum, organic compounds, iron oxides, quartz, and feldspar particles. A large number of siliceous as well as carbonaceous fly ash particles are commonly embedded in such crusts and high ratios of Fe-rich particles are detected. In the limestone samples the fly ash particles are firmly incorporated into the gypsum crust, surrounded by gypsum crystals and overgrown with sub-micron size gypsum crystals (Török et al. 2011). However, although fly ash particles are found embedded in the trachyte structure in the samples of Drachenfels trachyte, their incorporation into the crust is not as strongly wedded to the growth of gypsum crystals as is the case in the crust on limestone.



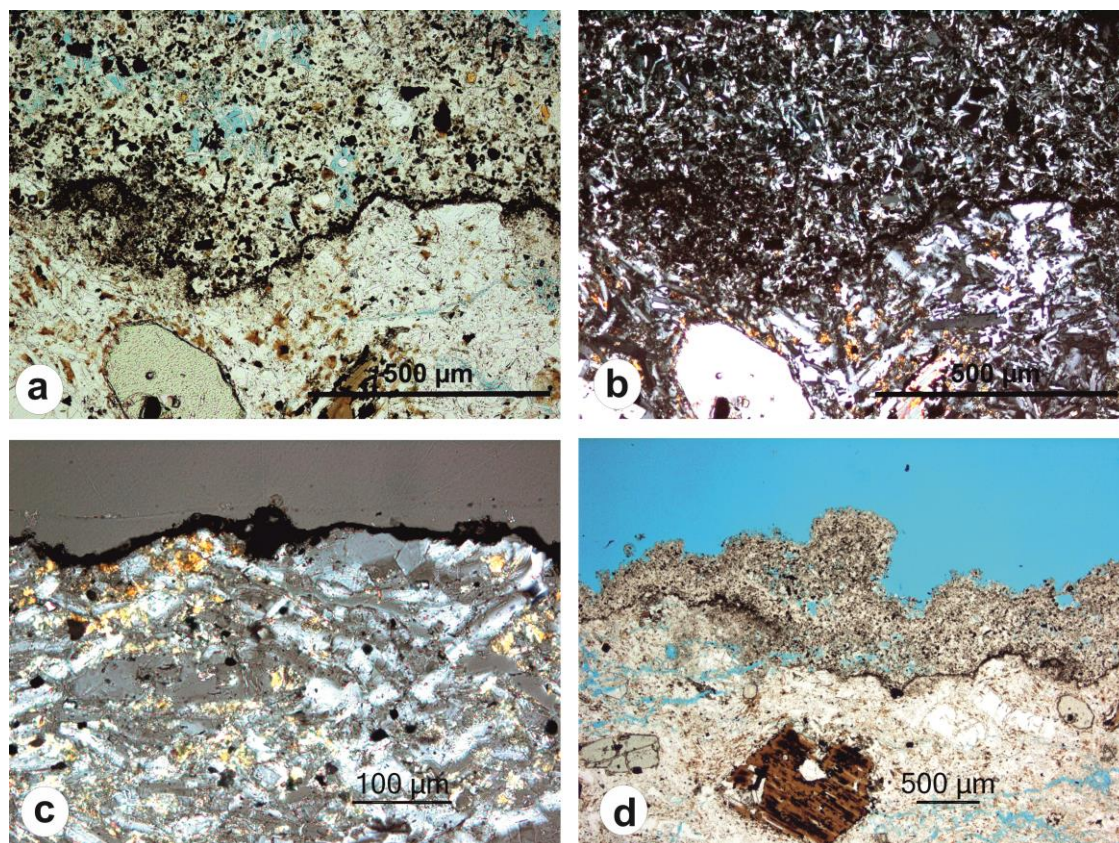


**Figure 8.2** Black weathering crusts on Drachenfels trachyte: **a.** framboidal crust (transmitted light) black interface layer, very porous poly-mineral composition with heterogeneous particle size; **b.** framboidal crust – same detail as Fig. 7a (crossed polars); **c.** laminar crust on Drachenfels trachyte, very thin opaque surface layer (crossed polars); **d.** thick framboidal crust with a black interface layer and surface parallel cracks in the host rock (crossed polars).

SEM-EDX analyses of the crust surface reveal a high gypsum concentration for framboidal crusts (Fig. 8.3a–d), whereas on laminar crusts a composition mainly of silicate and organic components is detected (Fig. 8.3e–f). The thin opaque black layer on the surface of the host rock marks the boundary of the stone, on which the crust forms. In some places, this defined line is distorted, which may be attributed to the structural disintegration of the stone material underneath. Surface parallel cracks are often observed in the host rock beneath the crust. These cracks not only run along grain boundaries, but also characteristically cut through larger grains and minerals (Fig. 8.2d). This structural degradation of the host rock finally leads to the detachment of the crust, including the upper superficial region of the host rock. The width of this detached zone is not limited to the crust but reaches into the host rock to a depth of 3–10 mm. The host rock shows further structural disintegration in the form of multiple flaking and exfoliation (Fig. 4.4).



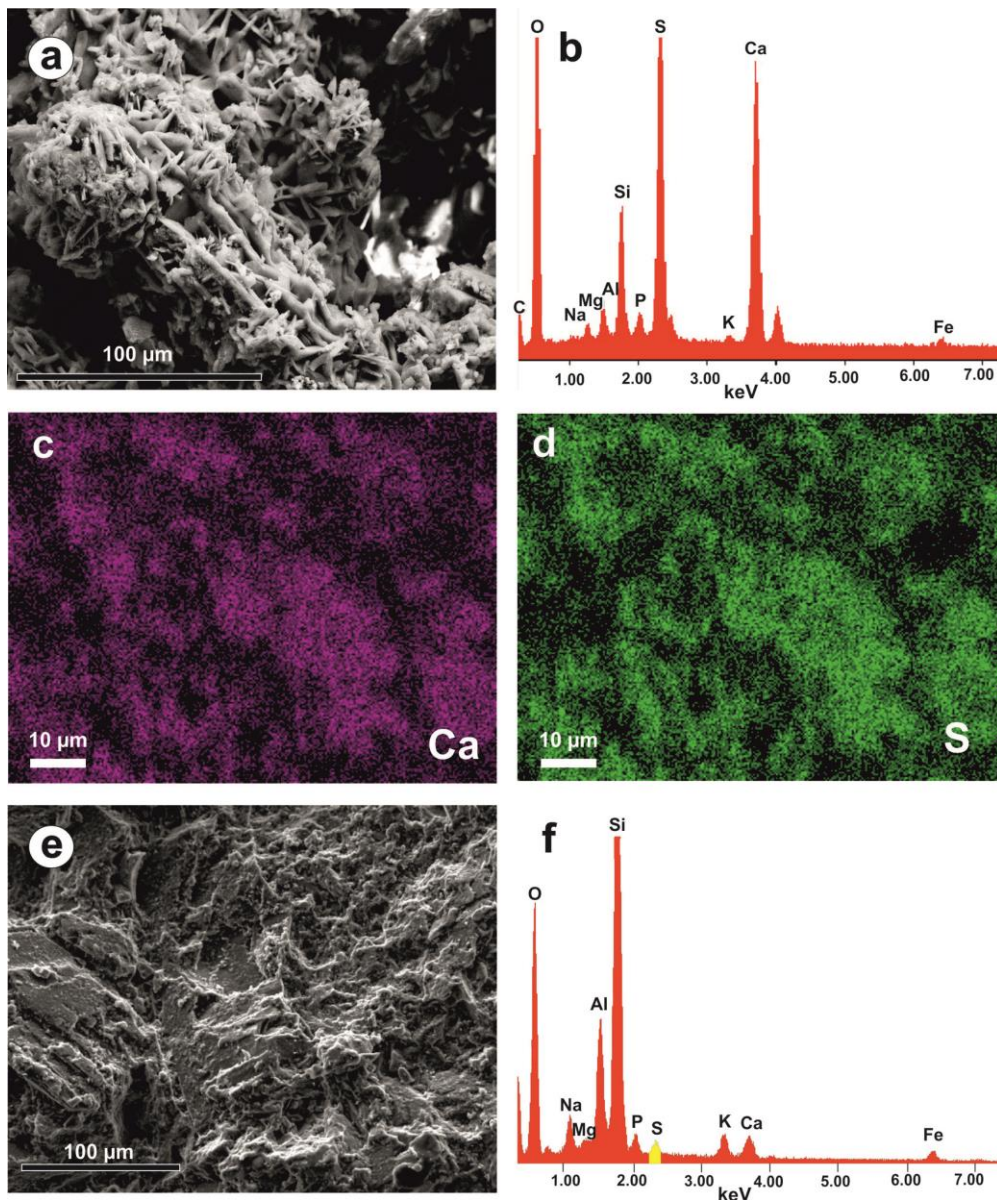


**Figure 8.3** Surface detections of black weathering crusts on Drachenfels trachyte: **a.** SEM picture (SE detection) of the outer surface of a framboidal crust; **b.** EDX spectrum of the outer surface of a framboidal crust; **c.** EDX map (calcium) of the outer surface of a framboidal crust; **d.** EDX map (sulfur) of the outer surface of a framboidal crust; **e.** SEM picture (SE detection) of the outer surface of a laminar crust; **f.** EDX spectrum of the outer surface of a laminar crust.

Laminar crusts are very thin (5–15 µm, where bulging occurs up to 50 µm) and have a dense composition of mainly organic compounds with parts of gypsum, iron oxides, quartz and feldspar particles (Fig. 8.2c). As observed with framboidal crusts, the host rock beneath laminar crusts also shows surface parallel cracking, with a lower quantity and latitude of the cracks. With laminar crusts, the structural disintegration of the stone is often manifested in the form of scales of 0.5–1.5 cm thickness.

### 8.2.3 Geochemical characterization

The results of the XRF analyses show a significant relative depletion of  $\text{SiO}_2$  (2–15 %) and of  $\text{Al}_2\text{O}_3$  (2–19 %) in the crust samples in respect to the host rock (Tab.8.1). Also,  $\text{K}_2\text{O}$  shows an average decrease of 10–22 % and  $\text{Na}_2\text{O}$  of 0.5–19 %. The mean enrichment of  $\text{Fe}_2\text{O}_3$  for the samples from Altenberg is 12 %, for the Xanten samples 16 %, and for the Cologne samples 11 %. The enormous increase of  $\text{P}_2\text{O}_5$  concentration is striking, which is three times higher for the Cologne samples. An enrichment of  $\text{CaO}$  within the crust is clearly noticeable for the samples from Cologne (factor 2.8) and from Xanten (factor 1.7). The average  $\text{CaO}$ -enrichment in the Altenberg samples is within the measurement accuracy. The increase in  $\text{SO}_3$ , the sulfur concentration, shows a similar tendency: the Cologne samples show an enrichment of sulfur with factor 139, the Xanten samples with factor 65 and the Altenberg samples with factor 7. The depletion of the oxides associated with silicate phases ( $\text{SiO}_2$ ,  $\text{Al}_2\text{O}_3$ ,  $\text{Na}_2\text{O}$ ,  $\text{K}_2\text{O}$ ) correlates with the increase in  $\text{SO}_3$ .

**Table 8.1** Main element composition of samples (data set of XRF analyses in wt. %)

sample	No. sample	$\text{SiO}_2$	$\text{TiO}_2$	$\text{Al}_2\text{O}_3$	$\text{Fe}_2\text{O}_3$	$\text{MnO}$	$\text{MgO}$	$\text{CaO}$	$\text{Na}_2\text{O}$	$\text{K}_2\text{O}$	$\text{P}_2\text{O}_5$	$\text{H}_2\text{O}$	$\text{CO}_2$	$\text{SO}_3$	$\Sigma$
host rock	n = 5	64.31	0.72	16.97	3.49	0.11	0.85	2.43	4.56	5.22	0.18	0.92	0.22	0.04	99.9
Altenberg	n = 3	63.17	0.77	16.68	3.92	0.09	0.63	2.41	4.58	4.69	0.19	1.56	1.21	0.30	100.2
Cologne	n = 10	54.45	0.65	13.79	3.86	0.09	0.68	6.72	3.71	4.05	0.51	0.92	0.92	5.90	100.3
Xanten	n = 5	59.80	0.71	15.12	4.06	0.14	0.74	4.24	4.24	4.39	0.22	0.99	0.54	2.77	99.8

In crusts on limestone, where the substrate consists almost entirely of  $\text{CaCO}_3$ , a depletion of  $\text{CaO}$  and an enrichment of  $\text{SiO}_2$  as well as aluminum and iron in the crust are detected (Török et al. 2011). The contrary is found for crusts on silicate stones: a relative depletion of oxides associated with silicate phases and an enrichment of  $\text{CaO}$  in the crust along with an enormous increase in sulfur, indicating high gypsum enrichment in the crust. The average sulfur concentrations normalized to the host rock correlate to gypsum contents for Altenberg (0.6 wt. %), Xanten (5.9 wt. %) and Cologne (12.6 wt. %). The sulfur concentration found in crust samples on limestone – investigated by Török et al. (2011) – correlates to an average gypsum amount of 22 wt. % in respect to the host rock. Gypsum concentrations in samples from marble and limestone from different sites range from 10.3 wt. % (Torfs and van Grieken 1997) to 23.3 wt. % (Fassina 1988) (Tab. 8.2).

**Table 8.2** Concentrations of sulfur (wt. %) (calculated from  $\text{SO}_4^{2-}$  content of soluble salts) detected in the black crusts on stone masonry from different urban sites in Europe

S (wt. %)	13.8	14.6 – 23.3	10.5 – 16.2	10.3 – 13.4	13.2 – 20.3
Investigated sites	Rome, Italy	Venice, Italy	Northern and central Italy	Mediterranean coast	Eleusis, Greece
	Brocco et al. 1988	Fassina 1988	Sabbioni & Zappia 1992a and 1992b	Torfs & Van Grieken 1997	Moropoulou et al. 1998

The data show a clear discrimination of framboidal and laminar crusts (Tab. 8.3). A stronger depletion for  $\text{SiO}_2$ ,  $\text{Al}_2\text{O}_3$  and  $\text{Na}_2\text{O}$ , as well as for  $\text{K}_2\text{O}$ , is detectable. The increase of  $\text{CaO}$  and  $\text{SO}_3$  concentrations from laminar to framboidal crusts is significant.

**Table 8.3** Enrichment factors of main elements in laminar and framboidal crust samples from Altenberg, Xanten and Cologne relative to the host rock

sample	No. sample	$\text{SiO}_2$	$\text{Al}_2\text{O}_3$	$\text{Fe}_2\text{O}_3$	$\text{CaO}$	$\text{Na}_2\text{O}$	$\text{K}_2\text{O}$	$\text{P}_2\text{O}_5$	$\text{SO}_3$
<b>laminar crusts</b>									
Altenberg	3	0.98	0.98	1.12	0.99	1.01	0.90	1.05	7.05
Xanten	5	0.99	0.96	1.19	1.03	1.02	0.90	1.25	1.41
Cologne	8	0.98	0.95	1.18	1.38	0.98	0.90	1.21	10.57
<b>framboidal crusts</b>									
Xanten	1	0.71	0.66	1.02	4.46	0.61	0.63	1.05	319.6
Cologne	2	0.33	0.27	0.81	8.33	0.16	0.29	9.55	651.8

The calculated content of gypsum in the analyzed samples of framboidal crusts from Cologne is about 60 wt. %, and in the samples of framboidal crusts from Xanten about 29 wt. %. However, the samples of laminar crusts show a quite similar low gypsum concentration for the three locations: Altenberg, 0.55 wt. % Xanten, 0.04 wt. % Cologne, 0.88 wt. %. In terms of the mineralogical determination by the Rietveld method, the gypsum concentrations of the laminar crust samples are below the detection limit for gypsum by XRD, but the framboidal crust samples clearly indicate gypsum content (Tab. 8.4; Fig. 8.4).

**Table 8.4** Main mineral phases of black crust and host rock (xxx: major, xx: medium, x: minor) (see sample description in Tab. A8.1 in Appendix)

sample code	cathedral	Quartz	Sanidine	Plagioclase	Pyroxen	Biotite	Gypsum
DT-03	-	x	xxx	xxx	x	x	
AL-02	Altenberg	xx	xxx	xxx	xx	x	
AL-03	Altenberg	xx	xxx	xxx	x	x	
CL-06	Cologne	xx	xxx	xxx	x	x	
CL-08	Cologne	xx	xxx	xxx	x	x	
CL-07	Cologne	xx	xxx	xxx	x	x	
CF-09	Cologne	x	xxx	xxx	x	x	x
XF-06	Xanten	x	xxx	xxx	x		x
XL-05	Xanten	x	xxx	xxx	xx	x	

The enrichment of  $\text{CO}_2$  in the samples for Altenberg (factor 5.6), Cologne (factor 4.2) and Xanten (factor 2.5) (Tab. 8.1) indicates a certain amount of carbonaceous fly ash particles in the investigated material as well as a partition of organic material, especially for the investigated samples from Altenberg. This again illustrates the importance of settling dust and particles in terms of weathering crust formation.

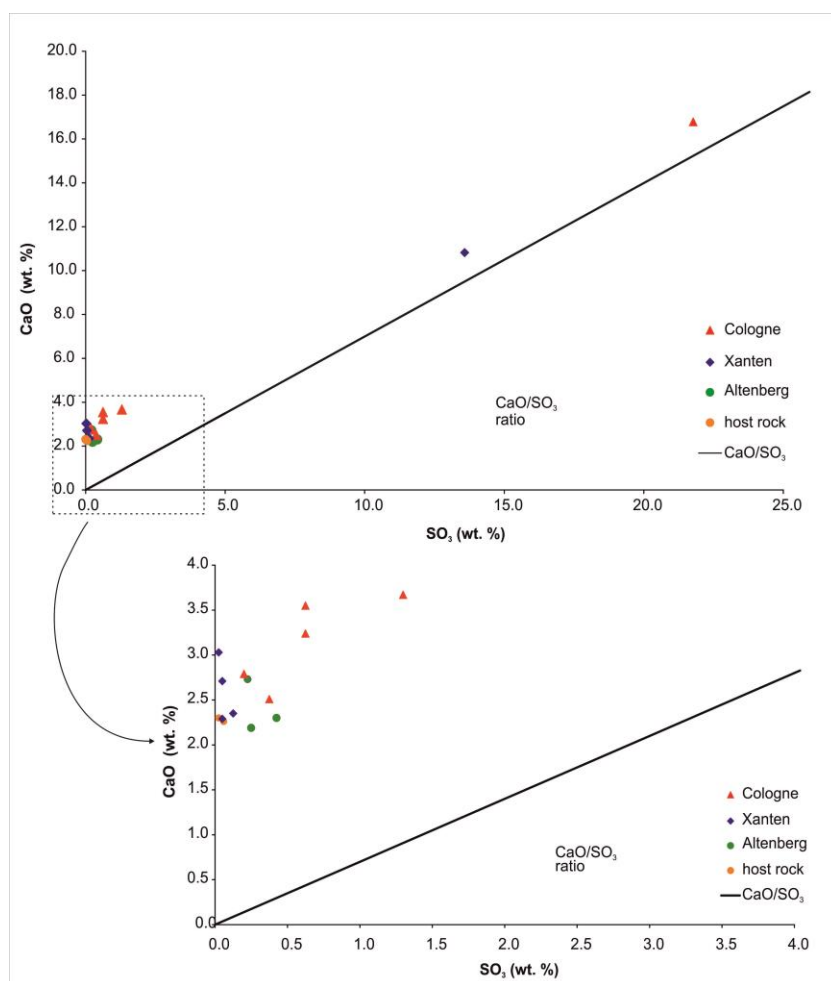


**Figure 8.4** CaO versus SO<sub>3</sub> content indicates the part of gypsum at the sample. The higher the amount of SO<sub>3</sub>, the higher the gypsum content of the sample. The molar ratio of calcium versus sulfur in gypsum (CaSO<sub>4</sub>·2H<sub>2</sub>O) is 1:1 (black line). The samples are above this molar ratio (Ca/S or CaO/SO<sub>3</sub> respectively), suggesting that the total sulfur in the samples is present as gypsum. The CaO content can be assigned to gypsum as well as to the rock-forming minerals (e.g., plagioclases). An enrichment of calcite (CaCO<sub>3</sub>) cannot be correlated (see also Tab. 8.4).

## 8.2.4 Microscale chemical investigation

LA-ICP-MS analyses show clear trends in terms of major and trace element distribution in the black crusts and the host rock. The microscale chemical investigation also reveals little change in oxides associated with the silicate phases. An enrichment of sulfur, lead, antimony, bismuth and arsenic in black weathering crusts developed on Drachenfels trachyte is detected (Fig. 8.5). The crusts of the Cologne cathedral show an average concentration of 1,849 ppm Pb and those of Xanten 1,944 ppm Pb, while the crusts of Altenberg only show 890 ppm Pb – which corresponds to enrichment factors of 105, 110 and 50 in respect to the host rock (Tab. 8.5; Fig. 8.5).

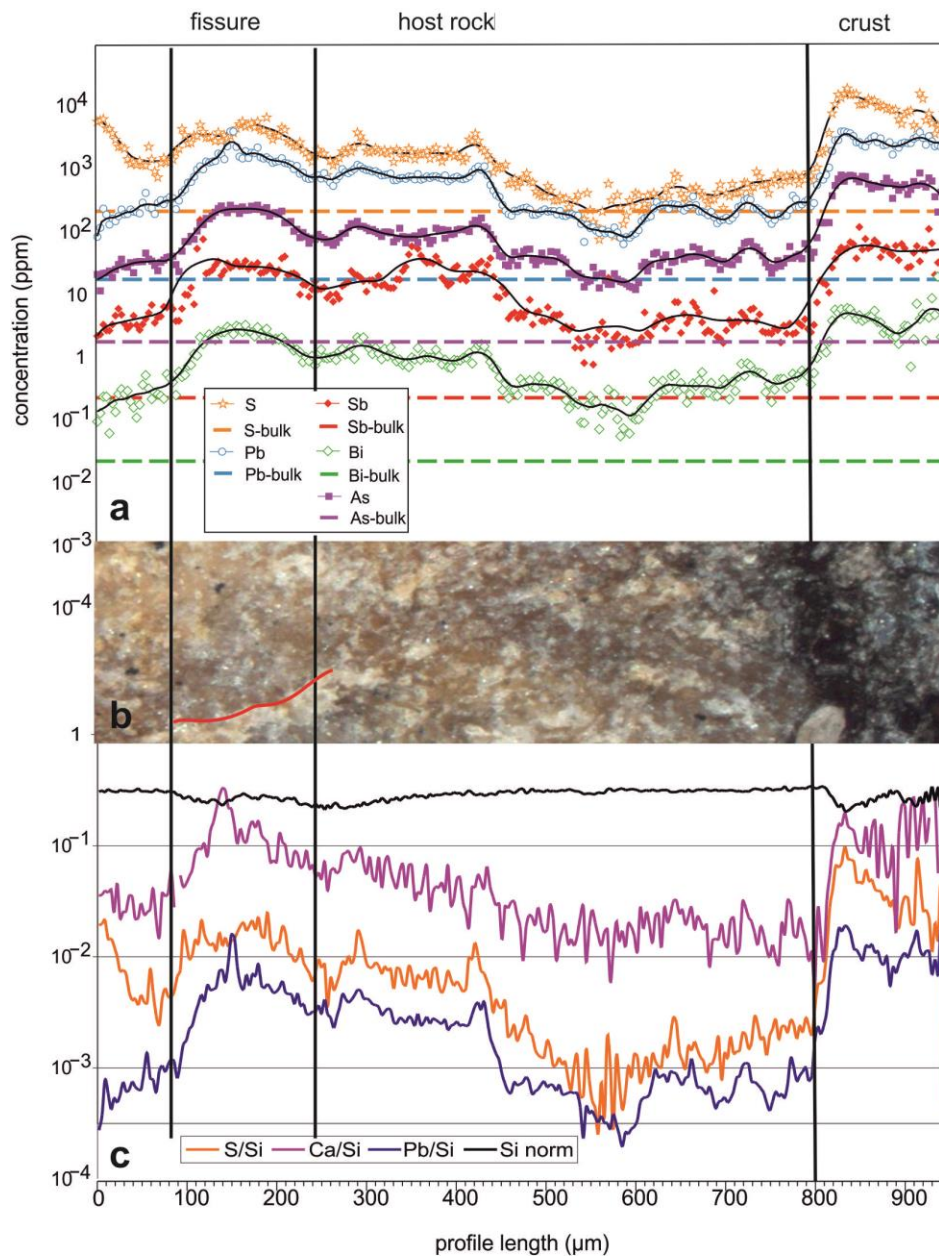


**Figure 8.5** LA-ICP-MS analyses along a profile perpendicular to the surface on a thin cut of a black weathering crust (Drachenfels trachyte; Cologne cathedral): **a.** concentration profiles of S, Pb, Sb, Bi and As; **b.** microscopic picture of the ablated line; **c.** S/Si, Ca/Si and Pb/Si ratios (and normalized Si content) plotted against the length of the line.

**Table 8.5** Mean values for S, Ca, Pb, Sb, Bi, and As in the host rock and in the crust from the Altenberg, Cologne, and Xanten samples

	sample No.	sulfur (S)		calcium (Ca)		lead (Pb)		antimony (Sb)		bismuth (Bi)		arsenic (As)	
		value	increase factor	value	increase factor	value	increase factor	value	increase factor	value	increase factor	value	increase factor
	n	ppm		%		ppm		ppm		ppm		ppm	
host rock	n = 1	215		1		18		0		0		2	
Altenberg	n = 1	5044	23	2	2	890	50	12	37	1	48	28	16
Cologne	n = 2	6313	29	3	3	1849	105	37	114	3	145	367	205
Xanten	n = 4	40785	190	5	4	1944	110	16	48	3	117	50	28



The samples from the three locations are clearly distinguishable. Comparing industrial, urban and rural samples, the data show high concentrations of heavy metals (e.g., Pb, and Bi), As and Si in black crust samples collected from the industrial and urban sites (Cologne and Xanten). The samples from the rural area (Altenberg) contain significantly lower concentrations of heavy metals (Tab. 8.5). This clearly indicates a very strong pollution impact for the Cologne and Xanten samples, since the content of these elements is due to an intense impact of combustion emissions (Fig. 8.6).

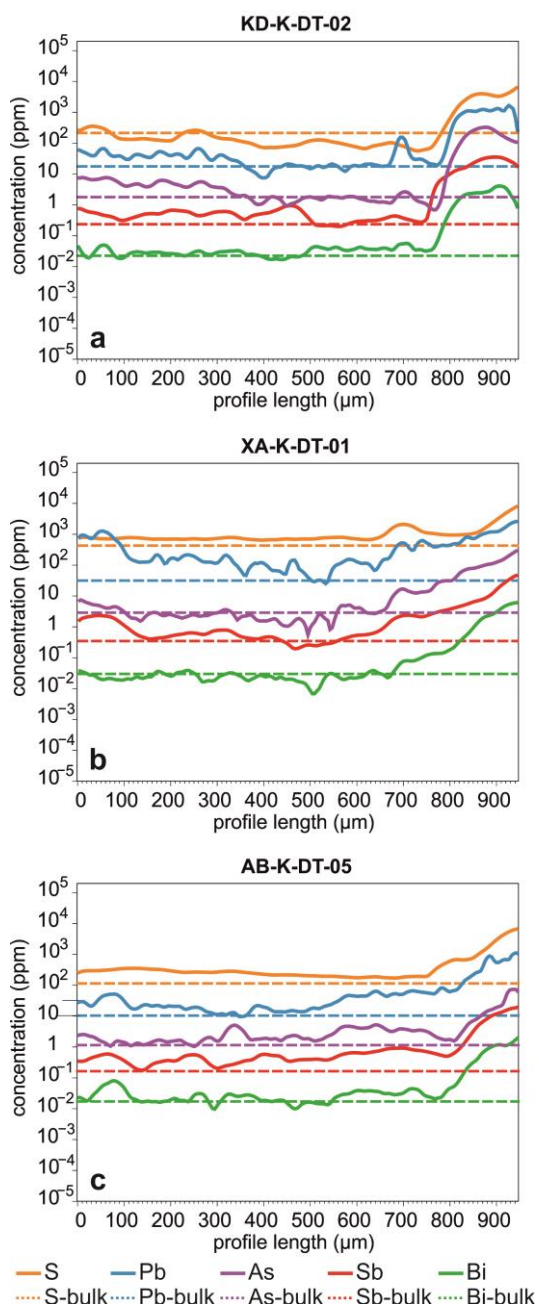


**Figure 8.6** Distribution of sulfur (S), lead (Pb), antimony (Sb), bismuth (Bi) and arsenic (As) in black weathering crusts developed on Drachenfels trachyte normalized to earth crust values (blk) in **a.** Altenberg, **b.** Cologne, and **c.** Xanten. LA-ICP-MS analyses, perpendicular to the sample surface (concentrations are in ppm), showing an enrichment of S, Pb, Sb, Bi, and As in the crust.

**Table 8.6** Concentrations (ppm) of lead (Pb) detected in the black crusts on stone masonry from different urban sites in Europe

location	lead (Pb)	stone substrate
	Pb (ppm)	
Cologne	1,849	trachyte
Xanten	1,944	trachyte
Halle, GER *	2,000	limestone
Budapest *	1,000	limestone
Milan °	883	marble and limestone
Venice °	123	marble and limestone
Rome °	532	marble and limestone
Bologna °	427	marble and limestone
Eleusis °	300	marble and limestone
Brussels °	516	sandstone and calcarenite
Bologna °	160	sandstone and calcarenite
Granada °	40	sandstone and calcarenite

\*Török et al . 2011, ° after Sabbiono 21003

In view of decreasing SO<sub>2</sub> fluxes, the ban on leaded petrol, and emission regulations, the high concentrations of heavy metals as *anthropogenic combustion tracers* in the samples from Cologne result not only from recent air pollution but show the long history of industrial

development at this location. The high lead concentrations in the Xanten samples can be traced back to the strong impact of the industrial area of Arnhem (NL) over a long period of time.

The weathering crusts show high enrichment of the detected elements, whereas within the first 100–300  $\mu\text{m}$  of the surface of the host rock a general decrease is detectable (Fig. 8.5). An accumulation can be observed in cracks and small cavities of the host rock (Fig. 8.5). This correlates well with the phenomenon observed by Török et al. (2011) that in the porous zone below the crust an increase of Pb is observed, which marks the accumulation of lead not only within the crust but in the pores, too. The enrichment in the cracks demonstrates that pollutants are not only superficially fixed to the crust, but also penetrate deeper into the stone and accumulate in structurally altered zones.

The plots of the S/Si, Ca/Si and Pb/Si ratios show a sharp increase in the crust, indicating a high enrichment of Pb and S, as well as of Ca, in the crust (Fig. 8.5). The major atmospheric impact is indicated by the enormous enrichment of heavy metals, which, as *anthropogenic combustion tracers*, clearly refer to an atmospheric source. This is reaffirmed by the content of siliceous and carbonaceous fly ash particles in the crust.

If Pb concentrations are compared on an international scale, similar concentrations are found for Cologne, Xanten and Halle (Tab. 8.6). Values from these sites, as well as from Budapest, Milan, Rome, and Brussels, can be related to higher combustion emission impacts for example from domestic heating, power plants, coal combustion and vehicle exhausts (Sabbioni 2003).

### 8.2.5 The polycyclic aromatic hydrocarbon fingerprint

Microscopic analyses reveal particulate matter is abundant on the stones' surfaces and in the weathering crusts (Lefèvre and Ausset 2003). The detection of the polycyclic aromatic hydrocarbon (PAH) compounds reveals the organic fingerprint of the particulates of the settling dust. PAH as compounds indicative of air pollution are detected in selected samples of black weathering crusts, scales and disaggregated material, as well as from dust. PAH mainly arise from the incomplete combustion of fossil fuels, organic matter or wood. The detected concentrations are referred to the values of the host rock. The range of the detected 21 PAH compounds are from acenaphthylene ( $m/z$  152) to dibenzo(ah)-pyrene ( $m/z$  302).

The total concentrations of the PAH compounds varies from 62  $\mu\text{g/kg OS}$  (laminar crust from Xanten cathedral) to 13,525  $\mu\text{g/kg OS}$  (dust sample from Cologne cathedral) (Tab. 9). The high-end values belong to samples from Cologne cathedral and are typical for samples from an industrial area. The PAH concentrations of the samples from Xanten and Altenberg are in a close range (Tab. 8.7). A clear relationship can be drawn between PAH concentration and sample type. If the Cologne samples are compared to each other, samples of dust, framboidal weathering crusts and strongly deteriorated stone material (scale and

disaggregated stone) generally show higher PAH concentrations (1,362– 13,525  $\mu\text{g/kg OS}$ ); samples of laminar crusts and slightly weathered stone show lower values (247–482  $\mu\text{g/kg OS}$ ).

**Table 8.7** PAH and  $\text{SO}_4^{2-}$  concentrations of samples from Altenberg, Cologne and Xanten, as well as Hungary and the city centers of Budapest and Halle

sample code	stone	description	PAH total $\mu\text{g/kg OS}$	$\text{SO}_4$ $\text{mg/kg}$
DT-01	Drachenfels trachyte	host rock	179.12	299.92
AL-02	Drachenfels trachyte	laminar crust	82.11	5,092.30
AL-03	Drachenfels trachyte	laminar crust	669.13	2,995.47
AF-04	Krensheimer Muschelkalk	framboidal crust	226.89	43,364.10
CL-06	Drachenfels trachyte	laminar crust	481.54	1,497.74
CL-07	Drachenfels trachyte	laminar crust	3,872.46	3,295.02
CD-07	Drachenfels trachyte	disaggregated material behind scale	5,121.95	6,590.04
CL-08	Drachenfels trachyte	laminar crust	246.65	898.64
CD-08	Drachenfels trachyte	disaggregated material behind scale	1,362.24	6,290.49
CF-11	Krensheimer Muschelkalk	host rock	5,004.50	165,368.64
CS-01	Obernkirchner Sandstein	dust surface deposition	13,525.07	
XL-05	Drachenfels trachyte	laminar crust	420.47	599.09
XL-07	Drachenfels trachyte	laminar crust	62.25	33,549.29

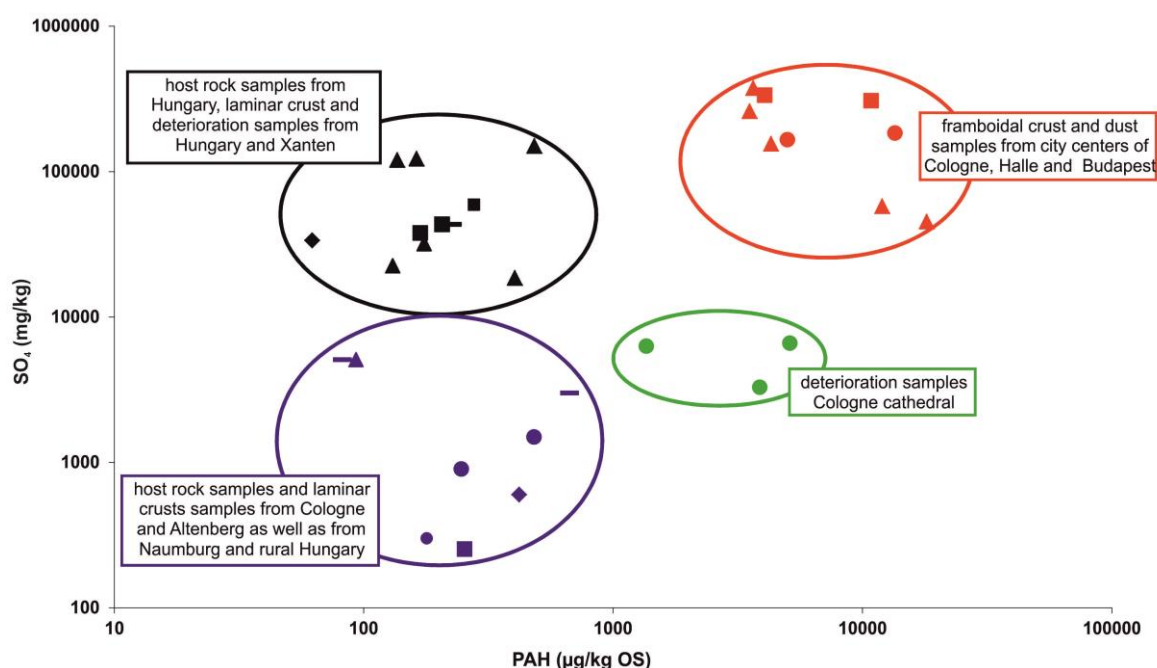


**Figure 8.7** PAH versus  $\text{SO}_4^{2-}$  concentrations of studied samples. The data set shows distinct fields with different origin of samples, indicating the difference in composition of dust, black weathering crusts and host rock.

When data from Török et al. (2011) are included, the higher PAH concentrations are in dust samples and from framboidal crusts from Cologne, Budapest and Halle (Fig. 8.7; red ellipse). This group of samples also shows high  $\text{SO}_4^{2-}$  concentrations. A second group of low PAH but higher  $\text{SO}_4^{2-}$  concentrations (Fig. 8.7; black ellipse) contains mainly laminar crusts from rural areas in Hungary as well as from Xanten and Altenberg, besides four samples from



Hungarian host rock. Except for one sample from Xanten (Drachenfels trachyte), these crust and host rock samples derive from limestone. A third group is formed by deterioration samples from Cologne cathedral on Drachenfels trachyte (Fig. 8.7; green ellipse). These samples show certain enrichment in  $\text{SO}_4^{2-}$ , but a stronger increase of PAH. A fourth group with low  $\text{SO}_4^{2-}$  and moderate PAH concentrations (Fig. 8.7; blue ellipse) contains a host rock sample of Drachenfels trachyte, and further consists of samples of light weathered stone and laminar crusts from Cologne, Altenberg and Naumburg, as well as rural areas in Hungary.

### 8.3 Discussion

#### 8.3.1 Crust formation on Drachenfels trachyte in comparison to limestone

As the investigations and mapping show, gypsum crusts not only build on calcareous stones but also on silicate stones. In comparison to black weathering crusts on limestone, the crusts on the silicate Drachenfels trachyte are lower in gypsum content (223 g/kg on average on limestone, 126 g/kg on average on Drachenfels trachyte – relative to the corresponding host rock). Also, framboidal crusts are less frequent than laminar crusts on Drachenfels trachyte than on limestone. This is easily explained by the calcium source for the gypsum. The limestone displays a vast source of calcium ions for the formation of gypsum crusts, as a matter of transformation from  $\text{CaCO}_3$  into  $\text{CaSO}_4 \cdot 2 \text{H}_2\text{O}$ . The Drachenfels trachyte, however, has an original concentration of 2.43 wt. % CaO, which is mainly contained in silicate minerals and is not easily available for the formation of gypsum.

For crusts on limestone, a significant difference in chemical composition between host rock and crust is reported (Török et al. 2011). This is not the case for black weathering crusts on Drachenfels trachyte, where the crusts show a similar chemical composition to the host rock, with a depletion of oxides associated with silicate phases and enrichment in Ca and S. The morphology and composition of the crusts' surfaces on limestone and on silicate trachyte differ significantly. Török et al. (2011) found a surface composition of primarily gypsum crystals as well as calcite. They found idiomorphic rosette-like gypsum crystals in samples from industrial environments, and slightly dissolved gypsum crystals commonly associated with calcite in samples from rural places in Hungary and Germany. The crusts on the silicate trachyte showed higher content of siliceous compounds and organic matter and smaller content of gypsum compared to crusts on limestone. At Cologne cathedral the crust formation on limestone shows a very dense crust without any transitional zone, whereas the black crusts on the Drachenfels trachyte are a very porous poly-mineral composition with heterogeneous particle size.

### 8.3.2 Sulfur and calcium sources

The crust samples on Drachenfels trachyte have a higher sulfur as well as higher calcium content in correlation to the fresh stone (enrichment factor for S: 7–139; enrichment factor for Ca: 1–3). The chemical analyses reveal very low calcium (1.74 wt. %) and sulfur (<0.02 wt. %) concentration in the Drachenfels trachyte (Tab. 8.1). This indicates that, for both sulfur and calcium, external sources are responsible for the crust formation.

Sulfur derives from anthropogenic pollution impact and imports via wet and dry deposition. The most important sulfur sources are SO<sub>2</sub> deposition from air and SO<sub>4</sub><sup>2-</sup> from rainwater (Neumann et al. 1993). Torfs and Van Grieken (1997) mention that gypsum formation is more likely related to SO<sub>2</sub>, which is the airborne sulfur, indicating the major impact of dust and dry deposition. This correlates to the investigation by Furlan and Girardet (1983), who state that, especially in highly polluted areas, the impact of dry deposition is far more important than wet deposition as a source of building stone decay. Laboratory analyses of sulfate-rich fog water confirmed that 60 h after a main fog event, gypsum crystals were formed (Del Monte and Rossi 1997). This indicates that the SO<sub>4</sub><sup>2-</sup> import from rainwater and fog, as well as the dry deposition of SO<sub>2</sub> in the context of corresponding humidity (e.g., fog, condensation), function as sulfur sources for the gypsum formation.

The calcium import comes from aerosol deposition and leaching products from mortars (e.g., joint mortar) (Snethlage and Wendler 1997; Kraus 1980; Hughes et al. 1998) as well as from adjacent calcareous stones.

The role of particulate matter in the form of dry and wet deposition, and their contribution to the formation of black weathering crusts, has already been discussed (Amoroso and Fassina 1983; Bonazza et al. 2004 and 2005; Del Monte and Vittori 1985; Del Monte et al. 2001; Fassina et al. 2002; Lefèvre and Ausset 2002; Moropoulou et al. 1998; Smith et al. 1988; Trudgill et al. 2001; Viles 1994; Thornbush and Viles 2004). The dry deposition of airborne particles also includes calcium-rich aerosols, which therefore play their part in calcium import (Charola and Ware 2002). The total suspended particulate matter (TSP) is to be differentiated into PM<sub>10</sub> and PM<sub>2.5</sub> not only based on size, but also to differences in source, amount of emission, and physical and chemical behavior (Kainka et al. 1997). The composition of PM<sub>10</sub> is generally dominated by large soot agglomerates, particles from tire abrasion and geogenic clay minerals and silica particles. In industrial areas it may also contain slag, xenomorphic silica, salts, and gypsum and metallic particles. The coarse PM<sub>10</sub> fraction from clean air regions contains particles mostly of biogenic and geogenic origin, but also clay minerals and quartz. Typical components from combustion are soot conglomerates (sometimes with ball-like morphology) charcoal, fly ash particles of different sizes, xenomorphic silicates and sulfates including gypsum. The finer PM<sub>2.5</sub> fraction contains single soot particles or small soot agglomerates and fly ash particles (small balls). The latter

are amorphous silica material with a high content of heavy metals. The fine PM<sub>2.5</sub> fraction from clean air regions contains silicates and a few soot particles. The amount of PM<sub>2.5</sub> can be smaller than PM<sub>10</sub> in clean air regions. Geogenic particles, for example silicates, derive from mechanical abrasion and are found mostly in coarse fractions (PM<sub>10</sub>). The particulate air pollution caused by traffic is highly concentrated in the fine fraction (PM<sub>2.5</sub>), which is detected in all areas, and also in clean air regions (Kainka et al. 1997). Thus, in industrialized areas, generally higher PM concentrations are measured with high contents of soot, charcoal and particles from tire abrasion as well as slag and salts, e.g., gypsum and metallic particles. In general, a higher ratio of particulate air pollution is found, which is caused by traffic and contains large amounts of heavy metals. In clean air regions, however, particulate matter is dominated by biogenic and geogenic components, as well as clay minerals, silicates (e.g., quartz), and a few soot particles, with an overall lower ratio of particulate air pollution caused by traffic.

Calcareous and sulfur compounds are constituents of weathering crusts and they participate in their formation in different ways. Dust and soot particles – especially when containing hygroscopic salts – can serve as condensation nuclei for droplets and thus provide sufficient moisture for further reactions (Charola and Ware 2002; Moroni and Poli 2000). Higher content of metallic compounds in the PM of industrial environments and higher concentration of carbonaceous particles enhance the  $\text{SO}_4^{2-}$  formation on stone surfaces (Charola and Ware 2002; Zappia et al. 1998). Metals are mentioned to act as catalysts for the oxidation of  $\text{SO}_2$  into  $\text{SO}_4^{2-}$ . Soot particles containing heavy metals and metallic components of the particulate matter, e.g., abrasion material from tires, may function as reaction catalysts for the formation of calcium sulfate dihydrate, thus contributing to gypsum crust formation and stone decay. The experimental studies by Zappia et al. (1998) indicate two different reaction mechanisms for the formation of calcium sulfate dihydrate: an intermediate state of hemihydrate calcium sulfite or a direct formation of calcium sulfate dihydrate. The latter is linked to the presence of efficient catalysts, e.g., metallic compounds and strong oxidants.

Even though  $\text{SO}_2$  concentrations have been higher in the past and their effect on rock weathering might have been more significant than today, the  $\text{SO}_2$  concentrations today still have an effect on the stone deterioration, especially in the context of increasing particulate matter. The  $\text{NO}_x$  concentration of the air pollution plays a specific role. On the one hand,  $\text{NO}_2$  can function as an oxidant and increase the reaction rates of the sulfation processes significantly (Johansson et al. 1988). On the other hand,  $\text{NO}_x$  gases can be oxidized by lithotrophic bacteria to nitric acid, thus contributing to stone decay (Fuchs 2006).

The different incorporation of particulates, e.g., fly ash particles, into the gypsum crusts on limestone or on Drachenfels trachyte clearly indicates a very different formation process of the black weathering crusts. The limestone itself delivers the calcium component for the

transformation of calcite into gypsum as an intense crystal growth takes place, where extrinsic particles, e.g., fly ash particles, are firmly incorporated. On the Drachenfels trachyte, a siliceous rock, calcium components are transported from external sources, as are other particles, e.g., fly ash particles. As the crust builds, it forms as a more or less loose and porous mixture of the different particles delivered by the pollution fluxes.

Already Grün (1931) considered the mortars used as a potential source for the deterioration. Wolff (1972) addressed the formation of gypsum crusts on Obernkirchen sandstone – sandstone with very little calcium content – to leaching alkaline components of the joint mortars. Mortars with latently hydraulic binders, e.g., puzzolana and diatomaceous earth, or cement components are commonly known for their capability to release water-soluble forms of sodium, potassium, calcium and magnesium components (Arnold 1981, 1992; Bläuer-Böhm 2005; Kraus 2002; Kraus and Droll 2009; Schwiete et al. 1965). At Cologne cathedral, it can be observed that in many places the decay on the Drachenfels trachyte starts from the joints, which is indicated by gypsum crusts, flaking and scaling (Graue et al. 2011).

Besides alkaline mortars, neighboring calcareous stones, especially limestone, are also considered as a possibly contributing calcium source. As surface roughness evaluations on several calcareous stones show, a continuous increase of roughness is detectable, indicating the solution of the calcite stone (Grimm and Völkl 1983). The erosion is very much dependent on the exposition. Higher deterioration correlated roughness is detectable on the weather-exposed side within a factor of 1.5 in correlation to the protected side. Grimm and Völkl (1983) measured 0.002–0.005 mm/year material loss on the weather-exposed side for the investigated stones. On the Krensheim Muschelkalk at Cologne cathedral a surface roughness is observable (Fig. 8.8a). The calculated rate of diluted calcium ions from one square meter of Krensheim Muschelkalk with a matrix density of  $2.72 \text{ g/cm}^3$  (Lukas 1990), a calcium concentration of 37.14 wt. % and an average thickness of material loss due to corrosion of 0.0035 mm/year is about  $9.52 \text{ g/sq m} \cdot \text{year}$  Krensheim Muschelkalk, and thus  $3.54 \text{ g/sq m} \cdot \text{year Ca}$ . This would correlate to  $12 \text{ g/sq m} \cdot \text{year CaSO}_4$  or  $15.2 \text{ g/sq m} \cdot \text{year gypsum (CaSO}_4 \cdot 2\text{H}_2\text{O)}$ . The possibly diluted calcium ions are probably not transferred into gypsum at a 1:1 ratio. The higher share is probably lost as dust in air turbulences.

The acid buffering capacity of eight tested natural building stones was measured by titration with hydrochloric acid and the resulting solute ions buffering the acid at pH 4 were detected. As expected, the experiments on the eight tested stones revealed similar amounts for volcanic stones and sandstones. The carbonate rich sandstone (Schlaitdorf sandstone) buffers a volume of HCl, which is 12 times higher. The limestone (Krensheim Muschelkalk) shows an acid binding capacity enlarged by factor 320 (Fig. 8.8b). On the one hand these experiments indicate a higher liability for crust formation of stone with higher acid buffering capacity. On the other hand they reflect that, upon an acidic impact, the limestone also

readily solutes and provides calcium ions, which therefore may be transported to other stones and contribute to the formation of gypsum crusts (Fig. 8.9).

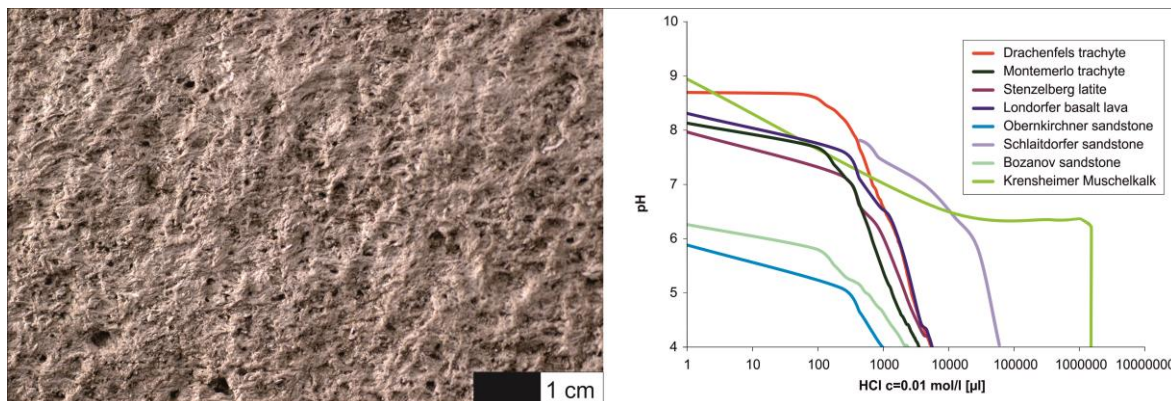


**Figure 8.8 (a)** Weathered surface of Krensheim Muschelkalk showing surface roughness; **(b)** tests on the acid binding capacity showing the extent of material solution.

In terms of a stone-immanent calcium source, it must firstly be considered that Drachenfels trachyte as host rock has a low calcium concentration, which is mainly associated with feldspars as rock-forming minerals, e.g., plagioclases. The decrease of the alkali metals within the crust ( $K_2O$ : 10–28 %;  $Na_2O$ : 0.5–27 %) indicates certain feldspar corrosion. However, the much higher calcium concentration of the investigated crusts in respect to the host rock indicates an external source for calcium and a stone-immanent calcium source is of minor impact.

### 8.3.3 Interferences of adjacent stones

Already Kraus (1985a, b), Mirwald et al. (1988) and von Plehwe-Leisen et al. (2007) noted that there are strong indications that the decay of the Drachenfels trachyte is especially critical when it is placed adjacent to carbonate stones. Investigations on site reveal that crust formation on Drachenfels trachyte can be enhanced by neighboring limestone, depending on the exposition of the affected section of the wall (Fig. 8.9. Krensheim Muschelkalk exposed to an acidic environment solutes into its ion compounds. Rainwater leaches the rock components of the limestone. This calcium ion loaded water runs off and is directly transported to the building stones in the flow direction. It is absorbed by the Drachenfels trachyte and accumulates in the cavities. Additionally, these cavities are a preferred location for the deposition of pollutants – on the one hand due to the rock's surface character and secondly due to the better adsorption of airborne particles onto humid surfaces (Charola and Ware 2002). Due to the environmental impact of sulfuric pollutants, salt, e.g., gypsum, formation takes place. As illustrated in Fig. 8.9, the affected wall section has to be in the relevant flow direction. Water transport and input have to be in a relation allowing enough ions to be dissolved and transported. At the same time, the appropriate amount of water has to guarantee the formation and precipitation of salts. This means that interferences are

strongly dependent on the exposition of the wall section concerned and the placement of adjacent stones in relation to each other. However, neighboring calcareous stones do not play an initial role in the formation of crusts, but may contribute if extrinsic factors such as environmental impact, exposition, and localization are already present.

The Drachenfels trachyte not only shows enhanced crust formation and stronger decay in cavities, but also along joints. These deterioration features can be ascribed to the dissolution of alkaline components of the mortars as well as to a perturbation of the flow of water.

The dissolution of the carbonate rock and the impact of alkaline components increase the pH of the floating solutions. The Drachenfels trachyte, with an  $\text{SiO}_2$  content of >63% due to the quartz concentration (13 %) and the high abundance of feldspars, can be referred to as an acid silicate rock. If the described alkaline waters come into contact with the Drachenfels trachyte, a stronger deterioration of the volcanic rock takes place, because of the increased solution of quartz and feldspars in the alkaline milieu.

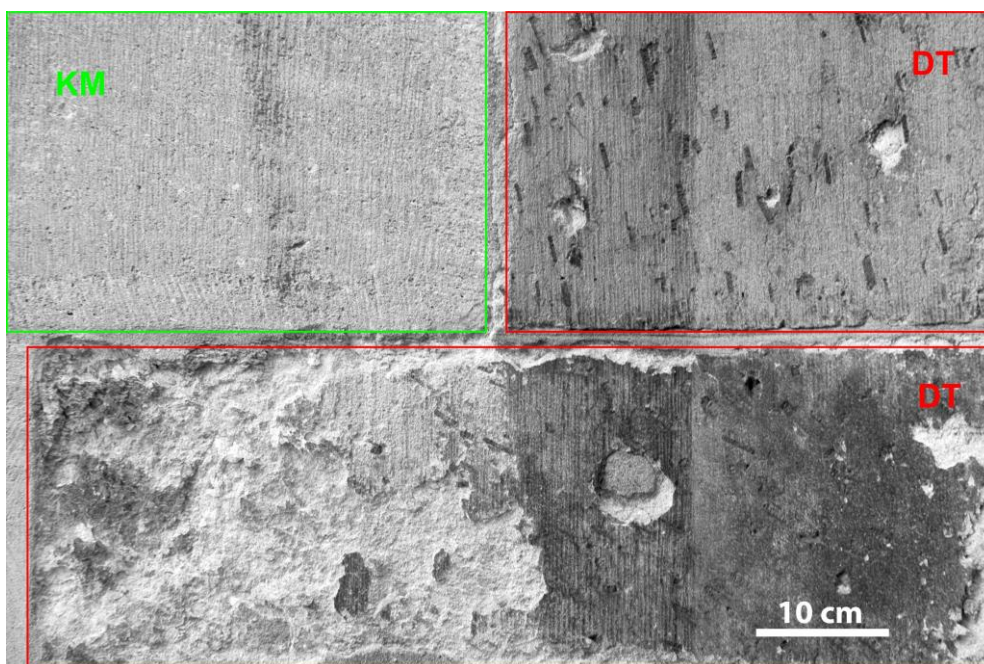


**Figure 8.9** Wall section at Cologne cathedral. Upper left stone: Krensheim Muschelkalk (KM); upper right and lower layer stones: Drachenfels trachyte (DT). The left side of the lower Drachenfels trachyte is in the flow direction of ion-loaded water from the limestone, which enhances the crust formation and decay. Also, a stronger deterioration of the Drachenfels trachyte is observed close to the joints, where alkaline leaching products of the mortar might have a certain impact. The massive erosion on the left side of the lower layered Drachenfels trachyte correlates with the coverage of the top Krensheim Muschelkalk.

Furthermore, a higher pH together with the calcite particles increases the oxidation rate for  $\text{SO}_4^{2-}$  from  $\text{SO}_2$  (Charola and Ware 2002; Zappia et al. 1998). Wiese et al. (2012) ascertained that, for the deposition velocity of  $\text{SO}_2$  on silicate stone, the relative humidity is not as relevant as the buffering capacity available for the dissolution reaction of  $\text{SO}_2$ . The solubility of  $\text{SO}_2$  strongly decreases with decreasing pH. Therefore, a rise of pH through the



impact of calcite adjacent stones may enhance  $\text{SO}_2$  deposition velocity and contribute to the sulfation process. If the aforementioned extrinsic factors are present, these aspects contribute to a stronger crust formation on the Drachenfels trachyte.

Continuous *in situ* measurements of temperature and humidity inside the different stone materials indicate higher water content for the Krensheim Muschelkalk than for the Drachenfels trachyte at a depth of 32 mm (Fig. 8.10a). It can be seen that the data logger in the Drachenfels trachyte with little distance to the Krensheim Muschelkalk shows higher values of relative humidity than the data logger in the center of the ashlar (Fig. 8.10b). These observations may indicate on the one hand a higher water import through the joints, where the alkaline mortar sits. On the other hand, the Krensheim Muschelkalk might serve as a long-term source of water for the Drachenfels trachyte. In both cases the Drachenfels trachyte is provided with ion-loaded water over an extended period of time where this stone would not have absorbed either as much water or as high a volume of alkaline components. Even though no direct water flow over the surface of the stone is provided, a potential import of alkaline components arises, raising the pH and delivering ions for the formation of damaging salts.

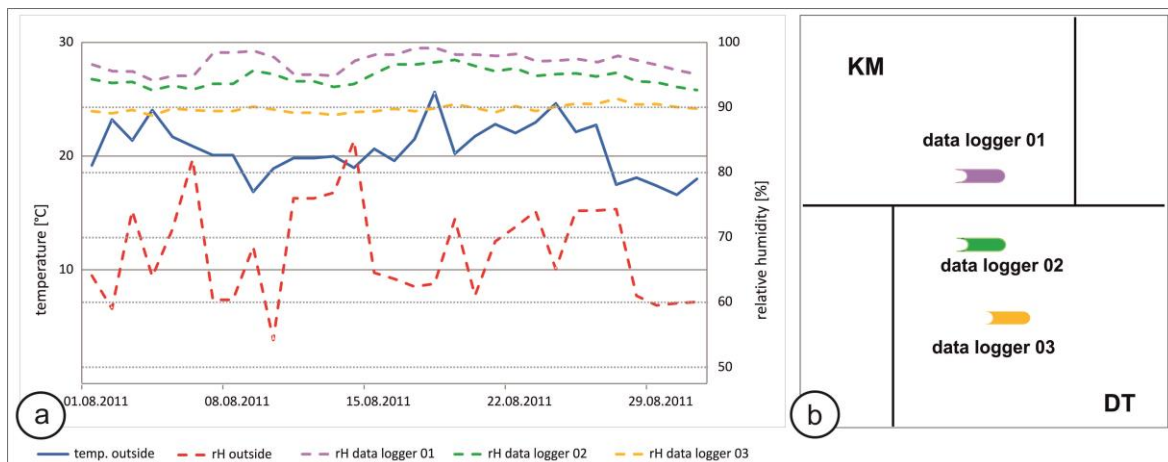


**Figure 8.10 (a)** *In situ* measurements of temperature and relative humidity (rH) at Cologne cathedral, August 2011: outside temperature (blue), outside rH (red), data logger 1 rH (purple), data logger 2 rH (green), data logger 3 rH (yellow); **(b)** scheme of sensors: data logger 1 is placed in the Krensheim Muschelkalk (KM), data logger 2 is placed in the Drachenfels trachyte (DT) with little distance to Krensheim Muschelkalk (KM) and the joint, and data logger 3 is placed centered in the Drachenfels trachyte (DT).

### 8.3.4 Exposition and crust formation

Besides the question of material import as a factor for crust formation, another vital point is the surface character and exposition of the building stone. Laminar crusts are observed on vertical and smooth stone surfaces. Black framboidal crusts build in sheltered areas and show significant formation in cavities on even stone surfaces as well. In sheltered areas the dry deposition of particulate matter is stronger than on unprotected surfaces. A higher pollutant concentration and higher moisture are expected, leading to significant acidity

(Charola and Ware 2002). Due to relevant air turbulences in sheltered areas the transport mechanisms provoke an accumulation of airborne particles. These particles are then firmly deposited and are not washed off by direct rain water. The necessary moisture for the crust formation is provided by higher relative humidity, especially in the case of fog or dew (Amoroso and Fassina 1983; Del Monte and Rossi 1997), as well as by indirect water input (Kraus 1985a). Furthermore, these protected zones stay moist for longer, further contributing to adhesion conditions appropriate for the deposition of particles. The deposition of particles provides nucleation sites for the growth of gypsum crystals (Charola and Ware 2002; Sabbioni 2003), which develop better in sheltered, protected zones where evaporation is retarded. The morphology of these framboidal crusts provides a larger reaction surface, not only for intensive particulate deposition but also for the condensation of fog and dew or high relative humidity in general. This clearly indicates that the growth of framboidal crusts is an exponential reaction.

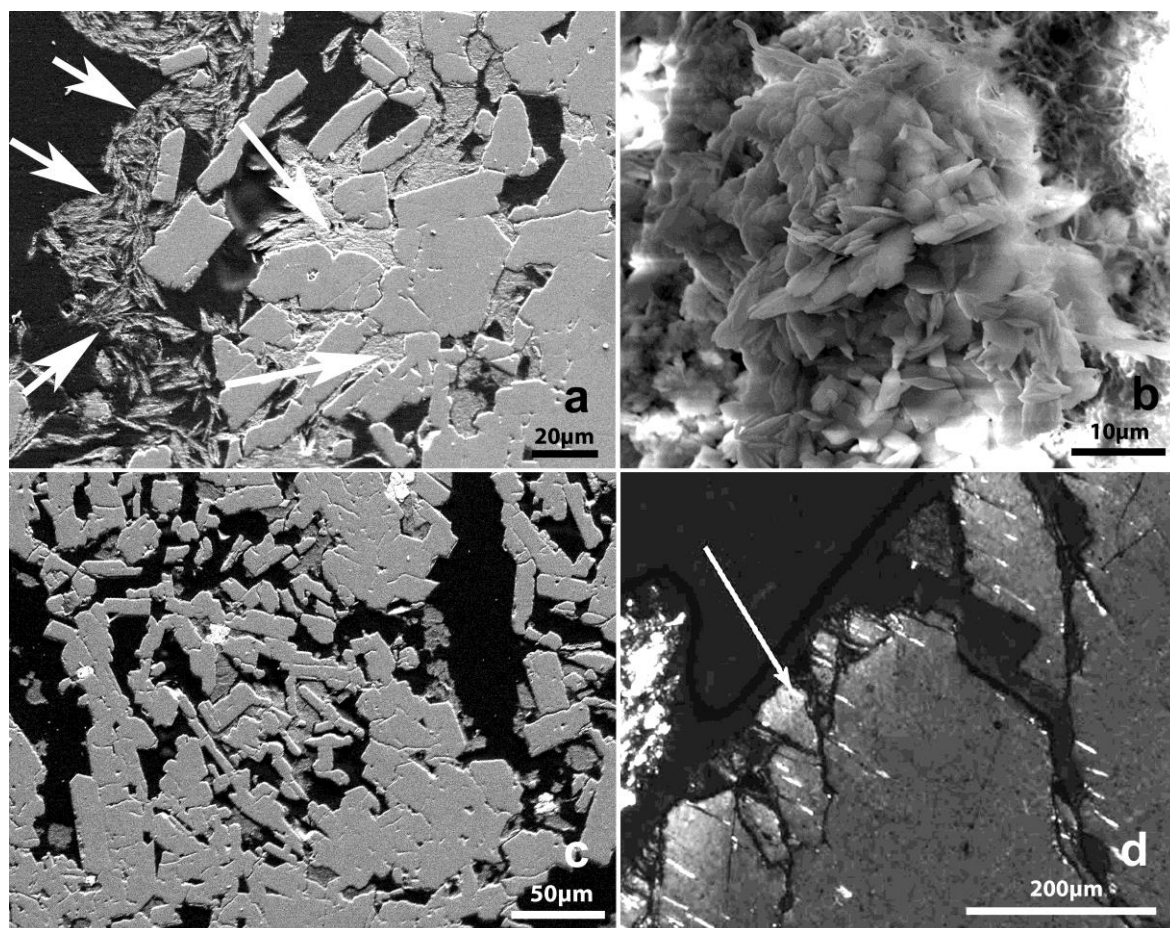


**Figure 8.11** (a) Gypsum (marked by arrows) is enriched in the crust as well as in the cracks (SEM); (b) rosette-shaped gypsum crystals on the reverse of a scale (SEM); (c) structurally disturbed zones where no gypsum is detected, indicating corrosion of feldspar grains (SEM); (d) fine-grained birefringent secondary minerals (marked by arrow) formed along the cleavage surfaces of sanidine phenocryst.



#### 8.4 Correlation of crust formation and stone decay

The investigation shows that crust formation is strongly correlated to the structural disintegration of the Drachenfels trachyte. Depth-specific samples and analyses reveal a gypsum distribution which is coherent with the detected decay phenomena. Microscopic, SEM and EDX analyses clearly indicate that gypsum enrichment is not only found within the crust but also in deeper zones of the disintegrated stone material. In deteriorated areas gypsum accumulates in cracks (Fig. 8.11a) and on the backside of the detached scales, where significant gypsum formation is observed (Fig. 8.11b). The disaggregated stone material underneath the scale is the zone where salts, e.g., gypsum, mainly precipitate and the highest concentrations are found (Fig. 8.12a). In deeper zones of the stone, sulfur decreases as the stone material becomes unaffected by environmental impact and salt migration, as the analyses of drill cores reveal (Fig. 8.12a).

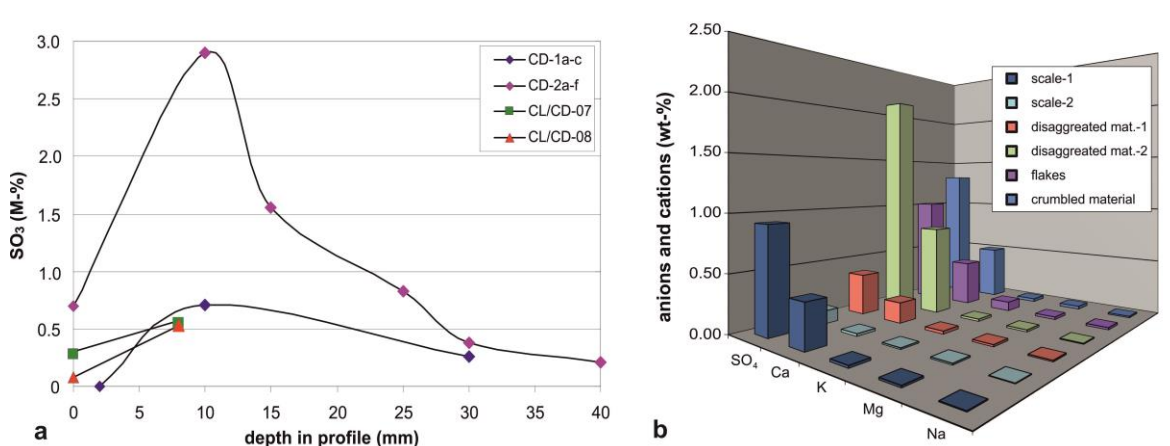


**Figure 8.12 (a)** SO<sub>3</sub> distribution in a depth profile of Drachenfels trachyte (SO<sub>3</sub> concentrations of depth specific samples) indicating a zone where salts (e.g., gypsum) preferably precipitate (sample index see Table A8.1 in the appendix); **(b)** anions and cations from water extractions of deteriorated stone material (IC-analysis) indicating high salt concentrations in the disaggregated material on the reverse of scales as well as in other deteriorated material.

Dependent on the moisture distribution in the building stone, a zone of maximum moisture defines. In this zone, salts preferably accumulate and precipitate, causing structural disintegration and leading to a zone of disruption (Snethlage and Wendler 1997). Gypsum has a comparably low solubility and shows little migration; therefore, it tends to accumulate in the pore space (Charola et al. 2007). Higher moisture conditions, e.g., retarded drying due to pore clogging through gypsum or crust formation, allow for an increased solubility and migration of the less soluble gypsum (Charola et al. 2007). A small amount of the saturated gypsum in the pore space is diluted again. If the diluted gypsum recrystallizes in fissures or interstitial areas at grain contacts, the stress induced by the growth of gypsum crystals may cause the disintegration of the fabric (Charola et al. 2007). Furthermore, calcium sulfate

solutions tend to supersaturate and may provide for the generation of high crystallization pressures (Steiger 2005).

Salt analyses confirm the on-site observations and SEM analyses. Gypsum is found in the water extractions from scale samples, and the enrichment of Ca and  $\text{SO}_4^{2-}$  is significantly higher in the disaggregated zone and the backside of the scales (Fig. 8.12b). In the samples of flaking and crumbling, high concentrations of Ca and  $\text{SO}_4^{2-}$  are detected as well (Fig. 8.12b). This indicates that even though the gypsum content in the crusts themselves is not as high as in the crusts built on limestone, gypsum clearly contributes to the damage process of flaking, scaling and crumbling to total fabric collapse of the Drachenfels trachyte.

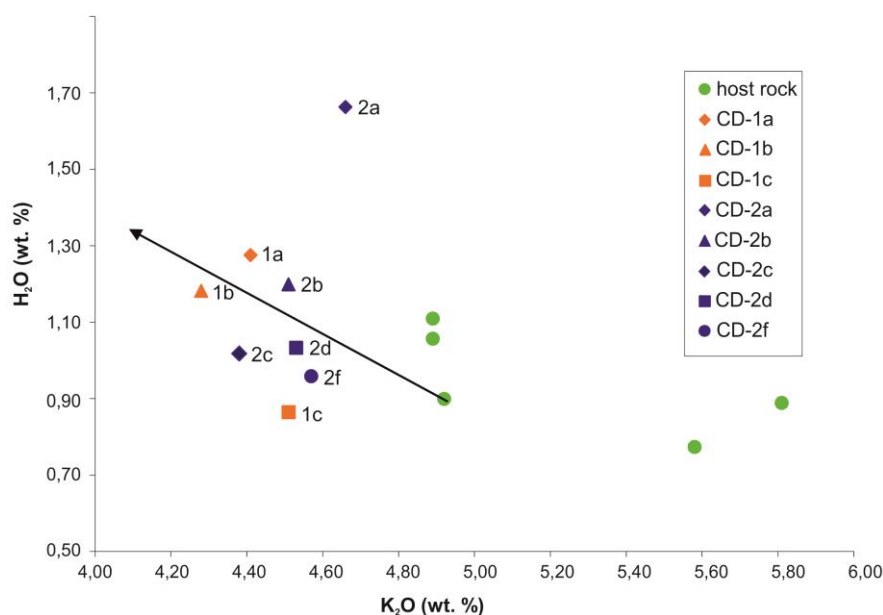


**Figure 8.13** K<sub>2</sub>O depletion and H<sub>2</sub>O increase in deterioration samples indicating the formation of phyllosilicates (sample index see Table A8.1 in the appendix).

Structurally disturbed zones, where no gypsum is found, are detected as well (Fig. 8.11c). This suggests that preexisting fabric and especially mineral in-homogeneities are disrupted due to a chemical and mechanical deterioration impact. Microscopic analyses not only show the displacement of separate grains but also detect the opening of cleavage surfaces in minerals and their disruption (Fig. 8.11d). Leaching experiments on the Drachenfels trachyte in different pH solutions show the dilution of alkali and alkaline earth metals (Na, K, Mg, Ca), indicating feldspar breakdown. The chemical analyses show a decrease of K<sub>2</sub>O (14 %) and an enrichment of H<sub>2</sub>O (22 %) in the depth-specific samples, indicating clay mineral, e.g., kaolinite, formation from the alteration of feldspars and volcanic glass fractions (Fig. 8.13).

SEM analyses detect high porosity of the aforementioned altered volcanic glass fractions of the mesostasis (Fig. 8.14). Due to the high capillarity of the altered glass fractions, caused by the distinct porosity of their very fine recrystallized grain structure, these interstitial fillings are very sensitive to penetrating pore water. Vieten 1961 and Koch 2006 attribute a certain content of montmorillonite to these recrystallized glass fractions. Microprobe analyses identify the areas of altered glass fractions through higher magnesium concentrations (Fig.

8.15a and b). If sections of un-weathered stone material (Fig. 8.15a and b) are compared to altered material (Fig. 8.15c and d), the interstitial area of the fabric, where the glass fraction is originally located, seems to be replaced by secondary gypsum formation (Fig. 8.15c and d).

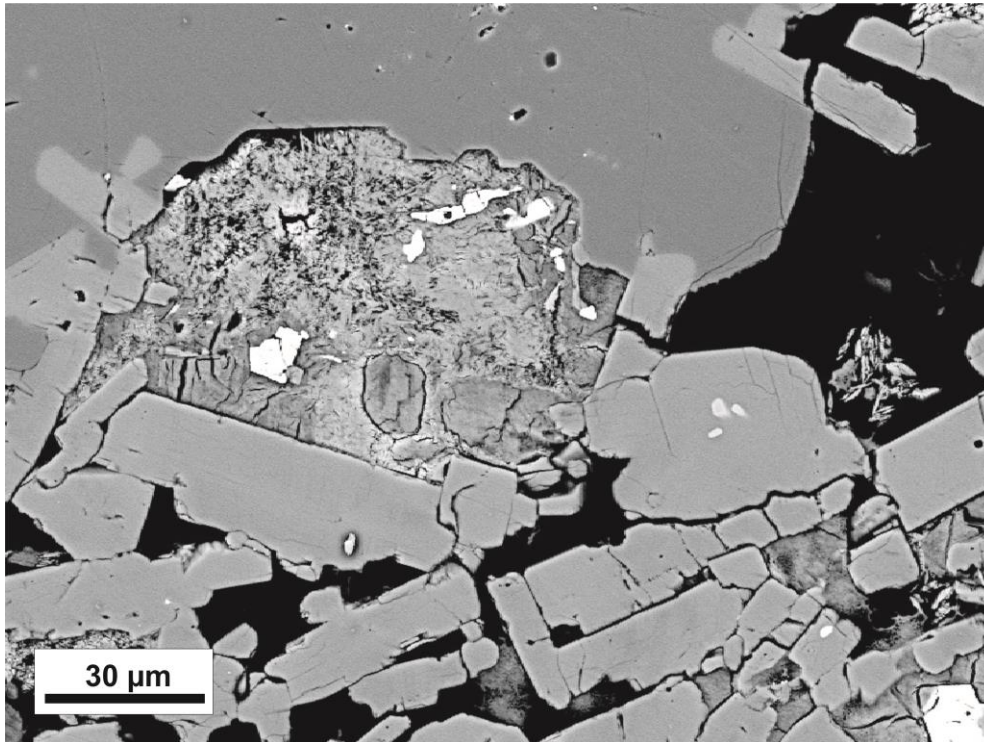


**Figure 8.14** The very fine recrystallized grain structure of the altered volcanic glass fractions in the interstitial area of the Drachenfels trachyte show high and distinct porosity and alteration to montmorillonite (microprobe backscattered electron image in composition mode).

These observations lead to a model for the deterioration of the Drachenfels trachyte. Primarily through a certain water uptake, ion-loaded water reaches the pore space of the Drachenfels trachyte. Mechanical and chemical deterioration processes of the rock-forming minerals take place: moisture dilatation provokes a grain displacement. Snethlage et al. (1996) ascertained a three- to four-fold higher hydric expansion induced by a saturated gypsum solution compared to dilatation with pure water. Mineral grains corrode and decompose along inherent weak points, e.g., cleavage planes as predetermined breaking points. These processes enlarge the pore space, giving rise to water impact and import of pollutants. Due to the higher concentration of pollutants in the pore water and a decrease of pH, the chemical corrosion of the rock-forming minerals increases, resulting in the further comminution of the mineral grains and the disintegration of the fabric (Fig. 8.11c). With increasing moisture supply, the fractions of altered volcanic glass in the aforementioned mesostasis become more affected. The montmorillonite concentrated in these areas causes significant stress onto the surrounding grains due to its strong swelling behavior. Due to the forming of new pathways through changes of pore space and the high capillarity of the interstitial areas of recrystallized volcanic glass, the ion-loaded water penetrates into the



interstitial areas and gypsum accumulates. Gypsum gets confined and accumulates in these delimited areas. The continuous crystal growth provided by the transport from the supersaturated gypsum solution, high crystallization pressures are generated (Steiger 2003). The swelling and shrinking behavior of the montmorillonite, which is found abundant in the Drachenfels trachyte, further contributes to degradation and mechanical deterioration processes. As leaching experiment showed, cation exchange processes of gypsum and clay minerals take place intensifying deterioration processes.

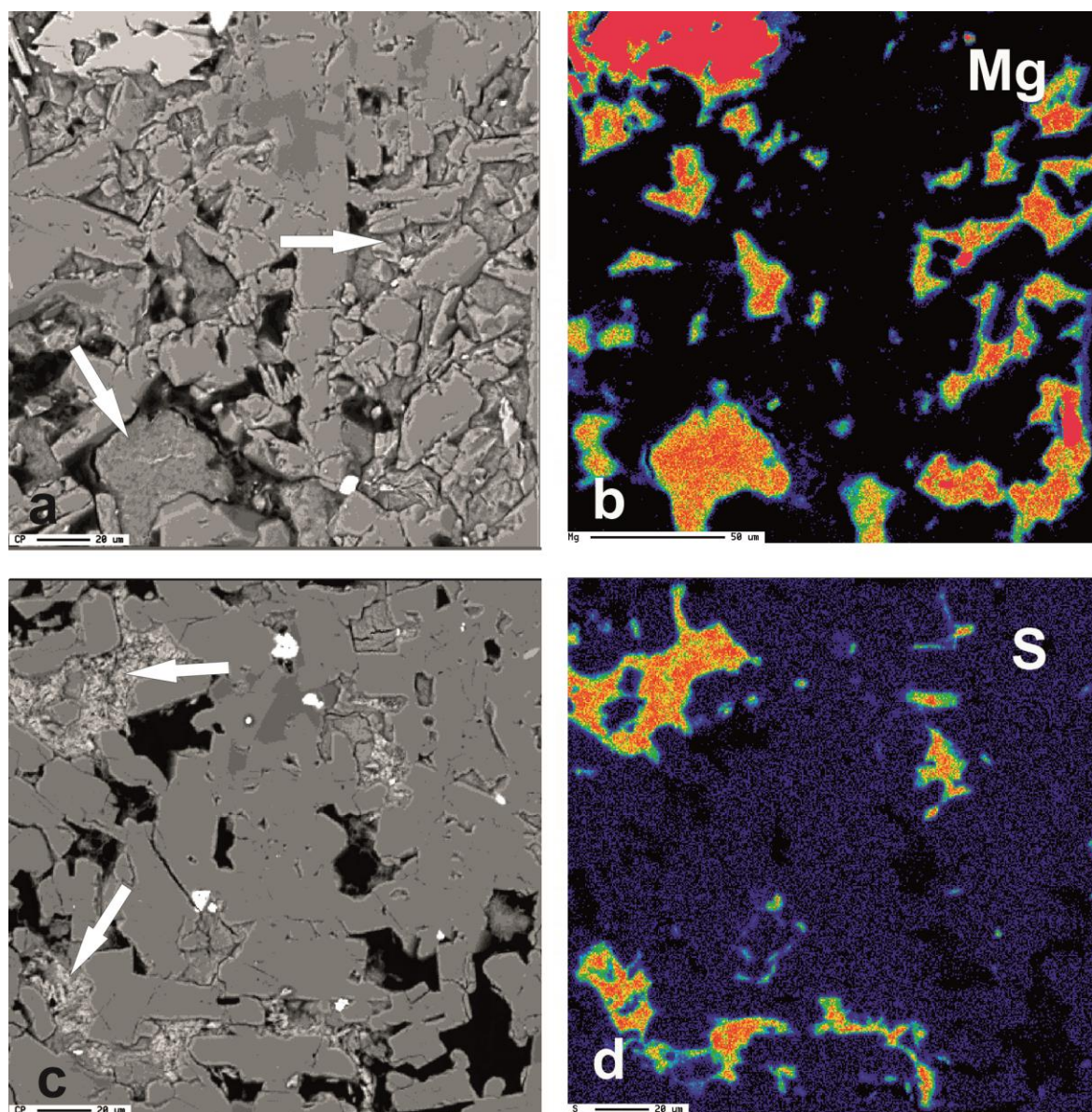


**Figure 8.15** Microprobe mapping **(a)** Backscattered electron image in composition mode of unweathered Drachenfels trachyte, *arrows* marking areas of volcanic glass fractions altered to montmorillonite; **(b)** magnesium mapping of the same area as Fig. 8.15a, the *yellow-orange-red* areas indicating higher magnesium concentration of the altered volcanic glass fractions (montmorillonite); **(c)** backscattered electron image in composition mode of weathered Drachenfels trachyte, *arrows* marking areas of pore spaces filled with gypsum –the altered glass fractions are originally located in these interstitial areas, but are now replaced through secondary gypsum formation; **(d)** sulfur mapping of the same area as Fig. 8.15c, the *yellow-orange-red* areas marking higher sulfur concentration as an indication of gypsum

Through the corrosion of the rock-forming minerals, the degradation of the altered volcanic glass fractions, and the swelling of the clay minerals, porosity changes and salt solutions are given new pathways. With repetitive wetting and drying cycles, different zones of moisture and evaporation form and the ion content of the pore water increases. Salts precipitate, produce and manifest the displacement of the grains; hence the structural disintegration. The interaction of these decay mechanisms is characterized by their coupled feedback mechanism, e.g., moisture dilatation is much more significant in the presence of salts, leading to structural degradation (Snethlage et al. 1996; Snethlage and Wendler 1997). Whereas dilatation processes have been seen to be reversible in salt-free systems, they become intensified and irreversible in salt-containing systems. Due to constantly repeating dilatation and contraction processes caused by moisture, temperature, clay minerals, and ionic species (salts), grains are permanently displaced relative to each other. The deterioration processes are interactive, leading to proceeding decay phenomena from surface parallel formation, e.g., scaling and flaking, to non-directional manifestations such as crumbling. Surface deterioration may start with crust formation, as well as contour scaling and the detachment of these scales. The weathered surface may then progress into flaking and crumbling, resulting in total fabric collapse.

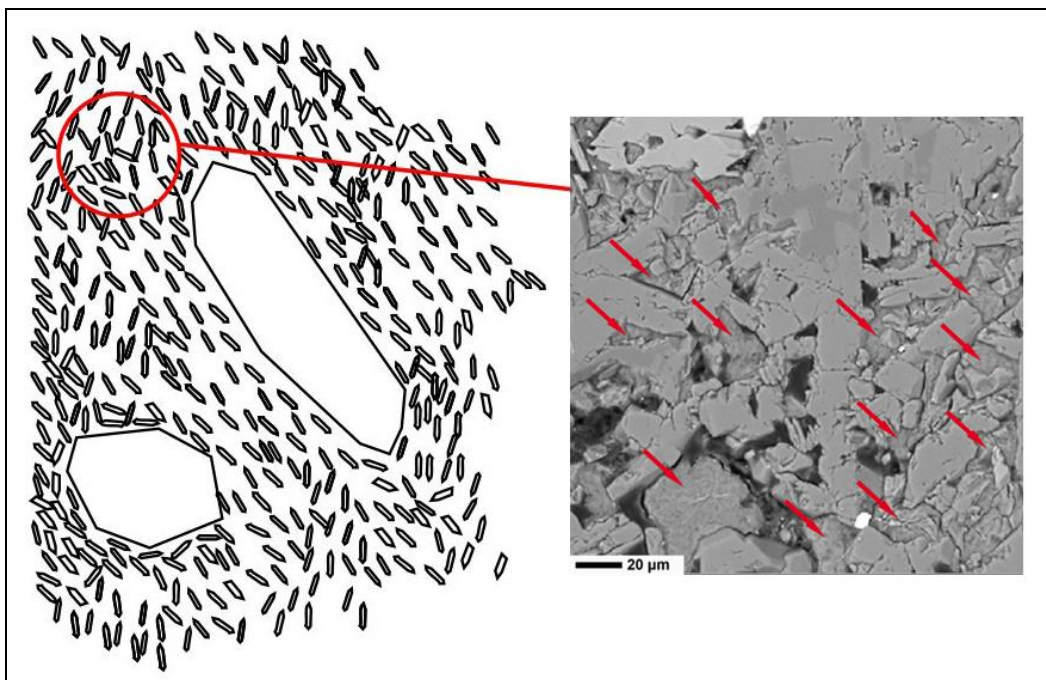


**Figure 8.16 (a)** Deterioration model of the Drachenfels trachyte: The unweathered trachyte has a porphyritic texture with feldspar phenocrysts tracing the flow direction. The small lath-shaped feldspars of the groundmass show a local flow fabric around the larger crystals forming interstitial areas. In these interstitial areas volcanic glass is detected, which is partially altered to montmorillonite (marked with red arrows).



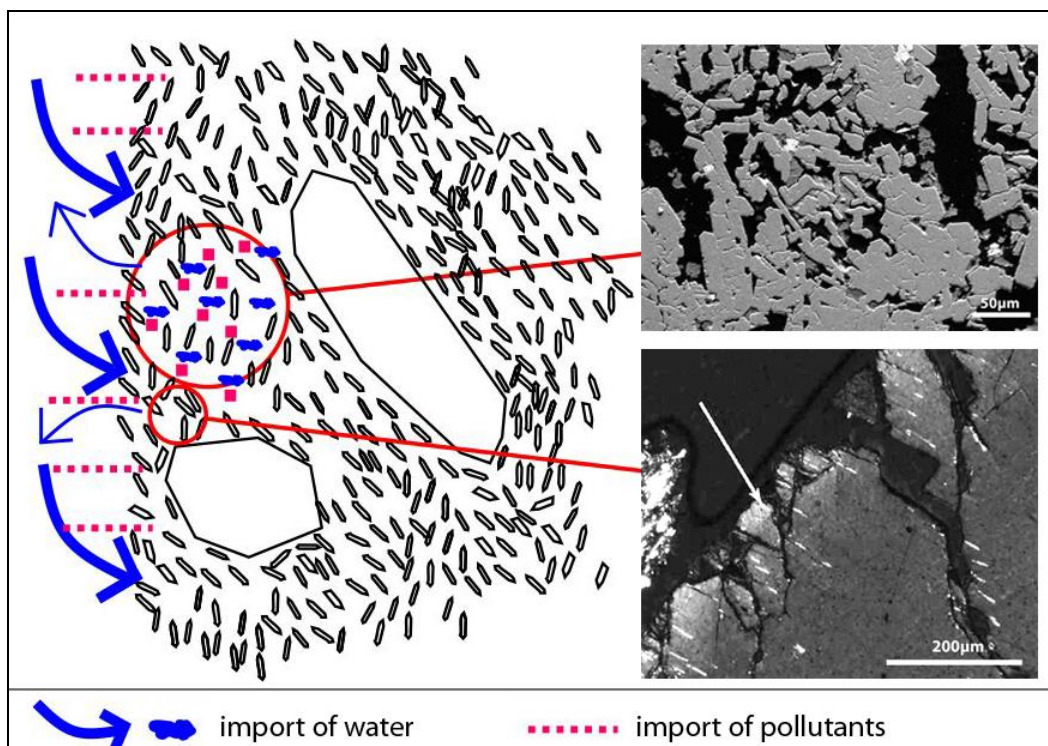


**Figure 8.16 (b)** Deterioration model of the Drachenfels trachyte: The import of water and pollutants leads to the corrosion of the feldspars due to the acidic impact. Mineral grains corrode and decompose along inherent weak points, e.g. cleavage planes (lower right picture). This results in the comminution of the mineral grains and the enlargement of the pore space (upper right picture).

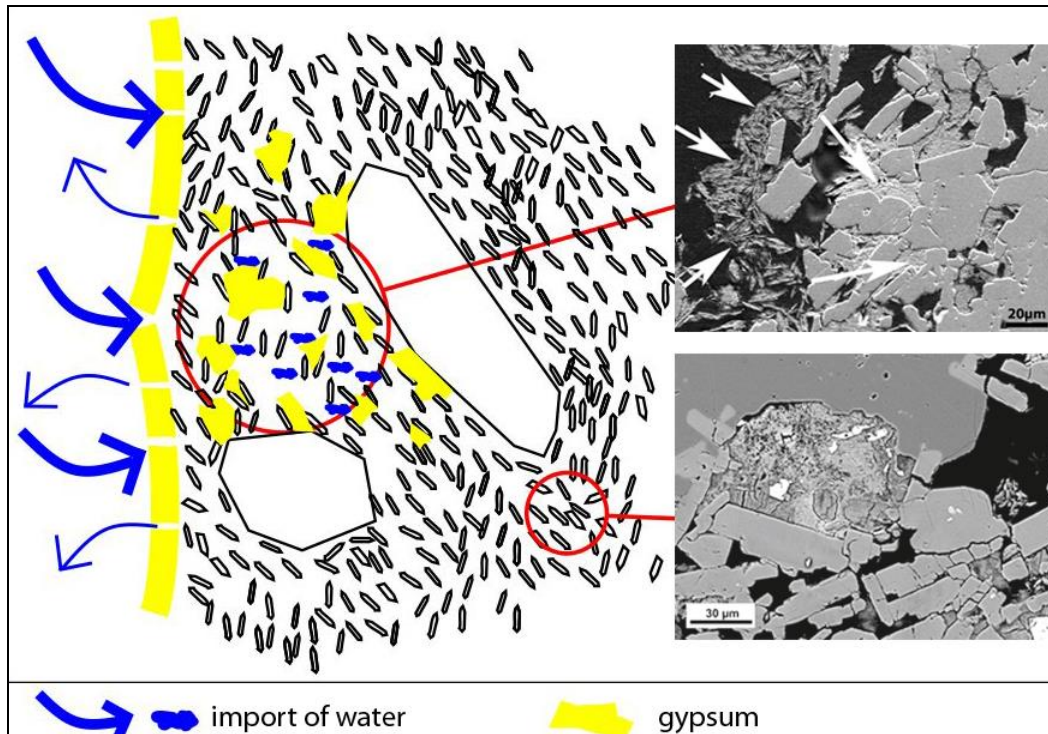


**Figure 8.16 (c)** Deterioration model of the Drachenfels trachyte: Gypsum crusts form on the surface of the stone due of the import of sulfuric and calcium components. Underneath these thick framboidal crusts water retain longer leading to a more pronounced solution of the gypsum. The salt migrates into deeper zones of the stone fabric and accumulates (upper right picture). Again, the higher water content enhances the chemical corrosion of the rock-forming minerals. The lower right picture shows an interstitial area of volcanic glass altered to montmorillonite.

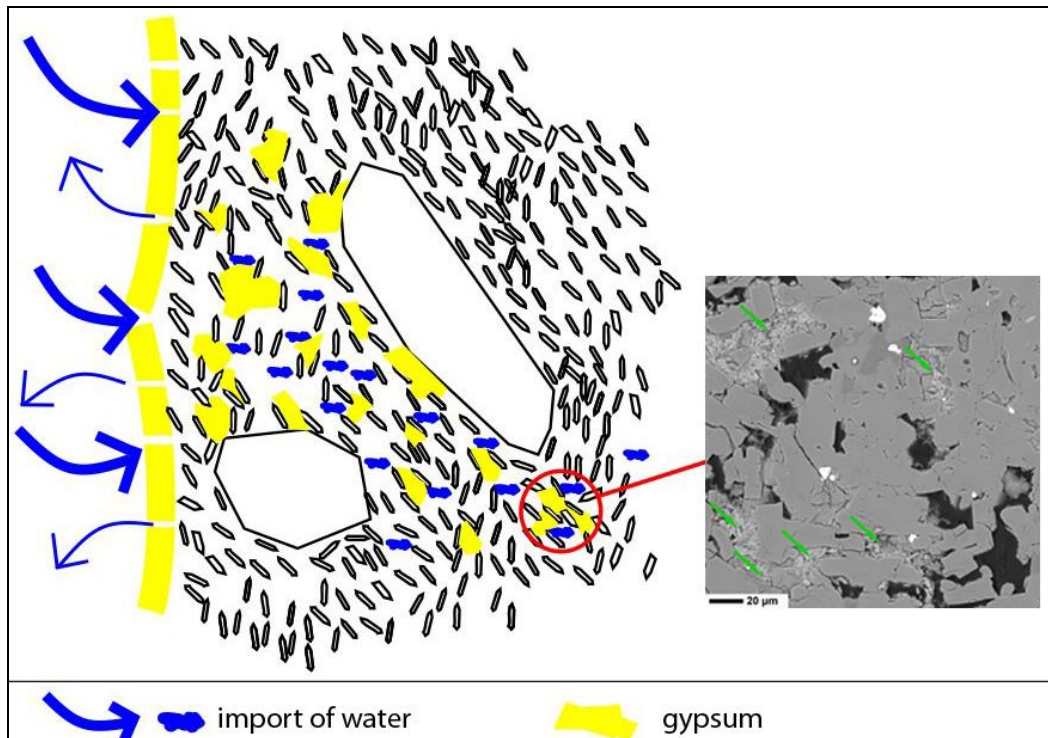


**Figure 8.16 (d)** Deterioration model of the Drachenfels trachyte: The several processes lead to the disintegration of the fabric and the formation of new pathways. Ion-loaded water penetrates into the interstitial areas, where gypsum gets confined and accumulates in these delimited areas. The swellable montmorillonite expands at water impact and enhances the dilatation processes leading to significant grain displacement. Severe crack formation and crumbling of the stone matrix takes place.

### 8.5 The clay mineral content in the Drachenfels trachyte

The significant deterioration behavior of the Drachenfels trachyte in the form of a total fabric collapse leads to assumptions about strong deterioration mechanisms once water reaches sensitive areas. Moisture dilatation processes are attributed to the presence in micropores and the resulting disjoining pressure as well as to the swelling of clay minerals (Ruedrich et al. 2011).

Mineralogical investigations focused upon the content of swellable clay minerals in the Drachenfels trachyte were carried out. The clay mineral composition was determined by X-ray diffraction (XRD) on the grain size fraction of  $<2\ \mu\text{m}$  (Fig. 8.16). A second XRF analysis was conducted after the ethylene glycol solvation of the fine grain size fraction (Fig. 8.17). In addition, the cation exchange capacity (CEC) – an indicator for the presence of expansive clay minerals – was determined on bulk samples. The CEC measurements employed the cupric-triethylene-tetramine method (Dohrmann and Kaufhold 2009, modified following Meier and Kahr 1999).

In figure 8.17 the results of the XRF are shown, clearly indicating the content of montmorillonite as shown by the peaks.

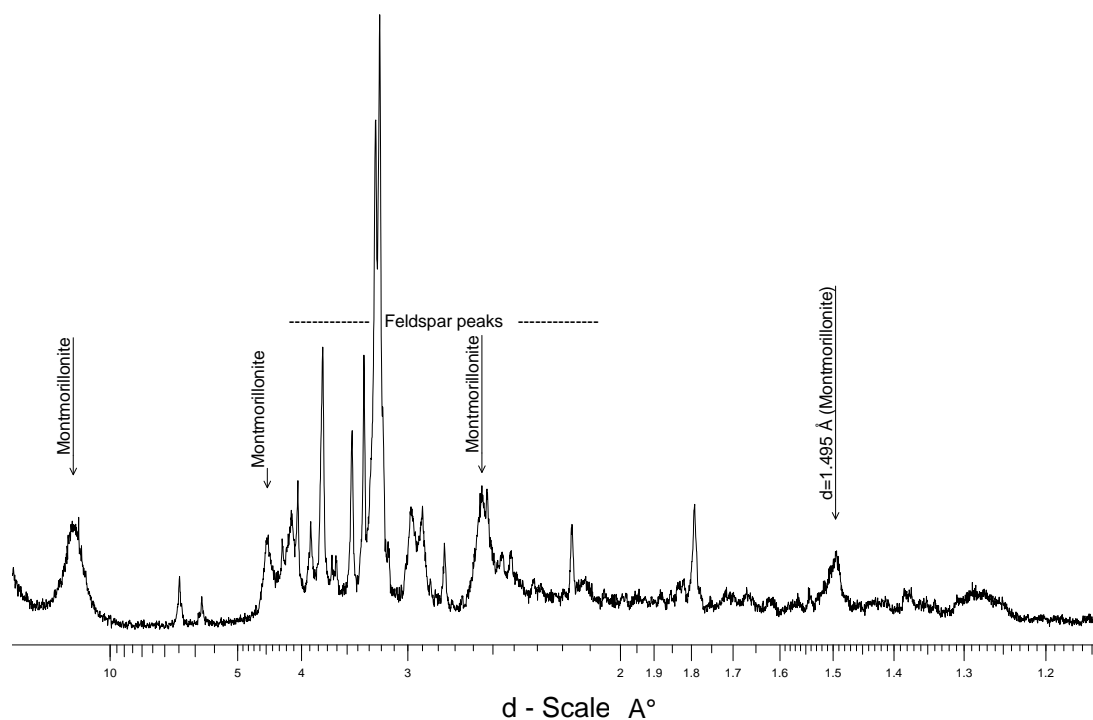


**Figure 8.17** Powder XRD of the < 2  $\mu\text{m}$  fraction prepared. The smectite is clearly identified as montmorillonite based on the peak at 1.5  $\text{\AA}$ . Even in the clay fraction feldspars are present (Dohrmann 2013)

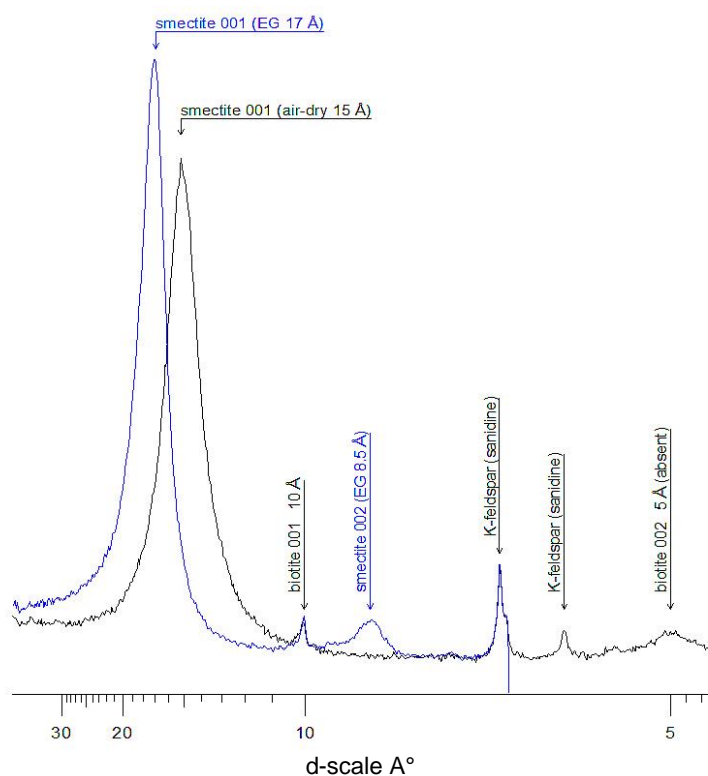


**Figure 8.18** XRD of the < 2  $\mu\text{m}$  fraction prepared as oriented slides. Black=air-dry, blue=ethylene glycol solvated (EG). Montmorillonite is clearly identified as the major clay mineral of the clay fraction (Dohrmann 2013)



The second X-ray analysis after the ethylene glycol solvation indicates swellable clay minerals (Fig. 8.18). Smectite is detected, the group to which montmorillonite belongs. Noticeable is the content of K-feldspar, which is still detected in this very fine powdered fraction ( $<2\ \mu\text{m}$ ). The cation exchange capacity (CEC) proved 4 meq/100g. This indicates a montmorillonite concentration of 3 – 5 wt. % in the Drachenfels trachyte, at an assumed CEC of  $100 \pm 30$  meq/100g for the pure montmorillonite (Dohrmann 2013).

The analyses detected a concentration of 3 – 5 wt. % of montmorillonite in the Drachenfels trachyte. This swellable clay mineral belonging to the smectite group is abundant in the pore space of the rock and notably found in the enclosed interstitial areas between feldspar grains (Fig. 8.19).

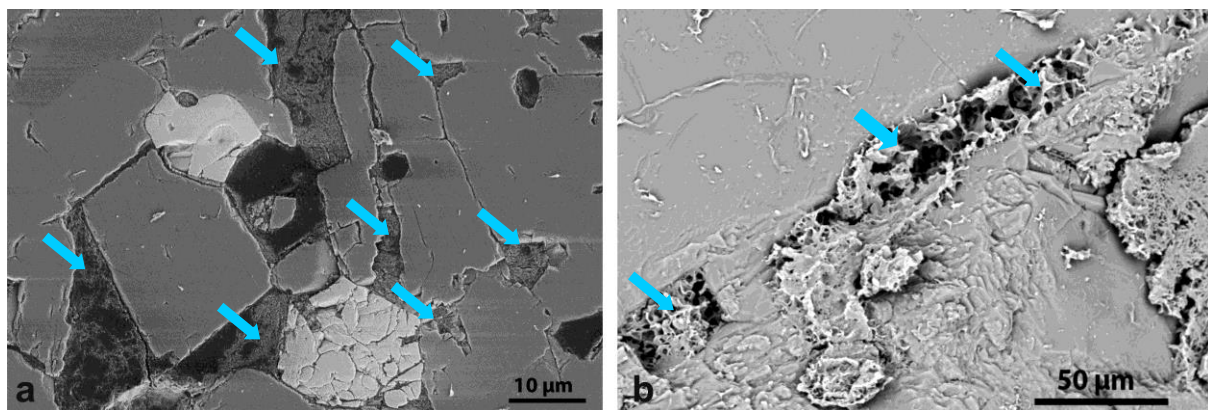


**Abb. 8.19** SEM-images of swellable montmorillonite (marked with arrows) **(a)** enclosed in the interstitial areas between the feldspar grains (secondary electron picture) **(b)** nestling in small fractures of Na-K-feldspar (backscattered electron image)

Montmorillonite is an alteration product of volcanic glasses. These volcanic glasses are abundant in the rock, indicating the fast cooling process of the Drachenfels trachyte when extruded as a krypto-dome. Through relaxation processes during the cooling of the magmas, the Kali-feldspars and the plagioclases show significant crack formation. These fissures may provide sufficient pathways for fluids for the alteration of the metastable glass fractions.

Smectite shows the highest CEC of all clay minerals with 70 – 120 meq/100g (Lagaly 1993). A high exchange capacity correlates with a significant swelling behavior. With water impact and especially at impregnation with ion loaded pore waters, these clay minerals show extensive swelling behavior and contribute to the deterioration of the natural stone.

## 8.6 Conclusions

Investigations on the crust formation on Drachenfels trachyte clearly identify the impact of pollution. The elevated contents of S, Ca, As, Pb, Sb, Bi and As in the crusts result from the impact of anthropogenic pollution mainly deriving from combustion. The analyses show an enrichment of sulfur associated with the higher abundance of gypsum. The lack of an

important intrinsic source for calcium and sulfur in Drachenfels trachyte for the formation of gypsum crusts demonstrates the major environmental impact of pollution as a source. Although  $\text{SO}_2$  in air has shown a strong decrease in concentration over the past 30 years, the pollutants are still present in the building stones and degradation in context with weathering crusts is still observed. This indicates that not only recent emission but also the pollutant concentrations of the past have to be considered, and that the impact of particulate matter in the form of settling dust plays an important role today.

In addition, the formation of gypsum crusts can be enhanced by interferences between different building materials, e.g., mortars and adjacent stones (e.g., limestone). Furthermore, the surface character and exposition of the relevant building stones pose a crucial question for the formation of the weathering crusts, promoting or hindering the deposition of settling dust, as well as the formation processes coupled to corresponding moisture supply.

If gypsum formation is compared using the data obtained from the three different cathedrals, the data from XRF analyses are consistent with the observations under the SEM. Gypsum formation on samples from Cologne shows a high accumulation of large, occasionally rosette-like, gypsum crystals. In comparison, gypsum crystals in Xanten are smaller and less abundant. In the samples from Altenberg, the gypsum crystals are even finer grained and normally only present in the form of a salt efflorescence (Fig. 8.20). These observations correlate well to the environmental  $\text{SO}_2$  concentrations and the intensity of the decay at the different locations. The trace element distribution in the crusts from industrial areas shows increasing values for lead and other heavy metals, which generally can be linked as typical pollutants to traffic and industry.

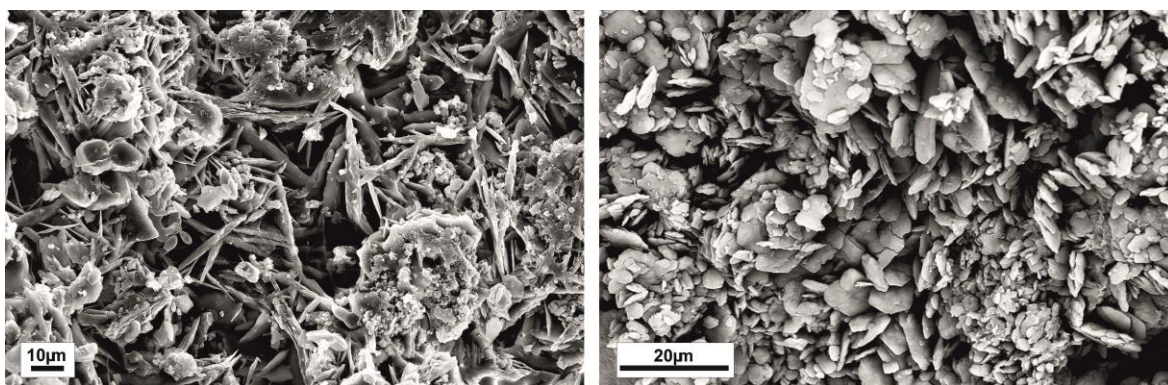


**Figure 8.20** SEM picture of gypsum formation on samples (a) from Cologne, showing an accumulation of large gypsum crystals; (b) from Altenberg, displaying gypsum crystals of smaller grain size and number.

Although crust formation on the Drachenfels trachyte is not as significant as on limestone, black crust formation on the silicate stone more strongly correlates with structural degradation (Graue et al. 2012b). The formation of gypsum crusts and salt deterioration play an essential part in the structural disintegration of the Drachenfels trachyte. The chemical corrosion of the rock-forming minerals, the further alteration of volcanic glass fractions, and

the swelling of clay minerals, i.e. montmorillonite, also contribute to the disintegration, besides mechanical decay processes. Mechanical deterioration processes (e.g., frost weathering, moisture dilatation) in a feedback mechanism with chemical corrosion of rock-forming minerals, degradation due to salt deterioration and swell-able clay minerals lead to an exponential disintegration of the rock fabric to total material collapse. The environmental impact in terms of pollutant import as well as climatic factors plays a key role.

A model for the deterioration of the Drachenfels trachyte is therefore concluded: gypsum crusts enhance moisture-related deterioration processes by hindering drying. Moisture and temperature cycles as well as varying moisture distribution promote the enrichment of gypsum in characteristic zones. Moisture dilatation is enhanced by the presence of gypsum salts. The acidic impact of anthropogenic pollution, e.g., the  $\text{SO}_2$  and  $\text{NO}_x$  concentrations in the atmosphere and the import of pollutants, leads to chemical weathering in the form of the alteration of feldspars and volcanic glass fractions, and enhances the stress caused by the swelling pressure of the montmorillonite. This is shown by the structural degradation and corrosion of the minerals and the increase of  $\text{H}_2\text{O}$  concentration. These chemical and physico-mechanical decay processes open the pore space through mineral comminution and grain displacement. The fabric becomes structurally impaired and the pore space is altered; thus, water and pollutant import increases. Through these newly opened pathways, gypsum, which usually scarcely migrates, reaches the interstitial areas of high capillarity. In these confined areas the crystallization of gypsum possibly generates high crystallization pressures. The stress already induced onto these regions by the swelling and shrinking of montmorillonite intensifies due to the enhanced cation exchange from gypsum towards the clay mineral.

The sum of these factors leads to stress and fabric decomposition as well as the degradation of the rock-forming minerals; hence the deterioration of the stone in the form of scaling, flaking and crumbling.

Regarding these deterioration mechanisms as solitary processes, not a single one is distinctively significant or could be addressed as the key mechanism for the deterioration of Drachenfels trachyte. However, their feedback interaction and their permanent repetition in continuous cycles lead to a material fatigue which finally results in the collapse of the material.



## 9 Multifactorial selection system for replacement stones

### 9.1 Introduction

The investigations ascertain a great variety of mineralogical und petrophysical properties, which characterize the different “cathedral stones”. Significantly different behavior in varying chemical milieu, i.e. acidic attack, and in the anthropogenic pollution environment is ascertained for the building materials. The individual stones show typical deterioration phenomena (see chapter four), which are controlled by specific deterioration processes (see chapters six and seven). For the building context in the monument, where the stones are placed together, compatibility of the used stones with each other is crucial. In a building environment several interferences of the stones with each other may occur; e.g. leached calcium ions from the Krenshelm Muschelkalk may contribute to the formation of gypsum crusts on the silicate Drachenfels trachyte. Variances of water balance within the stones can be observed, where a stone with originally lower water content shows increased water balance through the impact of an adjacent stone with generally higher water content (see chapter 8.4.3).

At weather exposed building sections, an increased water import might occur into the higher absorptive stone enhanced by neighboring less absorptive ashlar. As an example, when the Stenzelberg latite or the Londorf basalt lava are adjacent to the Drachenfels trachyte or other stones with higher water uptake, an increased water absorption of the latter might be considered. In case of heavy rainfall water will only be absorbed to low degrees by the latite or the basalt lava and rain will mainly run off. Thus, the increased water supply for the higher absorptive stone, e.g. Drachenfels trachyte, might yield higher water concentrations in this stone.

In the building environment context the moisture distribution within the building’s structure is of high relevance for the deterioration of natural building stones, since decay processes are moisture related (Snethlage 1985). A huge water exchange in the microstructure of the stone is generally correlated with a huge rise of pollutants, which not only supports a decay potential for salt and frost deterioration, but provides the necessary elements for chemical deterioration. Thus, moisture properties of the stones are of major interest. As an example, if the capillary water absorption of the Bozanov and Schlaitdorf sandstones is compared to that of the Obernkirchen sandstone, the first two coarse grained sandstones show much higher values (Tab. 5.1). In terms of drying behavior the Bozanov and Schlaitdorf sandstones release about 70–75 % of their water content within two days at 80% RH and 23 °C. The Obernkirchen sandstone, however releases about 60 % of its water content within two days, even though it is capable of releasing most of its water content via capillary transport (Fig. 6.1). If these three stones are compared to each other, Bozanov and Schlaitdorf sandstones

have a higher leveled water balance through their general high absorption. Obernkirchen sandstone shows relatively lower, but stable absolute water content. Thus, this sandstone stays more balanced when moist, while the Bozanov and Schlaitdorf sandstones might show strong changing moisture distributions and undergo several wetting-drying cycles. This again has a major impact on several deterioration processes, i.e. salt deterioration, which becomes significantly intensified at continual wetting-drying cycles. Additionally, in the Schlaitdorf sandstone a high sensitivity to chemical, i.e. acidic attack is observed due to its dolomite cement (see Fig. 7.2; 7.4; 7.14). Due to the environmental pollution impact the sandstone tends to form gypsum within its pore space (Kraus 1985a). For the Obernkirchen as well as the Bozanov sandstone very little sensitivity to chemical, i.e. acidic attack is observed (see Fig. 7.2; 7.4; 7.14). Thus, a primary weather resistivity can be noted. This becomes diminished in the Bozanov sandstone, when damaging salts from the ambience are adsorbed. Then the high capillary water uptake and the ascertained drying behavior of the Bozanov sandstone may evoke strong damage. If the originally weather resistant Obernkirchen sandstone is neighbored to these stones, negative interferences might be conceivable. Through the high water supply of the Bozanov and Schlaitdorf sandstones moisture as well as damaging salts might be transferred to a certain degree.

The observations and investigations contribute to a better understanding of the deterioration processes *in situ*. Furthermore, they may support the planning of preservation strategies for cultural heritage. The knowledge of deterioration processes taking place is prerequisite for the conception of adequate conservation proposals – preventive conservation, conservation treatments and the development of methods and materials. The main target is the stabilization of the stones' condition and the minimization of the progressing stone decay (E.C.C.O. 2002). At Cologne cathedral the primary objective is the preservation of the medieval Drachenfels trachyte as well as the other historic building stone ashlar through conservation measures. In many cases the replacement of historic stone material is crucial for the building's static safety. In general, it is aimed to use the same stone material as the historic one, which needs to be replaced. Since 1829 this has been impossible for the Drachenfels trachyte. Thus, this medieval construction material is found in masonry bonds with many other building stones at Cologne cathedral.

At the beginning the selection of replacement stones was determined by economic aspects and optic properties. Since the middle of the 19<sup>th</sup> century the deterioration resistivity of the stones became more important. Nowadays, the selection of appropriate replacement material ensues mineralogical and petrophysical comparability and geological similarity as well as optic properties. At this point it becomes crucial, that not only the comparability of the replacement stones with the original stone is given, but the compatibility with all other stones in the masonry bond as well. General requirements for replacement stones are optical,

textural (coarse, medium, or fine grained) as well as mineralogical properties, where a high similarity is demanded. At the same time a weather resistant material shall be chosen. In literature, general requirements for replacement stones are given in terms of their petrophysical properties (Snethlage 2005). Porosity, pore size distribution and capillary water uptake as well as water transport characteristics and strength properties ought to be in the same range as the original and the replacement stone. If several different natural building stones are placed in one building section, it is highly improbable to find a replacement stone, which is comparable in all its petrophysical parameters with those of all other adjacent stones. Thus, it is important to assess the mentioned parameters in regard to their significance for the characterization of the original stone. This has to be done in terms of the petrophysical characteristics, that specify the stone, and in respect to the typical deterioration behavior of the original stone as well. The assessments will score the parameters leading to the most important ones: these *key-parameters* of the original stone shall then be compatible with the replacement stone. The *key-parameters* are to be collated with those of the other stones in the masonry bond to achieve compatibility with each other (Graue et al. 2012a).

## **9.2 General requirements for replacement stones**

At the Cologne cathedral exists a material mix of sandstones and carbonates as well as volcanic rocks. This diversity of material on one building is an exception and a great challenge. Owing to the long building history and the continuous repair works, Drachenfels trachyte is found in masonry bonds together with Obernkirchen sandstone, Krensheim Muschelkalk, Stenzelberg latite, and Londorf basalt lava. Due to current restoration works, Montemerlo trachyte is integrated into the masonry bond. Occasionally the Schlaitdorf sandstone is also found together with the mediaeval Drachenfels trachyte. This indicates, that a potential replacement stone for Drachenfels trachyte has to be compatible with all other stone materials, i.e. its basic properties have to go with all the other stone materials. Bozanov sandstone is used as a replacement material for the Schlaitdorf sandstone.

To assess the compatibility of weathered and fresh stones, Snethlage (2005) suggests that the properties of a replacement stone should be in a similar range as the original stone. The mineralogical composition and the optical appearance are important criteria for replacement stones. Furthermore, it is necessary to determine the porosity, the pore size distribution, the capillary water uptake, water uptake by water vapor adsorption, the degree of saturation, the water vapor diffusion value and the strengths as well as the Young's modulus of elasticity (E-modulus). Many of the parameters required according to Snethlage (2005) are determined in the present study (see chapter five).



***Mineralogy***

In terms of the mineralogical phase composition the implemented stones at the Cologne cathedral cover a wide range. Since the different building stones (sandstones, carbonates, and volcanic rocks) exist together in the masonry bonds, it is not possible to find the particular replacement material of the same mineralogical classification. Therefore it is of major importance, that the petrophysical data, especially porosity and moisture behavior are compatible.

***Optical properties***

In general, all building stones of the Cologne cathedral show gray to black surfaces when weathered or are originally grayish-black, except for the Krensheim Muschelkalk in rain-washed areas. Quarry-fresh stones show varying optical appearances. Stenzelberg latite and Londorf basalt lava are both dark gray stones. Drachenfels trachyte and Krensheim Muschelkalk are originally light grayish to beige stones. While the weathered Drachenfels trachyte at the Cologne cathedral shows black surface crusts, the carbonate rock also forms black gypsum crusts in rain-protected wet areas. However, where the stone is washed, the light beige-gray color may even bleach somewhat. Schlaitdorf and Obernkirchen sandstones originally show similar light beige to yellow and orange color, but weather differently. While the Obernkirchen sandstone develops a grayish black surface layer, the Schlaitdorf sandstone forms dark brown gypsum crusts, but also tends to show some greenish microbiological growth. Besides the color matching, also structural features i.e. grain sizes are critical for the optical properties. The employed sandstones have different appearances in respect of their grain sizes. The Obernkirchen sandstone is a fine-grained sandstone, while Schlaitdorf sandstone is coarse-grained. The current replacement stone for the Schlaitdorf sandstone is the coarse-grained sandstone from Bozanov. The Bozanov sandstone, weathers slower and only minor formation of dark crusts can be anticipated, since high pollution impact has changed since the 1970/80's. Moreover, the Bozanov is free of carbonate minerals, and is therefore less sensitive to the formation of gypsum crusts.

Today's replacement material for Drachenfels trachyte, the Italian trachyte from Montemerlo, has a similar trachytic matrix, but is slightly more brownish in color intensity. From an aesthetical point of view, the stone is visually well compatible with the slightly weathered Drachenfels trachyte. However, in areas where the medieval building stone is weathered and shows intense black crusts, the newly inserted Italian trachyte stands out quite significantly. Even stronger is the difference of weathered Schlaitdorf to Bozanov sandstone. To cope with the situation of these different appearances, the Obernkirchen sandstone and Drachenfels trachyte were painted in the beginning of the 20<sup>th</sup> century to color adjust to the light gray Krensheim Muschelkalk (Schumacher 2004). The latest discussion on matching optical

properties is whether to apply an “aqua sporka” onto the new stones or to clean the old weathered stones.

### ***Petrophysical criteria***

In terms of porosity, all investigated stones except the Stenzelberg latite belong to a medium porosity class (Snethlage 2005; Siegesmund and Dürrast 2011). Moreover, both the trachytes and Londorf basalt lava are in the lower range of medium porosity (see also Stück et al. 2008).

In regard to the pore size classes clear distinctions are registered. Figure 5.3 shows that the stones from the Cologne cathedral diverge in terms of their pore size distribution. The Drachenfels trachyte, Schlaitdorf, Obernkirchen and Bozanov sandstones as well as the Krensheim Muschelkalk have 83.3 – 89.6 % capillary active pores. Londorf basalt lava and Montemerlo trachyte show 65.8% and 62.8% capillary pores. Stenzelberg latite is the other extreme with 95.4% micropores and only 4.6% capillary pores. Due to its high percentage of micropores Stenzelberg latite probably shows the effect of capillary condensation. Montemerlo trachyte and Londorf basalt lava might possibly show little effect as well.

Comparing the pore size distribution of the Drachenfels trachyte and the other stones used at the Cologne cathedral, it is obvious that the Drachenfels trachyte does not have a close match (Fig. 5.3). The Obernkirchen sandstone has a wider distribution than the Drachenfels trachyte with 67.6% of pores  $> 1 \mu\text{m}$ , whereas the Drachenfels trachyte only has 35.1% of that range. Stenzelberg latite and Montemerlo trachyte have relatively high percentages of micropores. Londorf basalt lava and Krensheim Muschelkalk have an even but very unsorted pore size distribution from 0.0064 to 64  $\mu\text{m}$ , respectively 0.0064 to 82  $\mu\text{m}$ . The Londorf basalt lava has 65.8% capillary pores, whereas the Krensheim Muschelkalk shows 85.0%. Only the Schlaitdorf and Bozanov sandstones may be grouped as „heavy soakers“ – stones with a high water absorption – with 83.3 % and 89.6% capillary active pores and 47.8%, respectively 68.7% pores  $> 10 \mu\text{m}$ .

Snethlage (2005) suggests using a replacement stone with a low to medium water suction value when replacing damaged parts, which originally consisted of stones with higher water suction value.

All the w-values of the samples are in the range from 0.3  $\text{kg/m}^2 \cdot \sqrt{\text{h}}$  to 6.9  $\text{kg/m}^2 \cdot \sqrt{\text{h}}$  (Tab. 5.1). The original building stone, the Drachenfels trachyte, shows a w-value of 0.6  $\text{kg/m}^2 \cdot \sqrt{\text{h}}$ . The Schlaitdorf and Bozanov sandstones can be classified as belonging to the group of strongly absorbing stones. Montemerlo, Obernkirchen and Krensheim, however, are medium absorbing stones. The maximum water content attainable by capillary water uptake was not determined, since it does not play an essential role in nature. In general, the

penetration depth of rain is smaller than the thickness of building components. The stones used in the cathedral and the evaluated replacement stones show a strong divergence when considering the capillary water uptake, and thus do not meet the necessary suitability requirements (Fig. 9.1).

The s-value is a factor for the determination of the frost resistance of natural building stones. The degrees of saturation (s-value) of the investigated stones are between 0.59 and 0.76 (Tab. 5.1). According to the limit value of  $s < 0.75$  (DIN 52103) only the Stenzelberg latite has a higher water saturation coefficient (Fig. 9.1).

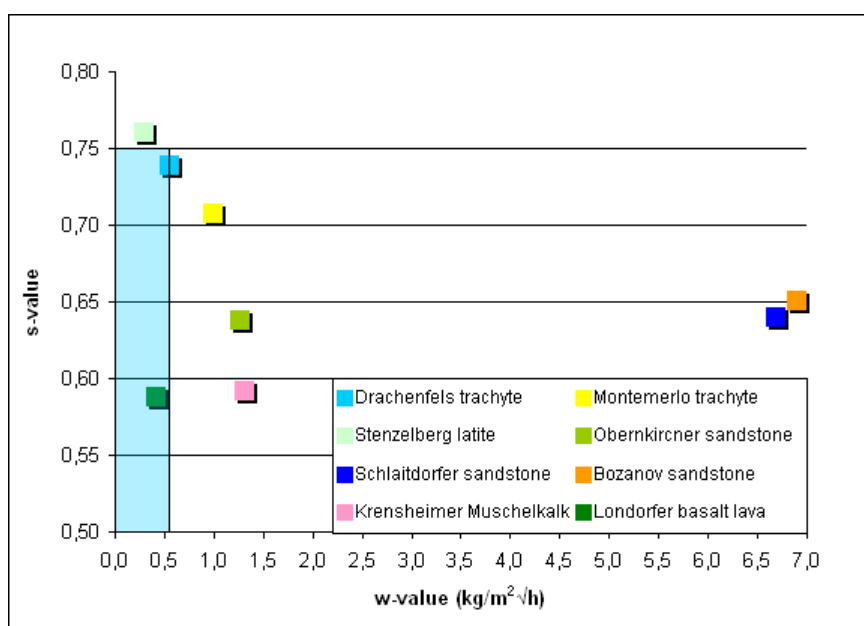


**Figure 9.1** Capillary water uptake (w-value) and saturation degree (s-value) of the stones from the Cologne cathedral show much divergence. If the proposed requirements on these two parameters are set in comparison to the Drachenfels trachyte (marked area), only the Londorf basalt lava shows appropriate s- and w-values

The water uptake by adsorption plays an important role in the deterioration of natural building stones due to the central European climate. The Stenzelberg latite has a very high water uptake by adsorption, whereas Drachenfels and Montermerlo trachyte as well as the Londorf basalt lava have a medium water uptake by adsorption. The three sandstones and the Krensheim Muschelkalk absorb water only by a small degree due to their pore size distribution and the lack of a well communicating pore space. Moreover, salt contamination e.g. due to pollution and deterioration may cause significant increases of the water uptake by adsorption in exposed building stones (Kraus 1985a).

Until now, no guidelines are available to evaluate the water uptake by adsorption in respect of replacement materials. Analogous to the guideline for the capillary water uptake, water uptake by adsorption of the replacement stone should be the same or less as the original stone. Thus, only Stenzelberg latite does not fit into this scheme (Tab. 5.1 and Fig. 9.2).

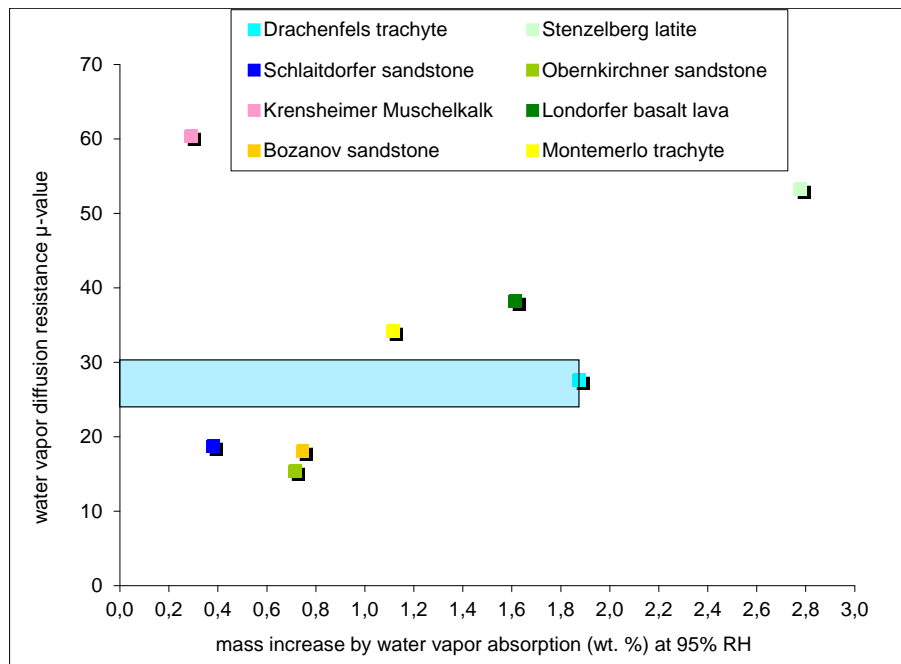


**Figure 9.2** Diagram showing the sorption and water vapor diffusion resistance of the investigated stones. Setting the proposed requirements in correlation to the Drachenfels trachyte (marked area), shows that for one parameter e.g. sorption, all building stones except the Stenzelberg latite might be suitable. A second parameter, the water vapor diffusion, shows the insufficient compatibility of the different stones

Since water is a driving factor for deterioration, drying processes and their length play an important role for the decay resistance. Kraus (1985) ascertained drying durations for Schlaitdorf sandstone of 11 days, for the Krensheim Muschelkalk and Obernkirchen sandstone of 13 days and for the Drachenfels trachyte and the Londorf basalt lava longer than 15 days. Krensheim Muschelkalk shows moderate drying despite a high water vapor diffusion resistance (Kraus 1985a). The latter is determined by the low connectivity of the pores. With respect to drying, Kraus (1985) determined that salt-contamination as well as dirt depositions on the stone surfaces decelerate the drying process. As a requirement for replacement stones, these should dry in a moderate period of time. The newly inserted stone should not stay humid longer than the neighboring original one, thereby not functioning as water supply.

The investigated stones from the Cologne cathedral show a broad distribution in terms of water vapor diffusion resistance. Following the outline of a maximum divergence of 10% for the water vapor diffusion value (Snethlage 2005), it becomes obvious that the building stones at the Cologne cathedral are not compatible with each other (Tab. 5.1; Fig. 5.6a & 9.2).

Moisture and thermal expansion are volume changes of natural building stones induced by extrinsic factors (exposition, climatic situation, and building physics). A critical hydric swelling is observed at the Montemerlo and the Drachenfels trachyte as well as the Stenzelberg latite and the Londorf basalt lava. On the building stones from the Cologne cathedral it can be

observed, that with increasing amount of micropores hygric swelling increases as well (Fig. 9.3a), which indicates, that the main driving factor for moisture related length changes could be caused by disjoining pressure in small pores (Wangler and Scherer 2008). Furthermore, a smaller mean pore radius can be correlated to a higher hygric dilatation. The stones from the Cologne cathedral with a high capillary water uptake do not necessarily show high hygric dilatation, however high sorption values can be correlated to higher hygric and hydric expansion, indicating a damage potential; as it may be interpreted for the Stenzelberg latite, Londorf basalt lava, Montemerlo and Drachenfels trachyte (Fig. 9.3b).

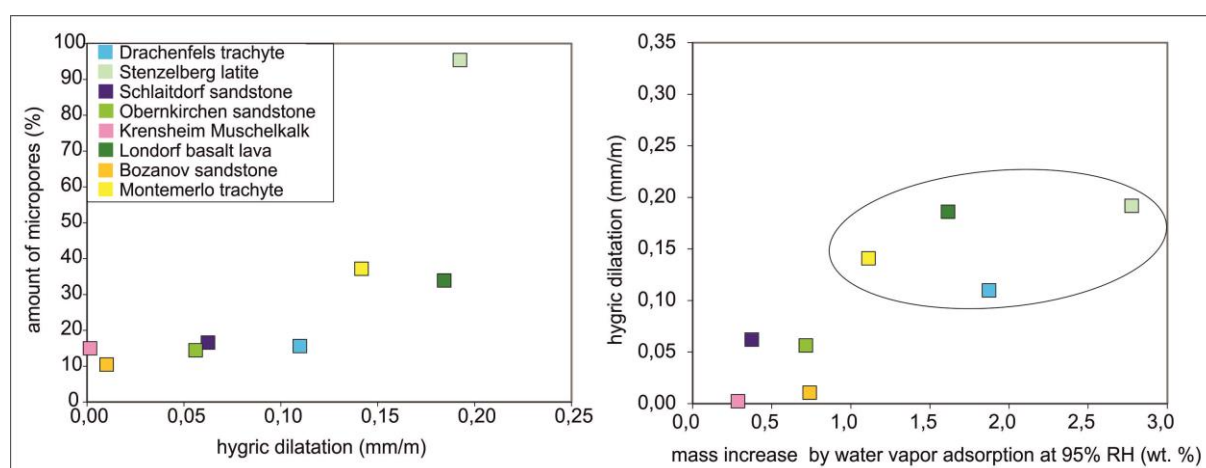


**Figure 9.3 (a)** The building stones from the Cologne cathedral show that a higher percentage of micropores indicates stronger hygric dilatation, which again might be due to disjoining pressure in small pores. **(b)** Higher water sorption values can be correlated to higher hygric dilatation, indicating a potential damage source for Drachenfels trachyte, Stenzelberg latite, Londorf basalt lava and Montemerlo trachyte

For both moisture and thermal dilatation, lower expansion should be the aim for the replacement stones being employed. Since the investigated stones show no residual strain in terms of thermal dilatation this is of minor importance.

In respect of strength properties the following evaluation of the investigated stones is based on the proposed criterion of 80 – 120% of the strength value of the original building stone (Snethlage 2005). In respect of the uniaxial compressive strength only the Londorf basalt lava would be compatible in terms of the strength values with the Drachenfels trachyte (Fig. 9.4a). A compatible flexural strength to the Drachenfels trachyte is shown by the Montemerlo trachyte and Schlaitdorf sandstone (Fig. 9.4b). Assuming that 80 – 120% of the tensile strength of the original building stone would be suitable, the Drachenfels and Montemerlo trachytes as well as Schlaitdorf and Bozanov sandstones are of one comparable range (Fig. 9.4c).

If the limitations are extended to 70 – 130%, for uniaxial compressive strength, all investigated stones except the Stenzelberg latite will be suitable. For flexural strength the Obernkirchen sandstone could be added. In terms of tensile strength it would be the same grouping as at 80-120% limitation (Fig. 9.4).

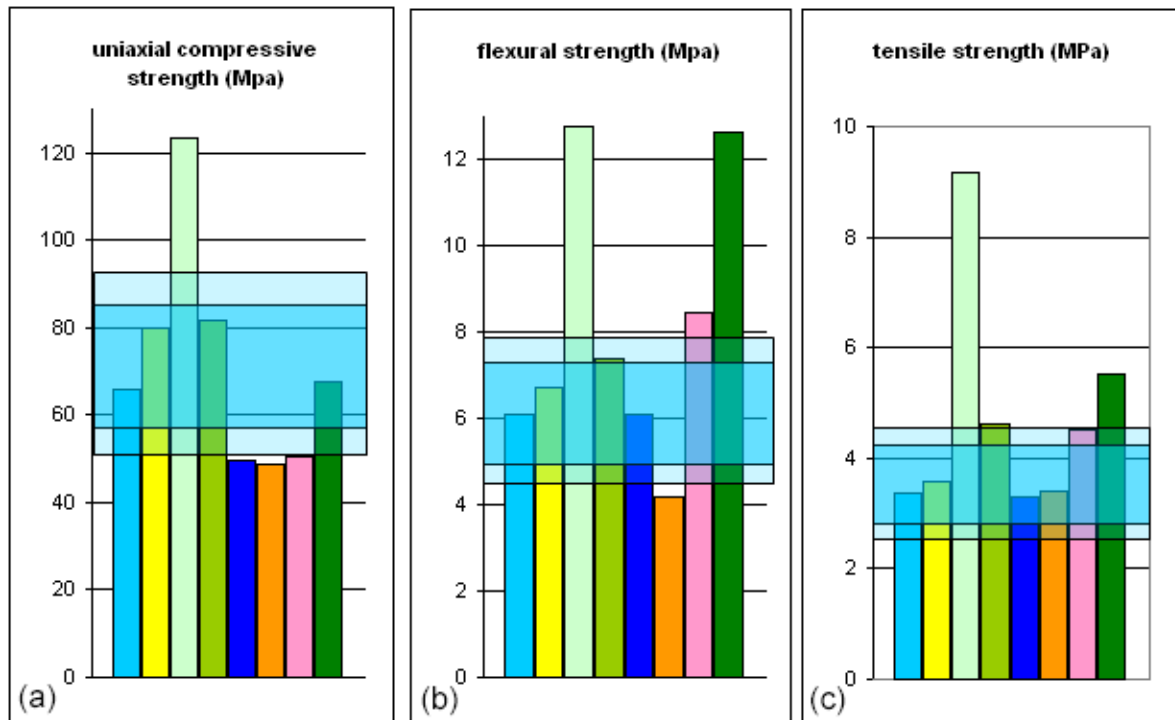


**Figure 9.4** Diagrams showing the strength values of the investigated stones from the Cologne cathedral **(a)** uniaxial compressive strength, **(b)** flexural strength and **(c)** tensile strength. Each have the proposed constraint of 80-120% of the original strength value (Snethlage 2005) in correlation to the Drachenfels trachyte (dark blue marked area), and widened limitations of 70-130% (light blue marked area)

One aspect contributing to the evaluation of the deterioration and interferences of the different stones is missing within the discussion of the present work. Thermal conductivity and head storage capacity are two parameters which influence water balances within natural building stones (e.g., drying properties). Thermal properties are characterized by the thermal conductivity, the temperature conductivity and the specific heat (Siegesmund and Dürrast 2011). Although, head storage capacity will probably be similar in the investigated stones, a higher porosity is correlated with a lower thermal conductivity. Furthermore, the mineralogical composition, rock fabric features, pressure and temperature, as well as the type and degree of fluid saturation, determine the *in situ* thermal conductivity of rocks (Siegesmund and Dürrast 2011). Temperature distribution measurements were carried out on site (chapter 3.2). Laboratory data was detected but was not available for data progressing, at least thus far; the inclusion of this data remains outstanding.

### 9.3 Recognition and measurement of parameters

The different building stones employed at Cologne cathedral show a diverse petrography and mineralogical composition as well as a broad variety of petrophysical properties. The comparison with valid guidelines reveals the broad spectrum of the used materials. The strong divergence of the ascertained parameters of the stones (i. e mineral composition, porosity, water absorption and saturation, drying characteristics, moisture and thermal

dilatation, strength properties, etc.) shows, that the constraints for replacement materials make it almost impossible to find an ideal stone, if parameters are not differentiated.

Afore described requirements for replacement stones weight the parameters equally. As shown, it is difficult to find a stone material, which displays all required parameters within the limit values. At the same time it is not sufficient to restrict the selective parameters only to optical and geological-mineralogical aspects.

Within the present systematic approach for the determination of criteria for replacement stones the parameters are recognized and measured by a multi-factorial assessment analysis following four working steps: A. assessment; B. ranking; C. correlation; D. matching.

Step A: Firstly the ascertained parameters of the stone in question are assessed in terms of their relevance to each other for material characterization and secondly in respect of their significance to each other for the deterioration behavior of the natural building stone.

Step B: The single valuations – “material index” and “decay index” – are compiled and the parameters are ranked.

Step C: The correlation of the two rankings (material relevance and deterioration significance) indicates the imperative “key parameters”, which determine the relevant criteria for the selection of an appropriate replacement stone. These *key parameters* should be met within afore stated requirements for a replacement stone.

Step D: The *key parameters* of the “original” stone and the potential replacement stones are matched.

### **9.3.1 Assessment and ranking**

As an example the multi-factorial analysis is shown for the Drachenfels trachyte. Fabric and pore space parameters, mineralogical and petrophysical properties are correlated in terms of their significance to each other for material characteristics and behavior as well as in respect to their influence on decay processes.

The Drachenfels trachyte has a porphyritic fabric with a strong magmatic foliation. Large phenocrysts of sanidine are embedded with preferred orientation in a matrix with strongly aligned microcrystalline feldspar laths. The fabric can be divided in three structural components: the large phenocrysts, secondly the microcrystalline matrix, composed mainly of feldspar and third a mesostasis consisting mainly of recrystallized interstitial volcanic glass, which in many places is altered to montmorillonite.

In contrast to the relatively high porosity of 12 % and the high ratio of capillary active pores (84 %), the stone shows a low capillary water uptake ( $0.55 \text{ kg/m}^2\sqrt{\text{h}}$ ). This may indicate a lack of connectivity of the pore space. The water uptake by adsorption and the saturation degree measured are high, analogous to the values of Snethlage 2005. Larger mineral grains show a lot of cracks and breakages, which are to be considered as part of the pore space. The Drachenfels trachyte shows medium water vapor diffusion resistance and drying



is retarded. Kraus 1985a reports that within 15 days the tested stone samples still contain rest moisture. This water has to be released via water vapor diffusion. The strength properties of the stone are medium to low: low compressive strength, medium flexural strength, very low tensile strength. Moisture dilatation is high compared to the other eight investigated stones, thermal dilatation is little.

The Drachenfels trachyte is very inhomogeneous not only in respect of grain sizes but also in terms of the mineralogical composition of the structural components (phenocrysts, matrix and mesostasis) and their specific properties. Phenocrysts and matrix consist of chemically fairly stable components in comparison to the mesostasis. The recrystallized glass in the mesostasis is liable to chemical decay impact and the fractions already altered to montmorillonite enhance deterioration processes due to the swelling properties of these clay minerals. Even though capillary water uptake is low, the high porosity, saturation degree, and water adsorption as well as the retarded drying suggest a susceptibility to moisture related processes. These parameters, which are significant for the Drachenfels trachyte, indicate that wetting-drying cycles are not very pronounced, but the stone stays humid over long periods of time. This involves a significant capacity for adsorption and transportation of pollutants and guarantees sufficient water supply for the degradation processes. In these terms, direct mechanical material reaction, e.g. moisture dilatation, can be considered minor, but pollution impact and salt weathering become more important in terms of initializing and accelerating deterioration processes.

For the assessment, at first a “material index” and second a “decay index” are generated. Based on these two indexes the parameters are ranked. In a matrix analogous to Visser and Mirwald 1998, the afore described fabric and pore space parameters as well as the petrophysical properties of the Drachenfels trachyte are evaluated from 0 to 3 (rating numbers) in terms of their significance to each other for the material behavior (Fig. 9.5). The higher their significance to each other is, the higher their rating number becomes. Through This assignemnet is an approach of a numeric estimatoion of the correlationens, which does not compensate the discussion in individual cases. With this numeric assignment of the correlationen a tabular overview is obtained.

This material-intern correlation points out the significance of distinct parameters in respect to the characteristic properties of this stone, e.g. the water uptake strongly correlates with porosity and PSD (rating number 3), whereas thermal dilatation is not interrelated to moisture properties (rating number 0). The digit sum of these rating numbers of one parameter is the degree of the material-intern correlation of the parameters, the “material index” of each parameter. This is shown by the lower left side of the matrix. In the upper right part of the matrix the parameters are correlated to each other in terms of their significance for the deterioration processes, again from 0 to 3, giving the “decay index” for each parameter.

Drachenfels trachyte		fabric														cmc		pore space properties		moisture properties								therm. dil.	strength properties			
		A	B	C	D	E	F	G	H	I	J	K	L	M	N	O	P															
A	components		3	2	2	1	1	1	1	1	2	1	2	2	2	3	2															
B	matrix	0		3	2	3	3	3	3	3	3	2	2	2	2	2	2															
C	mesostasis	0	0		3	3	3	2	3	2	3	1	2	1	1	1	1															
D	critical mineral content (calcite, clay minerals)	2	2	3		3	2	3	3	2	3	2	2	3	1	1	1															
E	porosity	1	3	3	2		3	3	2	2	2	2	2	1	2	2	2															
F	pore size distribution	1	3	2	2	3		3	3	2	3	3	2	2	2	2	2															
G	capillary water uptake	1	3	2	1	3	3		1	3	1	3	0	2	2	2	2															
H	sorptive water uptake	1	3	2	2	3	3	1		3	2	3	3	0	1	1	1															
I	saturation degree	1	3	2	1	3	2	3	3		0	3	2	0	2	2	2															
J	water vapor diffusion	2	3	2	2	3	3	1	2	0	1	3	0	1	1	1	1															
K	moisture expansion	1	2	3	3	2	3	3	3	0		1	0	1	2	1	1															
L	drying	1	2	1	2	2	3	3	3	3	2		0	1	1	1	1															
M	thermal dilatation	2	2	2	1	2	2	0	0	0	0	0		1	1	1	1															
N	compressive strength	3	3	2	1	3	3	1	1	1	1	1	0		0	0	0															
O	flexural strength	3	3	2	1	3	3	1	1	1	1	1	0	2		0	0															
P	tensile strength	3	3	2	1	3	3	1	1	1	1	1	0	2	2	2																
material intern correlation of the parameters																																
extrinsic impact correlation of the parameters (decay index)																																

**Figure 9.5** Correlation of fabric, mineral and petrophysical parameters of the Drachenfels trachyte in terms of their significance for material behavior (lower left triangle) and decay characteristics (upper right triangle)

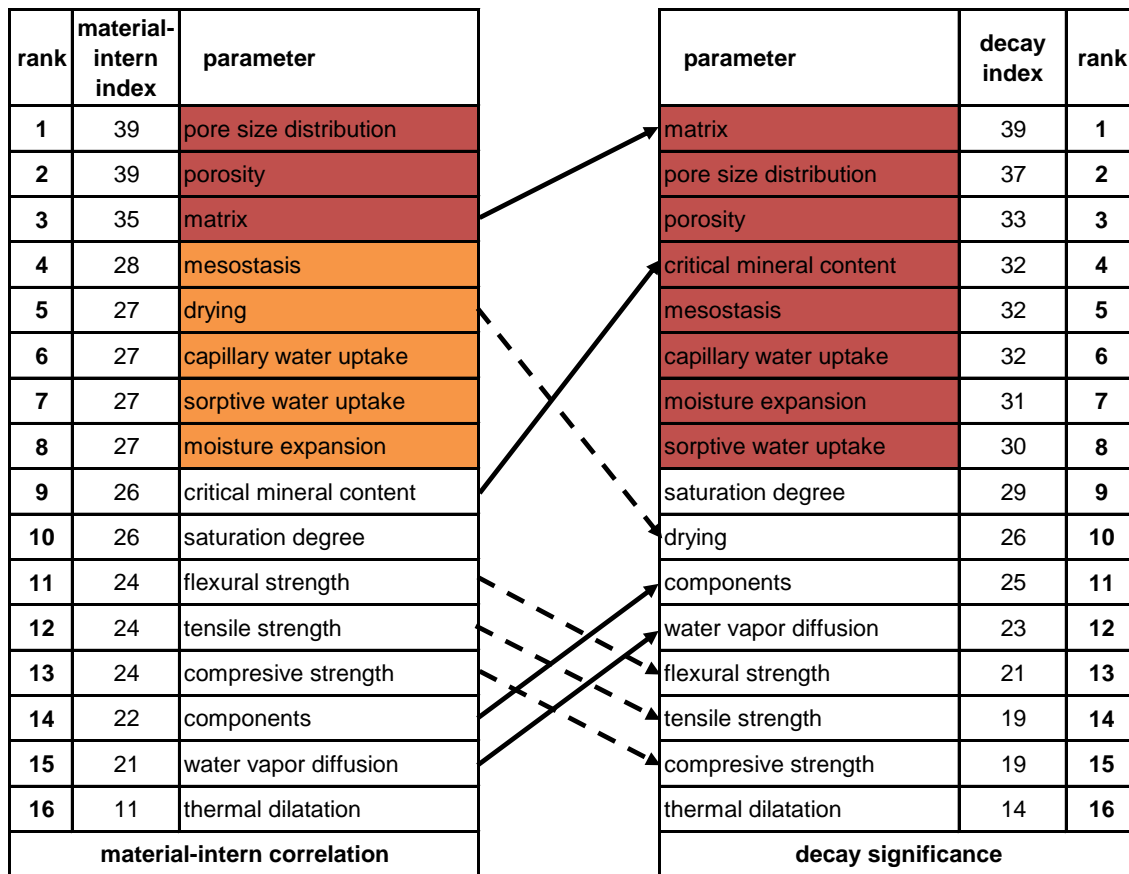


**Figure 9.6** Ranking of fabric, mineral and petrophysical parameters of the Drachenfels trachyte in terms of their significance for material behavior and deterioration, indicating eight “key parameters” for replacement criteria.

The ranking of the material parameters shows, that in the case of the Drachenfels trachyte mainly fabric parameters, characterized by the specific features of the matrix and mesostasis, and pore space properties such as PSD and porosity as well as moisture properties, e.g. drying and capillary and water uptake by adsorption, determine the behavior of the stone (Fig. 9.6). In respect to the decay of the stone mainly fabric and pore space parameters as well as moisture properties control the deterioration processes. The aspect of critical mineral content in terms of clay mineral concentration becomes more pronounced. Strength and thermal properties are of minor impact (Fig. 9.6).

### 9.3.2 Correlation and matching

The rankings are correlated and show the “key parameters” for the selection of an appropriate replacement material. The ranking of the parameters in terms of material behavior and deterioration impact (Fig. 9.6) and their correlation, indicate the relevance for replacement criteria of potential building stones. The material behavior of the Drachenfels trachyte is determined by fabric and pore space parameters as well as moisture properties especially pore size distribution, porosity and matrix. In terms of deterioration besides the mentioned parameters also critical mineral content, i.e. clay mineral content, mesostasis, and capillary as well as water uptake by adsorption and moisture dilatation become more

pronounced. These eight parameters characterize the Drachenfels trachyte and are significant for the behavior of the stone in terms of extrinsic impact and decay. These are the *key parameters* a replacement stone for the Drachenfels trachyte should match and they should be within the mentioned limit values (see chapter 9.2).

The last step of *recognition & measurement* is to match the key parameters with those of the planned or historic replacement stone. In terms of restoration and conservation any import of potentially harmful substances by a new material, e.g. critical mineral components in a replacement stone has to be avoided. Furthermore, the optical properties of the replacement stone should be similar to the original material considering aging and patination. In respect to petrophysical criteria, the replacement stone for the Drachenfels trachyte should have a comparable PSD and porosity. A stone with a homogeneous matrix, well cemented without possible inherited “weak spots” and without critical mineral content would be preferable. Moisture dilatation should not be pronounced and water uptake – capillary as well as by vapor adsorption – should be low. Generally the s-value should be less than 0.75. Although strength and thermal properties play a minor role in deterioration processes in the Drachenfels trachyte, the replacement stone should be in a range of 80-120% of the strength values (Snethlage 2005) and thermal dilatation should be less than the original stone.

For the matching those stones are of interest, which are placed in a masonry bond together with other stones, i.e. adjacent to other natural building stones. Within the present example of the Drachenfels trachyte at Cologne cathedral, these would be the Obernkirchen sandstone and the Krensheim Muschelkalk as well as Londorf basalt lava and Schlaitdorf sandstone. In many areas at the towers and the choir of Cologne cathedral the Drachenfels trachyte is employed in masonry bonds together with the Obernkirchen sandstone and the Krensheim Muschelkalk (Fig. 4.1 and 4.2).

In geological terms these three stones belong to different classes. The Obernkirchen sandstone with a concentration of 98 % monocrystalline quartz is a very deterioration resistant quartz arenite (Graue et al. 2011), thus implying no harmful components for adjacent stones. Comparing their patination, both stones tend to show a grey surface of similar brightness. Porosity of the Obernkirchen sandstone (18.6 %) is higher than that of Drachenfels trachyte (11.9 %). The Obernkirchen sandstone shows fewer micropores (Fig. 5.3) and thus is not as sensitive to water absorption, higher water vapor diffusion resistance and moisture dilatation (Tab. 5.1 and Tab. 5.2; Fig. 9.2 and 9.3). Capillary water uptake is slightly raised in the Obernkirchen sandstone (1.26 kg/m<sup>2</sup>√h) but the saturation coefficient (0.64) is significantly lower than in the Drachenfels trachyte (Fig. 9.1). Drying is less retarded in the Obernkirchen sandstone than in the Drachenfels trachyte (Kraus 1985a; Fig. 6.1). Uniaxial compressive strength of the Obernkirchen sandstone is within the mentioned constraints (Snethlage 2005) of 80-120 %, flexural strength (122 %) and tensile strength (132

%) are slightly higher (Fig. 9.4). Thermal dilatation is pronounced in the Obernkirchen sandstone, but without any residual strain (Tab. 5.2). In respect to the *key parameters* of the Drachenfels trachyte for a replacement stone, the Obernkirchen sandstone shows a relatively good matching (Fig. 9.7).

The Krensheim Muschelkalk itself is a relatively weathering resistant natural building stone. In rain protected areas it tends to form massive gypsum crusts (Graue et al. 2013a) (Fig. 4.5f). In these areas the stone surface is black next to very white microkarst weathered surface areas. Thus, patination differs from that at the Drachenfels trachyte. Due to acid rain dissolution of the carbonate rock ion loaded waters may be transported from the Krensheim Muschelkalk to the silicate Drachenfels trachyte providing ions for salt formation and decreasing the pH, thus contributing to stronger decay of the Drachenfels trachyte (Graue et al. 2013a; see chapter 8.4.3). Porosity of the Krensheim Muschelkalk (16 %) is higher than that of the Drachenfels trachyte (11.9 %). The ratio of micropores is the same at the Krensheim Muschelkalk and the Drachenfels trachyte (Fig. 5.3). Krensheim Muschelkalk shows a medium capillary water uptake ( $1.3 \text{ kg/m}^2\sqrt{\text{h}}$ ), very low water absorption (Fig. 9.2) and a low saturation coefficient (0.59) (Fig. 9.1). Water vapor diffusion resistance in the Krensheim Muschelkalk is high (Fig. 9.2) but drying is less retarded than in the Drachenfels trachyte (Kraus 1985a; Fig. 6.1). Moisture and thermal dilatation of the Krensheim Muschelkalk is neglectable (Tab. 5.2 and 9.3). Uniaxial compressive strength of the Krensheim Muschelkalk is less (69 %) than the mentioned constraints (Snethlage 2005) of 80-120 %, flexural strength (145 %) and tensile strength (129 %) are higher (Fig. 9.4). The matching of the *key parameters* of the Drachenfels trachyte with the parameters of the Krensheim Muschelkalk indicates a partly compliance in terms of constraints (Fig. 09.7). The aspect of calcium ion transport from the Krensheim Muschelkalk at an building exposition for sufficient water impact and a higher moisture import from the Krensheim Muschelkalk to the Drachenfels trachyte (see chapter 8.4.3) must be seen critical.

The current replacement stone for the Drachenfels trachyte at Cologne cathedral is the Montemerlo trachyte from Italy. If the two stones are compared in respect of the mentioned constraints, it is to ascertain that the mineralogical composition and optical properties match almost perfectly. The porosity of both is similar (Tab. 5.1); the pore size distribution shows a higher ratio of micropores in the Montemerlo trachyte (37%). In the Drachenfels trachyte the ratio of micro to capillary pores is 16:84 (Graue et al. 2011). Moisture dilatation is slightly pronounced (Tab. 5.2); capillary water uptake is higher but water absorption and saturation coefficients are lower (Tab. 5.1). In terms of strength properties the Montemerlo trachyte is a slightly stronger stone, on average 112%, which is in the range of constraints. Thermal dilatation of the Montemerlo trachyte is comparable to the Drachenfels stone (Tab. 5.2), as well is drying (Fig. 6.1).

DT key parameter	OS	KM	MT
matrix	+	+	+
pore size distribution	+	+	-
porosity	-	-	+
critical mineral content	+	-	-
meso stasis	+	-	+
capillary water uptake	-	-	-
moisture expansion	+	+	-
sorptive water uptake	+	+	+
positive counts	6 of 8	4 of 8	4 of 8

**Figure 9.7** Matching of the key parameters of the Drachenfels trachyte (DT) with those of Obernkirchen sandstone (OS), Krensheim Muschelkalk (KM) and Montemerlo trachyte (MT) within the mentioned constraints.

In general, the parameters of the Drachenfels and Montemerlo trachyte are in a close comparability to the *key parameters* of the Drachenfels trachyte. The higher ratio of micropores, the higher capillary water uptake and the slightly pronounced moisture dilatation can be critical. In resemblance to the observation by Lazzarini et al. (2008), the Montemerlo trachyte shows little resistance to salt deterioration experiments. It was the first of the eight investigated stones losing 50% of its weight after 19 cycles; Drachenfels trachyte is the second after 30 cycles (Fig. 6.7). However, Koch (2006) reported of possible clay mineral content. This would explain the higher moisture dilatation and the high cation exchange capacity observed in the leaching tests (Fig. 7.11i and j). These aspects might not necessarily imply a negative influence on the deterioration behavior of the Drachenfels trachyte, but should be looked at in terms of the deterioration behavior of the Montemerlo trachyte.

#### 9.4 Multivariate statistics

The correlation of the fabric and pore space parameters, mineralogical and petrophysical properties with respect to their relevance for material characteristics and their influence on the decay processes in the stone is based on the collected data acquired by the previously described investigations and tests. The assignment of scores may be subject to discussion in one or another way. For achieving a higher degree of objectivity a multivariate statistical approach based on dimension reduction can be considered. Potential methods comprise correspondence analysis (Blasius 2001; Greenacre 1984), factor analysis (Weber 1974), multidimensional scaling (Mathar 1997) and multiple regression (Bosch 1998; Backhaus 2008). The objective is to reduce dimensions by compressing relevant information into fewer interpretable signals incorporating dependence structures among the variables and the data visualization by means of various types of diagrams (Fried 2013).

Factor analysis is based on the decomposition of a *range of correlated characteristics* by detecting structures and correlations, and the ascription of observed correlations into simpler unobserved variables, the *combination of features* or the so-called *factors*. As a statistical method it is based on correlation calculation and a number of test procedures. As a multivariate method it refers to a *range of correlated characteristics*, which is not determined by a single variable, but is captured through a group of *m* variables, which are recorded for *n* individuals in a representative sample. The values of one of the *m* variables (for *n* individuals) as well as the values of all *m* variables can be visualized as vectors. The distribution of the vectors and the correlation of the vector components are important for the interpretation, unlike single components, which are compared within the *n* individuals (which is common for univariate approaches). The quantitative character of the *m* variables is crucial for the calculations behind factor analysis. Qualitative variables have to be classified into a binary variable for further processing (Weber 1974). In statistics a representative sample of relevant data for a large number of *n* individuals is required. Some authors, such as Horst (1965), suggest that the number of individuals *n* has to be the three times the number of variables *m* ( $n \geq 3 m$ ).

Regarding the multifactorial selection system developed within this work, several aspects would have to be re-assessed for applying the previously mentioned statistical methods. At this point two of them should be mentioned:

- Some of the *variables* are not quantifiable and they cannot be coded binary. Thus, linear relations, on whom the factor analysis is based, are not applicable.
- The *range of correlated characteristics* “compatibility” does not solely refer to one kind of stone material, but is the alignment of the *range of correlated characteristics* of “sensitivity” for several stones. Thus, individuals are not similar and in terms of factor analysis they are not equitable.

These aspects lead to consider (multiple) correspondence analysis as the possible multivariate statistical method (Blasius 2001; Greenacre 1984). Within this approach the variables would be evaluated by the cross-tabulated frequencies for each stone. This could include (grouped) quantitative and qualitative variables.

The application of a multivariate statistical approach based on dimension reduction would contribute to a substantial assessment of the stones’ sensitivities and compatibilities. A common challenge in statistical applications is the data acquisition. Besides uncertainties of measured data, which can be minimized by increasing number of measured individuals, high amounts of data have to be available.



### **9.5 Development of a classification scheme for the selection of replacement stones**

The different building stones employed at Cologne cathedral show a diverse petrography and mineralogical composition as well as a broad variety of petrophysical properties. To understand possible interactive deterioration processes it is important to determine the basic petrophysical data and assess their significance to each other.

For the Drachenfels trachyte as an example the specific parameters are assessed in terms of their significance for material behavior and in view of the observed deterioration phenomena and processes. They are ranked as “material index” and as “decay index”. These rankings are correlated indicating the imperative *key parameters* the replacement stone should match. These chosen parameters should be met within the stated requirements for replacement stones.

This systematic multi-factorial analysis for the determination of specific material parameters for the selection of an appropriate replacement stone is ment to contribute to the reproductibility and the sustainability. The developed classification scheme contributes to the evaluation of the compatibility of historic and modern replacement stones and helps to assess preservation problems for historical monuments, which comprise more than one natural building stone material. The classification scheme could also be adapted to assess possibly critical parameters of the different stones in a masonry bond indicating “weak spots” of potential interferences.

Although the basic requirement catalog is enlarged by the evaluation and assessment of the parameters, the selection of an appropriate replacement material is still difficult. It is shown that not only material specific parameters are to be correlated. The comparability of the deterioration behavior of the several stones has to be comprised as well. Naturally, it is not possible to equate sensitivities of used stones, but deterioration sensibilities of potential replacement stones could be estimated and possible amplifying feedback mechanisms avoided. The fact shown by the historic examples that the selection of replacement stones is not restricted to petrographical identical stones further supports a successful choice. It shall be emphasized that the optical similarity of the stones is crucial for the preservation of a coherent overall view of the monument or building section. Top priority is to diminish further deterioration progress.

## 10 General conclusions

The preservation of cultural heritage as materialized witnesses of the history of mankind is assigned to society as a whole. Science is able to contribute to a better perception and understanding of this material and cultural patrimony through knowledge acquisition among the diverse aspects interweaving cultural heritage. The engagement of humanities and natural science once again shows the multifaceted character of this assignment. The present thesis focuses on the objective of contributing to a better understanding of stone deterioration as a function of material diversity built in an anthropogenic environment.

Stone procurement and stone preservation have together comprised a crucial question since the beginning of building. In the work present, this is distinctively shown for the cathedrals of Cologne, Xanten and Altenberg, all of which serves as examples for many other historic monuments. At the same time, the recurrent preservation measures indicate that the problem of stone deterioration is as old as the buildings themselves. The deterioration of stone is a feedback mechanism of the material itself and the environment in terms of physical, chemical and biological processes. The environment constitutes of the proximity within the building's structure and orientation, as well as the further ambience of the building's location in an industrial, urban or rural environment. For the three cathedrals investigated, three different environments are discerned. Their ambient climatic conditions do not differ significantly, but in terms of pollutant impact, strong divergences are ascertained. Cologne and Xanten show high fluxes of SO<sub>2</sub> and particulate matter, whereas Altenberg shows low values, similar to a clean air region.

Furthermore, measurements for building-physical data assessment were conducted. The measurements of temperature and relative humidity within several building stones in different building sections at Cologne cathedral determine a clear correlation with cardinal directions. In comparison with the outside climate, each individual climate within the stones has been detected. The various sensors placed at a deeper position inside the stones show generally higher values of relative humidity than those sensors positioned closer to the surface of the stones. This correlates well with numerous models for deterioration processes; e.g., scaling, where a zone of maximum moisture is defined within the stone at which salts preferably accumulate leading to a zone of disintegration and disruption. In the case of different adjacent natural building stones, the relative humidity measured in one stone correlates with the humidity values of the neighboring stone. In the proximity areas towards the adjacent stone with a higher water balance, the stone with originally lower humidity values shows increased moisture content. Thus, this may point to possible interferences on the part of different building materials and contribute to the understanding of observed deterioration phenomena.

For the eight investigated “cathedral stones”, the Drachenfels trachyte, the Stenzelberg latite, the Obernkirchen and Schlaitdorf sandstones, the Krensheim Muschelkalk, and the Londorf basalt lava as well as the Montemerlo trachyte and the Bozanov sandstone, typical deterioration phenomena were ascertained. In particular, the medieval Drachenfels trachyte shows severe deterioration in the form of scaling, flaking, crack formation and crumbling to total fabric collapse. If the Drachenfels trachyte is placed adjacent to carbonate stone, i.e., Krensheim Muschelkalk, an increased susceptibility to these decay phenomena can be noticed. The other stones investigated exhibit decay as well – most notably, crust formation is detected not only on the limestone but in the silicate stones as well. If the decay at the three locations of the cathedrals in the different industrial, urban and rural environmental situations is compared, a clear decreasing gradient of deterioration can be noticed from a higher to a decreased level of pollution impact, respectively. At all three cathedrals, the Drachenfels trachyte shows scaling and flaking, which are the typical deterioration phenomena of this stone and are due to its mineral compositional and textural features as well its petrophysical properties. The intensity of decay varies significantly from the industrial to rural environment, indicating a strong pollution impact on the decay of the stones.

To understand the deterioration behavior of the stones and possible interactive deterioration processes, it is important to determine the basic petrophysical data. The different building stones employed at Cologne cathedral show a diverse petrography and mineralogical composition, as well as a broad variety of petrophysical properties. The various ascertained parameters are correlated with the deterioration processes and the observed decay phenomena. Interactive processes are elucidated and possible decay scenarios are described. Moisture properties, which in turn are determined by petrophysical features, become the center of focus in terms of any evaluation of stone compatibility. A huge water exchange in the microstructure of the stone is generally correlated to a huge rise of pollutants, which not only supports the decay potential for salt and frost deterioration, but also provides the necessary elements for chemical deterioration.

The experimental assessment of the drying property, freeze-thaw resistivity and salt-weathering resistance of the “cathedral stones” all contribute to an understanding of the different physical deterioration processes of the stones. As expected, the drying properties of the eight investigated stones differ significantly, as does the salt-weathering resistivity. Here, the two trachyte stones – Montemerlo and Drachenfels – show the lowest resistance.

Chemical tests and experiments allow an empirical approach to be taken towards the chemical deterioration processes within the natural building stones investigated. Their general resistivity against acidic impact, e.g., from an industrial pollution environment, is detected. Furthermore, the solution in different leachants illustrates the different chemical weathering reactions taking place as regards the environment-related deterioration of the

stones. It is shown that the leachability of the various elements from the different stones differs significantly and is not just dependent upon the mineral composition of the individual stones or the weather resistivity of the rock-forming minerals. Leachability also depends upon the solute's composition and concentration, the reaction time and temperature, as well as mineral grain sizes and textural features. The experiments elucidate the many-faceted situation of environmental deterioration, whereby several concurrently weathering reactions and products enhance or hinder each other.

After the assessment of the different environmental situations at the three cathedrals and the ascertainment of the specific deterioration phenomena of the individual stones, and following from the empirical investigations of their material characteristics and behavior in terms of the impact of extrinsic factors – e.g., temperature, moisture, mechanical load, salts, the impact of chemicals – the next consequential step was the investigation and comparison of the pollution-related deterioration of the various stones *in situ* in the context of the buildings themselves at the three different locations.

Black weathering crusts are ascertained as an indicator for pollution-related stone deterioration. The investigation of this deterioration phenomenon discriminates between types of weathering crusts: laminar crusts tracing the surface and thick framboidal crusts, often associated with the disintegration of the stone material underneath. As element composition analyses show, these crusts mainly consist of gypsum. This is to be attributed to the high SO<sub>2</sub> immission of the anthropogenic pollution's impact, whereas the declining SO<sub>2</sub> concentrations in the air indicate that the impact of past pollution, which is still detectable within the stones, has to be considered as well. The formation of these gypsum crusts is not restricted to carbonate stone but can be observed on silicate stone as well, indicating the major extrinsic environmental impact in the form of atmospheric gases as well as particulate matter. Furthermore, the detection of increasing concentrations of heavy metals within the crusts indicates a strong correlation to anthropogenic combustion pollution from fossil fuels. It is shown that the form of the manifestation of the crusts differs significantly within the three locations. Crystal growth sizes are clearly distinguished, from larger crystals in samples from the Cologne cathedral to almost more or less minor salt efflorescence in the samples from the Altenberg cathedral. Especially in the industrial environment at Cologne, crust formation and the related structural deterioration is massive while, in the rural environment at Altenberg, crust formation is not very significant – thus correlated stone deterioration is less. Furthermore, it is shown that the formation of gypsum crusts can be enhanced by interferences between different building materials, e.g., mortars and adjacent stones (i.e., carbonate stone). The surface character and exposition of the relevant building stones pose a crucial question for the formation of the weathering crusts – the promotion or hindrance of the deposition of settling dust, as well the formation processes, are coupled with the

corresponding moisture supply. In addition, the *onsite* measurements of moisture and temperature distribution illustrate the possible feedback mechanisms of adjacent stones in terms of their water balance, leading to higher water importation into stones, which originally yield lower water content.

The sum of the investigations and observations made within the present work leads to a model for the deterioration of the Drachenfels trachyte. Through the environmental impact, a certain mineral corrosion of feldspar grains – especially from the cryptocrystalline matrix – takes place, leading to mineral grain comminution and the opening of new path-ways. As a result of the extrinsic import of calcite and sulfur components, gypsum crystal growth and the formation of weathering crusts are detected. The crusts in turn enhance moisture-related deterioration processes by hindering the drying of the stone. This higher moisture content has many-faceted consequences. The effect on the mesostasis of altered volcanic glass fractions becomes significantly intensified; through the high capillarity of these interstitial fillings, water import and moisture dilatation increase significantly in these areas delimited by surrounding feldspar crystals. The dilatation processes of the swell-able clay mineral montmorillonite – which is found within these areas as well as in the entire pore space of the Drachenfels trachyte – cause severe structural impairment, leading to an enlargement of secondary porosity. Due to this increased pore space in the stone and the higher moisture content within, the solubility of gypsum and the migration into sensitive zones are increased, leading to higher salt accumulation and intensified salt deterioration. In addition, moisture dilatation processes and the swelling of clay minerals become irreversible due to the ionic import through gypsum. The interaction of these feedback deterioration mechanisms leads to continuously advancing corrosion and the delocalization of mineral grains. Thus, the increasing disintegration of the stone material and crumbling further advances, finally resulting in total fabric collapse.

Regarding stone decay as a function of the material mix in an environmental-climatic and building-physical context, it is seen that the petrophysical and mechanical properties of the stones are highly relevant. Besides water uptake, strength properties and thermal behavior, the freeze-thaw-cycle stability and the salt deterioration resistivity are important as well. Through the mechanical degradation of the stone's framework and the mineral compound structure, the reaction surface for chemical weathering reactions is enlarged. The chemical weather resistivity of the natural building stones is determined by the mineral composition and mineral weather resistivity, as well as the textural features of the stones, depending upon the environmental pollution's impact and the building's physics (e.g., the exposure of the building section). The investigations described within the thesis indicate possible decay scenarios and the incompatibilities of different stones to each other. For the conservation and

preservation of natural building stone, it is important to understand these deterioration processes and to control and counteract them.

The preservation of historic monuments is informed by the choice of adequate construction materials. This holds for the origination of the building and for later renovation works as well – thus, it holds for the right choice of compatible replacement material. Within the literature, guidelines are given for the selection of adequate replacement stones, concerning their mineralogical composition, optical features and petrophysical properties. These general criteria are to be referred to with the original stone, which needs to be replaced. In many historic buildings, a number of different stones are used. Thus, a replacement stone must not only to be comparable to the original stone – which is replaced – but must also be compatible with all the other stones used within the masonry bond. At Cologne cathedral, the different building stones display a diverse petrography and mineralogical composition, as well as a broad variety of petrophysical properties. The comparison with valid guidelines reveals that the constraints given by the general criteria for replacement materials make it almost impossible to find an ideal stone. To support the selection of an adequate replacement material, the parameters are recognized and measured in a four-step process of assessment, ranking, correlation and matching in terms of a multi-factorial assessment analysis. This comprises the assessment of the ascertained petrophysical parameter according to a two-fold aspect: first, in terms of their relevance to each other for material characterization and, secondly, in respect of their significance to each other for the deterioration behavior of the natural building stone. The single valuations – *material index* and *decay index* – rank the parameters. The rankings are correlated and the *key parameters* are indicated by the highest scores. These *key parameters* are the relevant criteria for the selection of an appropriate replacement stone and should be met by the before mentioned requirements for replacement stones. Finally, the *key parameters* of the “original” stone and the potential replacement stone are matched along with the other stones in the masonry bond. This selection scheme can be used as an assessment tool for the selection of appropriate replacement material for buildings comprising more than one natural building stone. Moreover, it can be used for the evaluation of the possible deterioration interferences of different building stones placed in one building section and their decay phenomena. Thus, it contributes to the understanding of stone decay in a built environment and serves as a preservation measures for cultural heritage monuments

Cologne cathedral is an outstanding monument and a most challenging field of research. The insights gained by the present work seek to contribute to the assessment of stone preservation at Cologne cathedral and to also support the handling of essential preservation needs for any cultural heritage monument, especially those comprised of different building materials.





## 11 Outlook

The studies and methodological approaches presented in this work offer starting points for future research of the following aspects:

- The water balance of natural building stones within a building's context determines to a great extent, the deterioration of the stone. The methodic development, a technical approach and the evaluation of acquired data for long-term and outside measurements of material moisture and temperature distribution within natural building stones *in situ* offers a comprehensive field of work.
- The development of standard laboratory tests for the chemical weathering of natural building stones represents a broad subject for scientific research. The aspect relating to NO<sub>x</sub> immission needs further to be elucidated.
- Computer simulated numeric modeling of the acquired data would constitute a further important point of work, contributing to the evaluation and assessment of deterioration behavior and the interdependencies of different building materials.
- An underlying statistical view and thus concretization of the systematic approach for the selection of replacement stones opens an interdisciplinary field of work. The data reduction would support its use as an evaluation and prognosis tool for cultural heritage tasks.



## References

- Adamo P, Violante P (2000) Weathering of rocks and neogenesis of minerals associated with lichen activity. *Appl Clay Sci*, 16:229–256
- Aligizaki KK (2006) *Pore Structure of Cement-Based Materials: Testing Interpretation and Requirements*. Technology & Engineering. Taylor & Francis, London. 388p
- Altmann K (1970) Neues Feuchtigkeitsmessverfahren für Bauteile. *Die Bautechnik* 8:268–272
- Altschuler ZS, Dwornik EJ, Kramer H (1963) Transformation of montmorillonite to kaolinite during weathering. *Science* 141:148–162
- Amoroso GG, Fassina V (1983) *Stone decay and conservation*. Elsevier, Amsterdam, pp 1–453
- Antill SJ, Viles HA (1999) Deciphering the impacts of traffic on stone decay in Oxford: some preliminary observations from old limestone walls. In: Jones MS, Wakefield RD (eds.) *Aspects of stone weathering, decay and conservation*. Imperial College Press, London, pp 28–42
- Arendt C (1993) Praktischer Vergleich von Untersuchungsgeräten und –verfahren zur Feuchtemessung im Mauerwerk, Teil 1 und 2. *Bautenschutz +Bausanierung* 5:27–31 and 6: 10–14
- Armstrong JT (1991) Quantitative elemental analysis of individual microparticles with electron beam instruments. In: Heinrich KFJ, Newbury DE (eds.) *Electron Probe Quantitation*, Plenum Press, New York, London, pp 261–315
- Armstrong JT (1995) CITZAF: a package of correction programs for the quantitative electron microbeam X-ray analysis of thick polished materials, thin films, and particles. *Microbeam Anal.*, 4:177–200
- Arnold A (1981) Salzminerale in Mauerwerken. *Schweiz. Mineral. Petrogr. Mitt.*, 41:147–166
- Ausset P, Bannery F, Lefèvre RA (1992) Black-crust and air microparticles contents at Saint-Trophime, Arles. In: Delgado Rodrigues J, Henriques F, Telmo Jeremias F (eds.) *7<sup>th</sup> Int. Congress on Deterioration and Conservation of Stone*. Lab. Nat. Engenharia Civil, Lisbon, pp 325–334
- Backhaus K (2008) *Multivariate Analysemethoden eine anwendungsorientierte Einführung*. Berlin, Springer.
- Bader W (1949) *Der Dom zu Xanten*. Kevelaer
- Bader W (1964) Vom ersten Baumeister der gotischen Stiftskirche (1263 bis 1280). *Sechzehnhundert Jahre Xantener Dom*. Xantener Domblätter 6:103–140
- Banfield JF, Barker WW (1994) Direct observation of reactant–product interfaces formed in natural weathering of exsolved, defective amphibole to smectite: evidence for episodic, isovolumetric reactions involving structural inheritance. *Geochim. Cosmochim. Acta* 58:1419–1429
- Barcellona-Vero L, Montesila M (1978) Mise en évidence de l'activité des thiobacilles dans les altérations des pierres à Rome. In: *Symposium Deterioration and Protection of Stone Monuments*, Paris, Publ. Nr. 4.1
- Bergmann J, Friedel P, Kleeberg R (1998) BGMN: a new fundamental parameters based Rietveld program for laboratory X-ray sources, its use in quantitative analysis and structure investigations. *CPD Newsletter* 20 (Summer), pp 5–8
- Berliner MA (1980) *Feuchtemessung*. VEB Verlag Technik, Berlin
- Berres F (1996) *Gesteine des Siebengebirges*. Rheinlandia, Siegburg, 141p
- Beuckers K.G.: *Der Kölner Dom*. Darmstadt, 2005
- Bland, W., Rolfs, D., (1998) *Weathering, An Introduction to the Scientific Principles*. Arnold, London
- Blasius J (2001) *Korrespondenzanalyse*. München, Oldenbourg.
- Bläuer Böhm C (2005) Quantitative Salt Analysis in Conservation of Buildings. In: *Restoration of Buildings and Monuments*. Bauinstandsetzen und Baudenkmalfpflege, 11(6):409–418
- Blum AE, Stillings LL (1995) Feldspar dissolution kinetics. In: *Chemical weathering rates of silicate minerals*. In: *Reviews in Mineralogy*, 31. White AF, Brantley SL (eds.) *Min Soc Am*, Washington DC, pp. 176–195
- Bonazza A, Sabbioni C, Ghedini N (2005) Quantitative data on carbon fractions in interpretation of black crusts and soiling on European built heritage. *Atmos Environ* 39:2607–2618
- Bonazza A, Sabbioni C, Ghedini N, Favoni O, Zappia G (2004) Carbon data in black crusts on European monuments. In: Saiz-Jimenez C (ed.) *Air pollution and cultural heritage*. Taylor and Francis, London, pp 39–46
- Bonazza A, Sabbioni C, Ghedini N, Hermosin B, Jurado V, Gonzalez JM, Saiz-Jimenez C (2007) Did smoke from Kuwait oil well fires affect Iranian archeological heritage? *Environ Sci Technol* 41:2378–2386
- Bosch K (1998) *Statistik-Taschenbuch*. 3<sup>rd</sup> ed. München, Oldenbourg.
- Brakel J van, Modry S, Svata M (1981) Mercury porosimetry: state of the art. *Powder Technol* 29:1–12
- Brantley SL (2003) Reaction Kinetics of Primary Rock-forming Minerals under Ambient Conditions. In: *Treatise on Geochemistry*, Volume 5. Drever JL et al. (eds) Elsevier, p.73–117
- Brimblecombe P (2003) *The Effects of Air Pollution on the Built Environment*. *Air Pollution Reviews – vol. 2*. Imperial College Press, London, 428p
- Brocco D, Giovagnoli A, Laurenzi-Tabasso M, Marabelli M, Tappa R, Polesi R (1988) Air pollution in Rome and its role in the deterioration of porous building materials. *Durab. Build. Mater.*, 5:393–408
- Brownstein S, Stillman AE (1959) Proton Resonance Shifts of Acids in Liquid Sulfur Dioxide. *J. Phys. Chem.* 1959, 63:2061–2062
- Burch TE, Nagy KL, Lasage LA (1993) Free energy dependence of albite dissolution kinetics at 80 °C, and pH 8.8. *Chem Geol*, 105: 137–162
- Camuffo D (1992) Acid rain and deterioration of monuments: how old is the phenomenon? *Atmos Environ* 26B:241–247
- Camuffo D (1995) Physical weathering of stone. *Sci. Total Environ.*, 167:1–14
- Casey WH, Ludwig C (1995) Silicate mineral dissolution as a ligand exchange reaction. In: *Chemical weathering rates of silicate minerals*. In: *Reviews in Mineralogy*, 31. White AF, Brantley SL (eds.) *Min Soc Am*, Washington DC, pp. 241 – 294
- Charola AE (2000) Salts in the deterioration of porous materials: an overview. *J Am Inst Conserv* 39:327–343

- Charola AE, Pühringer J, Steiger M (2007) Gypsum: a review of its role in the deterioration of building materials. *Environ Geol*, 52:339–352
- Charola AE, Ware R (2002) Acid deposition and the deterioration of stone: a brief review of a broad topic. In: Siegesmund S, Vollbrecht A (eds.) *Natural Stone, Weathering Phenomena, Conservation Strategies and Case Studies*, Geological Society, London, Special Publication 205, pp 393–406
- Charola AE, Weber J (1992) The hydration/dehydration mechanisms of sodium sulphate. In: Delgado Rodrigues J (ed) *Seventh international congress on the deterioration and conservation of stone*. Lisbon, pp 581–590
- Chatterji S, Christensen P, Overgaard G (1979) Mechanisms of breakdown of natural stones caused by sodium salts. In: Badan B (ed) *Third international congress on the deterioration and conservation of stone*. Padova, pp 131–134
- Chou L, Wollast R (1984) Study of the weathering of albite at room temperature and pressure with a fluidized bed reactor. *Geochem. Cosmochem. Acta*, 48: 2205–2217
- Clayton JL (1986) An estimate of plagioclase weathering rate in the Idaho batholith based upon geochemical transport rates. In *Rates of Chemical Weathering of Rocks and Minerals* (eds. S. Colman and D. Dethier). Academic Press, Orlando, pp. 453–466
- Cloos H, Cloos E (1927) Die Quellkuppe des Drachenfels am Rhein. Ihre Tektonik und Bildungsweise. *Z. f. Vulkanologie* XI:33 – 40
- Colman SM, Dethier DP (1986) *Rates of Chemical Weathering of Rocks and Minerals*. Academic Press, Orlando, 603p.
- Colombra F (sa): Steine und Marmor aus dem Veneto. (in Vorbereitung)
- Correns CW (1962) Über die chemische Verwitterung von Feldspäten. *Norsk Geol. Tidsskrift*, 42: 272–282
- Correns CW, Steinborn W (1939) Über die Erklärung der sogenannten Kristallisationskraft. *Z Kristallogr* 101:117–133
- Correns CW, von Engelhardt W (1938) Neue Untersuchungen über die Verwitterung des Kalifeldspates. *Chemie der Erde*, 12:1–22
- Darwin CR (1839) *Journal of researches into the natural history and geology of the countries visited during the voyage of HMS Beagle round the world*. D. Appleton, New York
- De La Calle C, Suquet H (1988) Vermiculite. In: Bailey SW (ed) *Hydrous phyllosilicates. Reviews in Mineralogy*. Mineralogical Society of America, vol 19, pp 455–496
- Del Monte M, Ausset P, Forti P, Lefèvre RA, Tolomelli M (2001) Air pollution records on selenite in the urban environment. *Atmos Environ* 35:3885–3896
- Del Monte M, Rossi P (1997) Fog and gypsum crystals on building materials. *Atmos. Environ* 31:1637–1646
- Del Monte M, Sabbioni C, Vittori O (1981) Airborne carbon particles and marble deterioration. *Atmos. Environ* 15:645–652
- Del Monte M, Vittori O (1985) Air pollution and stone decay: the case of Venice. *Endeavour* 9:117–122
- Delgado Rodrigues J, Charola AE (1996) General report on water repellents. *Sci Technol Cult Heritage* 5:93–103
- Delgado Rodrigues J, Charola AE (1996) General report on water repellents. *Sci technol Cult Heritage* 5:93–103
- Derbez M, Lefèvre RA (1996) Le contenu microparticulaire des croûtes gypseuses de la Cathédrale Saint-Gatien de Tours: comparaison avec l'air et la pluie. In: Riederer J (ed.) *Proceedings of the 8<sup>th</sup> Int. Congress on Deterioration and Conservation of Stone*, Möller, Berlin, pp 359–370
- Derjaguin BV, Obukov EV (1936) Anomalien dünner Flüssigkeitsschichten. III *Acta Physicochim*. URSS 5(1):1–22
- Dienemann W, Burre O (1929) *Die nutzbaren Gesteine Deutschlands und ihre Lagerstätten mit Ausnahme der Kohlen, Erze und Salze*. Enke, Stuttgart. 485p
- DIN 22024 (1989) *Bestimmung der Spaltzugfestigkeit von Festgesteinen*. Beuth, Berlin
- DIN 52102 (1988) *Bestimmung von Dichte, Trockenrohddichte, Dichtigkeitsgrad und Gesamtporosität*. Beuth, Berlin
- DIN 52103 (1988) *Bestimmung von Wasseraufnahme und Sättigungswert*. Beuth, Berlin
- DIN 52104 (1982) Teil 1 und 2. *Prüfung von Naturstein; Frost-Tau-Wechsel-Versuch*. Beuth, Berlin
- DIN 66138 (2008) *Isothermal measurement of the sorption of vapours at solids*. Beuth, Berlin
- DIN EN 12370 (1999) *Prüfverfahren für Naturstein - Bestimmung des Widerstandes gegen Kristallisation von Salzen*. Beuth, Berlin
- DIN EN 12372 (1999) *Bestimmung der Biegezugfestigkeit unter Mittellinienlast*. Beuth, Berlin
- DIN EN 1925 (1995) *Bestimmung des Wasseraufnahmekoeffizienten infolge Kapillarwirkung*. Beuth, Berlin
- DIN EN 1926 (1999) *Prüfverfahren für Naturstein: Bestimmung der Druckfestigkeit*. Beuth, Berlin
- DIN EN ISO 12572 (2001) *Wärme- und feuchtetechnisches Verhalten von Baustoffen und Bauprodukten - Bestimmung der Wasserdampfdurchlässigkeit*. Beuth, Berlin
- Dixon JB, Weed SB (1989) *Minerals in soil environments*, 2nd edn. Soil Science Society of America, pp 1244
- Do J (2000) *Untersuchung der Verwitterung von Fassaden aus Naturstein – Vergleich an den Gebäuden der Museumsinsel in Berlin*. University of Berlin, Diss.
- Doehne E (1994) In situ dynamics of sodium sulfate hydration and dehydration in stone pores: observations at high magnification using the environmental scanning electron microscope. In: Fassina V, Ott H, Zezza F (eds) *The conservation of monuments in the Mediterranean Basin*. Venice, pp 143–150
- Doehne E (2002) Salt weathering: a selective review. In: Siegesmund S, Weiss T, Vollbrecht A (eds) *Natural stones, weathering phenomena, conservation strategies and case studies*. *Geol Soc Spec Publ* 205:43–56
- Dohrmann R (2013) *Tonmineralogie und REM-Untersuchungen am Trachyt vom Drachenfels, Deutschland*. BGR, Hannover. Unpublished report.
- Dohrmann R, Kaufhold S (2009) Three new, quick CEC methods for determining the amounts of exchangeable calcium cations in calcareous clays. *Clays and Clay Minerals* 57(3):251–265
- Dombauhütte Köln (2006) *Modellhafte Entwicklung von Konservierungskonzepten für den stark umweltgeschädigten Trachyt an den Domen zu Köln und Xanten*. Unpubl. Report, DBU

- Dornieden T, Gorbushina A (2000) New methods to study the detrimental effects of poikilotroph microcolonial micromycetes (PPM) on building materials. In: Fassina V (ed.) *Proceedings of the 9<sup>th</sup> Intern. Conf. on Deterioration and Conservation of Stone*, Elsevier, Amsterdam, Vol. 1. pp 461-468
- Dunham RL (1962) Classification of carbonate rocks according to depositional texture. In: Ham WE (ed) *Classification of carbonate rocks*. AAPG Mem., 1, Tulsa. pp 108-121
- Duttlinger W, Knöfel D (1993) Salzkristallisation und Salzschadensmechanismen. *Jahresbericht Steinerfall—Steinkonservierung 1991*, Ernst & Sohn Verlag, pp 197–213
- E.C.C.O. (2002) Professional guidelines. European Confederation of Conservator-Restorers' Organization, Brussels
- Efes Y (1980) Wasserdampfdurchlässigkeit von unverwitterten und verwitterten Naturbausteinen. *Bautenschutz & Bausanierung*, 3/3:91-95
- Efes Y, Lühr HP (1975) Ermittlung des Korrosionsablaufes an den am Kölner Dom verwendeten Natursteinen. Unpub. Report. University Aachen, 112p.
- Efes Y, Lühr HP (1976) Natursteine am Bauwerk des Kölner Doms und ihre Verwitterung. In: *Kölner Domblatt* 41:167–194
- Ehling A (2007) Eigenschaften, Abbau und Verwendung schlesischer Bausandsteine – ein aktueller Vergleich mit der Historie. *Z. dt. Ges. Geowiss.* 158/3:351–360
- Ehling A, Siedel H (2011) Bausandsteine in Deutschland. Band 2: Sachsen-Anhalt, Sachsen, Schlesien (Polen). BGR, Hannover, 324p.
- Esbert RM, Diaz-Pache F, Alonso FJ, Ordaz J, Wood GC (1996) In: Riederer (ed.) *Proceedings of the 8<sup>th</sup> Int. Congress on Deterioration and Conservation of Stone*, Möller, Berlin, 1:393–399
- Everett DM (1961) The thermodynamics of frost damage to porous solids. *Trans Faraday Soc* 57:2205–2211
- Fassina V (1988) Environmental Pollution in Relation to Stone Decay. *Durab. Build. Mat.*, 5:317–358
- Fassina V, Favaro M, Naccari A (2002) Principal decay patterns on Venetian Monuments. In: Siegesmund S, Weiss T, Vollbrecht A (eds.) *Natural stones, weathering phenomena, conservation strategies and case studies*. Geological Society, London Special Publication 205, pp 381–391
- Fischer H (1993) Schadensanalysen und bauphysikalisches Messen. Expert-Vlg, Renningen-Malsheim
- Fitzner B, Heinrichs K, Kownatzki R (1995) Weathering forms – classification and mapping. In: Snethlage R (ed) *Denkmalpflege und Naturwissenschaft, Natursteinkonservierung I*. Ernst & Sohn, Berlin. Pp 41-88
- Folk RL (1962) Spectral subdivision of limestone types. In: Ham WE (ed) *Classification of carbonate rocks*. AAPG Mem., 1, Tulsa. pp 62-84
- Franzen C (2002) Historische Bauwerksteine in Südtirol – Verteilung und Verwitterungsverhalten. Dissertation, University of Innsbruck. 111p
- Franzen C, Mirwald PW (2004) Moisture content of natural stone: static and dynamic equilibrium with atmospheric humidity. *Environ Geol* 46:391-401
- Franzini M, Gratzu C, Spampinato M. Degradazione del marmot per effecto di variazioni di temperatura. *Rendiconti Società Italiana di Mineralogia e Petrologia* 1984;39(1):47–58.
- Frediani P, Malesani PG, Vanucci S (1976) Weathering of Florentine stones: sulfatation and its determination. In: 2<sup>nd</sup> Intern. Symposium on Deterioration of Building Stones, pp 117–118
- Fried R (2013) Statistische Strukturerkennung in Zeitreihen. Mathematisches Kolloquium. KIT, Karlsruhe.
- Fuchs G (2006) Allgemeine Mikrobiologie. Georg Thieme, Stuttgart, pp 321-340
- Furlan V, Girardet E (1983) Considerations on the rate of accumulation and distribution of sulphurous pollutants in exposed stones. In: Wittmann EH (ed.) *Materials Science and Restoration. Lack und Chemie*, Filderstadt, pp 285-290
- Garrecht H (2005) Hygrothermische Wechselwirkung von Naturstein und Mörtelfuge. *Z. dt. Ges. Geowiss.*, 156/1: 221 – 229
- Garrels RM, Mackenzie FT (1967) Origin of the chemical composition of some springs and lakes. In: *Equilibrium Concepts in Natural Water Systems*, Adv. Chem. Series 67 (ed. W. Stumm). American Chemical Society, Washington, DC, pp. 222–242
- Goldich SS (1938) A study of rock weathering. *J. Geol.* 46, 17–58.
- Graniteland (2013) Bozanov Sandstein (<http://www.graniteland.de/naturstein/bozanov>). C & H Steimel GbR, Rotenburg
- Graue B, Siegesmund S, Middendorf B (2011) Quality assessment of replacement stones for the Cologne Cathedral: mineralogical and petrophysical requirements. *Environ. Earth Sci.*, 63:1799–1822
- Graue B, Siegesmund S, Middendorf B, Oyhantcaval P (2012a) Requirements for replacement stones at the Cologne cathedral – a systematic approach to general criteria of compatibility. 12th Int. Congr. Deterioration and Conservation of Stone. Columbia University, New York City
- Graue B, Siegesmund S, Oyhantcaval P, Naumann R, Licha T, Simon K (2013a) The effect of air pollution on stone decay: the decay of the Drachenfels trachyte in industrial, urban and rural environments– a case study of the Cologne, Altenberg and Xanten cathedrals. *Environ Earth Sci*. DOI. 10.1007/s12665-012-2161-6
- Graue B, Siegesmund S, Schumacher T (2013b) Steinverwitterung und Natursteinaustausch am Kölner Dom. In: *Naturstein als Element der Kulturlandschaft*. Siegesmund S, Snethlage R (eds.) (submitted)
- Graue B, Siegesmund S, Simon K, Licha T, Oyhantcaval P, Middendorf B (2012b) Environmental impact on stone decay: crust formation at the Cologne cathedral. 12th Int. Congr. Deterioration and Conservation of Stone. Columbia University, New York City
- Greenacre MJ (1984) *Theory and Applications of Correspondence Analysis*, Academic Press, London.
- Grimm WD (1990) *Bildatlas wichtiger Denkmalgesteine der Bundesrepublik Deutschland*. Arbeitsheft des Bayerischen Landesamtes für Denkmalpflege, Bd. 50, München. 655p
- Grimm WD, Völkl J (1983) Rauigkeitsmessungen zur Kennzeichnung der Naturwerksteinverwitterung/ [Measurement of Roughness for Characterization of Building Stone Decay] *ZDGG*, 134:387–411
- Grossi CM, Brimblecombe P, Harris I (2007) Predicting long term freeze-thaw risks on Europe built heritage and archaeological sites in a changing climate. *Sci Total Environ* 377:273–281
- Grün R (1931) Die Verwitterung von Steinen. In: *Die Denkmalpflege*, 33:168–183

- Grün R (1933) Verwitterung der Bausteine vom chemischen Standpunkt. In: *Chemikerztg.* 57:401-403
- Gründer J (1980) Über Volumenänderungsvorgänge in überkonsolidierten, diagenetisch verfestigten Tonen und ihre Bedeutung für die Baupraxis. *Geotechnik* 2:60–66 (Essen)
- Heim D (1990) Tone und Tonminerale: Grundlagen der Sedimentologie und Mineralogie. Enke Verlag, Stuttgart, p 157
- Henley, K (1967) In: *Proceedings Clean Air Conference*, Blackpool, pp 55–60
- Herscovici B (1910) Die Einwirkung der Rauchgase auf die gesteinsbildenden Mineralien. *Bautechnische Gesteinsuntersuchung*, Jg. 1, 2:37–46
- Hertel B (1927) Die Wiederherstellungsarbeiten am Kölner Dome. In: *Der Kölner Dom in Gefahr*. pp 39-91
- Heydasch-Lehmann S; Stürmer A; Faika K (2008) Altenberg – Der Bergische Dom. Lindenberg
- Heydemann A (1966) Über die chemische Verwitterung von Tonmineralen. *Geochem. Cosmochem. Acta*, 30: 995–1035
- Hilger H.P (2005) Der Dom zu Xanten. *Rheinische Kunststätten*, Heft 275. Neuss
- Hirschwald J (1908) Die Prüfung der natürlichen Bausteine auf ihre Verwitterungsbeständigkeit. Verlag Wilhelm Ernst & Sohn, Berlin
- Hirschwald J (1910) Die Bautechnisch verwertbaren Gesteins-Vorkommnisse des Preussischen Staates u. einiger Nachbargebiete. Kgl. Ministeriums d. öffentl. Arbeiten. Bornträger, Berlin
- Hirschwald J (1912) Bautechnische Gesteinsuntersuchungen: Mitgl. Mineralog.-geolog. Institut d Kgl. Techn. Hochschule Berlin. Jg.1.1910 - Jg.3. Bornträger, Berlin
- Holdren GR, Speyer PM (1986) Stoichiometry of Alkali Feldspar Dissolution at Room Temperature and Various pH Values. In: *Rates of Chemical Weathering of Rocks and Minerals* (eds. S. Colman and D. Dethier). Academic Press, Orlando, pp. 61–81
- Horst P (1965) Factor analysis of data matrices. Holt, Rinehart and Winston, New York.
- Huang WH, Keller WD (1970) Dissolution of rock-forming silicate minerals in organic acids: simulated first-stage weathering of fresh mineral surfaces. *Am. Min.* 55:2076–2094
- Hughes JJ, Bartos PM, Cuthbert SJ, Stewart RN, Valek J (1998) Microstructures in historic Scottish lime mortars. In: Jones MS, Wakefield RD (eds.) *Stone Weathering and Atmospheric Pollution Network*. Imperial College Press, London
- IBS (1990) Untersuchungsbericht N-30/90 Altenberger Dom. Institut für Baustoffuntersuchung, Saarbrücken. Unpublished report
- Jimenez Gonzalez I, Scherer G (2004) Effect of swelling inhibitors on the swelling and stress relaxation of clay bearing stones. *Environ Geol* 46:364–377
- Johansson L-G, Lindqvist O, Mangio RE (1988) Corrosion of calcareous stones in humid air containing SO<sub>2</sub> and NO<sub>2</sub>. In: Rosvall J, Aleby S (eds.) *Air Pollution and Conservation. Safeguarding our Architectural Heritage*. Elsevier, Amsterdam, pp 255–265
- Jones D, Wilson MJ (1985) Chemical activity of lichens on mineral surfaces: a review. *Int. Biodeterioration*, 5:99–104
- Jones MS, Wakefield RD, Forsyth G (2000) A study of biological decayed sandstone with respect to Ca and its distribution. In: Fassina V (ed.) *Proceedings of the 9<sup>th</sup> Intern. Conf. on Deterioration and Conservation of Stone*. Elsevier, Amsterdam, Vol. 1. pp 473–481
- Kainka E, Kramert G, Dudzeviciusij J (1997) Characterization of particulate matter PM10 and PM2.5 in North Rhine Westphalia, Saxony, and Lithuania – first results. *Ann. Occup. Hyg.*, Elsevier, Amsterdam, 41:54–59
- Kaiser E (1910) Wetterbeständigkeit einer Reihe von Kalksteinen mit besonderer Berücksichtigung der Verhältnisse am Kölner Dom. Unpubl. report, Gießen
- Kaiser E (1910a) Bericht über die Versuche der Verwitterung von vulkanischen Tuffen und eines Trachyts vom Drachenfels in der schwefelsauren Atmosphäre. Unpubl. report, Gießen
- Kaiser E (1910b) Angewandte Methode der Prüfung der Wetterbeständigkeit nebst Vorschlägen zu einem weiteren Ausbau dieser Methodik. Unpubl. report, Gießen
- Kaspar I (1978) Feuchtigkeitsmessung von Baumaterialien. *Wiss. Zeitsch. TU Dresden*, 27/2:467–470
- Kessler DW (1919) Physical and chemical tests on the commercial marbles of the US. *Technology papers of the Bureau of standards*, No. 123
- Kieslinger A (1932) Zerstörung an Steinbauten—Ihre Ursachen und ihre Abwehr. Verlag Deuticke, Leipzig-Vienna, 346p
- Klopfer H (1974) Wassertransport durch Diffusion in Feststoffen. *Bauverl.* Wiesbaden, 235p
- Klopfer H (1985) Feuchte. In: Lutz P et al. (ed) *Lehrbuch der Bauphysik*. Teubner, Stuttgart. pp329-472
- Knacke-Loy O (1988) Verwitterungsdifferenzierungen von Stubensandstein-Bauteilen des Kölner Doms. University of Tübingen
- Knacke-Loy O (1989) Der Schlaitdorf Sandstein und seine unterschiedliche Verwitterungsanfälligkeit am Kölner Dom. In: *Kölner Domblatt*, 54:61–72
- Knapp T, Dungs M (2004): Ausführungsbericht Sakristei Außenfassade. St. Viktor Dom. Dombauhütte Xanten.
- Knetsch G (1952) Geologie am Kölner Dom. *Int. J. Earth Sci.* 40/1:57 – 73
- Knöfel D (1979) Bautenschutz mineralischer Baustoffe. *Bauverl.*, Wiesbaden, 220p
- Koch A, Siegesmund S (2001) Gesteintechnische Eigenschaften ausgewählter Bausandsteine. *Z. dt. Ges. Geowiss.* 152:681–700
- Koch A, Siegesmund S (2004) The combined effect of moisture and temperature on the anomalous expansion behaviour of marble. *Environ Geol* 46: 350 – 363
- Koch R (2000) Vergleichende petrographische Untersuchung an Sandsteinen aus dem Steinbruch Pliezhausen und einem tschechischen Sandstein. Unpubl. report. University of Erlangen-Nürnberg
- Koch R (2001) Zur Geologie und Fazies eines Sandsteins aus Nordost-Tschechien (Gebiet um Bozanov-Teplice – Police). Unpubl. report. University of Erlangen-Nürnberg
- Koch R (2006) Trachyte aus dem Colli Euganei, Norditalien. In: *Dombauhütte Köln (2006) Modellhafte Entwicklung von Konservierungskonzepten für den stark umweltgeschädigten Trachyt an den Domen zu Köln und Xanten*. Unpubl. report, DBU. pp 9-42; 223–308

- Kraus (1983) Versuche zur Simulation der chemischen Verwitterung von Gesteinen. AG Naturwissenschaftliche Forschung an Kunstgütern aus Stein, BGR, Hannover, pp. 61–73
- Kraus K (1980) Verwitterungsvorgänge an Bausteinen des Kölner Doms : ein Beitrag zur Problematik der Naturstein-Verwitterung an Bau-Denkmalen im Stadtklima/ Köln. University of Cologne. 112p
- Kraus K (1985a) Experimente zur immissionsbedingten Verwitterung der Naturbausteine des Kölner Doms im Vergleich zu deren Verhalten am Bauwerk. Dissertation, University of Cologne. 208p
- Kraus K (1985b) Unterschiedliche Witterungsanfälligkeit der Kölner Dombausteine. Kölner Domblatt. 50:101-104
- Kraus K (1988) Verwitterung von Naturwerksteinen. Stand des Wissens und offene Fragen. In: Bautenschutz und Bausanierung 11, 5:143–149
- Kraus K (2002) Lösliche Alkalien in neuen Mörteln (Bestimmung, Gehalte, Bewertung, Untersuchungsbedarf und erste Ergebnisse). In: IFS-Bericht Nr. 14, Salze im historischen Natursteinmauerwerk, pp 11–18
- Kraus K, Droll K (2009) Investigations of soluble salt content in modern hydraulic lime mortars – Test method and first results. In: C. Groot (ed.) RILEM Proceedings pro 67: Repair Mortars for Historic Masonry, pp 207–213
- Kraus K, Jasmund K (1981) Verwitterungsvorgänge an Bausteinen des Kölner Domes. In: Kölner Domblatt, 46:175–190
- Krumbein WE (1988) Biotransfer in monuments - a sociobiological study. Durab. Build. Mater., 5:359–382
- Kupfer C (ed.) (1997) Materialfeuchtemessung. Expert-Verlag, Renningen-Malsheim.
- Lagaly G (1993) Reaktionen der Tonminerale. In: Jasmund K, Lagaly G (eds) Tonminerale und Tone. Steinkopff, Germany, p 490
- Laird DA (2006) Influence of layer charge on swelling of smectites. Appl Clay Sci 34:74–87
- LANUV (2010) Data from Landesamt für Natur, Umwelt und Verbraucherschutz Nordrhein-Westfalen. Stationen: Köln-Rodenkirchen, Wesel-Feldmark, Netphen-Rothaargebirge.
- Lauer W, Bendix J (2004) Klimatologie. Das geographische Seminar. 2. ed. Westermann, Braunschweig, 352p
- Lazzarini L, Antonelli F, Cancelliere S, Conventi A (2008) The deterioration of Euganean trachyte in Venice. 11th Int. Congr. Deterioration and Conservation of Stone. Nicolaus Copernicus Univ. Torun, Poland. pp 153-162
- Lefèvre RA, Ausset P (2002) Atmospheric pollution and building materials: stone and glass. In: Siegesmund S, Weiss T, Vollbrecht A (eds.) Natural stones, weathering phenomena, conservation strategies and case studies. Geological Society, London, Special Publication 205, pp.329–345
- Lehr R (2008) Die Pläner des Nordböhmisches-Sächsischen Kreideeckens und ihre Bedeutung als Naturwerkstein. Fazies, Diagenese, petrophysikalische und gesteintechnische Eigenschaften, Verwitterungsverhalten. Dissertation, University of Erlangen. 241p
- Lepsky S, Nußbaum N (2005) Gotische Konstruktionen und Baupraxis an der Zisterzienserkirche Altenberg. Bd. 1. Bergisch-Gladbach
- Leschnik W (1999) Feuchtemessung an Baustoffen – Zwischen Klassik und Moderne. DGZfP-Berichtsband BB 69. pp:1–23
- Loughnan FC (1969) Chemical weathering of the silicate minerals. Elsevier, New York, 154p.
- Luckat S (1973a) Die Einwirkung von Luftverunreinigungen auf die Bausubstanz des Kölner Domes. Teil I. In: Kölner Domblatt, 36/37:65–74
- Luckat S (1973b) Ein Schnelltestgerät zur Prüfung von Resistenzverhalten mineralischer Baustoffe gegenüber Luftverunreinigungen. Dt. Kunst- und Denkmalpflege, 31:51-53.
- Luckat S (1974) Die Einwirkung von Luftverunreinigungen auf die Bausubstanz des Kölner Domes. Teil II. . In: Kölner Domblatt, 38/39:95–106
- Luckat S (1975) Die Einwirkung von Luftverunreinigungen auf die Bausubstanz des Kölner Domes. Teil III. Kölner Domblatt 40:75-108
- Luckat S (1977) Die Einwirkung von Luftverunreinigungen auf die Bausubstanz des Kölner Domes. Teil IV. Kölner Domblatt 42:151-175
- Luckat S (1984) Beton, Stein und Eisen bricht. In: Guratzsch D (ed.) Baumlos in die Zukunft. Kindler, München, pp 225–237
- Lukas R (1990) Geologie und Naturwerksteine Baden-Württembergs. In: Grimm WD (ed.) Bildatlas wichtiger Denkmalgesteine der Bundesrepublik Deutschland. Arbeitsheft des Bayerischen Landesamtes für Denkmalpflege, München, 50:147–162
- Madsen FT, Müller-Vonmoos M (1989) The swelling behaviour of clays. Appl Clay Sci 4:143–156
- Martinez GM, Martinez EN (1991) In: Studies in conservation, 36:99–110
- Mathar R. (1997) Multidimensionale Skalierung: Mathematische Grundlagen und algorithmische Aspekte, Teubner Skripten zur Mathematischen Stochastik, Stuttgart.
- McBride M (1994) Environmental Chemistry of Soils. Oxford Press
- Meier LP, Kahr G (1999) Determination of the cation exchange capacity (CEC) of clay minerals using the complexes of copper (II) ion with triethylenetetramine and tetraethylenepentamine. Clays Clay Miner 47:386–388
- Middendorf B, Klein D (2012) Aktuelle Projektergebnisse der Arbeitsgruppe der Technischen Universität Dortmund. In: Untersuchung und Simulation der Verwitterung ausgewählter Naturwerksteine und ihrer Interdependenzen mit historischen und neuzeitlichen Baumaterialien am Dom zu Köln. Graue et al. (eds.) Unpubl. Report.
- Mirwald PW, Kraus K, Wolff A (1987) Stones of the Cathedral of Cologne and their damages. - Ms. University Dortmund
- Mirwald PW, Kraus K, Wolff A (1988) Stone deterioration on the Cathedral of Cologne. In: Durability of Building Materials 3/4, Elsevier, Amsterdam, 5:549–570
- Moore DM, Reynolds RC Jr (1997) X-ray diffraction and the identification and analysis of clay minerals. Oxford University Press, Oxford, p 332
- Morales Demarco M, Jahns E, Rüdrieh J, Oyhanthabal P, Siegesmund S (2007) The impact of partial water saturation in rock strength: an experimental study on sandstone. Z. dt. Ges. Geowiss. 158/4:869-882.
- Moroni B, Poli G (2000) Corrosion of limestone in humid air containing sulphur and nitrogen dioxide: a model study. In: Fassina V (ed.) Proceedings of the 9<sup>th</sup> Intern. Conf. on Deterioration and Conservation of Stone. Elsevier, Amsterdam, Vol. 1. pp 367–374

- Moropoulou A, Bisbikou K, Torfs K, Van Grieken R, Zezza F, Macri F (1998) Origin and growth of weathering crusts on ancient marbles in industrial atmosphere. *Atmos Environ* 32:967–982
- Mortensen H (1933) Die Salzsprengung und ihre Bedeutung für die regional-klimatische Gliederung der Wüsten. *Petermann's Mitteilungen aus Justus Perthes geographischer Anstalt* 79:130–135
- Mosch S (2008) Optimierung der Exploration, Gewinnung und Materialcharakterisierung von Naturwerksteinen. Dissertation, University of Göttingen. 277p
- Nesbitt HW, Fedo CM, Young GM (1997) Quartz and feldspar stability, steady and non steady state weathering and petrogenesis of siliciclastic sands and muds. *J Geol* 105: 137–191
- Neue J (1986) Kapazitive Feuchtemessung an Gasbeton. *Bauplanung – Bautechnik* 40/5:215–218
- Neumann HH, Steiger M, Wassmann A, Dannecker W (1993) Aufbau und Ausbildung schwarzer Gipskrusten und damit zusammenhängender Gefügeschäden von Naturwerksteinen am Beispiel des Leineschlösses (Hannover). *Jahresbericht Steinerzfall Steinkonservierung* 1991, pp. 150–167
- Nugent M A, Brantley SL, Pantano CG, Maurice PA (1998) The influence of natural mineral coatings on feldspar weathering. *Nature* 396:527–622
- Nußbaum N, Lepsky S (2010) Intermediate report on the building historical survey. Presentation, Colloquium Cologne cathedral, Nov. 2010
- Oelkers EH, Schott J (1995) Experimental study of anorthite dissolution and the relative mechanism of feldspar hydrolysis. *Geochim. Cosmochim Acta* 59:5039–5053
- Okrusch M, Matthes S (2009) Mineralogie. 8th rev. ed. Springer, Berlin Heidelberg, 658p.
- Parkhurst DL, Plummer LN (1993) Geochemical models. In *Regional Ground-Water Quality* (ed. W. M. Alley). Van Nostrand Reinhold, pp. 199–225
- Paul RC, Paul KK, Malhotra KC (1970) Solution chemistry in substituted Acids. *J. Chem. Soc. (A)*, pp. 2712–2715
- Peschel A (1983) Natursteine. VEB Dt. Vlg. Grundstoffindust., Leipzig. 448p
- Pielow HU (1997) Korrodierte Minerlgrenzflächen als Indikatoren für die Migration saline Fluide im Kristallin am Beispiel des KTB. GAGP 71, University of Göttingen, 55p.
- Pinna D, Salvadori O (2000) Endolithic lichens and conservation: an underestimated question. In: Fassina V (ed.) *Proceedings of the 9<sup>th</sup> Intern. Conf. on Deterioration and Conservation of Stone*. Elsevier, Amsterdam, Vol. 1. pp513–519
- Pleßow A, Bielert U, Heinrichs H, Steiner I (1997) Problematik der Grundwasserversauerung und das Lösungsverhalten von Spurenstoffen. In: *Geochemie und Umwelt*. Matschullat et al. (ed.) Springer, pp. 395–408
- Pohl W, Schneider J (2005) Geochemische Einflüsse endolithischer Mikroorganismen auf Gesteinsoberflächen. *Z. dt. Ges. Geowiss.*, 156/1:81–92
- Poschod K (1990) Das Wasser im Porenraum kristalliner Naturwerksteine. *Münchner Geowiss Abh.* B7
- Powers TW, Helmuth RA (1953) Theory of volume changes in hardened Portland cement paste during freezing. *Highw Res Board Proc* 32:285–297
- Press F, Siever R (2003) *Allgemeine Geologie. Einführung in das System Erde*. 3. Ed. Elsevier, München, 723p.
- Price C, Brimblecombe P (1994) Preventing salt damage in porous materials. In: Ashok R, Smith P (eds) *Prepr. Contr. Ottawa Congr. Preventive conservation-practice, theory and research IIC*, London, pp 90–93
- Přikryl R, Weishauptová Z, Novotná M, Přikrylová J, Štátná A (2010) Physical and mechanical properties of the repaired sandstone ashlars in the facing masonry of the Charles Bridge in Prague (Czech Republic) and an analytical study for the causes of its rapid decay. *Environ Earth Sci*. doi:10.1007/s12665-010-0819-5
- Putnis A, Mauthe G (2001) The effect of pore size on cementation in porous rocks. *Geofluids* 1:37–41
- Rachow-Seemann T, Leschnik W, Hauenschild C (1995) Zur Genauigkeit von klassischen Verfahren zur Bestimmung der Bauteilfeuchte. Berlin, BAM, Tagungsbericht pp:264–271
- Rathgen F, Koch J (1934) *Verwitterung und Erhaltung von Werksteinen: Beiträge zur Frage der Steinschutzmittel*. Zement & Beton, Berlin. 122p
- Rentsch W, Krompholz G (1961) Zur Bestimmung elastischer Konstanten durch Schallgeschwindigkeitsmessungen. *Fachzeitschrift der Bergakademie Freiberg* 7–8:492–504
- Renz K, Wachutka M, Werner W (2013) *Geokoffer – Bausteine des Landes*. www.geokoffer.de
- Rodríguez-Navarro C, Doehne E, Sebastián E (2000) How does sodium sulfate crystallize? Implications for the decay and testing of building materials. *Cement Concr Res* 16(3):947–954
- Rodríguez-Navarro C, Hansen E, Sebastián E, Ginell WS (1997) The role of clays in the decay of ancient Egyptian limestone sculptures. *J Am. Inst Cons* 36: 151–163
- Rodríguez-Navarro C, Sebastian E (1996) Role of particulate matter from vehicle exhaust on porous building stones (limestone) sulfation. *Sci. Total Environ.*, 187:79–91
- Rozas DF, Weaver J (1996) Ab ignition of the methylsulfonate and phenylsulfonate anions. *J. Chem. Soc., Perkin Trans. 2*: 461–465
- Rüdrich J, Kirchner D, Seidel M, Siegesmund S (2005) Beanspruchungen von Naturwerksteinen durch Salz- und Eiskristallisation im Porenraum sowie hygri-sche Dehnungsvorgänge. *Z. dt. Ges. Geowiss.* 156/1:59-73
- Rüdrich J, Bartelsen T, Dohrmann R, Siegesmund S (2011) Moisture expansion as a deterioration factor for sandstone used in buildings. *Environ. Earth Sci*, 63:1545–1564
- Rüdrich J, Kirchner D, Siegesmund S (2011) Physical weathering of building stones induced by freeze–thaw action: a laboratory long-term study. *Environ Earth Sci*. 63:1573-1586
- Rüdrich J, Siegesmund S (2006) Salt and ice crystallization in porous sandstones. *Environ Geol* 52(2):343-367
- Sabbioni C (1995) Contribution of atmospheric deposition to the formation of damage layers. *Sci. Total Environ.*, 167:49–56
- Sabbioni C (2003) Mechanism of air pollution damage to stone. In: Brimblecombe P (ed.) *The Effects of air pollution on the built environment*. *Air Pollut. Rev.*, 2:63–88
- Sabbioni C, Zappia G (1992a) Atmospheric-derived element tracers on damaged stone. *Sci. Total Environ.*, 126:35–48



- Sabbioni C, Zappia G (1992b) Decay of sandstone in urban areas correlated with atmospheric aerosol. *Water Air Soil Pollut.*, 63:305–316
- Saiz-Jimenez C (1993) Deposition of airborne organic pollutants on historic buildings. *Atmos. Environ.*, 27B:77–85
- Schäfer B (1980) Luftverschmutzung durch Schwefeldioxid. *Umweltbundesamt*. 123p.
- Scherer GW (1999) Crystallization in pores. *Cement Concr Res* 29:1347–1358
- Scheuren E (2004) Kölner Dom und Drachenfels. In: Schock-Werner und Lauer (ed) *Steine für den Dom. Kölner Dom*. pp 22–45
- Schlabach S (2000) Auflösungsexperimente von Kaolinit, Montmorillonit, Illit, Serizit und Talk in Batch- und Durchfluss-Reaktoren. University of Göttingen, Diss.
- Schlösser H (1991) Quantifizierung der Silikatverwitterung in karbonatfreien Deckschichten des Mittleren Buntsandsteins im Nordschwarzwald. *Tübinger Geowiss. Arb. C/9*. University of Tübingen, 93p.
- Schock-Werner B, Lengyel D, Toulouse C (2011) Bauphasen des Kölner Domes und seiner Vorgängerbauten. *Köln*
- Schuh H (1987) Physikalische Eigenschaften von Sandsteinen und ihren verwitterten Oberflächen. *Münchner Geowiss. Abh.*, 6: S.; Enke Verlag, Stuttgart, p 66
- Schuh J (1988) Klimawechsel in porösen Gesteinen. *AdR* 2/1988: 192 – 202
- Schumacher T (2004) Steine für den Dom. In: Schock-Werner und Lauer (ed) *Steine für den Dom. Kölner Dom* pp 46–77
- Schwiete HE, Kastanja P, Ludwig U (1965) Das mörteltechnische und chemische Verhalten verschiedener Trasse und Gesteinsmehle in Verbindung mit Kalk in wässrigen Lösungen. *Forschungsbericht des Landes NRW*, Nr. 1441, Westdeutscher Verlag, Cologne und Opladen
- Sebastián E, Cultrone G, Benavente D, Fernandez LL, Eleert K, Rodriguez-Navarro C (2008) Swelling damage in clay-rich sandstones used in the church of San Mateo in Tarifa (Spain). *J Cult Her* 9:66–76
- Setzer MJ (1999) Mikroislinnenbildung und Frostschaaden. Eilgehausen R. (Hrsg.): *Werkstoffe im Bauwesen—Theorie und Praxis (Construction materials—theory and application)*. Ibidem Stuttgart, pp 397–413
- Siedel H, Siegfried S, Sterflinger K (2011) Characterization of Stone Deterioration on Buildings. In: Siegesmund and Snethlage (ed.): *Stone in Architecture*. 4<sup>th</sup> ed., Springer, Berlin Heidelberg. pp 347–410
- Siegesmund S, Dürrast H (2011) Physical and Mechanical Properties of Rocks. In: Siegesmund and Snethlage (ed.): *Stone in Architecture*. 4<sup>th</sup> ed., Springer, Berlin Heidelberg. pp 97–225
- Siegesmund S, Grimm WD, Dürrast H, Rüdrieh J (2010) Limestones in architecture: the German view. In: Smith B, Gomez-Heras M, Viles H and Cassar J: *Limestone in the Built Environment: Present day Challenges to Preserve the Past*. *Geol. Soc. Spec. London* 331:37–59
- Siegesmund S, Kirchner D (2003) Frost-Tau-Verhalten von Marmor. *Naturstein* 2/2003:52–56.
- Siegesmund S, Mosch S, Scheffzük Ch, Nikolayev DI (2008) The bowing potential of granitic rocks: rock fabrics, thermal properties and residual strain. *Environ Geol* 55: 1437 – 1448
- Siegesmund S, Ruedrich J (2008) Marble bowing. In: *Proceedings 11th international congress on deterioration and conservation of stone*, Torun, Poland
- Siegesmund S, Ruedrich J, Koch A (2008) Marble bowing: comparative studies of three different public building facades. *Environ Geol*. doi:10.1007/s00254-008-1307-z
- Siegesmund S, Snethlage R, Vollbrecht A, Weiss T (1999) Themenheft Marmorkonservierung. *Z dt geol Ges* 150(2):406
- Siegesmund S, Snethlage R (2011) *Stone in Architecture*. 4<sup>th</sup> ed., Springer, Berlin Heidelberg. 552p
- Siegesmund S, Török A., Hüpers A, Müller C, Klemm W (2007) Mineralogical, geochemical and microfabric evidences of gypsum crusts: a case study from Budapest. *Environ. Geol.*, 52:358–397
- Siegesmund S, Ullemeyer K, Weiss T, Tschegg E (2000) Physical weathering of marbles caused by thermal anisotropic expansion. *Int J Earth Sci Vol* 89:170–182
- Simper M (1990) Geologie und Naturwerksteine Nordrhein-Westfalens. In: Grimm WD (ed.) *Bildatlas wichtiger Denkmalgesteine der Bundesrepublik Deutschland*. Arbeitsheft des Bayerischen Landesamtes für Denkmalpflege, Bd. 50, München, pp 191–201
- Smith BJ, Whalley WB, Fassina V (1988) Elusive solution to monumental stone decay. *New Sci.*, 1615:49–53
- Snäll S, Lilijefors T (2000) Leachability of major elements from minerals in strong acids. *J. Geochem. Expl.* 71:1–12
- Snethlage R (1984) Steinkonservierung 1979 – 1983. Report Volkswagenstiftung. Bayer. Landesamt für Denkmalpflege, Munic. 22:203p
- Snethlage R (1985) Zum Kenntnisstand von Verwitterungsvorgängen an Natursteinen Bayer. *LAD*, 31:20–27
- Snethlage R (2005) Leitfaden Steinkonservierung. *Fraunhofer IRB*, Stuttgart. 289p
- Snethlage R, Wendler E (1997) Moisture cycles and sandstone degradation. In: Baer NS, Snethlage R (eds.) *Saving our Architectural Heritage: Conservation of historic stone structures*. John Wiley and Sons Ltd, London, pp 7–24
- Snethlage R, Wendler E, Klemm DD (1996) Tenside im Gesteinsschutz – Bisherige Resultate mit einem neuen Konzept zur Erhaltung von Denkmälern aus Naturstein. In: Snethlage R (ed.) *Denkmalpflege und Naturwissenschaft, Natursteinkonservierung I*. Ernst und Sohn, Berlin, pp 127–146
- Sperling CHB, Cooke RU (1980) Salt weathering in arid environments. I. Theoretical considerations. *Bedford Coll Pap Geogr* 9:52
- Spittgerber H (1976) Spaltdruck zwischen Festkörpern und Auswirkungen auf Probleme in der Technik. *Cement Concrete Res* 6:29–34
- Stauffer RE. (1990) Granite weathering and the sensitivity of Alpine Lakes to acid depositon. *Limnol. Oceanogr.* 35:1112–1134
- Steiger M (2003) Crusts and salts. In: Brimblecombe P (ed.) *The effects of air pollution on the built environment*. *Air Pollut Rev* 2:133–181
- Steiger M (2005) Crystal growth in porous materials: I. The crystallization pressure of large crystals. *J Cryst Growth* 282:455–469
- Steiger M (2009) Modellierung von Phasengleichgewichten. In: Schwarz HJ, Steiger M (eds) *Salzschäden an Kulturgütern*. DBU Workshop 2008. Ri-Con, Hannover, pp 80–99

- Steiger M, Dannecker W (1998) Die Bedingungen für die Kristallisation verschiedener Salzhydrate am Beispiel Thenardit/Mirabilit. In: Jahresberichte Steinerzfall-Steinkonservierung, Band 6, 1994–1996. Fraunhofer IRB Verlag, Stuttgart, pp 123–133
- Steiger M, Neumann HH, Grodten T, Wittenburg C, Dannecker W (1998) Salze in Natursteinmauerwerk: Probenahme, Messung und Interpretation. In: Snethlage R (ed) Natursteinkonservierung 2. Fraunhofer IRB Verlag, Stuttgart, pp 61–91
- Steindlberger E (2003) Vulkanische Gesteine aus Hessen und ihre Eigenschaften als Naturwerksteine. Geologische Abhandlungen Hessen, Band 110, Wiesbaden
- Stillings LL, Drever JL, Brantley S, Sun Y, Oxburgh R (1996) Rates of feldspar dissolution at pH 3–7 with 0–8 M oxalic acid. *Chem. Geol.* 132: 79–89
- Stockhausen N (1981) Die Dilatation hochporöser Festkörper bei Wasseraufnahme und Eisbildung. Dissertation, Technical University of München, 163p.
- Strübel G, Zimmer SH (1991) Lexikon der Minerale. Enke, Stuttgart, 385p.
- Stück H, Forgó Z, Rüdlich J, Siegesmund S, Török A (2008) The behaviour of consolidated volcanic tuffs: weathering mechanisms under simulated laboratory conditions. In: Siegesmund S, Snethlage R, Ruedrich J: Monumental future: climate change, air pollution, stone decay and conservation. *Environmental Geology* 56: 699–713. doi: 10.1007/s00254-008-1337-6
- Taylor AS, Blum JD, Lasaga AC (2000) The dependence of labradorite dissolution and Sr isotope release rates on solution saturation state. *Geochim Cosmochim Acta* 64(14): 2389–2400
- Thornbush M, Viles H (2004) Integrated digital photography and image processing for the quantification of colouration on soiled limestone surfaces in Oxford, England. *J Cult Herit* 5:285–290
- Torfs KM, Van Grieken RE (1997) Chemical relations between atmospheric aerosols, deposition and stone decay layers on historic buildings at the Mediterranean coast. *Atmos Environ* 31:2179–2192
- Török A (2003) Surface strength and mineralogy of weathering crusts on limestone buildings in Budapest. *Build Environ.*, 38:1185–1192
- Török A (2008) Black crusts on travertine: factors controlling development and stability. *Environ. Geol.*, 56:583–597
- Török A, Licha T, Simon K, Siegesmund S (2011) Urban and rural limestone weathering; the contribution of dust to black crust formation; examples from Germany and Hungary. *Environ. Earth Sci.*, 63:675–693
- Török A, Müller C, Hüpers A, Hoppert M, Weiss T, Siegesmund S (2006). Differences in texture, physical properties and microbiology of weathering crust and host rock: a case study of the porous limestone of Budapest (Hungary). In: Prikryl R, Smith BJ (eds) Building stone decay: From Diagnosis to Conservation. Geological Society Special Publications 271:261–276
- Tournier B, Jeannette D, Destringenville C (2000) Stone drying: an approach of the effective evaporation surface area. In: Fassina V (ed.) Proceedings of the 9<sup>th</sup> Intern. Conf. on Deterioration and Conservation of Stone. Elsevier, Amsterdam, Vol. 1. pp 629–635
- Trudgill ST, Viles HA, Inkpen R, Moses C, Gosling W, Yates T, Collier P, Smith DI, Cooke RU (2001) Twenty-year weathering remeasurements at St Paul's Cathedral, London. *Earth Surf Processes Landf.*, 26:1129–1142
- Turpin BJ, Huntzicker JJ (1995) Identification of secondary organic aerosol episodes and quantification of primary and secondary organic aerosol concentrations during SCAQS. *Atmos. Environ.*, 29:3527–3544
- UBA (2011) Umweltdaten. Fachgebiet II Deutsches Umweltbundesamt, Dessau
- Vieten K (1961) Die Trachyt-Latit-Alkalibasalt-Assoziation des Siebengebirges am Rhein. Dissertation, University of Bonn.
- Viles HA (1994) Observations and explanations of stone decay in Oxford, UK. In: Thiel MJ (ed.) Conservation of stone and other materials. Causes of disorders and diagnosis. E and FN Spon—RILEM, London, 1:115–120
- Visser H, Mirwald P (1998) Baumberger Kalksandstein – Materialeigenschaften und Schadenspotential. In: Die Steinskulpturen am Zentralbau des Jagdschlusses Clemenswerth/Emsland, LAD Nieders. (vol. 15) 26–45. Hannover: Selbstverlag
- von Lasaulx A (1882) Die Bausteine des Kölner Domes. Cohen, Bonn, 83 p
- von Plehwe-Leisen E, Leisen H, Wendler E (2007) Der Drachenfels-Trachyt – ein wichtiges Denkmalgestein des Mittelalters – Untersuchungen zur Konservierung. Z. dt. Ges. Geowiss., 158/3:985–998
- Vos BH (1970) Measuring moisture content and distribution in constructions. *Build International* 3/1970:51–54
- Vos BH (1978) Hydric methods for the determination of behavior of stones. In: Proceedings of the Int symp deterioration and protection of stone monuments, UNESCO-REILEM Paris, pp 1–10
- Vos BH, Tammes E (1968) Flow of water in the liquid phase. Inst. TNO for Building Materials and Building Structures, report BI-68-38, Delft
- Walder J, Hallet B (1985) A theoretical model of the fracture of rock during freezing. *Geol Soc Am Bull* 96:336–346
- Wangler TP, Scherer GW (2008) Clay swelling mechanism in claybearing sandstones. *Environ Geol* 56:529–534
- Warscheid T, Petersen K, Krumbein WE (1990) A rapid method to demonstrate and evaluate microbial activity on decaying sandstone. *Studies in Conservation*, 35:137–147
- Weber D (1995) Technische Feuchtemessung in Gasen und Festkörpern. Vulkan-Verlag, Essen, 152p
- Weber E (1974) Einführung in die Faktorenanalyse. Fischer, Stuttgart
- Weimann MB (2001) Hygrische Eigenschaften von Polymerbeton im Vergleich zu porösen mineralischen Werkstoffen im Bauwesen. Diss. Technische Hochschule Zürich, 149p
- Weiss G (1992) Die Eis und Salzkristallisation im Porenraum von Sandsteinen und ihre Auswirkung auf das Gefüge unter besonderer Berücksichtigung gesteinspezifischer Parameter. Münchner Geowissenschaftliche Abhandlungen, Reihe Band 9:S62
- Weiss T, Siegesmund S, Kirchner D, Sippel J (2004) Insolation weathering and hygric dilatation: two competitive factors in stone degradation *Environ Geol* 46:402–413
- Wellman HW, Wilson AT (1965) Salt weathering, neglected geological erosive agent in coastal and arid environments. *Nature* 205:1097–1098
- Wellman HW, Wilson AT (1968) Salt weathering or fretting. In: Fairbridge RW (eds) The encyclopedia of geomorphology.

- Wesche K (1996) Baustoffe für tragende Bauteile Grundlagen 1. Bauverlag, Wiesbaden. 145p
- White AF (1995) Chemical weathering rates in soils. In: In: Chemical weathering rates of silicate minerals. White AF, Brantley SL (eds.) Min Soc Am, Washington DC, pp. 407–458
- White AF (2003) Natural Weathering Rates of Silicate Minerals. In: Treatise on Geochemistry, vol. 5. Drever JI et al. (eds) Elsevier, pp.133–168
- White AF, Blum AE, Stonestrom DA, Bullen TD, Schulz MS, Huntington TG, Peters NE (2001) Differential rates of feldspar weathering in granitic regoliths. *Geochim. Cosmochim Acta* 65:847–869
- White AF, Brantley SL (1995) Chemical weathering rates of silicate minerals. In: Reviews in Mineralogy. Mineral. Soc. Am., Washington DC, vol. 31, 584p
- Wierzchos J, Ascaso C (1998) Mineralogical transformation of bioweathered granitic biotite, studied by HRTEM: evidence for a new pathway in lichen activity. *Clay and Clay Min.*, 46/4:446–452
- Wiese U, Behlen A, Steiger M (2012) The influence of relative humidity on the SO<sub>2</sub> deposition velocity to building stones: a chamber study at very low SO<sub>2</sub> concentration. *Environ. Earth Sci.* doi10.1007/s12665-012-1872-z
- Wihr R (1986) Restaurierung von Steindenkmälern. Callwey, München, 236p
- Winkler EM (1968) Frost damage to stone and concrete: geological considerations. *Eng Geol* 2:315–323
- Winkler EM (1970) The importance of air pollution in the corrosion of stone and metals. *Eng. Geol.*, 4:327–334
- Winkler EM (1975) Stone: Properties, durability in man's environment. Springer, New York
- Winkler EM (1994) Stone in architecture, 3rd ed. Springer Berlin Heidelberg New York
- WMO-UN World Meteorological Organisation 2012
- Wolf C (2002) Urban air pollution and health: an ecological study of chronic rhinosinusitis in Cologne, Germany. *Health Place* 8:129–139
- Wolff A (1972) Die Gefährdung des Kölner Doms – Seine Steine und ihr Zustand im Jahr 1972. *Kölner Domblatt*, 32:7–28
- Wolff A (1986) Stone deterioration on the Cathedral of Cologne: Paper presented at the Symposium "Air Pollution and Conservation", Rome
- Wolff A (1992): Dombaubericht von Oktober 1991 bis September 1992: 10.1 Londorf Basaltlava und Schlaitdorf Sandstein. *Kölner Domblatt* 57:89-93
- Wolff A (2004) Steine für den Dom. In: Schock-Werner B and Lauer S (eds.) Steine für den Kölner Dom. Dom Vlg., Cologne, pp 8–21
- Wolff A (2005) Der Dom zu Köln. Köln
- Wolff A, Luckat S (1973) Untersuchungen zur Einwirkung von Luftverunreinigungen auf die Baumaterialien des Kölner Domes. In: Proceedings of the third International Clean Air Congress, VDI-Verlag, Düsseldorf, pp A90–A92
- Wollast R (1990) Rate and mechanism of dissolution of carbonates in the system CaCO<sub>3</sub>–MgCO<sub>3</sub>. In: Aquatic chemical kinetics. Reaction rates of processes in natural waters. Stumm W (ed.) John Wiley, New York, pp. 432–445
- WTA (1992) Sanierputzsysteme. Merkblatt 2-2-91 In: B+B15:59–63
- WTA (2004) Sachstandsbericht zur Messung der Feuchte von mineralischen Baustoffen. WTA 4.11. Rieche G (ed)
- Zappia G, Sabbioni C, Gobbi G (1998) Effects of carbonaceous particles and heavy metals on mortar-SO<sub>2</sub> reactions. *RILEM, Materials and Structure*, 31:480–486
- Zeisig A, Siegesmund S, Weiss T (2002) Thermal expansion and its control on the durability of marbles. *Geol. Soc. Spec. Publ.* 205: 64-79



## Acknowledgement

Die vorliegende Arbeit wäre ohne die Unterstützung von vielen verschiedenen Personen nicht zustande gekommen. Mein Dank gilt:

- der Deutschen Bundesstiftung Umwelt, die das Projekt gefördert und damit die Promotion ermöglicht hat;
- Prof. Dr. Siegfried Siegesmund und Prof. Dr. Rolf Snethlage für die Übernahme des Referats und Korreferats der Arbeit;
- Prof. Dr. Barbara Schock-Werner, die mein Promotionsvorhaben im Rahmen des DBU-geförderten Projektes von Anfang an unterstützt hat;
- Dr. Thomas Schumacher und Uwe Schäfer, den Mitarbeiterinnen und Mitarbeitern der Dombauhütte und der Dombauverwaltung für die vielfältige Unterstützung und die gute Zusammenarbeit;
- den im Projekt Beteiligten: Christian Knell und Felix Hüttenrauch, die mir bei Versuchen und Untersuchungen vor Ort mit großer Hilfsbereitschaft zur Seite standen; Prof. Dr. Bernhard Middendorf und Deborah Klein für die gute Projektzusammenarbeit;
- Dorothea Hause-Reitner, Dr. Andreas Kronz, Dr. Tobias Licha, Mechthild Rittmeier, Dr. Klaus Simon, Dr. Kirsten Techmer, Anke von Gaza vom Geowissenschaftlichen Zentrum der Universität Göttingen für ihre Unterstützung bei Untersuchungen und Versuchen;
- Dr. Reiner Dohrmann von der Bundesanstalt Geowissenschaften und Rohstoffe für die Tonmineralanalysen; Dirk Kirchner und Karin Kirchner vom Deutschen Bergbau-Museum Bochum sowie Rudolf Naumann vom Deutschen Geoforschungszentrum in Potsdam für ihre Unterstützung bei REM- und XRF-Analysen;
- Prof. Dr. Pedro Oyhantcabal, Universität Montevideo, und Dr. Rudolf Plagge, Technische Universität Dresden, für interessante Diskussionsanregungen;
- den Kolleginnen und Kollegen im Rheinischen Amt für Denkmalpflege für ihr Interesse und ihre Diskussionsbereitschaft;
- Johannes Schubert und Torsten Knapp, Dombauhütte Xanten, sowie den Verantwortlichen am Altenberger Dom und der Bezirksregierung für ihre Unterstützung der Untersuchung und Probenentnahme vor Ort;
- den Kolleginnen und Kollegen der Abteilung Struktur für die vielfältige Unterstützung des nicht immer einfachen Weges.

Ein besonderer Dank gilt meiner Familie, die schon immer an meinem beruflichen Werdegang mit großem Interesse teilgenommen hat und mir liebevollen Rückhalt gibt. Mein Mann, meine Mutter und mein Sohn sind ein unschlagbares Team! Vielen Dank!



## Curriculum Vitae

Birte Johanna Graue

geboren am 04.06.1971 in Lauterbach/Hessen  
Staatsangehörigkeit: deutsch

### Hochschulausbildung und wissenschaftlicher Werdegang

2009 - 2012	Wissenschaftliche Mitarbeit, Geowissenschaftliches Zentrum der Universität Göttingen
seit 2009	Mitarbeit, Restaurierungswerkstatt II, LVR-Amt für Denkmalpflege im Rheinland, Köln-Pulheim
2005 - 2009	Restauratorische und konservierungswissenschaftliche Beratung, Dombauverwaltung Köln
2007– 2009	Mitglied des Projektleitungsteams, Forschungsprojekt „Zur Wiedergewinnung altägyptischer Wandmalerei und Reliefdarstellungen - Methoden ägyptologischer Forschung und ihre Auswirkung am Beispiel der Tempelwand in der Grabkammer des Neferhotep, Theben“ (Gerda Henkel-Stiftung)
2004 – 2006	Mitglied des Projektleitungsteams, Forschungsprojekt „Wiederlesbarmachung altägyptischer Darstellungen zu ihrer Interpretation - Entwicklung neuer Methoden zur Oberflächenreinigung repräsentativ am Beispiel der Grabkammer des Neferhotep TT 49 (Theben, Ägypten)“ (Gerda Henkel-Stiftung)
2004 – 2006	Wissenschaftliche Mitarbeit, Forschungsprojekt „Modellhafte Entwicklung von Konservierungskonzepten für den stark umweltgeschädigten Trachyt an den Domen zu Köln und Xanten“, Dombauverwaltung Köln (Deutsche Bundesstiftung Umwelt)
2004	Wissenschaftliche Mitarbeit, Forschungsprojekt „Archäologische, philologische und material- und konservierungswissenschaftliche Erforschung des spätptolemäischen/ frühromischen Tempels von Athribis im 9. oberägyptischen Gau „ in Ägypten, Fachhochschule Köln (März – April) (Fritz-Thyssen-Stiftung/ Deutsche Forschungsgemeinschaft)
2003 – 2005	Wissenschaftliche Mitarbeit, „German Apsara Conservation Project Cambodia“, Fachhochschule Köln
2003	Mitarbeit, Sherman Fairchild Center for Objects Conservation, Metropolitan Museum of Art, New York City, USA (Januar – Oktober)
seit 2001	Freiberufliche Tätigkeit und Leitung einer Werkstatt für Restaurierung und Konservierung, Köln/Göttingen
seit 2000	Mitglied des Projektleitungsteams, Leitung der Steinkonservierung im Forschungs- und Konservierungsprojekt Neferhotep TT 49 – PROCON in Theben, Ägypten
1998	Mitarbeit, Canadian Conservation Institute, Ottawa/Canada (März, September – Oktober)
1997 – 1998	Studentische Mitarbeit, Canadian Museum of Civilization, Ottawa/Canada (Juni 1987 – Februar 1998) (Stipendium der Wilhelm Klein-Stiftung)
1995 – 2001	Studium, Restaurierung und Konservierung von Kunst und Kulturgut, Fachrichtung Wandmalerei und Objekte aus Stein, Fachhochschule Köln  Diplomthema: „Eisenverfärbungen im Stein im Zusammenhang mit Restaurierungs- und Konservierungsmaßnahmen – Untersuchungen zu Schadensmechanismen und Reinigung“





## Appendix

**Table A3.1** Measuring parameters of the sensors in MF01.

Messstelle	Klimasensor	Messbereich	Seriennummer	Kennwerte
M1	KS01	DT - Bohrlochtiefe: 1,8 cm	T09070-146	Temp., Feuchte, Taupunkt, Mischung
M2	KS02	OS - Bohrlochtiefe: 1,8 cm	T09070-147	Temp., Feuchte, Taupunkt, Mischung
M3	KS03	DT - Bohrlochtiefe: 3,2 cm	T09070-148	Temp., Feuchte, Taupunkt, Mischung
M4	KS04	OS - Bohrlochtiefe: 3,2 cm	T09070-149	Temp., Feuchte, Taupunkt, Mischung
M5	KS05	DT - OF	NiCr	Oberflächentemperatur
M6	KS06	OS - OF	NiCr	Oberflächentemperatur
M7	KS07	Außenfühler	T09070-150	Temp., Feuchte, Taupunkt, Mischung

**Table A3.2** Measuring parameters of the sensors in MF02x.

Messstelle	Klimasensor	Messbereich	Seriennummer	Kennwerte
M1	KS01	SS - Bohrlochtiefe: 3,7 cm	11030012	Temp., Feuchte, Taupunkt, Mischung
M2	KS02	DT - Bohrlochtiefe: 3,7 cm	11030018	Temp., Feuchte, Taupunkt, Mischung
M3	KS03	SS - Bohrlochtiefe: 2,3 cm	11010008	Temp., Feuchte, Taupunkt, Mischung
M4	KS04	DT - Bohrlochtiefe: 2,3 cm	11030015	Temp., Feuchte, Taupunkt, Mischung
M5	KS05	SS - OF	NiCr	Oberflächentemperatur
M6	KS06	DT - OF	NiCr	Oberflächentemperatur
M7	KS07	Außenfühler	11030013	Temp., Feuchte, Taupunkt, Mischung

**Table A3.3** Measuring parameters of the sensors in MF04.

**Gerät A**      **Seriennummer: T09070148**

Messstelle	Klimasensor	Messbereich	Seriennummer	Kennwerte	Bohrlochtiefe
M1	KS01	DT - entfernt KM-OS	T09070-138	Temp., Feuchte, Taupunkt, Mischung	3,2 cm
M2	KS02	DT - näher KM-OS	T09070-139	Temp., Feuchte, Taupunkt, Mischung	3,2 cm
M3	KS03	KM - nah an DT	T09070-140	Temp., Feuchte, Taupunkt, Mischung	3,2 cm
M4	KS04	KM - entfernt von DT	T09070-141	Temp., Feuchte, Taupunkt, Mischung	3,2 cm
M5	KS09	KM - OF	NiCr	Oberflächentemperatur	--
M6	KS11	DT - OF	NiCr	Oberflächentemperatur	--

**Gerät B**      **Seriennummer: T09070150**

Messstelle	Klimasensor	Messbereich	Seriennummer	Kennwerte	Bohrlochtiefe
M1	KS05	OS - entfernt KM-DT	T09070-142	Temp., Feuchte, Taupunkt, Mischung	3,2 cm
M2	KS06	OS - näher KM-DT	T09070-143	Temp., Feuchte, Taupunkt, Mischung	3,2 cm
M3	KS07	KM - nah an OS-DT	T09070-144	Temp., Feuchte, Taupunkt, Mischung	3,2 cm
M4	KS08	KM - entfernt von OS-DT	T09070-145	Temp., Feuchte, Taupunkt, Mischung	3,2 cm
M5	KS10	OS - OF	NiCr	Oberflächentemperatur	--
M6	KS12	Außenfühler	T09070-151	Temp., Feuchte, Taupunkt, Mischung	--

**Table A3.4** Measuring parameters of the sensors in MF07.

Messstelle	Klimasensor	Messbereich	Seriennummer	Kennwerte
M1	KS01	DT - Bohrlochtiefe: 1,8 cm	T09070-152	Temp., Feuchte, Taupunkt, Mischung
M2	KS02	DT - Bohrlochtiefe: 3,0 cm	T09070-153	Temp., Feuchte, Taupunkt, Mischung
M3	KS03	DT - OF	NiCr	Oberflächentemperatur
M4	KS04	OS - Bohrlochtiefe: 1,8 cm	T09070-154	Temp., Feuchte, Taupunkt, Mischung
M5	KS05	OS - Bohrlochtiefe: 3,0 cm	T09070-155	Temp., Feuchte, Taupunkt, Mischung
M6	KS06	OS - OF	NiCr	Oberflächentemperatur
M7	KS07	Außenfühler	T09070-156	Temp., Feuchte, Taupunkt, Mischung

**Table A.5.1** XRF analyses of the investigated stones

	SiO <sub>2</sub>	TiO <sub>2</sub>	Al <sub>2</sub> O <sub>3</sub>	Fe <sub>2</sub> O <sub>3</sub>	MnO	MgO	CaO	Na <sub>2</sub> O	K <sub>2</sub> O	P <sub>2</sub> O <sub>5</sub>	H <sub>2</sub> O	CO <sub>2</sub>	sum
	(%)	(%)	(%)	(%)	(%)	(%)	(%)	(%)	(%)	(%)	%	%	%
<b>Krensheim Muschelkalk</b>	0.70	0.01	1.52	0.19	0.05	0.45	52.25	0.70	0.05	0.08	0.40	43.28	99.68
<b>Schlaitdorf sandstone</b>	88.66	0.03	4.88	0.12	0.01	0.87	1.31	0.07	0.10	0.02	1.36	2.45	99.88
<b>Obernkirchen sandstone</b>	92.63	0.57	3.91	0.11	0.01	0.05	0.03	0.80	0.17	0.03	1.12	0.15	99.57
<b>Bozanov sandstone</b>	92.56	0.03	4.34	0.09	0.01	0.09	0.09	0.33	1.62	0.01	0.55	0.08	99.79
<b>Drachenfels trachyte</b>	63.66	0.66	17.46	3.23	0.11	0.78	2.40	4.44	5.58	0.17	0.76	0.12	99.36
<b>Montemerlo trachyte</b>	61.71	0.82	18.20	4.30	0.09	1.10	2.12	5.19	4.73	0.43	0.85	0.09	99.63
<b>Stenzelberg latite</b>	56.12	1.85	18.30	6.78	0.10	1.47	4.95	4.17	4.05	0.46	1.11	0.13	99.48
<b>Londorf basalt lava</b>	49.54	2.57	14.35	10.62	0.15	8.20	8.23	3.30	1.32	0.35	0.93	0.17	99.72

**Table A.7.0** Concentrations of MSA solutions

Stone	MSA (0.01 mol/l) ml	MSA (1 mol/l) ml	demin. aqua ml	pH after 24 h
Drachenfels trachyte	6.5		18.5	4.76
Montemerlo trachyte	4.2		20.8	5.11
Krensheim Muschelkalk 1		19.0	6.0	6.9
Krensheim Muschelkalk 2		19.5	5.5	2.28
Bozanov sandstone	2.8		22.2	4.18
Schlaitdorf sandstone		0.9	24.1	4.07
Londorf basalt lava	15.0		10.0	3.87
Stenzelberg latite	12.0		13.0	4.03
Obernkirchen sandstone	1.5		23.5	4.32

**Table A7.1** Preparation of leachents

<p><u>Buffer solution pH 3.4</u> analogous Kolthoff, concentration: 1/50</p> <p>Parent solution A: 19.1 g borax <math>\text{Na}_2\text{B}_4\text{O}_7 \cdot 10\text{H}_2\text{O}</math> in 1000ml (eq. 0,05m)</p> <p>Parent solution B: 5.9 g succinic acid <math>\text{C}_4\text{H}_6\text{O}_4</math></p> <p>37.44 ml solution B + 2.56 ml solution A, filled up with demin. water to 2000 ml</p>
<p><u>Buffer solution pH 7,0</u> analogous Palitzsch, concentration: 1/50</p> <p>Parent solution A: 19.1 g borax <math>\text{Na}_2\text{B}_4\text{O}_7 \cdot 10\text{H}_2\text{O}</math> in 1000ml (eq. 0,05m)</p> <p>Parent solution B: 0.2 mol/l boric acid, 12.368 g <math>\text{H}_3\text{BO}_3</math> diluted in 1000ml demin. water</p> <p>37.64 ml solution B + 2.36ml solution A, filled up with demin. water to 2000 ml</p>
<p><u>Buffer solution pH 8.4</u> analogous Palitzsch, concentration: 1/50</p> <p>Parent solution A: 19.1 g borax <math>\text{Na}_2\text{B}_4\text{O}_7 \cdot 10\text{H}_2\text{O}</math> in 1000ml (eq. 0,05m)</p> <p>Parent solution B: 0.2 mol/l boric acid, 12.368 g <math>\text{H}_3\text{BO}_3</math> diluted in 1000ml demin. water</p> <p>22.08 ml solution B + 17.92 ml solution A, filled up with demin. water to 2000 ml</p>
<p><u>Saturated gypsum solution</u> <math>\text{CaSO}_4 \cdot 2\text{H}_2\text{O}</math></p> <p>Gypsum powder is steeped in demin. water for several days. Supernatant is decanted, sediment is rinsed two times with diluted sulfuric acid pH 3 (3 drops/100 ml). Then two times rinsed with demin. water, with sedimentation time in between. Afterwards dried at 40 °C several days, clear supernatant removed: oversaturated gypsum solution is yielded.</p>

**Table A7.2** Data of the detected pH values **(a)** fine sample fraction; **(b)** coarse sample fraction

<b>a</b>							
<b>Fine sample fraction</b>		mean value of 3 measurements					
<i>stone material</i>	<i>leachant</i>	<i>Ch1Wo1</i>	<i>Ch1Wo2</i>	<i>Ch1Wo3</i>	<i>Ch2Wo4</i>	<i>Ch2Wo8</i>	<i>Ch3Wo12</i>
Schlaitdorfer sandstone	demin water	8.55	8.18	7.94	7.41	7.79	7.83
SS	pH 7.0	8.39	8.27	7.06	8.06	8.22	8.05
SS	pH 8.4	8.66	8.60	8.37	8.34	8.48	8.10
SS	oversat. gypsum sol.	7.85	7.80	8.55	7.47	7.67	7.88
Obernkirchner sandstone	demin water	6.98	7.22	7.41	7.34	7.23	7.35
OS	pH 3.4	6.53	6.79	6.53	7.17	6.67	7.23
OS	pH 7.0	6.79	7.08	7.13	7.25	7.23	7.62
OS	pH 8.4	7.77	8.16	8.35	7.49	7.77	7.48
OS	oversat. gypsum sol.	6.21	6.31	6.86	7.02	6.27	6.41
Bozanov sandstone	demin water	7.12	7.04	7.36	7.11	7.48	7.32
BS	pH 3.4	6.83	6.08	5.71	7.04	7.08	7.38
BS	pH 7.0	6.99	7.05	7.37	6.92	7.20	7.28
BS	pH 8.4	7.71	8.25	8.37	7.53	8.20	7.61
BS	oversat. gypsum sol.	6.28	6.03	6.84	6.48	6.31	6.17
Drachenfels trachyte	demin water	8.98	8.63	8.36	7.25	7.35	7.37
DT	pH 3.4	7.32	6.26	5.23	7.24	6.74	7.69
DT	pH 7.0	8.30	8.19	7.81	7.85	8.11	8.10
DT	pH 8.4	8.73	8.57	8.56	8.53	8.49	8.20
DT	oversat. gypsum sol.	7.88	7.71	7.43	7.40	7.12	7.11
Montemerlo trachyte	demin water	8.17	8.37	8.12	6.93	7.58	7.78
MT	pH 3.4	7.65	6.56	5.94	7.53	7.34	7.87
MT	pH 7.0	8.26	7.93	7.70	6.84	7.78	7.88
MT	pH 8.4	8.58	8.44	8.43	8.22	8.20	7.80
MT	oversat. gypsum sol.	7.57	7.07	7.14	7.33	7.10	7.20
Stenzelberg latite	demin water	8.28	7.88	7.45	7.74	7.58	8.05
SL	pH 3.4	7.99	7.06	6.81	7.68	7.60	8.12
SL	pH 7.0	8.01	7.31	7.21	7.61	7.35	7.71
SL	pH 8.4	8.55	8.20	8.35	7.78	7.54	7.90
SL	oversat. gypsum sol.	7.59	7.15	6.78	7.47	6.98	7.49
Londorfer basalt lava	demin water	9.01	8.62	7.76	7.69	7.95	7.95
LB	pH 3.4	8.03	7.14	6.19	7.69	7.60	8.19
LB	pH 7.0	8.44	7.94	7.86	8.07	7.89	8.10
LB	pH 8.4	8.77	8.53	8.48	8.51	8.33	8.09
LB	oversat. gypsum sol.	8.13	7.57	7.67	7.74	7.43	7.78

b

## Coarse sample fraction

mean value of 3 measurements

<i>stone material</i>	<i>leachant</i>	<i>Ch1Wo1</i>	<i>Ch1Wo2</i>	<i>Ch1Wo3</i>	<i>Ch2Wo4</i>	<i>Ch2Wo8</i>	<i>Ch3Wo12</i>
Schlaitdorfer sandstone	demin water	8.18	8.13	6.96	7.48	7.52	7.90
SS	pH 7.0	8.18	8.09	7.75	8.17	8.17	7.99
SS	pH 8.4	8.57	8.56	8.23	8.22	8.44	8.13
SS	oversat. gypsum sol.	7.68	7.58	8.49	6.69	6.98	7.32
Obernkirchner sandstone	demin water	6.96	6.59	6.97	7.23	6.66	6.91
OS	pH 3.4	6.88	6.65	6.79	7.40	7.01	7.05
OS	pH 7.0	6.92	6.90	6.60	7.24	6.67	6.79
OS	pH 8.4	7.55	7.85	7.89	7.42	7.17	7.19
OS	oversat. gypsum sol.	6.19	5.88	6.25	6.38	5.62	5.97
Bozanov sandstone	demin water	7.79	7.67	7.09	7.01	7.59	7.04
BS	pH 3.4	6.68	6.79	6.87	6.76	7.44	7.14
BS	pH 7.0	6.27	6.72	6.90	6.84	7.05	6.69
BS	pH 8.4	6.88	6.84	7.47	6.96	7.08	6.77
BS	oversat. gypsum sol.	4.40	4.72	4.72	4.63	4.48	4.48
Drachenfels trachyte	demin water	7.01	7.13	7.35	7.48	6.70	7.19
DT	pH 3.4	7.18	6.98	6.87	7.79	6.99	7.26
DT	pH 7.0	8.01	7.78	7.82	7.79	7.15	7.47
DT	pH 8.4	8.10	8.22	8.22	7.71	7.44	7.47
DT	oversat. gypsum sol.	7.44	7.26	7.09	7.43	6.68	7.11
Montemerlo trachyte	demin water	7.49	7.38	6.60	7.61	7.42	6.90
MT	pH 3.4	7.71	7.38	7.05	7.49	7.04	7.32
MT	pH 7.0	7.19	6.99	7.15	6.94	6.92	7.48
MT	pH 8.4	7.55	7.64	7.70	7.06	7.13	7.15
MT	oversat. gypsum sol.	7.30	7.00	7.43	6.83	6.41	6.77
Stenzelberg latite	demin water	6.80	6.82	6.91	7.20	7.10	6.88
SL	pH 3.4	6.66	6.49	6.90	7.15	6.53	6.82
SL	pH 7.0	6.94	6.84	7.20	7.17	6.54	6.51
SL	pH 8.4	7.62	7.98	8.02	7.44	7.01	6.97
SL	oversat. gypsum sol.	6.43	6.06	5.96	6.86	6.05	6.39
Londorfer basalt lava	demin water	7.04	6.64	6.68	7.23	6.63	6.91
LB	pH 3.4	7.10	6.67	6.84	7.42	6.71	7.03
LB	pH 7.0	7.37	6.98	6.87	7.53	6.92	6.99
LB	pH 8.4	7.95	7.79	8.05	7.64	7.35	7.52
LB	oversat. gypsum sol.	7.07	6.13	6.45	6.59	6.25	6.62
blank	demin water	5.74	6.52	5.73	5.75	6.13	6.04
BP	pH 3.4	3.66	3.69	3.60	3.65	3.86	3.90
BP	pH 7.0	7.88	6.97	6.77	6.81	6.80	6.46
BP	pH 8.4	8.35	8.27	8.28	7.76	8.23	7.73
BP	oversat. gypsum sol.	5.74	4.92	6.05	4.85	4.91	4.82

**Table A7.3** Concentrations of leached fractions (g/kg) from the Schlaitdorf sandstone (fine and coarse grain size)

SS fine fraction		concentration of leached element (g/kg)					
leachants		aq. demin.	pH 3,4	pH 7	pH 8	oversat. gypsum sol.	TOTAL
Ch1Wo1	Na	g/kg	0,03	0,04	0,18	-0,11	0,14
	K	g/kg	0,05	0,05	0,05	0,07	0,23
	Mg	g/kg	0,05	0,08	0,05	0,15	0,33
	Ca	g/kg	0,10	0,12	0,09	4,06	4,37
	TOTAL	g/kg	0,23	0,30	0,38	4,17	5,07
Ch1Wo2	Na	g/kg	0,01	0,00	0,14	-0,13	0,02
	K	g/kg	0,02	0,02	0,02	0,02	0,08
	Mg	g/kg	0,03	0,07	0,05	0,04	0,18
	Ca	g/kg	0,12	0,12	0,08	4,12	4,45
	TOTAL	g/kg	0,18	0,21	0,30	4,05	4,73
Ch1Wo3	Na	g/kg	0,00				
	K	g/kg	0,01				
	Mg	g/kg	0,03				
	Ca	g/kg	0,06				
	TOTAL	g/kg	0,10				
Ch2Wo4	Na	g/kg	0,04	0,05	0,18	-0,11	0,16
	K	g/kg	0,06	0,06	0,05	0,07	0,23
	Mg	g/kg	0,08	0,10	0,06	0,17	0,41
	Ca	g/kg	0,13	0,14	0,10	5,43	5,81
	TOTAL	g/kg	0,32	0,34	0,40	5,56	6,62

SS coarse fraction		concentration of leached element (g/kg)					
leachants		aq. demin.	pH 3,4	pH 7	pH 8	oversat. gypsum sol.	TOTAL
Ch1Wo1	Na	g/kg	0,04		0,03	0,08	-0,04
	K	g/kg	0,02		0,02	0,02	0,03
	Mg	g/kg	0,02		0,02	0,02	0,07
	Ca	g/kg	0,03		0,03	0,01	1,51
	TOTAL	g/kg	0,10		0,11	0,14	1,57
Ch1Wo2	Na	g/kg	0,00		0,00	0,05	-0,05
	K	g/kg	0,01		0,01	0,01	0,01
	Mg	g/kg	0,01		0,02	0,02	0,02
	Ca	g/kg	0,01		0,03	0,01	1,61
	TOTAL	g/kg	0,03		0,06	0,09	1,58
Ch1Wo3	Na	g/kg	0,00				
	K	g/kg	0,00				
	Mg	g/kg	0,01				
	Ca	g/kg	0,01				
	TOTAL	g/kg	0,03				
Ch2Wo4	Na	g/kg	0,01		0,01	0,01	0,00
	K	g/kg	0,00		0,00	0,00	0,00
	Mg	g/kg	0,01		0,01	0,01	0,03
	Ca	g/kg	0,01		0,02	0,01	0,01
	TOTAL	g/kg	0,02		0,04	0,03	0,11

**Table A7.4** Leachabilities of the individual fractions (% of wt. %) from the Schlaitdorf sandstone (fine and coarse grain size)

SS fine fraction		Leachability (% of wt. %)					
host rock (wt. %)		aq. demin.	pH 3.4	pH 7	pH 8	oversat. gypsum sol.	TOTAL
Ch1Wo1	Na	0,05	6,65	8,30	34,18	-21,45	27,67
	K	0,08	6,26	6,59	6,44	8,32	27,62
	Mg	0,52	0,95	1,47	1,04	2,91	6,37
	Ca	0,94	1,04	1,32	0,98	43,31	46,65
	TOTAL	1,60	1,46	1,87	2,36	26,10	31,80
Ch1Wo2	Na	0,05	1,28	0,84	27,44	-25,58	3,97
	K	0,08	2,49	2,20	2,63	2,17	9,49
	Mg	0,52	0,50	1,30	0,93	0,79	3,52
	Ca	0,94	1,30	1,24	0,90	44,05	47,48
	TOTAL	1,60	1,10	1,29	1,86	25,38	29,64
Ch1Wo3	Na	0,05	0,19				
	K	0,08	1,28				
	Mg	0,52	0,57				
	Ca	0,94	0,65				
	TOTAL	1,60	0,64				
Ch2Wo4	Na	0,05	8,50	8,95	35,51	-21,42	31,54
	K	0,08	6,65	6,73	6,35	8,28	28,00
	Mg	0,52	1,59	1,83	1,22	3,25	7,90
	Ca	0,94	1,44	1,54	1,06	58,04	62,08
	TOTAL	1,60	1,99	2,15	2,51	34,85	41,50

SS coars fraction		Leachability (% of wt. %)					
host rock (wt. %)		aq. demin.	pH 3.4	pH 7	pH 8	oversat. gypsum sol.	TOTAL
Ch1Wo1	Na	0,05	6,84		5,60	16,19	-6,99
	K	0,08	2,29		2,36	2,58	3,53
	Mg	0,52	0,36		0,46	0,36	1,31
	Ca	0,94	0,29		0,37	0,16	16,11
	TOTAL	1,60	0,63		0,67	0,87	9,84
Ch1Wo2	Na	0,05	0,72		0,55	9,39	-9,86
	K	0,08	0,83		0,82	1,19	0,80
	Mg	0,52	0,19		0,38	0,30	0,32
	Ca	0,94	0,09		0,31	0,13	17,18
	TOTAL	1,60	0,18		0,36	0,54	9,90
Ch1Wo3	Na	0,05	0,05				
	K	0,08	0,43				
	Mg	0,52	0,19				
	Ca	0,94	0,12				
	TOTAL	1,60	0,16				
Ch2Wo4	Na	0,05	1,20		1,37	1,37	-0,76
	K	0,08	0,19		0,24	0,25	0,19
	Mg	0,52	0,11		0,20	0,15	0,14
	Ca	0,94	0,10		0,20	0,15	0,13
	TOTAL	1,60	0,14		0,24	0,19	0,11

**Table A7.5** Concentrations of leached fractions (g/kg) from the Drachenfels trachyte (fine and coarse grain size)

DT fine fraction		concentration of leached element (g/kg)						
leachants		aq. demin.	pH 3,4	pH 7	pH 8	oversat. gypsum sol.	TOTAL	
Ch1Wo1	Na	g/kg	0,11	0,13	0,12	0,06	0,13	0,55
	K	g/kg	0,07	0,13	0,10	0,10	0,19	0,60
	Mg	g/kg	0,00	0,03	0,01	0,01	0,07	0,13
	Ca	g/kg	0,03	0,29	0,12	0,09	-0,28	0,24
	TOTAL	g/kg	0,21	0,58	0,35	0,26	0,12	1,52
Ch1Wo2	Na	g/kg	0,03	0,04	0,03	0,00	0,02	0,11
	K	g/kg	0,05	0,08	0,06	0,06	0,07	0,32
	Mg	g/kg	0,00	0,02	0,01	0,01	0,02	0,06
	Ca	g/kg	0,00	0,17	0,11	0,09	-0,04	0,35
	TOTAL	g/kg	0,09	0,30	0,21	0,16	0,08	0,84
Ch1Wo3	Na	g/kg	0,01	0,02	0,01	0,01	0,01	0,06
	K	g/kg	0,03	0,05	0,03	0,03	0,03	0,18
	Mg	g/kg	0,00	0,02	0,00	0,00	0,01	0,03
	Ca	g/kg	0,04	0,12	0,03	0,04	-0,01	0,21
	TOTAL	g/kg	0,08	0,20	0,08	0,08	0,04	0,48
Ch2Wo4	Na	g/kg	0,12	0,13	0,13	0,11	0,15	0,64
	K	g/kg	0,09	0,13	0,10	0,10	0,19	0,61
	Mg	g/kg	0,00	0,03	0,01	0,01	0,07	0,12
	Ca	g/kg	0,06	0,26	0,11	0,07	-0,48	0,01
	TOTAL	g/kg	0,27	0,55	0,35	0,28	-0,07	1,38

DT coarse fraction		concentration of leached element (g/kg)						
leachants		aq. demin.	pH 3,4	pH 7	pH 8	oversat. gypsum sol.	TOTAL	
Ch1Wo1	Na	g/kg	0,02	0,03	0,03	0,00	0,03	0,10
	K	g/kg	0,02	0,04	0,04	0,03	0,09	0,22
	Mg	g/kg	0,00	0,00	0,00	0,00	0,03	0,03
	Ca	g/kg	0,02	0,04	0,05	0,02	-0,12	0,01
	TOTAL	g/kg	0,06	0,11	0,12	0,05	0,03	0,36
Ch1Wo2	Na	g/kg	0,01	0,01	0,01	0,00	0,00	0,01
	K	g/kg	0,01	0,03	0,03	0,02	0,05	0,13
	Mg	g/kg	0,00	0,00	0,00	0,00	0,01	0,01
	Ca	g/kg	-0,01	0,02	0,03	0,01	0,02	0,08
	TOTAL	g/kg	0,01	0,06	0,07	0,02	0,08	0,24
Ch1Wo3	Na	g/kg	0,00	0,00	0,00	0,00	0,00	0,00
	K	g/kg	0,01	0,02	0,02	0,01	0,03	0,09
	Mg	g/kg	0,00	0,00	0,00	0,00	0,01	0,01
	Ca	g/kg	0,00	0,02	0,02	0,00	0,00	0,05
	TOTAL	g/kg	0,02	0,05	0,05	0,01	0,03	0,15
Ch2Wo4	Na	g/kg	0,02	0,03	0,03	0,02	0,03	0,12
	K	g/kg	0,05	0,05	0,04	0,04	0,09	0,26
	Mg	g/kg	0,00	0,00	0,00	0,00	0,02	0,04
	Ca	g/kg	0,08	0,07	0,03	0,05	-0,10	0,14
	TOTAL	g/kg	0,15	0,15	0,10	0,12	0,04	0,56

**Table A7.6** Leachabilities of the individual fractions (% of wt. %) from the Drachenfels trachyte (fine and coarse grain size)

DT fine fraction		Leachability (% of wt. %)						
host rock (wt. %)		aq. demin.	pH 3.4	pH 7	pH 8	oversat. gypsum sol.	TOTAL	
Ch1Wo1	Na	3,29	0,33	0,40	0,36	0,18	0,41	1,67
	K	4,63	0,16	0,29	0,22	0,22	0,41	1,30
	Mg	0,47	0,05	0,63	0,25	0,18	1,57	2,68
	Ca	1,72	0,17	1,66	0,70	0,50	-1,63	1,41
	TOTAL	10,11	0,21	0,57	0,35	0,26	0,12	1,50
Ch1Wo2	Na	3,29	0,09	0,11	0,08	-0,01	0,07	0,34
	K	4,63	0,11	0,17	0,12	0,14	0,15	0,69
	Mg	0,47	0,03	0,40	0,21	0,17	0,49	1,29
	Ca	1,72	0,03	0,99	0,66	0,55	-0,21	2,01
	TOTAL	10,11	0,09	0,30	0,20	0,16	0,08	0,83
Ch1Wo3	Na	3,29	0,04	0,05	0,04	0,03	0,04	0,19
	K	4,63	0,07	0,11	0,06	0,07	0,07	0,39
	Mg	0,47	0,04	0,33	0,08	0,07	0,20	0,72
	Ca	1,72	0,21	0,67	0,20	0,21	-0,08	1,20
	TOTAL	10,11	0,08	0,20	0,08	0,08	0,04	0,48
Ch2Wo4	Na	3,29	0,35	0,41	0,39	0,32	0,46	1,94
	K	4,63	0,19	0,29	0,22	0,21	0,40	1,31
	Mg	0,47	0,10	0,54	0,23	0,18	1,57	2,61
	Ca	1,72	0,34	1,49	0,63	0,42	-2,82	0,06
	TOTAL	10,11	0,27	0,54	0,34	0,28	-0,07	1,36

DT coars fraction		Leachability (% of wt. %)						
host rock (wt. %)		aq. demin.	pH 3.4	pH 7	pH 8	oversat. gypsum sol.	TOTAL	
Ch1Wo1	Na	3,29	0,06	0,08	0,08	0,00	0,09	0,30
	K	4,63	0,05	0,08	0,08	0,05	0,20	0,47
	Mg	0,47	0,02	0,05	0,05	0,02	0,59	0,74
	Ca	1,72	0,09	0,23	0,30	0,12	-0,69	0,04
	TOTAL	10,11	0,06	0,10	0,12	0,05	0,03	0,36
Ch1Wo2	Na	3,29	0,02	0,02	0,02	-0,01	0,01	0,04
	K	4,63	0,03	0,06	0,06	0,04	0,10	0,29
	Mg	0,47	0,00	0,03	0,03	0,01	0,25	0,32
	Ca	1,72	-0,04	0,13	0,19	0,04	0,12	0,45
	TOTAL	10,11	0,01	0,06	0,07	0,02	0,08	0,24
Ch1Wo3	Na	3,29	0,01	0,01	0,01	-0,01	0,00	0,01
	K	4,63	0,03	0,05	0,04	0,03	0,05	0,20
	Mg	0,47	0,01	0,03	0,04	0,01	0,12	0,21
	Ca	1,72	0,01	0,12	0,14	0,02	-0,01	0,28
	TOTAL	10,11	0,02	0,04	0,05	0,01	0,03	0,15
Ch2Wo4	Na	3,29	0,07	0,08	0,08	0,06	0,09	0,38
	K	4,63	0,11	0,10	0,08	0,09	0,20	0,57
	Mg	0,47	0,08	0,08	0,04	0,07	0,50	0,77
	Ca	1,72	0,45	0,43	0,20	0,32	-0,58	0,81
	TOTAL	10,11	0,15	0,15	0,10	0,12	0,04	0,56

**Table A7.7** Concentrations of leached fractions (g/kg) from the Montemerlo trachyte (fine and coarse grain size)

MT fine fraction		concentration of leached element (g/kg)						
leachants		aq. demin.	pH 3,4	pH 7	pH 8	oversat. gypsum sol.	TOTAL	
Ch1Wo1	Na	g/kg	0,08	0,11	0,09	0,06	0,11	0,46
	K	g/kg	0,03	0,05	0,03	0,04	0,08	0,24
	Mg	g/kg	0,01	0,05	0,02	0,01	0,19	0,27
	Ca	g/kg	0,01	0,10	0,03	0,02	-0,34	-0,19
	TOTAL	g/kg	0,12	0,31	0,17	0,14	0,04	0,79
Ch1Wo2	Na	g/kg	0,02	0,03	0,02	0,01	0,03	0,12
	K	g/kg	0,02	0,04	0,02	0,03	0,03	0,13
	Mg	g/kg	0,00	0,03	0,01	0,00	0,05	0,10
	Ca	g/kg	0,02	0,07	0,01	0,01	-0,32	-0,21
	TOTAL	g/kg	0,06	0,18	0,06	0,05	-0,21	0,14
Ch1Wo3	Na	g/kg	0,01	0,02	0,01	0,01	0,01	0,06
	K	g/kg	0,01	0,03	0,01	0,02	0,02	0,09
	Mg	g/kg	0,00	0,03	0,00	0,00	0,02	0,05
	Ca	g/kg	0,00	0,06	0,01	0,00	-0,03	0,04
	TOTAL	g/kg	0,03	0,13	0,04	0,03	0,02	0,25
Ch2Wo4	Na	g/kg	0,10	0,11	0,10	0,10	0,14	0,55
	K	g/kg	0,04	0,05	0,04	0,04	0,09	0,26
	Mg	g/kg	0,01	0,04	0,02	0,02	0,20	0,29
	Ca	g/kg	0,02	0,07	0,04	0,02	-0,47	-0,32
	TOTAL	g/kg	0,17	0,27	0,20	0,18	-0,05	0,78

MT coarse fraction		concentration of leached element (g/kg)						
leachants		aq. demin.	pH 3,4	pH 7	pH 8	oversat. gypsum sol.	TOTAL	
Ch1Wo1	Na	g/kg	0,01	0,02	0,01	0,00	0,01	0,04
	K	g/kg	0,01	0,01	0,01	0,01	0,01	0,04
	Mg	g/kg	0,02	0,03	0,01	0,02	0,10	0,16
	Ca	g/kg	0,07	0,10	0,01	0,06	-0,16	0,09
	TOTAL	g/kg	0,11	0,15	0,03	0,08	-0,04	0,33
Ch1Wo2	Na	g/kg	0,00	0,00	0,00	-0,01	0,00	0,00
	K	g/kg	0,00	0,00	0,00	0,00	0,01	0,02
	Mg	g/kg	0,00	0,01	0,00	0,01	0,03	0,06
	Ca	g/kg	0,00	0,05	0,00	0,03	-0,06	0,01
	TOTAL	g/kg	0,01	0,06	0,01	0,03	-0,02	0,09
Ch1Wo3	Na	g/kg	0,01	0,00	0,00	0,00	0,00	0,01
	K	g/kg	0,00	0,00	0,00	0,00	0,00	0,01
	Mg	g/kg	0,00	0,01	0,00	0,00	0,01	0,02
	Ca	g/kg	0,01	0,03	0,00	0,01	-0,01	0,04
	TOTAL	g/kg	0,03	0,04	0,01	0,01	0,00	0,08
Ch2Wo4	Na	g/kg	0,01	0,01	0,01	0,01	0,02	0,06
	K	g/kg	0,01	0,00	0,00	0,01	0,01	0,03
	Mg	g/kg	0,02	0,01	0,01	0,01	0,10	0,14
	Ca	g/kg	0,08	0,02	0,02	0,02	-0,20	-0,07
	TOTAL	g/kg	0,12	0,04	0,04	0,03	-0,07	0,16

**Table A7.8** Leachabilities of the individual fractions (% of wt. %) from the Montemerlo trachyte (fine and coarse grain size)

MT fine fraction		Leachability (% of wt. %)						
host rock (wt. %)		aq. demin.	pH 3.4	pH 7	pH 8	oversat. gypsum sol.	TOTAL	
Ch1Wo1	Na	3,85	0,21	0,29	0,24	0,16	0,29	1,20
	K	3,93	0,07	0,14	0,09	0,11	0,20	0,60
	Mg	0,66	0,08	0,72	0,28	0,20	2,86	4,14
	Ca	1,52	0,08	0,63	0,19	0,13	-2,26	-1,24
	TOTAL	9,96	0,13	0,31	0,17	0,14	0,04	0,79
Ch1Wo2	Na	3,85	0,06	0,08	0,06	0,03	0,07	0,30
	K	3,93	0,04	0,09	0,05	0,07	0,09	0,34
	Mg	0,66	0,01	0,52	0,11	0,05	0,79	1,49
	Ca	1,52	0,14	0,49	0,08	0,04	-2,11	-1,36
	TOTAL	9,96	0,06	0,18	0,06	0,05	-0,21	0,14
Ch1Wo3	Na	3,85	0,03	0,04	0,03	0,01	0,03	0,15
	K	3,93	0,04	0,07	0,04	0,04	0,05	0,24
	Mg	0,66	0,03	0,41	0,06	0,01	0,28	0,79
	Ca	1,52	0,02	0,39	0,04	0,02	-0,20	0,27
	TOTAL	9,96	0,03	0,13	0,04	0,03	0,02	0,25
Ch2Wo4	Na	3,85	0,25	0,29	0,27	0,26	0,37	1,43
	K	3,93	0,09	0,13	0,11	0,11	0,22	0,65
	Mg	0,66	0,19	0,59	0,33	0,24	3,02	4,36
	Ca	1,52	0,14	0,48	0,24	0,16	-3,12	-2,10
	TOTAL	9,96	0,17	0,27	0,20	0,18	-0,05	0,78

MT coars fraction		Leachability (% of wt. %)						
host rock (wt. %)		aq. demin.	pH 3.4	pH 7	pH 8	oversat. gypsum sol.	TOTAL	
Ch1Wo1	Na	3,85	0,03	0,04	0,02	-0,01	0,03	0,11
	K	3,93	0,02	0,02	0,01	0,02	0,03	0,10
	Mg	0,66	0,31	0,38	0,08	0,24	1,46	2,47
	Ca	1,52	0,47	0,65	0,09	0,39	-1,03	0,58
	TOTAL	9,96	0,11	0,15	0,03	0,08	-0,04	0,34
Ch1Wo2	Na	3,85	0,00	0,01	0,00	-0,02	0,00	-0,01
	K	3,93	0,01	0,01	0,01	0,01	0,01	0,05
	Mg	0,66	0,06	0,17	0,02	0,10	0,50	0,85
	Ca	1,52	0,01	0,32	0,02	0,17	-0,42	0,09
	TOTAL	9,96	0,01	0,07	0,01	0,03	-0,02	0,09
Ch1Wo3	Na	3,85	0,04	0,00	0,00	-0,01	0,00	0,03
	K	3,93	0,01	0,01	0,01	0,01	0,01	0,03
	Mg	0,66	0,04	0,10	0,01	0,03	0,18	0,36
	Ca	1,52	0,06	0,20	0,01	0,05	-0,08	0,24
	TOTAL	9,96	0,03	0,04	0,01	0,01	0,00	0,08
Ch2Wo4	Na	3,85	0,03	0,03	0,03	0,01	0,05	0,15
	K	3,93	0,01	0,01	0,01	0,02	0,03	0,09
	Mg	0,66	0,33	0,08	0,10	0,08	1,54	2,12
	Ca	1,52	0,55	0,10	0,12	0,11	-1,34	-0,46
	TOTAL	9,96	0,12	0,04	0,04	0,03	-0,07	0,16



**Table A7.9** Concentrations of leached fractions (g/kg) from the Obernkirchen sandstone (fine and coarse grain size)

OS fine fraction		concentration of leached element (g/kg)						
leachants		aq. demin.	pH 3,4	pH 7	pH 8	oversat. gypsum sol.	TOTAL	
Ch1Wo1	Na	g/kg	0,01	0,01	0,01	-0,05	0,01	-0,01
	K	g/kg	0,04	0,05	0,03	0,01	0,07	0,21
	Mg	g/kg	0,00	0,01	0,00	0,00	0,01	0,02
	Ca	g/kg	0,01	0,02	0,00	0,00	-0,08	-0,04
	TOTAL	g/kg	0,06	0,10	0,05	-0,03	0,01	0,18
Ch1Wo2	Na	g/kg	0,00	0,00	0,00	-0,01	0,00	-0,01
	K	g/kg	0,02	0,02	0,01	0,01	0,02	0,08
	Mg	g/kg	0,00	0,00	0,00	0,00	0,00	0,00
	Ca	g/kg	-0,04	0,01	0,00	0,00	0,04	0,01
	TOTAL	g/kg	-0,03	0,04	0,02	0,01	0,05	0,08
Ch1Wo3	Na	g/kg	0,00	0,00	0,00	0,00	0,00	0,00
	K	g/kg	0,01	0,01	0,01	0,01	0,02	0,06
	Mg	g/kg	0,00	0,00	0,00	0,00	0,00	0,00
	Ca	g/kg	0,00	0,00	0,00	0,00	-0,02	-0,01
	TOTAL	g/kg	0,01	0,02	0,01	0,01	0,01	0,05
Ch2Wo4	Na	g/kg	0,01	0,02	0,01	0,00	0,02	0,06
	K	g/kg	0,04	0,04	0,04	0,02	0,07	0,21
	Mg	g/kg	0,00	0,00	0,00	0,00	0,01	0,01
	Ca	g/kg	0,00	0,00	0,00	0,00	-0,20	-0,19
	TOTAL	g/kg	0,05	0,06	0,05	0,02	-0,10	0,09

OS coarse fraction		concentration of leached element (g/kg)						
leachants		aq. demin.	pH 3,4	pH 7	pH 8	oversat. gypsum sol.	TOTAL	
Ch1Wo1	Na	g/kg	0,01	0,01	0,00	-0,01	0,00	0,01
	K	g/kg	0,01	0,01	0,01	0,01	0,01	0,05
	Mg	g/kg	0,00	0,00	0,00	0,00	0,01	0,01
	Ca	g/kg	0,00	0,00	0,00	0,00	-0,01	-0,01
	TOTAL	g/kg	0,02	0,02	0,01	0,00	0,01	0,07
Ch1Wo2	Na	g/kg	0,00	0,00	0,00	-0,01	0,00	0,00
	K	g/kg	0,00	0,01	0,00	0,00	0,01	0,02
	Mg	g/kg	0,00	0,00	0,00	0,00	0,00	0,00
	Ca	g/kg	0,00	0,01	0,00	0,00	-0,01	0,00
	TOTAL	g/kg	0,00	0,01	0,01	0,00	0,00	0,02
Ch1Wo3	Na	g/kg	0,00	0,00	0,00	0,00	0,00	0,00
	K	g/kg	0,00	0,00	0,00	0,00	0,00	0,01
	Mg	g/kg	0,00	0,00	0,00	0,00	0,00	0,00
	Ca	g/kg	0,00	0,00	0,00	0,00	0,13	0,13
	TOTAL	g/kg	0,00	0,00	0,00	0,00	0,13	0,13
Ch2Wo4	Na	g/kg	0,01	0,01	0,01	0,00	0,00	0,03
	K	g/kg	0,01	0,01	0,01	0,00	0,00	0,04
	Mg	g/kg	0,00	0,00	0,00	0,00	0,01	0,01
	Ca	g/kg	0,00	0,00	0,00	0,00	-0,01	-0,01
	TOTAL	g/kg	0,02	0,02	0,02	0,01	0,00	0,06

**Table A7.10** Leachabilities of the individual fractions (% of wt. %) from the Obernkirchen sandstone (fine and coarse grain size)

OS fine fraction		Leachability (% of wt. %)						
host rock (wt. %)		aq. demin.	pH 3.4	pH 7	pH 8	oversat. gypsum sol.	TOTAL	
Ch1Wo1	Na	0,59	0,15	0,24	0,21	-0,85	0,15	-0,10
	K	0,14	2,62	3,88	2,46	1,05	4,72	14,74
	Mg	0,03	0,37	2,14	0,27	0,00	4,21	7,00
	Ca	0,02	4,30	11,48	0,98	0,40	-35,78	-18,61
	TOTAL	0,79	0,72	1,27	0,64	-0,44	0,14	2,33
Ch1Wo2	Na	0,59	0,00	0,05	0,03	-0,13	-0,08	-0,12
	K	0,14	1,20	1,28	1,03	0,87	1,07	5,46
	Mg	0,03	-0,42	1,19	0,27	0,00	0,34	1,39
	Ca	0,02	-20,46	4,84	0,38	0,40	17,33	2,50
	TOTAL	0,79	-0,36	0,45	0,23	0,07	0,62	1,01
Ch1Wo3	Na	0,59	0,00	0,02	0,03	-0,01	-0,01	0,03
	K	0,14	0,69	0,61	0,51	0,50	1,70	4,01
	Mg	0,03	0,00	0,49	0,14	0,00	0,15	0,77
	Ca	0,02	-0,36	1,94	0,31	0,22	-8,12	-6,01
	TOTAL	0,79	0,11	0,19	0,13	0,09	0,08	0,61
Ch2Wo4	Na	0,59	0,17	0,27	0,24	0,04	0,27	0,99
	K	0,14	2,80	3,17	2,68	1,45	4,71	14,82
	Mg	0,03	0,27	0,12	0,28	0,26	4,00	4,94
	Ca	0,02	0,12	0,71	0,04	0,04	-91,35	-90,44
	TOTAL	0,79	0,64	0,80	0,68	0,30	-1,29	1,13

OS coars fraction		Leachability (% of wt. %)						
host rock (wt. %)		aq. demin.	pH 3.4	pH 7	pH 8	oversat. gypsum sol.	TOTAL	
Ch1Wo1	Na	0,59	0,09	0,15	0,07	-0,15	0,04	0,20
	K	0,14	0,92	1,03	0,47	0,39	0,86	3,67
	Mg	0,03	0,09	0,09	0,09	0,09	2,31	2,67
	Ca	0,02	0,50	0,32	0,19	0,27	-4,11	-2,82
	TOTAL	0,79	0,25	0,31	0,15	-0,03	0,16	0,83
Ch1Wo2	Na	0,59	0,01	0,02	0,01	-0,13	0,02	-0,07
	K	0,14	0,34	0,37	0,19	0,20	0,42	1,53
	Mg	0,03	-0,04	0,11	0,09	0,09	0,23	0,47
	Ca	0,02	-0,10	2,39	0,77	0,18	-2,99	0,24
	TOTAL	0,79	0,06	0,15	0,07	-0,06	0,02	0,24
Ch1Wo3	Na	0,59	-0,01	0,01	0,00	-0,05	0,00	-0,05
	K	0,14	0,18	0,23	0,11	0,10	0,05	0,66
	Mg	0,03	0,00	0,00	0,00	0,00	0,06	0,06
	Ca	0,02	-0,15	-0,14	0,06	0,07	58,80	58,65
	TOTAL	0,79	0,02	0,04	0,02	-0,02	1,62	1,69
Ch2Wo4	Na	0,59	0,11	0,13	0,15	0,03	0,08	0,50
	K	0,14	0,78	0,64	0,70	0,29	0,25	2,66
	Mg	0,03	0,09	0,01	0,09	0,09	2,31	2,58
	Ca	0,02	0,01	0,01	0,01	0,01	-5,33	-5,28
	TOTAL	0,79	0,23	0,21	0,24	0,08	0,05	0,81

**Table A7.11** Concentrations of leached fractions (g/kg) from the Bozanov sandstone (fine and coarse grain size)

BS fine fraction		concentration of leached element (g/kg)						
leachants		aq. demin.	pH 3,4	pH 7	pH 8	oversat. gypsum sol.	TOTAL	
Ch1Wo1	Na	g/kg	0.01	0.01	0.00	-0.07	0.00	-0.05
	K	g/kg	0.03	0.06	0.03	0.01	0.11	0.25
	Mg	g/kg	0.00	0.01	0.00	0.00	0.09	0.10
	Ca	g/kg	0.00	0.03	0.00	0.00	-0.27	-0.24
	TOTAL	g/kg	0.05	0.11	0.03	-0.06	-0.07	0.06
Ch1Wo2	Na	g/kg	0.00	0.00	0.00	-0.03	0.00	-0.03
	K	g/kg	0.02	0.03	0.02	0.01	0.03	0.11
	Mg	g/kg	0.00	0.01	0.00	0.00	0.01	0.02
	Ca	g/kg	-0.02	0.02	0.00	0.00	-0.02	-0.02
	TOTAL	g/kg	0.00	0.07	0.02	-0.01	0.02	0.08
Ch1Wo3	Na	g/kg	0.00	0.00	0.00	-0.01	0.00	0.00
	K	g/kg	0.02	0.02	0.01	0.01	0.01	0.07
	Mg	g/kg	0.00	0.01	0.00	0.00	0.00	0.01
	Ca	g/kg	0.00	0.01	0.00	0.00	0.06	0.07
	TOTAL	g/kg	0.02	0.04	0.01	0.01	0.07	0.15
Ch2Wo4	Na	g/kg	0.00	0.00	0.00	-0.03	0.01	-0.01
	K	g/kg	0.04	0.05	0.03	0.02	0.11	0.26
	Mg	g/kg	0.00	0.00	0.00	0.00	0.08	0.09
	Ca	g/kg	0.00	0.00	0.00	0.00	-0.46	-0.45
	TOTAL	g/kg	0.05	0.06	0.04	-0.01	-0.25	-0.12

BS coarse fraction		concentration of leached element (g/kg)						
leachants		aq. demin.	pH 3,4	pH 7	pH 8	oversat. gypsum sol.	TOTAL	
Ch1Wo1	Na	g/kg	0.00	0.01	0.00	-0.05	0.00	-0.04
	K	g/kg	0.00	0.01	0.00	0.00	0.01	0.02
	Mg	g/kg	0.00	0.00	0.00	0.00	0.04	0.04
	Ca	g/kg	0.00	0.00	0.00	0.00	-0.11	-0.10
	TOTAL	g/kg	0.01	0.02	0.00	-0.05	-0.06	-0.08
Ch1Wo2	Na	g/kg	0.00	0.00	0.00	-0.04	0.00	-0.05
	K	g/kg	0.00	0.00	0.00	0.00	0.00	0.01
	Mg	g/kg	0.00	0.00	0.00	0.00	0.01	0.01
	Ca	g/kg	-0.01	0.00	0.00	0.00	0.01	0.00
	TOTAL	g/kg	-0.01	0.00	0.00	-0.04	0.02	-0.03
Ch1Wo3	Na	g/kg	0.00	0.00	0.00	-0.03	0.00	-0.03
	K	g/kg	0.00	0.00	0.00	0.00	0.00	0.00
	Mg	g/kg	0.00	0.00	0.00	0.00	0.00	0.00
	Ca	g/kg	0.00	0.00	0.00	0.00	0.03	0.03
	TOTAL	g/kg	0.00	0.00	0.00	-0.03	0.04	0.01
Ch2Wo4	Na	g/kg	0.00	0.00	0.00	-0.03	0.00	-0.03
	K	g/kg	0.00	0.00	0.00	0.00	0.01	0.02
	Mg	g/kg	0.00	0.00	0.00	0.00	0.04	0.04
	Ca	g/kg	0.00	0.00	0.00	0.00	-0.10	-0.10
	TOTAL	g/kg	0.00	0.00	0.00	-0.03	-0.05	-0.08

**Table A7.12** Leachabilities of the individual fractions (% of wt. %) from the Bozanov sandstone (fine and coarse grain size)

BS fine fraction		Leachability (% of wt. %)						
host rock (wt. %)		aq. demin.	pH 3.4	pH 7	pH 8	oversat. gypsum sol.	TOTAL	
Ch1Wo1	Na	0.24	0.33	0.27	0.16	-3.02	0.12	-2.13
	K	1.34	0.26	0.48	0.21	0.10	0.81	1.86
	Mg	0.05	0.20	2.16	0.13	0.13	16.52	19.14
	Ca	0.06	0.27	4.15	0.18	0.11	-42.10	-37.39
	TOTAL	1.71	0.27	0.64	0.20	-0.35	-0.40	0.36
Ch1Wo2	Na	0.24	0.00	0.10	-0.02	-1.20	-0.13	-1.26
	K	1.34	0.14	0.26	0.12	0.10	0.23	0.85
	Mg	0.05	-0.21	1.23	0.13	0.13	2.17	3.45
	Ca	0.06	-3.40	3.45	0.11	0.11	-3.37	-3.10
	TOTAL	1.71	-0.03	0.39	0.10	-0.08	0.11	0.48
Ch1Wo3	Na	0.24	0.00	0.03	0.02	-0.22	0.00	-0.17
	K	1.34	0.12	0.16	0.08	0.08	0.09	0.53
	Mg	0.05	0.00	1.01	0.06	0.00	0.50	1.57
	Ca	0.06	-0.08	1.82	0.11	0.08	9.19	11.13
	TOTAL	1.71	0.10	0.23	0.07	0.03	0.43	0.86
Ch2Wo4	Na	0.24	0.15	0.20	0.16	-1.22	0.47	-0.24
	K	1.34	0.30	0.39	0.24	0.14	0.84	1.91
	Mg	0.05	0.19	0.12	0.15	0.15	15.10	15.72
	Ca	0.06	0.07	0.16	0.01	0.01	-70.79	-70.53
	TOTAL	1.71	0.27	0.34	0.22	-0.06	-1.46	-0.69

BS coars fraction		Leachability (% of wt. %)						
host rock (wt. %)		aq. demin.	pH 3.4	pH 7	pH 8	oversat. gypsum sol.	TOTAL	
Ch1Wo1	Na	0.24	0.10	0.24	0.03	-2.01	0.09	-1.56
	K	1.34	0.02	0.04	0.02	0.00	0.09	0.17
	Mg	0.05	0.07	0.19	0.05	0.00	7.06	7.37
	Ca	0.06	0.68	0.66	0.12	0.00	-17.29	-15.83
	TOTAL	1.71	0.06	0.10	0.03	-0.29	-0.35	-0.45
Ch1Wo2	Na	0.24	0.00	-0.02	-0.13	-1.78	-0.06	-1.98
	K	1.34	0.01	0.01	0.00	0.00	0.02	0.05
	Mg	0.05	-0.06	0.00	0.00	0.00	1.49	1.43
	Ca	0.06	-1.27	-0.01	0.04	0.04	1.49	0.29
	TOTAL	1.71	-0.04	0.01	-0.01	-0.25	0.11	-0.19
Ch1Wo3	Na	0.24	0.00	-0.03	-0.13	-1.11	0.00	-1.27
	K	1.34	0.00	0.01	0.00	0.00	0.01	0.02
	Mg	0.05	0.00	0.02	0.00	0.00	0.39	0.42
	Ca	0.06	-0.05	-0.01	0.02	0.05	5.15	5.17
	TOTAL	1.71	0.00	0.00	-0.02	-0.16	0.21	0.04
Ch2Wo4	Na	0.24	0.02	-0.07	0.01	-1.28	0.13	-1.18
	K	1.34	0.01	0.01	0.01	0.00	0.08	0.12
	Mg	0.05	0.05	0.00	0.05	0.05	6.92	7.07
	Ca	0.06	0.00	0.00	0.00	0.00	-15.63	-15.61
	TOTAL	1.71	0.02	0.00	0.02	-0.18	-0.29	-0.44

**Table A7.13** Concentrations of leached fractions (g/kg) from the Stenzelberg latite (fine and coarse grain size)

SL fine fraction		concentration of leached element (g/kg)						
leachants		aq. demin.	pH 3,4	pH 7	pH 8	oversat. gypsum sol.	TOTAL	
Ch1Wo1	Na	g/kg	0.13	0.18	0.16	0.08	0.20	0.75
	K	g/kg	0.03	0.07	0.05	0.04	0.12	0.31
	Mg	g/kg	0.00	0.03	0.01	0.00	0.19	0.23
	Ca	g/kg	0.01	0.09	0.03	0.01	-0.74	-0.60
	TOTAL	g/kg	0.17	0.36	0.24	0.13	-0.23	0.68
Ch1Wo2	Na	g/kg	0.03	0.05	0.05	0.01	0.04	0.18
	K	g/kg	0.02	0.04	0.03	0.02	0.06	0.17
	Mg	g/kg	0.00	0.01	0.00	0.00	0.07	0.09
	Ca	g/kg	-0.04	0.04	0.01	0.00	-0.27	-0.26
	TOTAL	g/kg	0.01	0.14	0.09	0.04	-0.10	0.18
Ch1Wo3	Na	g/kg	0.03	0.02	0.03	0.00	0.02	0.11
	K	g/kg	0.02	0.03	0.02	0.02	0.03	0.12
	Mg	g/kg	0.00	0.01	0.01	0.00	0.03	0.05
	Ca	g/kg	0.01	0.03	0.01	0.00	-0.01	0.04
	TOTAL	g/kg	0.07	0.09	0.07	0.02	0.08	0.32
Ch2Wo4	Na	g/kg	0.17	0.19	0.18	0.14	0.22	0.90
	K	g/kg	0.05	0.07	0.06	0.05	0.14	0.36
	Mg	g/kg	0.01	0.02	0.01	0.01	0.20	0.26
	Ca	g/kg	0.02	0.07	0.04	0.02	-0.65	-0.50
	TOTAL	g/kg	0.25	0.35	0.28	0.23	-0.09	1.01

SL coarse fraction		concentration of leached element (g/kg)						
leachants		aq. demin.	pH 3,4	pH 7	pH 8	oversat. gypsum sol.	TOTAL	
Ch1Wo1	Na	g/kg	0.05	0.05	0.06	0.02	0.07	0.26
	K	g/kg	0.01	0.01	0.01	0.01	0.03	0.07
	Mg	g/kg	0.00	0.00	0.00	0.00	0.10	0.11
	Ca	g/kg	0.02	0.02	0.01	0.01	-0.23	-0.17
	TOTAL	g/kg	0.08	0.08	0.08	0.04	-0.03	0.26
Ch1Wo2	Na	g/kg	0.01	0.01	0.01	-0.01	0.01	0.01
	K	g/kg	0.00	0.00	0.00	0.00	0.02	0.03
	Mg	g/kg	0.00	0.00	0.00	0.00	0.05	0.05
	Ca	g/kg	0.00	0.00	0.00	0.00	-0.06	-0.06
	TOTAL	g/kg	0.00	0.01	0.01	-0.01	0.01	0.03
Ch1Wo3	Na	g/kg	0.00	0.01	0.00	-0.01	0.00	0.01
	K	g/kg	0.00	0.00	0.00	0.00	0.01	0.02
	Mg	g/kg	0.00	0.00	0.00	0.00	0.03	0.03
	Ca	g/kg	0.00	0.00	0.00	0.00	-0.02	-0.02
	TOTAL	g/kg	0.01	0.01	0.01	-0.01	0.01	0.03
Ch2Wo4	Na	g/kg	0.05	0.06	0.05	0.05	0.08	0.29
	K	g/kg	0.01	0.01	0.01	0.01	0.03	0.07
	Mg	g/kg	0.01	0.01	0.00	0.01	0.11	0.13
	Ca	g/kg	0.02	0.02	0.01	0.02	-0.28	-0.21
	TOTAL	g/kg	0.09	0.10	0.07	0.09	-0.06	0.29

**Table A7.14** Leachabilities of the individual fractions (% of wt. %) from the Stenzelberg latite (fine and coarse grain size)

SL fine fraction		Leachability (% of wt. %)						
host rock (wt. %)		aq. demin.	pH 3.4	pH 7	pH 8	oversat. gypsum sol.	TOTAL	
Ch1Wo1	Na	3.09	0.42	0.59	0.51	0.27	0.64	2.42
	K	3.36	0.10	0.20	0.14	0.12	0.37	0.92
	Mg	0.89	0.04	0.31	0.10	0.04	2.10	2.59
	Ca	3.54	0.03	0.25	0.07	0.03	-2.08	-1.70
	TOTAL	10.88	0.16	0.33	0.22	0.12	-0.21	0.63
Ch1Wo2	Na	3.09	0.11	0.16	0.16	0.02	0.14	0.59
	K	3.36	0.05	0.11	0.09	0.07	0.18	0.49
	Mg	0.89	-0.01	0.15	0.05	0.01	0.79	0.99
	Ca	3.54	-0.11	0.12	0.03	0.01	-0.77	-0.73
	TOTAL	10.88	0.01	0.13	0.09	0.03	-0.09	0.17
Ch1Wo3	Na	3.09	0.11	0.07	0.10	0.02	0.07	0.37
	K	3.36	0.07	0.08	0.07	0.05	0.09	0.36
	Mg	0.89	0.04	0.11	0.07	0.00	0.37	0.59
	Ca	3.54	0.02	0.08	0.03	0.01	-0.03	0.10
	TOTAL	10.88	0.06	0.08	0.07	0.02	0.07	0.30
Ch2Wo4	Na	3.09	0.54	0.62	0.57	0.46	0.72	2.91
	K	3.36	0.15	0.20	0.16	0.15	0.40	1.07
	Mg	0.89	0.11	0.24	0.15	0.11	2.28	2.88
	Ca	3.54	0.07	0.19	0.11	0.07	-1.85	-1.42
	TOTAL	10.88	0.23	0.32	0.26	0.21	-0.09	0.93

SL coars fraction		Leachability (% of wt. %)						
host rock (wt. %)		aq. demin.	pH 3.4	pH 7	pH 8	oversat. gypsum sol.	TOTAL	
Ch1Wo1	Na	3.09	0.17	0.17	0.18	0.07	0.23	0.83
	K	3.36	0.03	0.03	0.03	0.03	0.09	0.20
	Mg	0.89	0.04	0.05	0.03	0.03	1.14	1.29
	Ca	3.54	0.05	0.05	0.04	0.03	-0.66	-0.49
	TOTAL	10.88	0.08	0.08	0.08	0.04	-0.03	0.24
Ch1Wo2	Na	3.09	0.02	0.03	0.02	-0.05	0.02	0.05
	K	3.36	0.00	0.01	0.01	0.01	0.05	0.08
	Mg	0.89	-0.01	0.00	0.00	0.00	0.57	0.56
	Ca	3.54	-0.01	0.00	0.00	0.00	-0.17	-0.18
	TOTAL	10.88	0.00	0.01	0.01	-0.01	0.01	0.03
Ch1Wo3	Na	3.09	0.02	0.02	0.01	-0.03	0.01	0.02
	K	3.36	0.00	0.01	0.00	0.01	0.03	0.05
	Mg	0.89	0.00	0.00	0.00	0.00	0.30	0.30
	Ca	3.54	0.00	0.00	0.00	0.00	-0.07	-0.07
	TOTAL	10.88	0.01	0.01	0.01	-0.01	0.01	0.02
Ch2Wo4	Na	3.09	0.18	0.20	0.16	0.16	0.25	0.95
	K	3.36	0.03	0.03	0.02	0.04	0.10	0.22
	Mg	0.89	0.06	0.06	0.03	0.07	1.26	1.47
	Ca	3.54	0.05	0.06	0.02	0.07	-0.80	-0.60
	TOTAL	10.88	0.08	0.09	0.06	0.08	-0.05	0.26

**Table A7.15** Concentrations of leached fractions (g/kg) from the Londorf basalt lava (fine and coarse grain size)

LB fine fraction		concentration of leached element (g/kg)						
leachants		aq. demin.	pH 3,4	pH 7	pH 8	oversat. gypsum sol.	TOTAL	
Ch1Wo1	Na	g/kg	0.07	0.10	0.09	0.04	0.11	0.41
	K	g/kg	0.01	0.02	0.02	0.02	0.04	0.11
	Mg	g/kg	0.01	0.08	0.04	0.03	0.27	0.42
	Ca	g/kg	0.02	0.14	0.06	0.04	-0.53	-0.28
	TOTAL	g/kg	0.11	0.34	0.20	0.12	-0.11	0.66
Ch1Wo2	Na	g/kg	0.03	0.03	0.02	0.01	0.02	0.12
	K	g/kg	0.01	0.01	0.01	0.01	0.02	0.06
	Mg	g/kg	0.00	0.07	0.02	0.01	0.08	0.19
	Ca	g/kg	-0.04	0.10	0.03	0.02	-0.14	-0.03
	TOTAL	g/kg	0.00	0.21	0.09	0.06	-0.02	0.34
Ch1Wo3	Na	g/kg	0.02	0.02	0.02	0.01	0.01	0.07
	K	g/kg	0.01	0.01	0.01	0.01	0.01	0.04
	Mg	g/kg	0.01	0.06	0.01	0.00	0.04	0.12
	Ca	g/kg	0.01	0.09	0.02	0.01	-0.17	-0.04
	TOTAL	g/kg	0.05	0.18	0.05	0.04	-0.11	0.20
Ch2Wo4	Na	g/kg	0.10	0.11	0.11	0.08	0.13	0.53
	K	g/kg	0.01	0.02	0.02	0.02	0.04	0.11
	Mg	g/kg	0.02	0.09	0.04	0.03	0.26	0.44
	Ca	g/kg	0.02	0.13	0.06	0.04	-0.70	-0.44
	TOTAL	g/kg	0.15	0.36	0.23	0.16	-0.27	0.64

LB coarse fraction		concentration of leached element (g/kg)						
leachants		aq. demin.	pH 3,4	pH 7	pH 8	oversat. gypsum sol.	TOTAL	
Ch1Wo1	Na	g/kg	0.00	0.01	0.00	-0.02	0.01	0.00
	K	g/kg	0.00	0.00	0.00	0.00	0.01	0.01
	Mg	g/kg	0.00	0.01	0.01	0.01	0.16	0.19
	Ca	g/kg	0.01	0.02	0.01	0.01	-0.27	-0.22
	TOTAL	g/kg	0.02	0.04	0.02	0.00	-0.10	-0.01
Ch1Wo2	Na	g/kg	0.00	0.00	0.00	-0.01	0.00	-0.01
	K	g/kg	0.00	0.00	0.00	0.00	0.01	0.01
	Mg	g/kg	0.00	0.01	0.00	0.00	0.07	0.08
	Ca	g/kg	0.00	0.01	0.00	0.00	-0.10	-0.08
	TOTAL	g/kg	0.00	0.02	0.01	-0.01	-0.03	0.00
Ch1Wo3	Na	g/kg	0.00	0.00	0.00	-0.01	0.00	0.00
	K	g/kg	0.00	0.00	0.00	0.00	0.00	0.01
	Mg	g/kg	0.00	0.00	0.00	0.00	0.03	0.04
	Ca	g/kg	0.00	0.01	0.00	0.00	-0.04	-0.03
	TOTAL	g/kg	0.00	0.02	0.01	0.00	-0.01	0.01
Ch2Wo4	Na	g/kg	0.01	0.01	0.01	0.00	0.01	0.03
	K	g/kg	0.00	0.00	0.00	0.00	0.01	0.02
	Mg	g/kg	0.01	0.01	0.01	0.01	0.17	0.20
	Ca	g/kg	0.01	0.02	0.01	0.01	-0.27	-0.22
	TOTAL	g/kg	0.02	0.04	0.03	0.02	-0.08	0.02

**Table A7.16** Leachabilities of the individual fractions (% of wt. %) from the Londorf basalt lava (fine and coarse grain size)

LB fine fraction		Leachability (% of wt. %)						
host rock (wt. %)		aq. demin.	pH 3.4	pH 7	pH 8	oversat. gypsum sol.	TOTAL	
Ch1Wo1	Na	2.45	0.29	0.40	0.36	0.16	0.46	1.67
	K	1.10	0.10	0.19	0.15	0.17	0.35	0.96
	Mg	4.94	0.01	0.16	0.07	0.05	0.55	0.85
	Ca	5.88	0.04	0.23	0.10	0.06	-0.90	-0.47
	TOTAL	14.37	0.08	0.24	0.14	0.08	-0.08	0.46
Ch1Wo2	Na	2.45	0.11	0.13	0.10	0.06	0.08	0.47
	K	1.10	0.07	0.13	0.09	0.12	0.16	0.57
	Mg	4.94	0.00	0.14	0.05	0.02	0.16	0.38
	Ca	5.88	-0.06	0.17	0.05	0.03	-0.23	-0.04
	TOTAL	14.37	0.00	0.15	0.06	0.04	-0.01	0.24
Ch1Wo3	Na	2.45	0.06	0.07	0.07	0.06	0.05	0.30
	K	1.10	0.06	0.11	0.06	0.07	0.07	0.38
	Mg	4.94	0.02	0.12	0.03	0.01	0.07	0.25
	Ca	5.88	0.02	0.15	0.03	0.02	-0.29	-0.07
	TOTAL	14.37	0.03	0.12	0.04	0.03	-0.08	0.14
Ch2Wo4	Na	2.45	0.40	0.45	0.45	0.34	0.53	2.18
	K	1.10	0.13	0.20	0.16	0.15	0.33	0.97
	Mg	4.94	0.03	0.19	0.08	0.05	0.53	0.88
	Ca	5.88	0.04	0.23	0.11	0.07	-1.19	-0.75
	TOTAL	14.37	0.11	0.25	0.16	0.11	-0.19	0.44

LB coars fraction		Leachability (% of wt. %)						
host rock (wt. %)		aq. demin.	pH 3.4	pH 7	pH 8	oversat. gypsum sol.	TOTAL	
Ch1Wo1	Na	2.45	0.01	0.02	0.02	-0.08	0.03	0.01
	K	1.10	0.01	0.02	0.01	0.02	0.08	0.14
	Mg	4.94	0.01	0.02	0.01	0.02	0.33	0.39
	Ca	5.88	0.02	0.04	0.02	0.02	-0.47	-0.37
	TOTAL	14.37	0.01	0.03	0.01	0.00	-0.07	-0.01
Ch1Wo2	Na	2.45	0.00	0.01	0.00	-0.05	0.00	-0.04
	K	1.10	0.01	0.01	0.01	0.01	0.05	0.09
	Mg	4.94	0.00	0.01	0.00	0.00	0.14	0.16
	Ca	5.88	0.00	0.02	0.01	0.01	-0.17	-0.14
	TOTAL	14.37	0.00	0.02	0.01	0.00	-0.02	0.00
Ch1Wo3	Na	2.45	0.00	0.00	0.01	-0.02	0.00	-0.01
	K	1.10	0.01	0.01	0.01	0.01	0.03	0.07
	Mg	4.94	0.00	0.01	0.00	0.00	0.06	0.08
	Ca	5.88	0.00	0.01	0.00	0.00	-0.07	-0.05
	TOTAL	14.37	0.00	0.01	0.00	0.00	-0.01	0.01
Ch2Wo4	Na	2.45	0.03	0.03	0.03	-0.02	0.05	0.12
	K	1.10	0.01	0.02	0.02	0.01	0.08	0.14
	Mg	4.94	0.01	0.02	0.02	0.01	0.34	0.40
	Ca	5.88	0.02	0.03	0.02	0.02	-0.46	-0.37
	TOTAL	14.37	0.02	0.03	0.02	0.01	-0.06	0.02

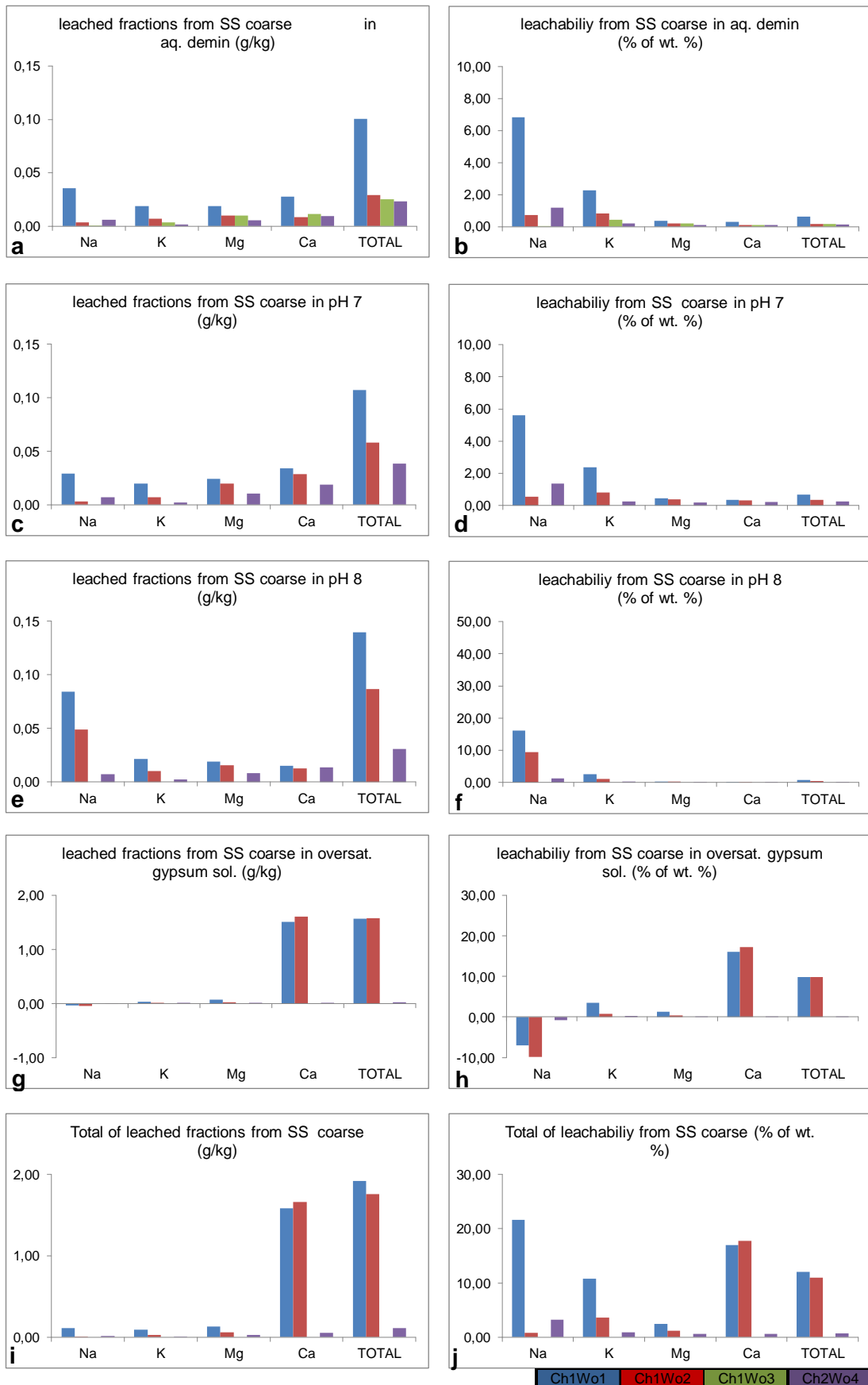


**Figure A7.1** Leachabilities of the individual leached fractions (% of wt. %) from the Schlaitdorf sandstone (coarse grain size) (please note the different scales).

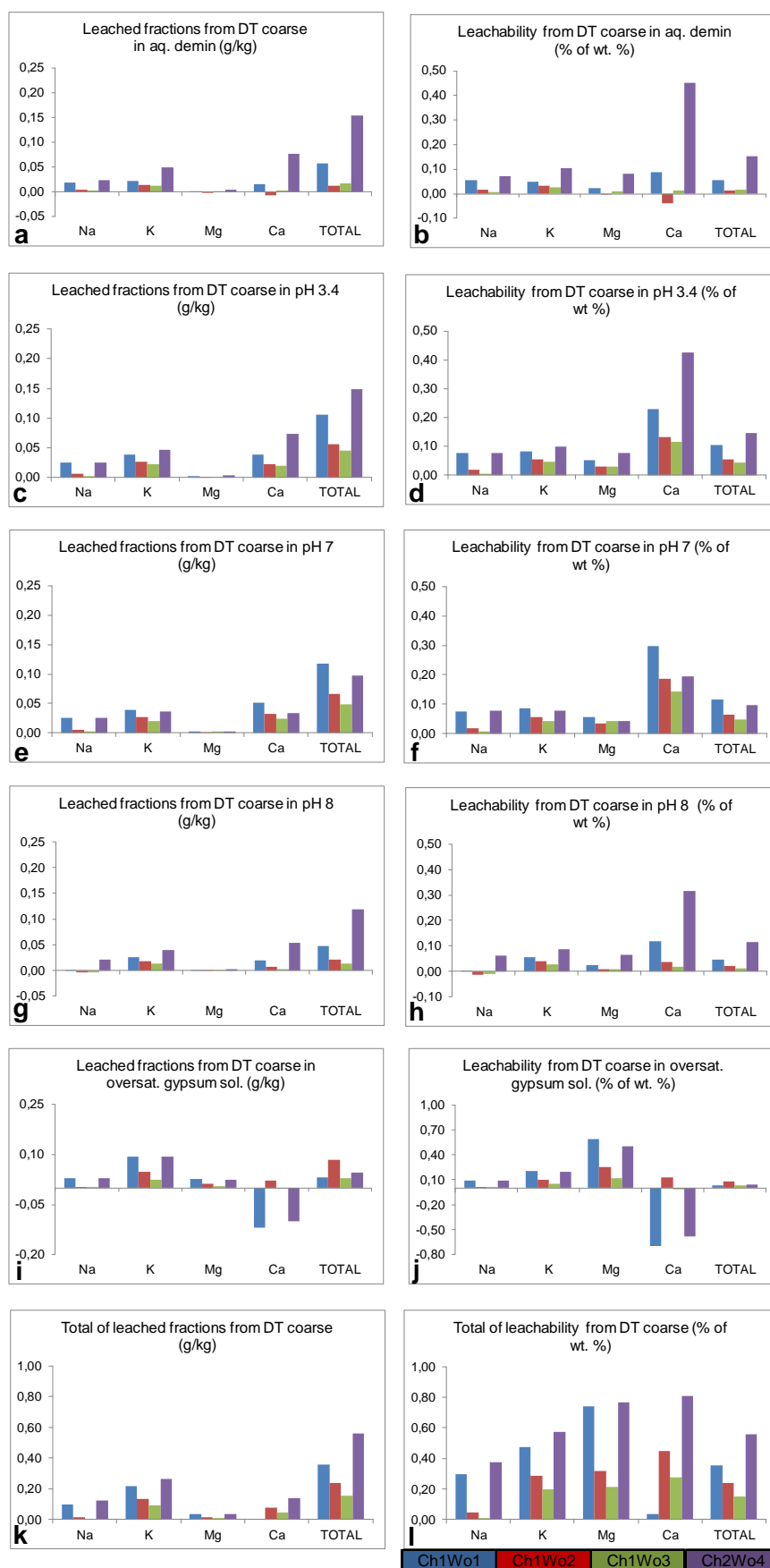


**Figure A7.2** Leachabilities of the individual leached fractions (% of wt. %) from the Drachenfels trachyte (coarse grain size) (please note the different scales).

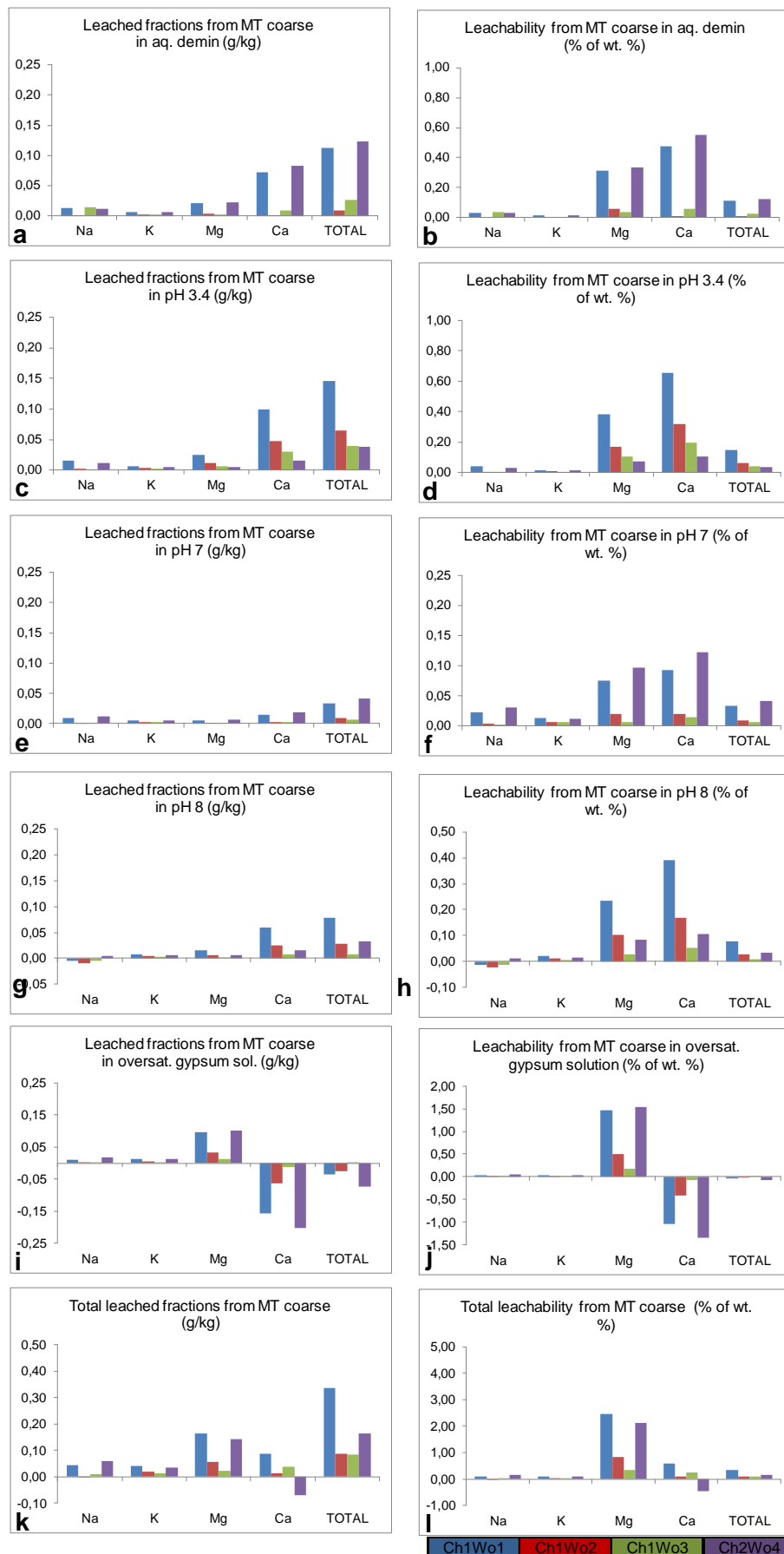


**Figure A7.3** Leachabilities of the individual leached fractions (% of wt. %) from the Montemerlo trachyte (coarse grain size) (please note the different scales).

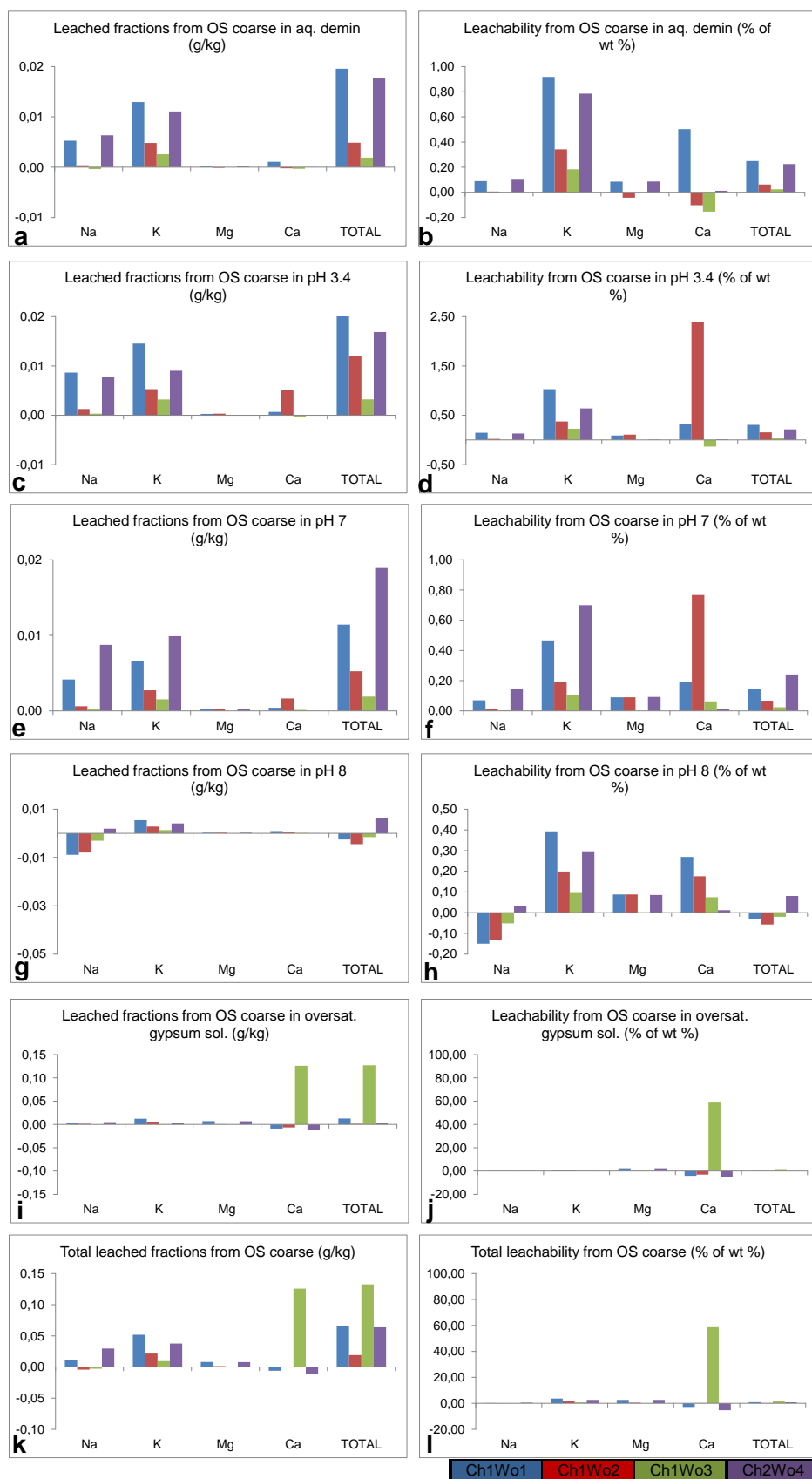


**Figure A7.4** Leachabilities of the individual leached fractions (% of wt. %) from the Obernkirchen sandstone (coarse grain size) (please note the different scales).



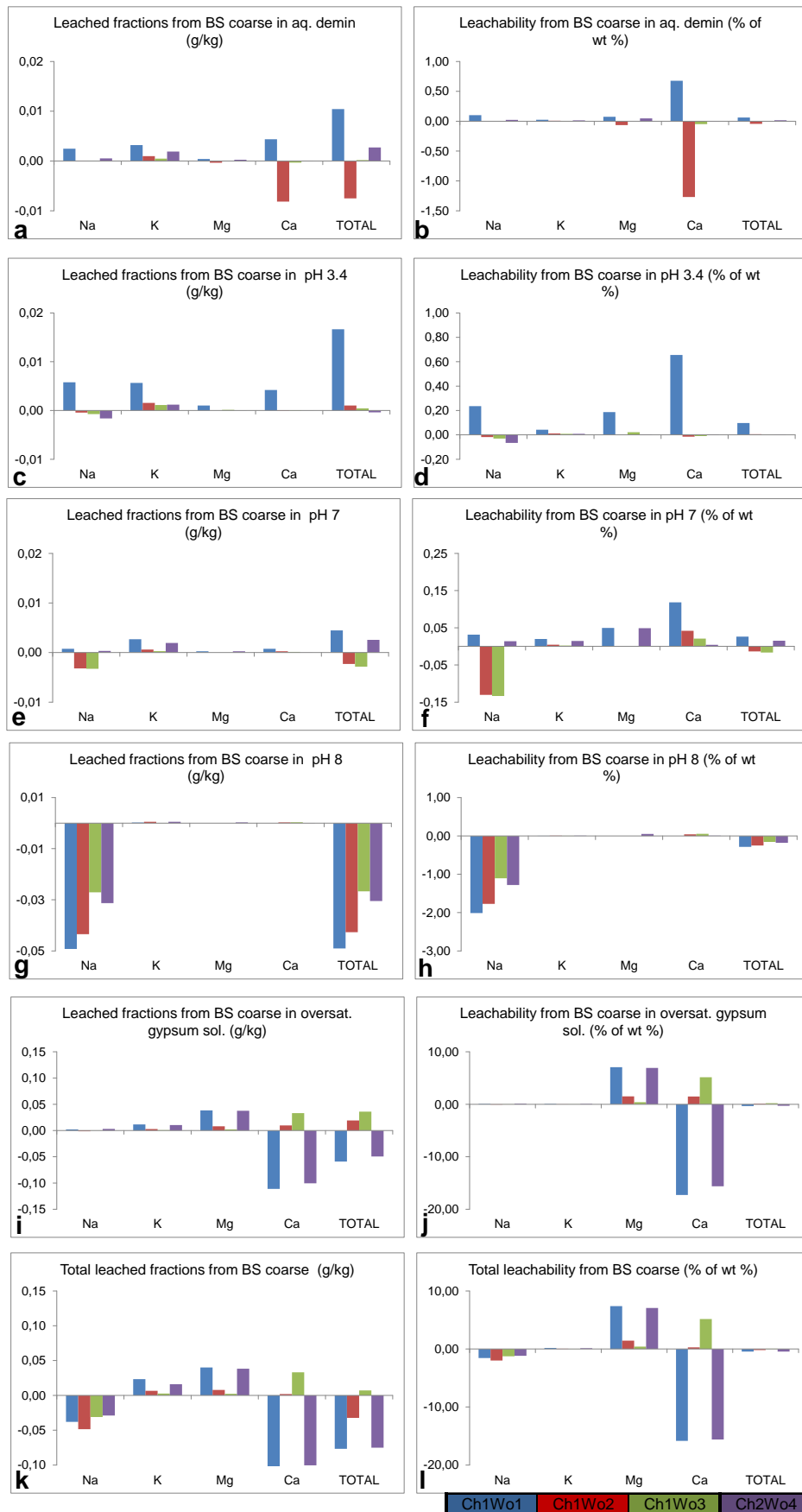


**Figure A7.5** Leachabilities of the individual leached fractions (% of wt. %) from the Bozanov sandstone (coarse grain size) (please note the different scales).

**Table A8.1** Index of analyzed samples

sample code	cathedral	stone	descripton
DT-1	-	Drachenfels trachyte	host rock
DT-2	-	Drachenfels trachyte	host rock
DT-3	-	Drachenfels trachyte	host rock
DT-4	-	Drachenfels trachyte	host rock
DT-5	-	Drachenfels trachyte	host rock
AL-01	Altenberg	Drachenfels trachyte	laminar crust
AL-02	Altenberg	Drachenfels trachyte	laminar crust
AL-03	Altenberg	Drachenfels trachyte	laminar crust
AF-04	Altenberg	Krensheimer Muschelkalk	framboidal crust
CL-01	Cologne	Drachenfels trachyte	laminar crust
CL-02	Cologne	Drachenfels trachyte	laminar crust
CL-03	Cologne	Drachenfels trachyte	laminar crust
CL-04	Cologne	Drachenfels trachyte	laminar crust
CL-05	Cologne	Drachenfels trachyte	laminar crust
CL-06	Cologne	Drachenfels trachyte	laminar crust
CL-07	Cologne	Drachenfels trachyte	laminar crust
CL-08	Cologne	Drachenfels trachyte	laminar crust
CF-09	Cologne	Drachenfels trachyte	framboidal crust
CF-10	Cologne	Drachenfels trachyte	framboidal crust
CF-11	Cologne	Krensheimer Muschelkalk	framboidal crust
XL-01	Xanten	Drachenfels trachyte	laminar crust
XL-02	Xanten	Drachenfels trachyte	laminar crust
XL-03	Xanten	Drachenfels trachyte	laminar crust
XL-04	Xanten	Drachenfels trachyte	laminar crust
XL-05	Xanten	Drachenfels trachyte	laminar crust
XF-06	Xanten	Drachenfels trachyte	framboidal crust
CD-1a	Cologne	Drachenfels trachyte	scale (0.5 mm thickness)
CD-1b	Cologne	Drachenfels trachyte	drill core behind scale (0-10 mm)
CD-1c	Cologne	Drachenfels trachyte	drill core behind scale (11-31 mm)
CD-2a	Cologne	Drachenfels trachyte	scale (1 mm thickness)
CD-2b	Cologne	Drachenfels trachyte	disaggregated material behind scale
CD-2c	Cologne	Drachenfels trachyte	decay material from flaking
CD-2d	Cologne	Drachenfels trachyte	drill core behind scale (0-10 mm)
CD-2e	Cologne	Drachenfels trachyte	decay material crumbled area
CD-2f	Cologne	Drachenfels trachyte	drill core behind scale (11-31 mm)
CD-07	Cologne	Drachenfels trachyte	disaggregated material behind scale
CD-08	Cologne	Drachenfels trachyte	disaggregated material behind scale
CS-01	Cologne	Obernkirchner Sandstein	dust surface deposition